IntechOpen

PID Control for Industrial Processes

Edited by Mohammad Shamsuzzoha

PID CONTROL FOR INDUSTRIAL PROCESSES

Edited by **Mohammad Shamsuzzoha**

PID Control for Industrial Processes
http://dx.doi.org/10.5772/intechopen.69592
Edited by Mohammad Shamsuzzoha

Contributors

Juwari Purwo Sutikno, Nur Hidayah, Renanto Handogo, Jyh-Cheng Jeng, Nasser Mohamed Ramli, Adel Taieb, Abdelkader Chaari, Jorge-Humberto Urrea-Quintero, Jesús Hernandez-Riveros, Nicolás Muñoz-Galeano, Hidehiro Ikeda, Štefan Bucz, Alena Kozakova, Moonyong Lee, Rodrigue Tchamna, Thamiles Melo, Nathália Monteiro, Danilo Pequeno, Jaidilson Silva, Jose Sergio Da Rocha Neto

Notice

First published in London, United Kingdom, 2018 by IntechOpen
eBook (PDF) Published by IntechOpen, 2019
IntechOpen is the global imprint of INTECHOPEN LIMITED, registered in England and Wales, registration number: 11086078, The Shard, 25th floor, 32 London Bridge Street
London, SE19SG – United Kingdom
Printed in Croatia

British Library Cataloguing-in-Publication Data
A catalogue record for this book is available from the British Library

Additional hard and PDF copies can be obtained from orders@intechopen.com

PID Control for Industrial Processes
Edited by Mohammad Shamsuzzoha

p. cm.

Print ISBN 978-1-78923-700-9

Online ISBN 978-1-78923-701-6

eBook (PDF) ISBN 978-1-83881-401-4

Meet the editor

Dr. Mohammad Shamsuzzoha holds a Ph.D. in Chemical Engineering with specialization in process design and control and an MBA in Entrepreneurship and Leadership. He works as a senior process simulation engineering at ADNOC Refining Research Center (ARRC), Abu Dhabi, UAE.

Prior to joining ARRC, he worked at King Fahd University of Petroleum and Minerals, Saudi Arabia, as an assistant professor and at the Norwegian University of Science and Technology Norway as a postdoctoral research fellow. He was intensively involved in research and industrial projects to develop theory and applications in the area of process design, optimization, and control. He has published more than 30 technical papers in refereed chemical engineering journals and around 75 papers in proceedings in international conferences.

Contents

Preface

This book is devoted to proportional–integral–derivative (PID) controller theory and its application. PID controllers are probably the most widely used industrial controller in the process industries. They remain important control tools for three reasons: past record of success, wide availability, and simplicity of use. Their stability analysis is extremely easy to carry out and the design trade-off between performance and robustness is clearly understood.

PID Control for Industrial Processes presents a clear, multidimensional representation of PID control for both students and specialists working in the area of PID control. It mainly focuses on the theory and application of PID control in industrial processes. It incorporates recent developments in PID control technology in industrial practice. Emphasis has been given to finding the best possible approach to develop a simple and optimal solution for industrial users. This book includes several chapters that cover a broad range of topics and priority has been given to subjects that cover real-world examples and case studies. The book is focused on approaches for controller tuning, i.e., method bases on open-loop plant tests and closed-loop experiments.

Briefly, Chapter 1 presents a novel data-based PID controller tuning method that can be applied to stable, integrating, and unstable plants. The tuning method is developed under the virtual reference feedback tuning (VRFT) design framework where the reference model of VRFT is coordinately optimized with the controller on the basis of the model-reference criterion to ensure the validity of the VRFT approach. Chapter 2 finds the PID setting parameters of two degrees of freedom control structure based on model uncertainty. This tuning method is able to obtain reasonable controller parameters even under process uncertainties on standard two degrees of freedom internal model control. Chapter 3 demonstrates that when using advanced evolutionary algorithms, whatever the adopted system model (SOSPD, non-minimum phase, oscillatory, or non-linear), it is possible to find optimal parameters of PID controllers satisfying simultaneously the behavior of the system and a performance index such as Absolute Integral Error. Multidynamics Algorithm for Global Optimization is used to solve the control problem with PID controllers. Chapter 4 is a concise survey showing the persistent demand for PID tuning algorithms that integrate performance requirements into the tuning algorithm. The proposed frequency-domain PID controller design method guarantees closed-loop performance in terms of commonly used time-domain specifications. Chapter 5 emphasizes the problem of controlling the Takagi-Sugeno fuzzy model by PID controllers using particle swarm optimization. A new algorithm is proposed that relies on the use of a new objective function taking into account both the performance indices and the error signal.

In Chapter 6 steady-state simulation and dynamic simulation for a debutanizer column are performed using a process simulator. The main objective is to study the process variables of each controller at the column by using different tuning relations. The other part is to identify the best tuning methods for the controllers to optimize the performance of the column. Chapter 7 introduces the closed-form analytical design of proportional-integral controller parameters for optimal control subjected to operational constraints. The main idea of the design is not only to minimize the control performance index but also to cope with the constraints in the process variable, controller output, and its rate of change. The proposed optimization-based approach is examined to regulatory and servo control of integrating processes. Chapter 8 presents the design and implementation of a decoupling control strategy for an experimental platform pilot plant, dedicated to the study of the fouling phenomena that occurs in industrial tubes. The concept of a soft sensor was applied to monitor the output variables of the experimental platform for better performance of the decoupling control. Chapter 9 provides two off-line tuning methods for a digital PID-type controller for a two-mass resonance system to suppress its mechanical resonance vibrations. These methods include a coefficient diagram method and a fictitious reference iterative tuning method. The first method uses a nominal mathematical model of the object while the second method uses only the initial experimental data without use of the mathematical model.

Dr. Mohammad Shamsuzzoha
ADNOC Refining Research Center
Abu Dhabi, UAE

Chapter 1

Data-Based Tuning of PID Controllers: A Combined Model-Reference and VRFT Method

Jyh-Cheng Jeng

Additional information is available at the end of the chapter

http://dx.doi.org/10.5772/intechopen.75835

Abstract

This chapter presents a novel data-based proportional-integral-derivative (PID) controller tuning method that can be applied to stable, integrating, and unstable plants. The tuning method is developed under the virtual reference feedback tuning (VRFT) design framework, where the reference model of VRFT is coordinately optimized with the controller on the basis of the model-reference (MR) criterion to ensure the validity of the VRFT approach. In the proposed MR-VRFT method, a set of closed-loop plant data are directly exploited without resorting to a process model. Because of its closed-loop tuning capability, the MR-VRFT method can be applied online to improve (retune) existing underperforming controllers. Moreover, the tuning method includes a robustness specification based on the maximum sensitivity that enables the designer to explicitly address the trade-off between performance and robustness. Simulation studies, including the application to an unstable biochemical reactor, are presented to demonstrate the effectiveness of MR-VRFT method.

Keywords: PID controller, process control, data-driven control, model-reference control, virtual reference feedback tuning, integrating process, unstable process

1. Introduction

Proportional-integral-derivative (PID) controllers have been the most widely used process control technique for many decades in the chemical process industry. Although a PID controller has only three adjustable parameters, the optimization of these parameters in the absence of a systematic procedure is not a trivial task. It has been reported that numerous controllers are poorly tuned in practice [1]. A typical category of methods for tuning PID controllers is based on the model-based design approach. With the availability of plant

models, both analytic and empirical rules can be applied for PID design; see Ref. [2] for an extensive collection of methods. With the development of engineering technologies, industrial plants are becoming more and more complex, and therefore, modeling and identifying industrial plants are more challenging and demand considerable engineering effort. Furthermore, the performance of model-based controllers is highly dependent on the model accuracy. The model-based methods can give satisfactory PID design when the controlled plant dynamics are reasonably described by the low-order models, but the effectiveness of these methods degrades for complex and/or higher-order process dynamics owing to the inevitable modeling error.

An attractive approach to relieving the efforts of identifying a complicated process and mitigating the drawback of a plant-model mismatch is to design controllers directly from plant input–output data without the intermediate step of model identification. In the past two decades, a number of data-based control design methods have been developed; see Ref. [3] for a brief survey of the existing data-based control methods. Virtual reference feedback tuning (VRFT) [4, 5] is a one-shot discrete-time controller tuning method that only needs a set of plant input–output data to compute the controller parameters. Under the VRFT framework, the controller tuning problem is transformed into a controller parameter identification problem through introducing the virtual reference signal with a predefined reference model. The controller parameters are then obtained by solving an optimization problem formulated to minimize the VRFT criterion, that is, the deviation between the virtual controller output and actual plant input. The closed-loop behavior with the controller designed by VRFT is determined by the reference model. It is critical but not an easy step to properly determine a reference model because the plant model is unknown. However, VRFT is basically studied as an identification problem, and how to determine the optimal reference model is not addressed in traditional VRFT methods. Recently, VRFT has been extended to the design of continuous-time PID controllers [6–10] and, to determine the reference model appropriately, the parameter in the reference model was optimized by evaluating the VRFT criterion. In fact, the original objective of VRFT is to search the optimal controller parameters which minimize a model-reference (MR) criterion. The VRFT criterion shares with the MR criterion the same minimizer only when the adopted controller structure allows a perfect model matching [5]. However, the PID controller may not belong to the ideal controller set that allows a perfect model matching. The reference model determined by minimizing the VRFT criterion does not guarantee an effective model-reference control and therefore the performance of the designed PID controller becomes unpredictable.

To solve this problem, a novel model-reference VRFT (MR-VRFT) method is presented in this chapter. The PID controller is designed with VRFT based on an optimal reference model determined by minimizing the MR criterion, and consequently, the design objective of model-reference control can be effectively achieved. The MR-VRFT method can be applied to stable, integrating, and unstable plants by choosing appropriate reference model structures. The proposed design method includes robustness consideration that allows the designer to deal with the trade-off between control performance and system robustness by specifying a desired robustness level in terms of the maximum sensitivity.

http://dx.doi.org/10.5772/intechopen.75835

The rest of this chapter is organized as follows. Section 2 presents the PID controller design based on VRFT approach. Section 3 presents the specification of the reference model and proposed MR-VRFT method. Section 4 summarizes the controller tuning procedures. Section 5 presents several simulation examples showing the effectiveness of the proposed method. Finally, concluding remarks are presented in Section 6.

2. PID controller design based on VRFT approach

Consider the feedback control system shown in **Figure 1**, which consists of a plant $G(s)$ and a PID controller $C(s)$ given by

$$C(s) = K_C\left(1 + \frac{1}{\tau_I s} + \tau_D s\right) \tag{1}$$

where K_C, τ_I, and τ_D denote the proportional gain, the integral time, and the derivative time of the controller, respectively. Assume that the plant $G(s)$ is unknown and only a set of input–output data, $u(t)$ and $y(t)$, collected during an experiment on the plant is available for tuning the PID controller. The target of control design in the proposed method is assigned via a reference model, $M(s)$, that describes the desired closed-loop transfer function of the system shown in **Figure 1**. The control objective is the minimization of the following model-reference (MR) criterion:

$$J_{\mathrm{MR}}(K_C, \tau_I, \tau_D) = \left\| \left(\frac{G(s)C(s)}{1 + G(s)C(s)} - M(s) \right) W(s) \right\|_2^2 \tag{2}$$

where $W(s)$ is a user-specified weighting function.

Because $G(s)$ is unknown, the minimization of J_{MR} cannot be performed. The traditional approach is to identify a model of $G(s)$ using a set of input–output data of the plant and then minimize J_{MR} by replacing $G(s)$ with its model. However, this renders modeling difficult and introduces inevitable modeling error. The VRFT approach [5] avoids the procedure of model identification by creating a virtual reference signal $\tilde{r}(t)$ from the measured output $y(t)$:

$$\tilde{R}(s) = M(s)^{-1} Y(s) \tag{3}$$

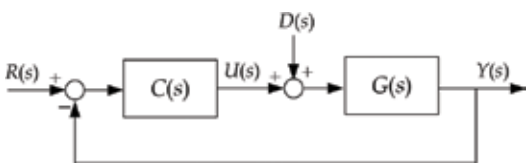

Figure 1. Feedback control system.

where $\tilde{R}(s)$ and $Y(s)$ is the Laplace transform of $\tilde{r}(t)$ and $y(t)$, respectively. Such a reference signal is called "virtual" because it was not used to generate $y(t)$. As $Y(s)$ is considered to be the desired output of the closed-loop system when the reference signal is specified by $\tilde{R}(s)$, the corresponding controller's output can be calculated by

$$\tilde{U}(s) = C(s)\left[\tilde{R}(s) - Y(s)\right] = K_C\left(1 + \frac{1}{\tau_I s} + \tau_D s\right)\left[M(s)^{-1} - 1\right]Y(s) \tag{4}$$

When the plant is fed by the measured input signal $u(t)$, it generates $y(t)$ as the output. Therefore, a controller that shapes the closed-loop transfer function to the reference model is one that generates $u(t)$ or its Laplace transform $U(s)$ when the error signal is given by $\tilde{R}(s) - Y(s)$, as depicted in **Figure 2**. The model-reference control design is then transformed into the problem of searching for a controller to minimize the difference between $U(s)$ and $\tilde{U}(s)$ given in Eq. (4).

Substituting $s = j\omega$ into Eq. (4) yields

$$\tilde{U}(j\omega) = \left[\Omega(j\omega) \quad \frac{\Omega(j\omega)}{j\omega} \quad \Omega(j\omega)j\omega\right]\mathbf{p} \tag{5}$$

where

$$\Omega(j\omega) = \left[M(j\omega)^{-1} - 1\right]Y(j\omega) \tag{6}$$

$$\mathbf{p} = \left[K_C \quad \frac{K_C}{\tau_I} \quad K_C\tau_D\right]^T \tag{7}$$

Minimizing the difference between $U(s)$ and $\tilde{U}(s)$ can be formulated in the frequency domain to minimize the difference between $U(j\omega)$ and $\tilde{U}(j\omega)$ in a frequency range $[0, \omega_{\max}]$. Choosing ω_i, $i = 1, 2, \cdots, n$, such that $0 < \omega_1 < \omega_2 < \cdots < \omega_n = \omega_{\max}$. The PID parameters are obtained by solving

$$\min_{\mathbf{p}} J_{\text{VRFT}}(\mathbf{p}) = \left\|\boldsymbol{\varphi} - \boldsymbol{\Psi}\mathbf{p}\right\|_2^2 \tag{8}$$

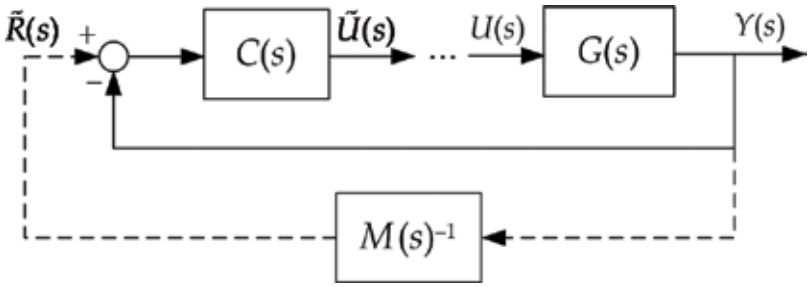

Figure 2. Schematic diagram of VRFT.

where

$$\begin{aligned}\boldsymbol{\varphi} &= \begin{bmatrix} U(j\omega_1) & U(j\omega_2) & \cdots & U(j\omega_n) \end{bmatrix}^T \\ \boldsymbol{\Psi} &= \begin{bmatrix} \psi_1 & \psi_2 & \cdots & \psi_n \end{bmatrix}^T \\ \psi_i &= \begin{bmatrix} \Omega(j\omega_i) & \frac{\Omega(j\omega_i)}{j\omega_i} & \Omega(j\omega_i)j\omega_i \end{bmatrix}^T \end{aligned} \tag{9}$$

The frequency responses of $U(j\omega_i)$ and $Y(j\omega_i)$ at selected frequency points ω_i ($i = 1, 2, \ldots, n$) can be evaluated by performing discrete Fourier transform for plant input and output measurements, which can be efficiently calculated using the fast Fourier transform (FFT) algorithm. The sampling rate to collect plant data must be large enough so that significant plant information is not lost. The frequency $\omega_{\max}$ denotes the upper bound of the frequency range for the minimization problem, and it is closely related to the controller design. Because the controller usually operates under the critical frequency, $\omega_{\max}$ can be specified as the critical frequency, ω_c, at which the phase angle of $GC(j\omega)$ equals $-\pi$. Based on the reference model $M(s)$, the critical frequency can be calculated according to the following equation:

$$\angle \frac{M(j\omega)}{1 - M(j\omega)}\bigg|_{\omega=\omega_c} = -\pi \tag{10}$$

After algebraic calculations, Eq. (8) is recast as

$$\min_{\mathbf{p}} J_{\mathrm{VRFT}}(\mathbf{p}) = \left\| \tilde{\boldsymbol{\varphi}} - \tilde{\boldsymbol{\Psi}}\,\mathbf{p} \right\|_2^2 \tag{11}$$

with

$$\tilde{\boldsymbol{\varphi}} = \begin{bmatrix} \mathrm{Re}(\boldsymbol{\varphi}) \\ \mathrm{Im}(\boldsymbol{\varphi}) \end{bmatrix}; \quad \tilde{\boldsymbol{\Psi}} = \begin{bmatrix} \mathrm{Re}(\boldsymbol{\Psi}) \\ \mathrm{Im}(\boldsymbol{\Psi}) \end{bmatrix} \tag{12}$$

where $\mathrm{Re}(\mathbf{A})$ and $\mathrm{Im}(\mathbf{A})$ denote the real matrix (or vector), and the elements are the real and imaginary parts of a complex matrix (or vector) $\mathbf{A}$, respectively. Eq. (11) can be solved by the least-squares method as

$$\mathbf{p}^* = \left(\tilde{\boldsymbol{\Psi}}^T \tilde{\boldsymbol{\Psi}}\right)^{-1} \tilde{\boldsymbol{\Psi}}^T \tilde{\boldsymbol{\varphi}} \tag{13}$$

which is used to obtain the parameters of the PID controller according to Eq. (7).

3. Specification of the reference model and MR-VRFT method

The reference model must be specified prior to calculation of the PID parameters using Eq. (13). The specification of the reference model is crucial to the performance of the resulting closed-loop system. Basically, the condition $M(0) = 1$ should be satisfied to achieve an offset-

free tracking. In addition, other conditions should be imposed on the reference model when the controlled plant is integrating or unstable. Here, the reference models for stable, integrating, and unstable plants are presented.

For stable plants, the reference model can be specified as

$$M(s) = \frac{1}{\lambda s + 1} e^{-\theta s} \tag{14}$$

For integrating plants, the following asymptotic tracking constraint must be satisfied to enable the step-load disturbances to be counteracted to eliminate the offset.

$$\lim_{s \to 0} \frac{d}{ds} [1 - M(s)] = 0 \tag{15}$$

In this case, the reference model for integrating plants is chosen as

$$M(s) = \frac{(2\lambda + \theta)s + 1}{(\lambda s + 1)^2} e^{-\theta s} \tag{16}$$

For unstable plants, $[1 - M(s)]$ should have zeros at unstable poles of the plant to guarantee the internal stability of the closed-loop system [11]. When the plant has an unstable pole up, the following condition should be satisfied:

$$1 - M(s)|_{s=up} = 0 \tag{17}$$

Therefore, the reference model for unstable plants can be chosen as

$$M(s) = \frac{\alpha s + 1}{(\lambda s + 1)^2} e^{-\theta s} \tag{18}$$

where α must be determined so that Eq. (17) is satisfied. In the reference models, θ is related to the apparent time delay of the plant, and λ is an adjustable parameter to manage the trade-off between control performance and system robustness.

The peak value of the sensitivity function (maximum sensitivity), M_S, defined in the following, has been widely used as a measure of system robustness.

$$M_S = \max_{\omega} \left| \frac{1}{1 + GC(j\omega)} \right| \tag{19}$$

As the maximum sensitivity decreases, the closed-loop system becomes more robust. The use of the maximum sensitivity as a robustness measure is advantageous because lower bounds for the gain and phase margins can be assured [1]. Because the plant is not known, M_S can be evaluated on the basis of the reference model as follows:

$$M_S = \max_{\omega} |1 - M(j\omega)| \tag{20}$$

Therefore, the parameter λ can be selected to match a designer-specified robustness level in terms of the maximum sensitivity. For a given value of the reference model parameter ρ, where $\rho = \theta$ for stable and integrating plants and $\rho = \{\theta, \alpha\}$ for unstable plants, the following correlated robust design criterion provides the required value of λ to achieve a specified value of M_S.

$$\lambda = \frac{-0.7289 M_S + 1.555}{M_S - 1.006}\theta, \quad 1.2 \le M_S \le 2.0; \quad \text{for stable plants} \tag{21}$$

$$\lambda = \frac{-0.4105 M_S + 2.044}{M_S - 1.012}\theta, \quad 1.2 \le M_S \le 2.0; \quad \text{for integrating plants} \tag{22}$$

$$\lambda = \frac{b_1 M_S + b_0}{M_S + a}\theta, \quad 1.5 \le M_S \le 3.0; \quad \text{for unstable plants} \tag{23}$$

where

$$\begin{aligned} b_1 &= 0.1395\left(\tfrac{\alpha}{\theta}\right)^{0.7266} - 0.18 \\ b_0 &= 0.6371\left(\tfrac{\alpha}{\theta}\right)^{0.4992} + 0.0521 \\ a &= -0.178\left(\tfrac{\alpha}{\theta}\right)^{-0.7623} - 0.6712 \end{aligned} \tag{24}$$

Eq. (24) is valid for $1 \le \alpha/\theta \le 10$. With the robust design criterion, the value of λ can be determined conveniently.

When a desired value of M_S is specified, the optimal solution given in Eq. (13) is a function of the reference model parameter ρ, that is, $\mathbf{p}^* = \mathbf{p}^*(\rho)$. As pointed out before, it is unreasonable to determine the reference model without information on the controlled plant. To determine the reference model appropriately, we propose for the first time that the reference model parameter ρ is optimized by minimizing the model-reference criterion given in Eq. (2). Namely, the proposed method seeks an appropriate reference model, which is most achievable for the controlled plant under the desired robustness level, to design the PID controller in the framework of VRFT.

Given a value of the reference model parameter ρ, the corresponding PID controller parameter $\mathbf{p}^*(\rho)$ can be calculated and a PID controller $C(s; \mathbf{p}^*(\rho))$ is the result. The virtual reference signal $\tilde{R}_\rho(s)$ that has to be applied in a closed loop employing the PID controller $C(s; \mathbf{p}^*(\rho))$ to obtain $u(t)$ and $y(t)$ (the available data for controller design) as the closed-loop response can be calculated by

$$\tilde{R}_\rho(s) = C(s; \mathbf{p}^*(\rho))^{-1} U(s) + Y(s) \tag{25}$$

Therefore, the closed-loop transfer function resulting from $C(s; \mathbf{p}^*(\rho))$ can be expressed by

$$T_\rho(s) = \frac{G(s)C(s; \mathbf{p}^*(\rho))}{1 + G(s)C(s; \mathbf{p}^*(\rho))} = \frac{Y(s)}{\tilde{R}_\rho(s)} \tag{26}$$

and its frequency response can be obtained as follows:

$$T_\rho(j\omega) = \frac{Y(j\omega)}{\tilde{R}_\rho(j\omega)} = \frac{Y(j\omega)}{C(j\omega;\mathbf{p}^*(\rho))^{-1}U(j\omega) + Y(j\omega)} \tag{27}$$

A model-reference criterion based on the framework of VRFT for PID controller design is then defined by

$$J_{\text{MR-VRFT}}(\rho) = \sum_{i=1}^{n} \left| \left[T_\rho(j\omega_i) - M(j\omega_i;\rho) \right] W(j\omega_i) \right|^2 \tag{28}$$

where the weighting function can be simply chosen as $W(j\omega_i) = 1/(j\omega_i)$. The optimal reference model parameter, ρ^*, is determined by solving the following minimization problem:

$$\rho^* = \arg\min_{\rho} J_{\text{MR-VRFT}}(\rho) \tag{29}$$

and its corresponding solution $\mathbf{p}^*(\rho^*)$ is the optimal PID controller parameter proposed by the MR-VRFT method.

4. Controller tuning procedure

The MR-VRFT method directly utilizes closed-loop plant data for controller tuning without requiring a priori knowledge of the plant and the existing (possibly roughly tuned) controller. For stable plants, open-loop data can also be used for controller tuning. Suppose that the existing control system has been brought to a steady state and a closed-loop test is applied. We recommend using a set-point step test because it is the simplest and most commonly used test in process control applications. The plant input $u(t)$ and output $y(t)$ are collected during the set-point change until a new steady state is reached. It is noted that $u(t)$ and $y(t)$ represent deviation variables and are defined on the basis of the original steady state.

In sum, the proposed MR-VRFT method for tuning PID controllers can be implemented as follows:

Step 1. Collect the plant data, $u(t)$ and $y(t)$, from a plant test and calculate their frequency responses, $U(j\omega_i)$ and $Y(j\omega_i)$. To calculate $Y(j\omega_i)$, the output $y(t)$ is decomposed into $y(t) = \Delta y(t) + y_s$, where $\Delta y(t)$ and y_s represent the transient part and the final steady-state value of $y(t)$, respectively. The Fourier transforms of $y(t)$ at discrete frequencies ω_i are then obtained by

$$Y(j\omega_i) = \Delta Y(j\omega_i) + \frac{y_s}{j\omega_i} \tag{30}$$

where $\Delta Y(j\omega_i)$ can be calculated by applying the FFT to $\Delta y(t)$. Similar procedures apply to the calculation of $U(j\omega_i)$ from $u(t)$.

Step 2. Set the prescribed searching range of ρ and the desired level of system robustness in terms of M_S. The recommended values for M_S are typically within the range $1.2 < M_S < 2.0$ [12]. However, specifying a higher value of M_S is required for particular unstable plants (e.g., those that involve a large time delay).

Step 3. Solve the minimization problem given in Eq. (29) by iteration. For each chosen ρ, perform the following steps.

1. Calculate the corresponding λ using the robust design criterion and specify the reference model $M(s)$.
2. Obtain the critical frequency ω_c using Eq. (10) and set $\omega_{\max} = \omega_c$.
3. Calculate $\mathbf{p}^*$ using Eq. (13).
4. Calculate the frequency response $T_\rho(j\omega_i)$ using Eq. (27) and evaluate the criterion $J_{\text{MR-VRFT}}$ given in Eq. (28).

Repeat (1) to (4) for other values of ρ in the searching range until the minimal $J_{\text{MR-VRFT}}$ is identified.

Step 4. Obtain the PID controller parameters from $\mathbf{p}^*$ corresponding to the optimal value of ρ, i.e., $\mathbf{p}^*(\rho^*)$.

5. Illustrative examples

Simulation examples are presented to demonstrate the effectiveness of the MR-VRFT method for PID controller tuning. In each example, the closed-loop plant data, $u(t)$ and $y(t)$, were generated by introducing a step change in the set point of an initial (existing) closed-loop system (**Figure 1**). To implement the proposed method, a priori knowledge of the existing controller settings is not required. Therefore, the effectiveness of the MR-VRFT method, proposed as a closed-loop tuning method, is not affected by the existing controller parameters used for generating the closed-loop data, as confirmed by the following example.

In all simulations, the PID controller was implemented as follows to avoid the derivative kick:

$$U(s) = K_C\left[\left(1+\frac{1}{\tau_I s}\right)E(s) - \frac{\tau_D s}{\gamma\tau_D s+1}Y(s)\right] \tag{31}$$

The derivative filter parameter γ was set to 0.1. Two metrics were used to evaluate the controller performance. The integrated absolute error (IAE) is defined as

$$\text{IAE} = \int_0^\infty |r(t) - y(t)|\, dt \tag{32}$$

To evaluate the required control effort, the total variation (TV) of the manipulated input u was calculated:

$$\mathrm{TV} = \sum_{i=1}^{\infty} |u(i) - u(i-1)| \tag{33}$$

TV is an effective measure of the "smoothness" of a signal and should be as small as possible [13].

5.1. Example 1: stable plant

Consider a fifth-order plant given by the following transfer function:

$$G(s) = \frac{1}{(2s+1)^3(s+1)^2} e^{-6s} \tag{34}$$

To illustrate that the effectiveness of the MR-VRFT method is unaffected by the plant data used for controller design, three sets of plant data, that is, one set of open-loop step response data and two sets of closed-loop data generated by initially poorly tuned PID controllers, collected with a sampling interval of 0.1, were separately used to implement the MR-VRFT method. As illustrated in **Figure 3**, the first set of closed-loop data (initial tuning 1: $K_C = 0.4$, $\tau_I = 10$, and $\tau_D = 1$) exhibited a sluggish set-point step response whereas the second set of closed-loop data (initial tuning 2: $K_C = 0.4$, $\tau_I = 4$, and $\tau_D = 0.5$) exhibited an oscillatory response. Using the reference model given in Eq. (14) with the desired level of robustness set as M_S = 1.58, the resulting three PID controllers are summarized in **Table 1**, where the controller parameters obtained by the MR-VRFT are almost indistinguishable in spite of different plant data used for controller design. Furthermore, the resulting closed-loop system has M_S = 1.59, which is close to the design value. **Figure 4** shows the closed-loop responses for the initial and retuned (MR-VRFT) controllers for a unit step set-point change at t = 0 and a unit step load disturbance at

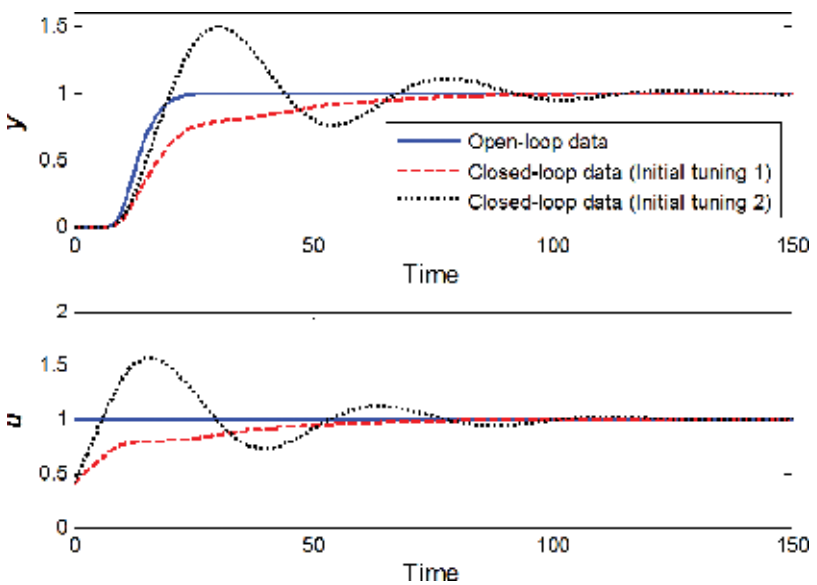

Figure 3. Three sets of plant data used for controller design in Example 1.

Data set	θ^*	λ	K_C	τ_I	τ_D	M_S
Open-loop data	8.91	6.26	0.508	7.71	2.58	1.59
Closed-loop data (initial tuning 1)	8.91	6.26	0.508	7.71	2.57	1.59
Closed-loop data (initial tuning 2)	8.94	6.28	0.505	7.69	2.51	1.59

Table 1. Results of controller design using three different sets of plant data for Example 1.

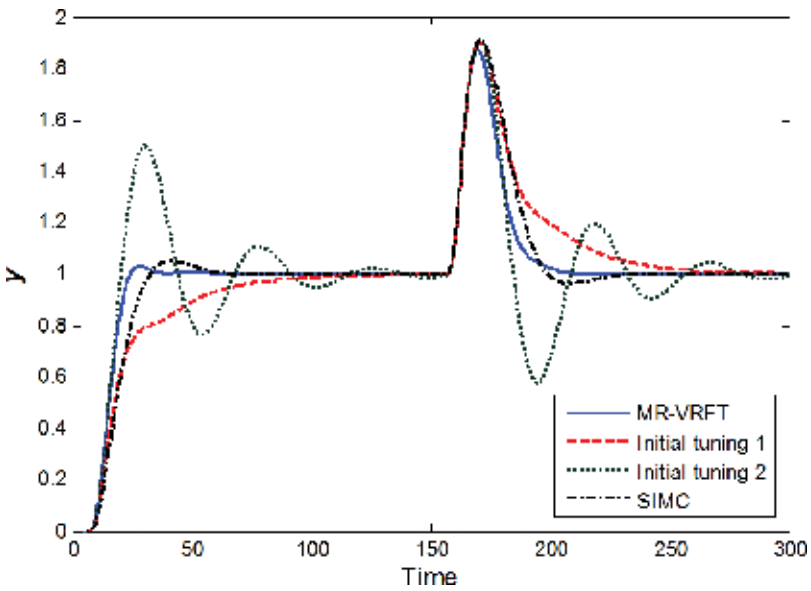

Figure 4. Closed-loop responses for Example 1.

t = 150. Control performance can be improved significantly using the MR-VRFT method, regardless of the initial controller parameters used for collecting the closed-loop data.

We compared the proposed PID design method with the model-based design method of Skogestad internal model control (SIMC) [13]. In the SIMC method, the plant in Eq. (34) was approximated as a second-order plus time delay (SOPTD) model:

$$G_m(s) = \frac{1}{(3s+1)(2s+1)} e^{-9s} \tag{35}$$

The controller parameters were obtained as $K_C = 0.278$, $\tau_I = 5$, and $\tau_D = 1.2$. The resulting closed-loop system also has M_S = 1.59, which facilitated a comparison of controller performance for controllers with the same level of robustness. The closed-loop response for the PID controller tuned by SIMC method is also shown in **Figure 4**. The values of IAE and TV for the controllers are presented in **Table 2**. **Figure 4** shows that the proposed PID controller provides faster set-point response and disturbance attenuation than the SIMC PID controller, demonstrating the superior performance of MR-VRFT method.

	Tuning method	K_C	τ_I	τ_D	Set point		Disturbance	
					IAE	TV	IAE	TV
Ex. 1	MR-VRFT	0.508	7.71	2.58	15.9	1.16	15.2	1.00
	SIMC [13]	0.278	5	1.2	19.9	1.12	19.4	1.09
Ex. 2	MR-VRFT	0.209	17.4	2.29	13.0	0.487	8.43	0.156
	SIMC [13]	0.177	25.5	1.41	14.0	0.416	14.4	0.157
Ex. 3	MR-VRFT	3.98	9.79	1.86	7.69	15.6	2.52	3.03
	Lee et al. [14] (first-order model)	3.26	10.6	1.63	8.84	12.5	3.31	2.96
	Lee et al. [14] (second-order model)	3.99	11.4	1.89	8.0	15.8	2.86	3.05
Ex. 4	MR-VRFT	−0.935	3.84	0.422	0.729	0.954	0.719	0.191
	Ref. [15]	−0.952	5.62	0.530	0.790	1.36	1.03	0.224

Table 2. PID controller settings and performance indices for the examples.

5.2. Example 2: integrating plant

Consider the following integrating plant:

$$G(s) = \frac{1}{s(s+1)^4} e^{-0.5s} \tag{36}$$

To implement the MR-VRFT method, an initial control system with a roughly tuned PID controller ($K_C = 0.3$, $\tau_I = 10$, and $\tau_D = 1$) was considered for generating closed-loop data, with a sampling interval of 0.05.

Using the reference model given in Eq. (16) with the design target M_S = 1.62, we determined the optimal θ value to be $\theta^* = 2.98$ ($\lambda = 6.75$). The corresponding PID controller parameters are $K_C = 0.209$, $\tau_I = 17.4$, and $\tau_D = 2.29$, and the resulting closed-loop system has an M_S value nearly identical to the design target. **Figure 5** shows the closed-loop responses for the initial and retuned (MR-VRFT) controllers for a unit step set-point change at t = 0 and a step-load disturbance of magnitude 0.1 at t = 120. The response for the initial controller is rather oscillatory. In fact, the initial closed-loop system has an M_S value of 3.92, indicating poor robustness. Control performance can be considerably improved after the retuning using the MR-VRFT method.

The proposed PID controller was compared with the SIMC PID controller which was tuned using the following model:

$$G_m(s) = \frac{1}{s(1.5s+1)} e^{-3s} \tag{37}$$

The SIMC controller parameters were obtained as $K_C = 0.177$, $\tau_I = 25.5$, and $\tau_D = 1.41$. The resulting closed-loop system also has M_S = 1.62. The closed-loop response for the PID controller tuned by SIMC method is also shown in **Figure 5**. The values of IAE and TV for the

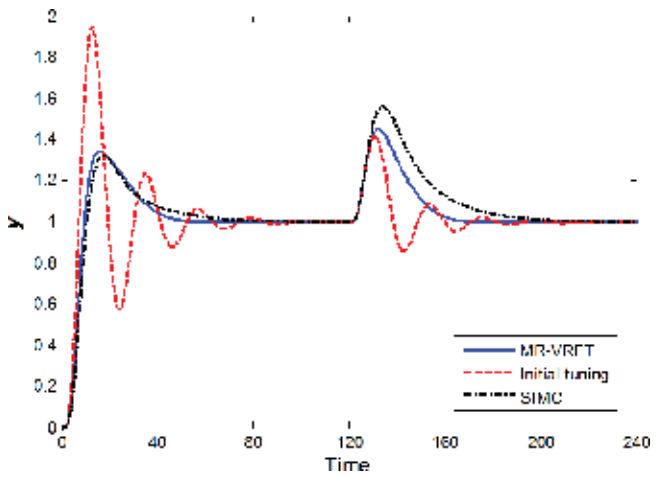

Figure 5. Closed-loop responses for Example 2.

controllers are presented in **Table 2**. Clearly, the proposed MR-VRFT method provides favorable control performance, especially for disturbance rejection, compared with the model-based method of SIMC.

In practice, plant data are inevitably corrupted by measurement noise. **Figure 6** shows closed-loop plant data that were corrupted by Gaussian white noise with a variance of 0.005; the data were used to tune the controller by the MR-VRFT method. The optimal θ value was determined to be $\theta^* = 2.99$ ($\lambda = 6.77$), and the resulting controller parameters were $K_C = 0.211$,

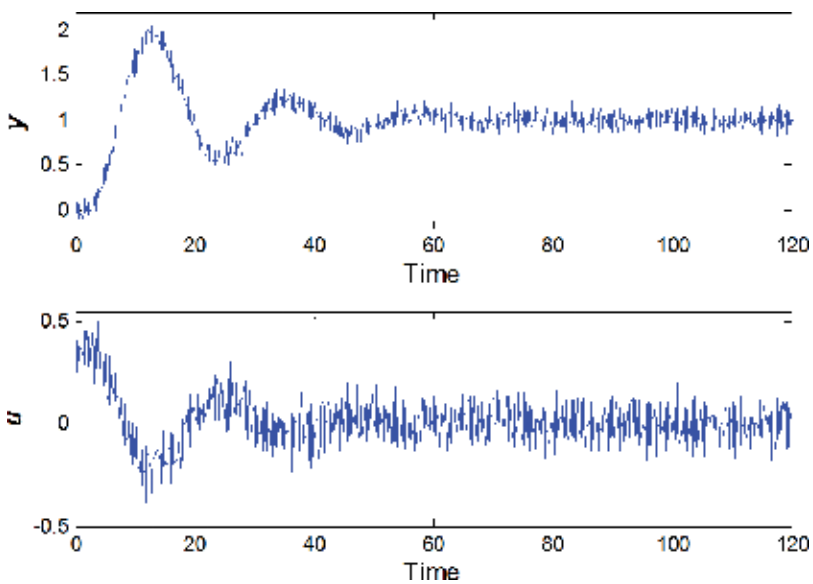

Figure 6. Noisy closed-loop data used for controller design in Example 2.

$\tau_I = 18.2$, and $\tau_D = 2.21$. By comparing the controller parameters obtained under noise conditions with those obtained under noise-free conditions, no dramatic change is observed, which verifies the applicability of the MR-VRFT method under realistic conditions. Moreover, simulation results show that fast sampling of plant data could reduce the sensitivity of the MR-VRFT method to the effect of measurement noise.

5.3. Example 3: unstable plant

Consider the following third-order delayed unstable plant studied in Lee et al. [14]:

$$G(s) = \frac{1}{(5s-1)(2s+1)(0.5s+1)} e^{-0.5s} \tag{38}$$

An initial closed-loop system with a roughly tuned PID controller ($K_C = 2$, $\tau_I = 20$, and $\tau_D = 1$) was assumed to generate plant data for controller design. The sampling interval was chosen as 0.1. We applied the MR-VRFT method to design the PID controller using the reference model given in Eq. (18), with an assigned M_S value of 2.25. The optimal reference model parameter was determined to be $\rho^* = \{\theta^*,\ \alpha^*\} = \{1.389,\ 8.033\}$ with $\lambda = 2.09$. The corresponding PID controller parameters are $K_C = 3.98$, $\tau_I = 9.79$, and $\tau_D = 1.86$, and the resulting closed-loop system has M_S = 2.20, which is close to the design target. To show the advantage of the MR-VRFT method over the previous VRFT method, the reference model parameter was also determined by minimizing the following VRFT criterion for comparison:

$$\rho^* = \arg\min_{\rho} J_{\text{VRFT}}(\rho) = \left\| \tilde{\boldsymbol{\varphi}} - \tilde{\boldsymbol{\Psi}}\, \mathbf{p}^*(\rho) \right\|_2^2 \tag{39}$$

The result was obtained as $\rho^* = \{\theta^*,\ \alpha^*\} = \{1.481,\ 9.645\}$ with $\lambda = 2.41$. The corresponding PID controller parameters are $K_C = 3.49$, $\tau_I = 11.7$, and $\tau_D = 1.77$, and the resulting closed-loop system has M_S = 2.07, which deviates from the design target. When a closed-loop system has an M_S value closer to the design target, the closed-loop system matches the reference model better. By comparing the M_S value of the closed-loop systems resulting from the MR-VRFT and VRFT methods, it clearly indicates that the MR-VRFT method achieves a more effective model-reference control design than the VRFT method does. **Figure 7** shows closed-loop responses for the initial and MR-VRFT controllers for a unit step set-point change at t = 0 and a unit step load disturbance at t = 50. The control performance evidently improves considerably after the retuning using the MR-VRFT method.

The proposed PID controller was compared with two PID controllers tuned by the model-based method of Lee et al. [14] on the basis of the following first-order and second-order models, respectively:

$$\begin{aligned} G_{m1}(s) &= \frac{1}{5.766s-1} e^{-3.282s} \\ G_{m2}(s) &= \frac{1}{(5s-1)(2.07s+1)} e^{-0.939s} \end{aligned} \tag{40}$$

Both models provide accurate approximations; however, the second-order model is more accurate.

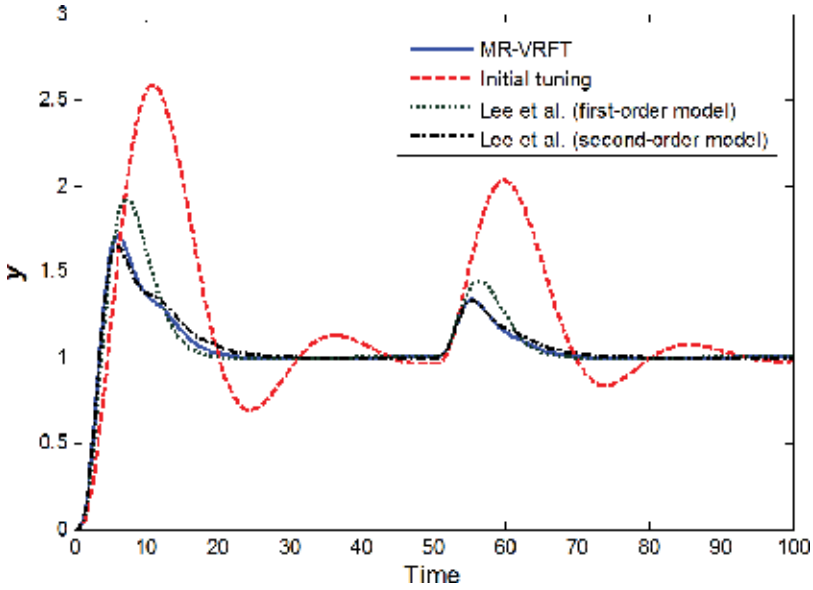

Figure 7. Closed-loop responses for Example 3.

The control systems using the model-based controllers were tuned to have the same robustness level of $M_S = 2.2$. The PID settings are shown in **Table 2** and the resulting closed-loop responses are shown in **Figure 7**. The values of IAE and TV for all of the controllers are presented in **Table 2**. As evident from the results in **Table 2** and **Figure 7**, the proposed MR-VRFT method performs better than the model-based design method with respect to both set-point tracking and disturbance rejection. In addition, the model-based controller based on the second-order model provides better performance than that based on the first-order model, which indicates that the model-based design method requires an accurate process model to obtain improved PID settings. Because the availability of accurate process models cannot be guaranteed, the proposed data-based method provides an obvious advantage in controller design.

5.4. Example 4: application of a biochemical reactor

The biochemical reactor plays a major role in most of the biotechnological and chemical industries. The MR-VRFT method was applied to the nonlinear biochemical reactor studied by Vivek and Chidambaram [15]. The bioreactor modeling equations are as follows.

$$\begin{aligned}
&\text{Biomass balance}: \frac{dx_1}{dt} = (\mu - D)x_1 \\
&\text{Substrate balance}: \frac{dx_2}{dt} = D(x_{2f} - x_2) - \frac{\mu x_1}{Y} \\
&\text{Specific growth rate}: \mu = \frac{\mu_{\max} x_2}{k_m + x_2 + k_1 {x_2}^2}
\end{aligned} \tag{41}$$

where x_1 is the biomass concentration, x_2 is the substrate concentration, x_{2f} is the substrate feed concentration, and D is the dilution rate. The yield Y is assumed to be a constant. The model parameters used for the simulation were

$$\mu_{\max} = 0.53\ \mathrm{h}^{-1};\ \ k_m = 0.12\ \mathrm{g/L};\ \ k_1 = 0.4545\ \mathrm{L/g};\ \ Y = 0.4;\ \ x_{2f} = 4.0\ \mathrm{g/L} \tag{42}$$

The nonlinear process has three steady-state operating points for a dilution rate of 0.3 h^{-1}. An unstable operating region with a steady-state value of (x_{1s}, x_{2s}) = (0.9951, 1.5122) is considered. The dilution rate is the manipulated variable used to control the biomass concentration at the unstable steady state. A time delay of 1 h is assumed in the measurement of x_1.

Vivek and Chidambaram [15] calculated the PID parameters (see **Table 2**) on the basis of the following identified unstable first-order plus time delay model:

$$G_m(s) = \frac{-5.5903}{5.6125s - 1} e^{-1.0152s} \tag{43}$$

An initial closed-loop system with the PID controller proposed by Vivek and Chidambaram [15] was considered to generate the plant data required to tune the controller. The MR-VRFT method was applied to retune the PID controller by introducing a step change of 10% in the set point of x_1. To simulate realistic conditions, Gaussian white noise, with a standard deviation of 0.005, was added to the measurements as the measurement noise. The noisy closed-loop data collected with a sampling interval of 0.01 h are shown in **Figure 8**. Using the reference model given in Eq. (18) with the design target M_S = 2.6, the optimal reference model parameter was determined to be $\rho^* = \{\theta^*,\ \alpha^*\} = \{1.084, 3.736\}$ with $\lambda = 0.966$, and the corresponding PID controller parameters are shown in **Table 2**.

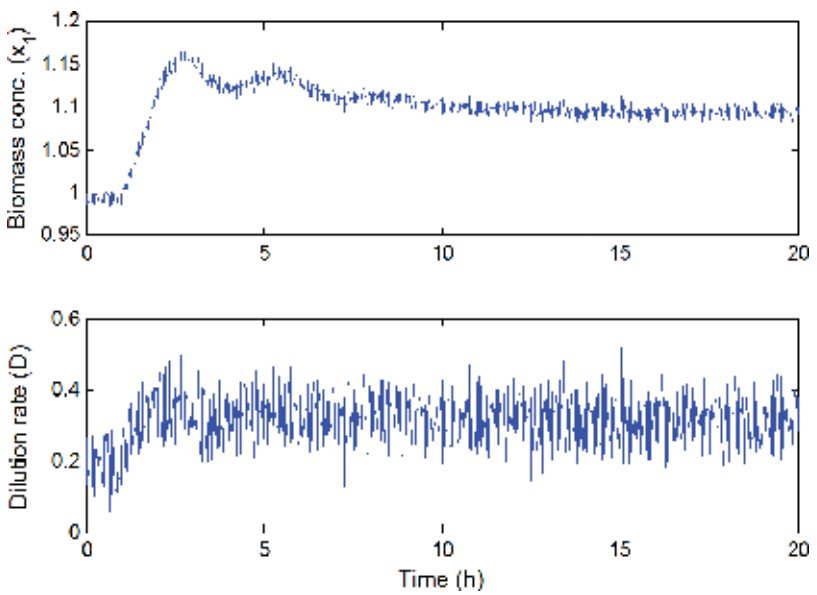

Figure 8. Noisy closed-loop data used for controller design in Example 4.

The proposed controller was compared with the initial model-based controller by simulating the nonlinear model equations of the bioreactor. **Figure 9** shows the closed-loop responses to a step change of 20% in the set point at $t = 0$, followed by a step disturbance of 4 g/L in the substrate

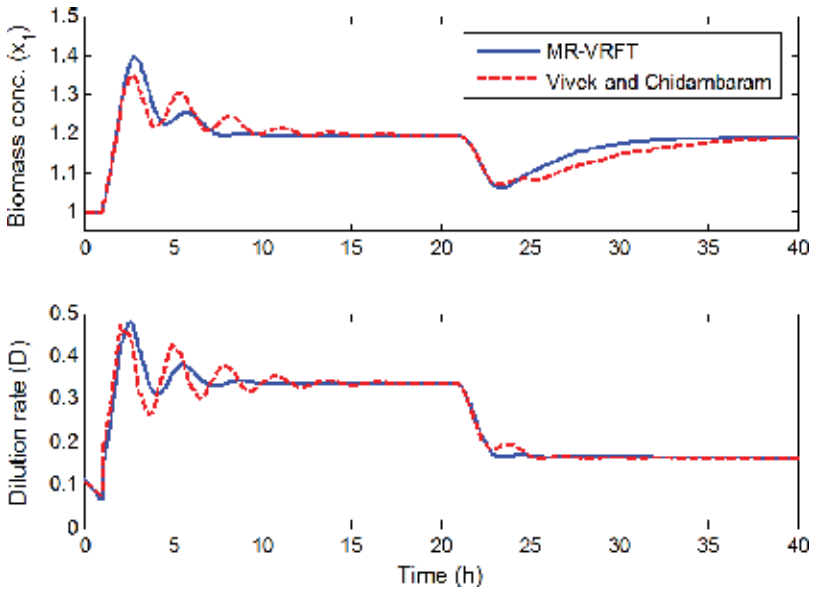

Figure 9. Closed-loop responses for Example 4.

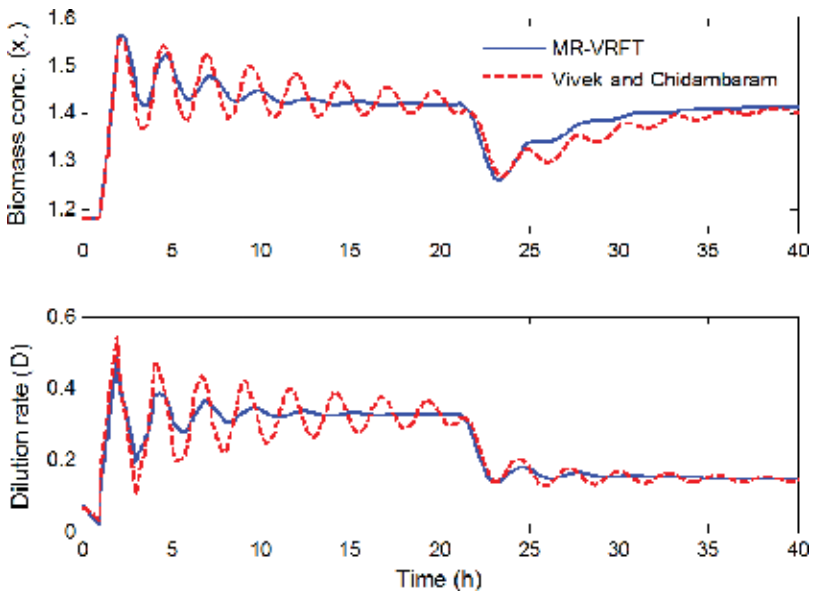

Figure 10. Closed-loop responses under variations in the process parameters for Example 4.

feed concentration x_{2f} at t = 20 h. The corresponding values of IAE and TV, as presented in **Table 2**, clearly indicate that the retuned control system using the MR-VRFT method outperforms the initial control system. The proposed controller shows a rapid attenuation of the disturbance. The overshoot in the set-point response for the proposed controller is moderately large, but the response is less oscillatory with a shorter settling time compared to that of Vivek and Chidambaram [15] (i.e., the initial controller). It is noted that the excessive overshoot can be reduced by applying the set-point weighting to the proportional mode of a PID controller.

Figure 10 shows the closed-loop responses of the controllers when a 30% increase in the process parameters k_m and k_1 has occurred. The response for the controller of Vivek and Chidambaram [15] became highly oscillatory compared with that of the proposed controller, indicating the superior robust performance of the proposed controllers. This example demonstrates that the MR-VRFT method is promising for industrial applications.

6. Conclusions

In this chapter, a novel and systematic data-based PID design method based on combined model-reference and virtual reference feedback tuning is presented. With the optimized reference model using the model-reference criterion, the optimal PID controller can be efficiently designed in the framework of VRFT. By choosing an appropriate structure of the reference model, the proposed MR-VRFT method applies to a wide variety of process dynamics and deals with stable, integrating, and unstable processes using the same unified procedure. Simulation studies show that PID controllers designed by the MR-VRFT method fulfill the user-defined robustness specification, indicating that an effective model-reference control design is achieved, and they also exhibit favorable control performance when compared to the model-based PID controllers. Therefore, the MR-VRFT method is a promising PID controller design method for industrial application, and it can be used to improve the performance of existing underperforming PID controllers through the retuning of the controller parameters using routine operating data.

Acknowledgements

The author thanks the Ministry of Science and Technology of Taiwan for supporting this research under the grant of MOST 105-2221-E-027-128.

Author details

Jyh-Cheng Jeng

Address all correspondence to: jcjeng@ntut.edu.tw

Department of Chemical Engineering and Biotechnology, National Taipei University of Technology, Taipei, Taiwan

References

[1] Åström KJ, Hägglund T. Advanced PID Control. Research Triangle Park: ISA; 2005

[2] O'Dwyer A. Handbook of PI and PID Controller Tuning Rules. London: Imperial College Press; 2006

[3] Hou ZS, Wang Z. From model-based control to data-driven control: Survey, classification and perspective. Information Sciences. 2013;**235**:3-35

[4] Guardabassi GO, Savaresi SM. Virtual reference direct design method: An off-line approach to data-based control system design. IEEE Transactions on Automatic Control. 2000;**45**:954-959

[5] Campi MC, Lecchini A, Savaresi SM. Virtual reference feedback tuning: A direct approach for the design of feedback controllers. Automatica. 2002;**38**:1337-1346

[6] Yang X, Xu B, Chiu MS. PID controller design directly from plant data. Industrial & Engineering Chemistry Research. 2011;**50**:1352-1359

[7] Jeng JC, Liao SJ. A simultaneous tuning method for cascade control systems based on direct use of plant data. Industrial & Engineering Chemistry Research. 2013;**52**:16820-16831

[8] Jeng JC, Tseng WL, Chiu MS. A one-step tuning method for PID controllers with robustness specification using plant step-response data. Chemical Engineering Research and Design. 2014;**92**:545-558

[9] Jeng JC, Fu EP. Closed-loop tuning of set-point-weighted proportional-integral-derivative controllers for stable, integrating, and unstable processes: A unified data-based method. Industrial & Engineering Chemistry Research. 2015;**54**:1041-1058

[10] Jeng JC, Ge GP. Disturbance-rejection-based tuning of proportional-integral-derivative controllers by exploiting closed-loop plant data. ISA Transactions. 2016;**62**:312-324

[11] Nasution AA, Jeng JC, Huang HP. Optimal H_2 IMC-PID controller with set-point weighting for time-delayed unstable processes. Industrial & Engineering Chemistry Research. 2011;**50**: 4567-4578

[12] Åström KJ, Panagopoulos H, Hägglund T. Design of PI controllers based on non-convex optimization. Automatica. 1998;**34**:585-601

[13] Skogestad S. Simple analytic rules for model reduction and PID controller tuning. Journal of Process Control. 2003;**13**:291-309

[14] Lee Y, Lee J, Park S. PID controller tuning for integrating and unstable processes with time delay. Chemical Engineering Science. 2000;**55**:3481-3493

[15] Vivek S, Chidambara M. An improved relay auto tuning of PID controllers for unstable FOPTD systems. Computers and Chemical Engineering. 2005;**29**:2060-2068

Chapter 2

Maximum Peak-Gain Margin (Mp-GM) Tuning Method for Two Degree of Freedom PID Controller

Juwari Purwo Sutikno, Nur Hidayah and
Renanto Handogo

Additional information is available at the end of the chapter

http://dx.doi.org/10.5772/intechopen.74293

Abstract

The specification of controller setting for a standard controller typically requires a trade-off between set point tracking and disturbance rejection. For this reason, two simple strategies can be used to adjust the set point and disturbance responses independently. These strategies are referred as controllers that have two degree of freedom. Unfortunately, the tuning parameters of the model uncertainty at two degree of freedom structure controller are difficult to obtain. Maximum peak-gain margin (Mp-GM) tuning method has been introduced to obtain the setting parameters of two degree of freedom structure controller based on model uncertainty. This tuning method is able to obtain reasonable controller parameters even under process uncertainties on standard two degree of freedom IMC. This research was conducted to develop maximum peak-gain margin tuning method for another two degree of freedom structure controller such as two degree of freedom IMC by Kaya [9] and two degree of freedom PID. The simulation results show that the maximum peak-gain margin tuning method can give a good target set point tracking, disturbance rejection, and robustness in two degree of freedom structure controller system.

Keywords: two degree of freedom structure controller, IMC, PID, maximum peak, gain margin

1. Introduction

The process control is one of the important component parts in industries which is useful to keep and maintain the operating conditions of processes working on the desired performance. The development of this issue had begun since 1940. It is characterized by using PID controller in industries. Nowadays, PID control system is widely used as the basic control technology,

because the PID controller uses a simple control algorithm [1]. Although the development of PID controller is rapid, it still does not produce maximum results especially for the process with large time delay. This is due to the disturbance that is not detected immediately (only can be detected until a certain time with delay) and also control actions based on the delay that are not in accordance with the purpose of information and need some time to determine its effects on the process.

To overcome this weakness, a new structure controller has been developed. This structure controller is called as internal model control (IMC) controller (**Figure 1**) [2, 3]. The philosophy of this structure stated that if the process model is an exact representation of the process that will be controlled, then it is possible to obtain the ideal control in 1DOF-IMC without any feedback. But in fact, the process model may not be invertible and some disturbances may enter the system so that the feedback path control is still necessary. Unfortunately, IMC design is intended only for the set point problem and the disturbance rejection responses still cannot be expected in many cases. So, this controller provides a good response for the set point tracking and a very slow response for the disturbance rejection case [4].

The specification of controller settings for a standard controller typically requires a trade-off between set point tracking and disturbance rejection. For many single-loop controllers, it is extremely difficult to obtain the specification in one degree of freedom structure controller settings. Fortunately, there are two simple strategies that can be used to adjust the set point and disturbance responses independently. These strategies are referred as controllers with two degree of freedom structure controller [5]. The design of these control systems is a multiobjective problem, so that a two degree of freedom (abbreviated as 2DOF) controller system has more advantages than a one degree of freedom (abbreviated as 1DOF) controller system. This fact was already stated by Horowitz, but it did not attract the general attention from engineers for a long time, until 1984, two decades after Horowitz's work, when a research to exploit the advantages of the 2DOF structure for PID control systems was eventually started [6].

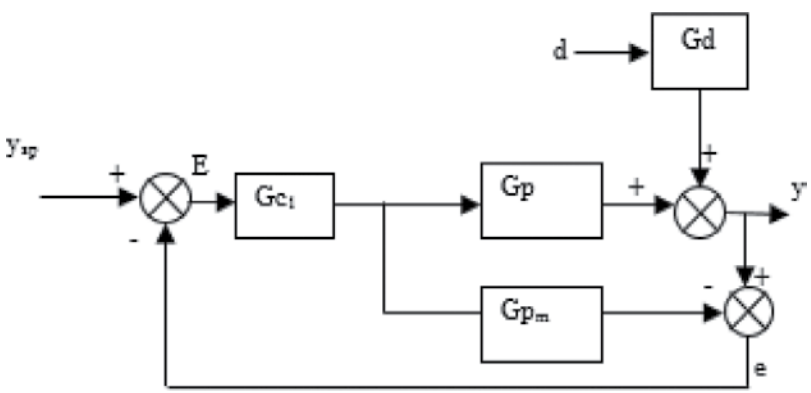

Figure 1. The structure of one degree of freedom IMC controller.

http://dx.doi.org/10.5772/intechopen.74293

Many researches have proposed new various configurations of 2DOF structure control for PID, IMC, fuzzy logic controller, etc. Unfortunately, this is not followed by the study of 2DOF controller tuning method. The research conducted for 2DOF tuning method is still very rare, especially for the process with uncertainty. Maximum peak-gain margin (Mp-GM) tuning method has been proposed to obtain setting parameter of 2DOF structure controller based on model uncertainty. This tuning method is able to obtain the good controller parameter even under process uncertainties on standard 2DOF IMC structure controller [7]. The stability and robust Mp-GM tuning method has potential to be implemented into the other 2DOF structure controllers, both 2DOF PID controller and 2DOF IMC controller. This chapter studies the analytical procedure of implementation of Mp-GM tuning method to the other 2DOF structure controller under process uncertainties.

2. Two degree of freedom PID structure controller

For many single-loop controls, disturbance rejection is more precedent to be attained than set point tracking. Hence, the tuning methods hold a dominant role to reach this goal. Unfortunately, 1DOF structure controller can only arrange one parameter so that a trade-off between set point tracking and disturbance rejection cannot be reached. If the parameters give good enough response for set point tracking, it will give a slow response for the disturbance rejection and vice versa. This leads to the difficulty for stabilizing the control response simultaneously between set point tracking and disturbance rejection [5]. To overcome this weakness, a new simple control strategy has been developed to arrange the set point tracking and disturbance rejection controller independently without affecting each other. This method is called as (2DOF) strategy controller. The research of 2DOF strategy control for PID controller began since 1984. In 2DOF PID structure control, controller which is used to control set point tracking and disturbance rejections can be in PI, PD, or PID form controller. In 2003, there are some new variations developed for 2DOF PID structure controller such as 2DOF PID filter set point as shown in **Figure 2** [6].

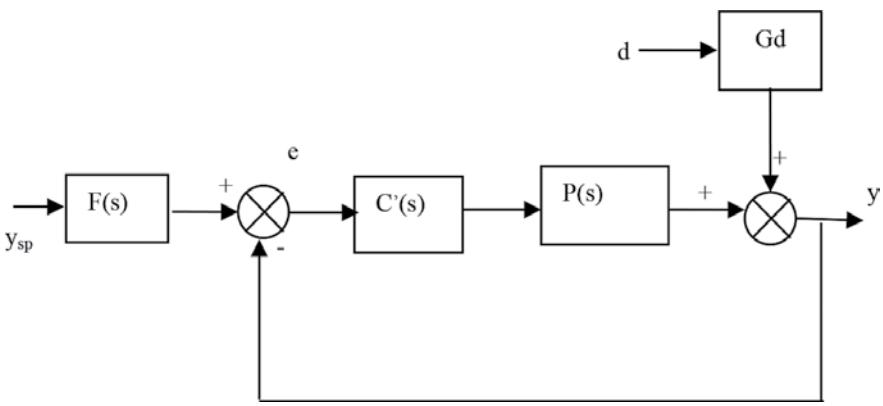

Figure 2. 2DOF-PID filter set point.

The structure of 2DOF-PID filter set point was developed by adding filter function in PID controller conventional (F(s)) that was used for controlling set point tracking, whereas PID parallel controller with approximate derivative was used for controlling disturbance rejection. Algorithm of F(s) and C′(s) controller for controlling set point tracking and disturbance rejection can be seen in Eqs. (1) and (2), respectively.

$$F(s) = \frac{1 + (1-a)\tau_I(s) + (1-\beta)\tau_I(s)\tau_D D(s)}{1 + \tau_I(s) + \tau_I(s)\tau_D D(s)} \tag{1}$$

$$C'(s) = k_p\left[1 + \frac{1}{\tau_I s} + \tau_D D(s)\right] \tag{2}$$

$$D(s) = \frac{s}{1 + \tau s} \tag{3}$$

Another variation of 2DOF-PID that is showed in **Figure 3** was developed by added feedback loop from output y directly to input u which will be compared with conventional PID controller ($C_y(s)$), which is called as feedback compensator that is used for controlling disturbance rejection). $C_r(s)$ will be used as set point tracking controller. Algorithm for $C_r(s)$ and $C_y(s)$ controller was given by Eqs. (4) and (5) [6]:

$$C_r(s) = k_p\left[(1-\alpha) + \frac{1}{\tau_I s} + (1-\beta)\tau_D D(s)\right] \tag{4}$$

$$C_y(s) = k_p\left[\alpha + \beta\tau_D D(s)\right] \tag{5}$$

In 2011, another structure called as 2DOF-PID Vilanova was developed and was given in **Figure 4**. **Figure 4** shows that $C_{sp}(s)$ is used as set point tracking, $C_{yd}(s)$ as disturbance rejection control, and P(s) as transfer function process. $C_{yd}(s)$ was placed in the feedback loop to give a significant influence in maintaining stability without depending on the weighting factor set point tracking. For set point tracking controller, a filter is inserted in the path of the

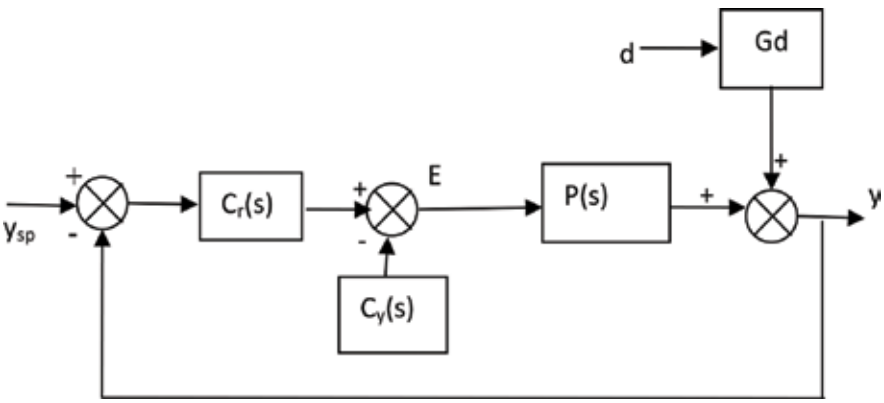

Figure 3. 2DOF-PID feedback.

http://dx.doi.org/10.5772/intechopen.74293

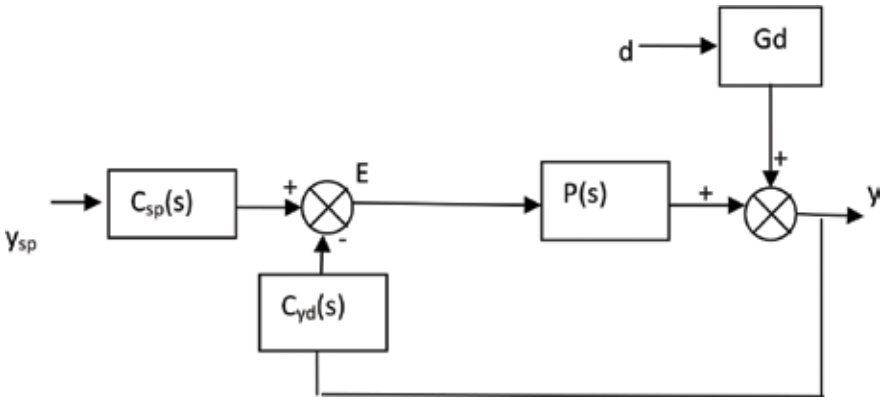

Figure 4. 2DOF-PID Vilanova.

conventional PID controller. Transfer function of C_{sp} and C_{yd} was given by Eqs. (6) and (7), respectively [8].

$$C_r(s) = k_c\left[\beta + \frac{1}{\tau_I s}\right] \tag{6}$$

$$C_y(s) = k_c\left[1 + \frac{1}{\tau_I s} + \tau_D\right] \tag{7}$$

where k_p is proportional to gain controller, τ_I the is integral time constant, τ_D is the derivative time constant as "basic parameters," and α and β variables as parameters for 2DOF controller. The range value of parameters α and β is between 0 and 1. All parameters in 2DOF-PID filter set point and feedback will be treated as adjustable parameters. The τ parameter in approximate derivative Eq. (3) is set as τ_D/δ, where δ is called the derivative gain. The fixed value of δ can be determined by traditional step. The research stated that the change of δ does not influence the optimal value of all parameters in this structure drastically [6], while in 2DOF-PID Vilanova, the controller parameters will be determined by analytical robust tuning (ART) method. This tuning method used approach of the robustness-performance to determine controller parameters [8].

Beside 2DOF-PID, research on 2DOF controller also performed on controller with model principle like 2DOF-IMC. 2DOF IMC (**Figure 5**) structure controller was developed which aimed to cover a very slow response for disturbance rejection at 1DOF-IMC. This controller consists of controller for set point tracking (G_{c1}) in the open loop and disturbance rejection (G_{c2}) in the feedback path as shown in **Figure 6**. This structure configuration shows if there are no errors in the model and there are no disturbance enter to the process, it will need open loop path control only to get the ideal control response where the output will be same with set point. In fact, none of the models exactly same with the process and disturbance will always enter to the process in the field so that will be required a feedback loop to overcome these problems [2].

$$y = \frac{G_{c1}G_p y_{sp} + (1 - G_{c2}G_{pm})G_d}{1 + G_{c2}(G_p - G_{pm})} \tag{8}$$

If $G_p = G_{pm}$,

$$e = (1 - G_p G_{c2})d - (1 - G_p G_{c2})Y_{sp} \tag{9}$$

From Eq. (9), it can be assumed that G_{c2} was designed for disturbance rejection (d). If G_{c2} was designed exactly with G_{c1}, then the disturbance rejections cannot be eliminated optimally. Therefore, it is necessary to do tuning to get an optimal control result [2]. Unfortunately, the research for 2DOF controller tuning method is still extremely rare. Most studies were conducted only on the development of the new structure configuration of 2DOF structure controller. As in 2004, a new structure configuration was proposed for 2DOF IMC called as 2DOF IMC Kaya. This structure was designed for controlling integrating process with small time delays. Besides that, this structure is also used for the tuning of proportional derivative

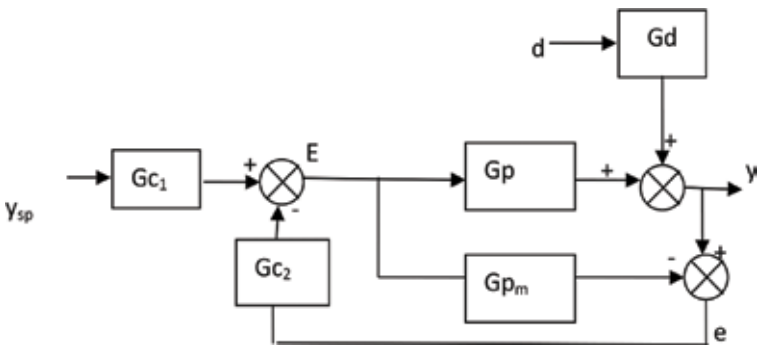

Figure 5. 2DOF-IMC standard.

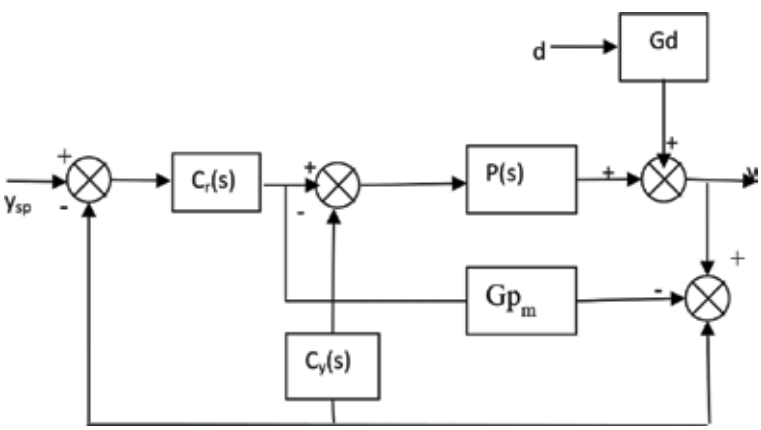

Figure 6. 2DOF-IMC Kaya.

http://dx.doi.org/10.5772/intechopen.74293

(PD) controller using gain and phase margin stability principle. As show in **Figure 6**, G_{c1} and G_{c2} in 2DOF-IMC Kaya are going to be located in the close loop of the structure. G_{c1} will be used for set point tracking and G_{c2} for disturbance rejection [9]. Besides 2DOF IMC controller, there is another controller that has model principle like Smith Predictor (SP), and nowadays, it is developed in 2DOF controller form. 2DOF SP structure controller has been applied on the integrating process with large time delay. The results show that 2DOF SP controller is able to gain fast and stable response for disturbance rejection [10].

3. Tuning method for two degree of freedom structure controller

The purpose of controller tuning is to determine the controller parameter to obtain appropriate control parameters in order to achieve stable closed-loop performance robustly. The controller performance is expected to be stable and robust when the variable control at desired set point and the disturbance can be eliminated as soon as possible [11]. The proposed 2DOF controller tuning method has been started since the structure developed in 1984. Tuning of 2DOF controller is developed in the form of proportional derivative (PD) or proportional integral derivative (PID) controller. Unfortunately, this tuning did not provide an analytical explanation for the controller parameters. Besides that, there is no guarantee that a stable response and robust process can be produced [4]. Furthermore, another tuning has been developed for 2DOF PID structure controller with principle multiplication from dominant pole on sensitivity and complementary sensitivity function [12]. This tuning has only been developed for the integrating process with small time delay. Additionally, this tuning involves weighting factor in variables for both proportional and derivative part in PID controller which is used for both set point tracking and disturbance rejections. In 2008, another research has been done to develop a tuning for 2DOF PI/PID structure controller with analytical approaching. This tuning was called as analytical robust tuning (ART), which is also using a weighting factor in variable of proportional controller for the case with perfect models. Analytical approaching in this tuning depends on the process being controlled. To control FOPDT process, the proportional integral (PI) controller will be used for set point tracking and disturbance rejection. Nevertheless, when SOPDT process is to be controlled, the proportional integral derivative (PID) controller will be used [4]. Tuning for 2DOF-PID filter set point has been done by Zhang et al. at 2006, but the tuning was used for integrating process and the dead time of process is approximated with two-order Pade approximation so that the equations become more complicated [13].

For the 2DOF IMC structure controller tuning, most of them are still being developed for the case with perfect model, where the transfer functions process and model are exactly equal. One of the researchers who developed a tuning for the case of uncertainties is Brosilow and Joseph. They used the principle of the resonant peak of the complementary sensitivity function to develop a tuning for 2DOF IMC structure. The tuning was called as maximum peak (Mp) tuning [14]. Unfortunately, this tuning can only be used for 1DOF IMC structure. Furthermore, it can be done by using the maximum peak (Mp) principle that was developed by Brosilow and Joseph, Stryczek et al. to propose IMCTUNE. This tuning can be implemented not only in

the 1DOF and 2DOF structure controller but also on the other structures, such as 1DOF PID and model state feedback (MSF)-IMC. Unfortunately, IMCTUNE needs partial sensitivity functions from the transfer function of disturbance which is difficult to be modeled [3]. To overcome this weakness, in 2013, maximum peak-gain margin (Mp-GM) tuning has been proposed to obtain setting parameter of 2DOF structure controller based on model uncertainty. By using maximum value of complementary sensitivity function of 1DOF IMC structure to determine parameter control for set point tracking and gain margin (GM) values to determine parameter control for disturbance rejection, this tuning method is able to obtain a good controller parameter when it is even under process uncertainties on standard 2DOF IMC. The steps for Mp-GM tuning will be explained more clearly in the next section [7].

4. Maximum peak-gain margin tuning method

One of the newest tuning method that was developed to handle the case control with parametric uncertainty is maximum peak-gain margin (Mp-GM) tuning method. This tuning method consists of three steps with all figure to determine the parameter value of Mp-GM tuning given in **Figure 7**. The initial step in Mp-GM tuning is determining the worst case of uncertainty model. Worst case is a condition when transfer function process is not same with model. The worst case can be found from the limit of the uncertainty model in terms of upper and lower on process model parameters. This condition usually occurs at the uncertainty model with the larger (upper limit) steady-state gain process, the larger the (upper limit) time delay, the smaller the (lower limit) process time constant. The worst case can be identified as the biggest maximum value of magnitude of frequency response of complementary sensitivity

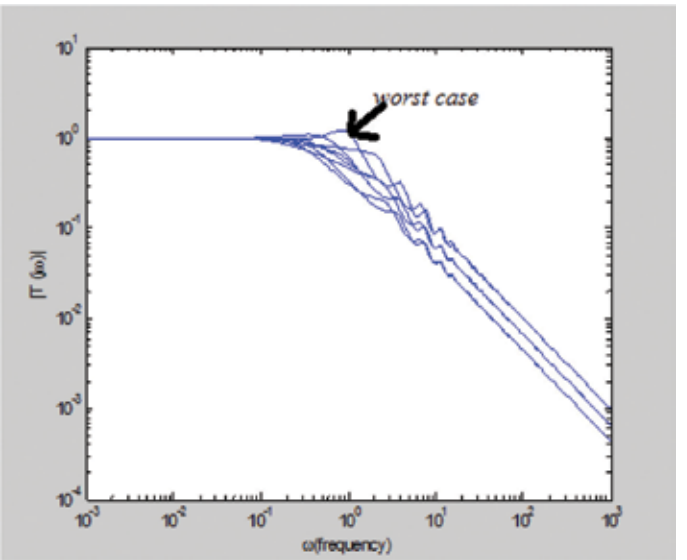

Figure 7. Magnitude of $|T(jw)|$ vs. frequency response (w) to get the worst case.

function which can be seen in the **Figure 7**. When determining the worst case, the filter time constant (τ) value will be set equal to the time delay of no error in the model [7].

The second step is specifying the parameter of set point controller (Gc_1) using complementary sensitivity function of 1DOF-IMC structure, based on the maximum peak stability criterion. By using algorithm of Eq. (10) below:

$$G_{c1} = \frac{1}{k}\frac{\tau_p s + 1}{\lambda_1 s + 1} \tag{10}$$

where k is the gain process, τ is the time constant process, and λ_1 is the filter time constant parameter, the parameter λ_1 is the parameter of set point controller. The filter time constant parameter can be obtained by looping the value of λ_1 (the filter time constant Gc_1) in calculating complementary sensitivity function so that acquired max $|T(j\omega)|$ will be 1.05 in the range of frequency ω equal to 10^{-3}–10^{3}. For the first looping, λ_1 will be set equal to the time delay (θ) of no error in the model divided by 20. Calculation results are displayed in the graphical frequency form which is shown in **Figure 8** [7].

The third step is obtaining parameter of disturbance rejection controller (G_{c2}) using open loop transfer function of 2DOF structure controller based on the gain margin criterion. The disturbance rejection parameter is obtained by looping the value of α in calculating transfer function open loop so that the acquired GM will be 2.4. For the first looping, α is set equal to the filter

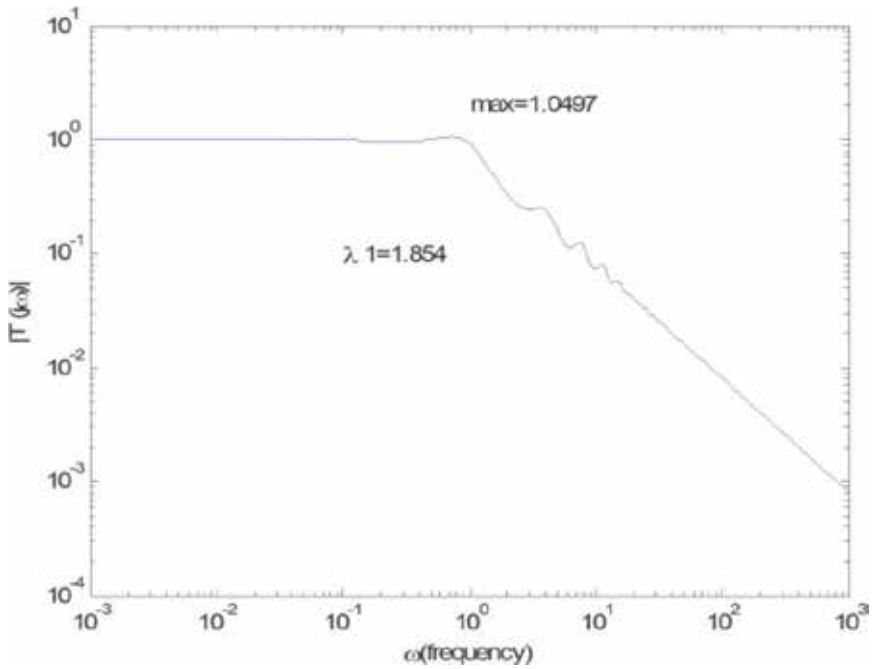

Figure 8. Magnitude of |T(*jw*)| vs. frequency response (*w*) to determine λ_1.

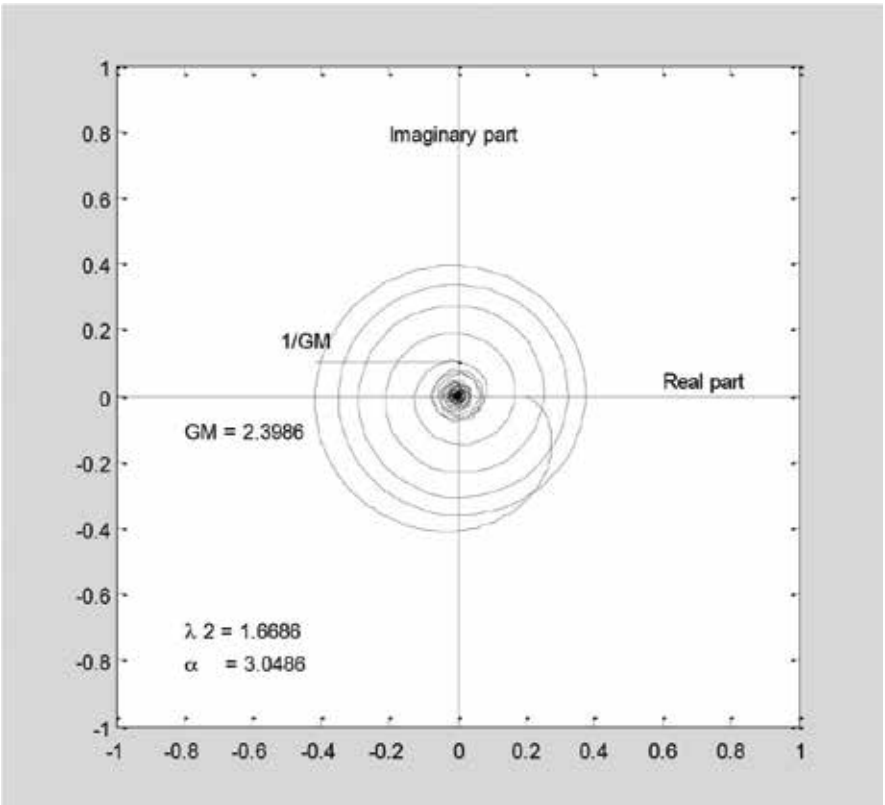

Figure 9. Nyquist plot to determine λ_2 and α.

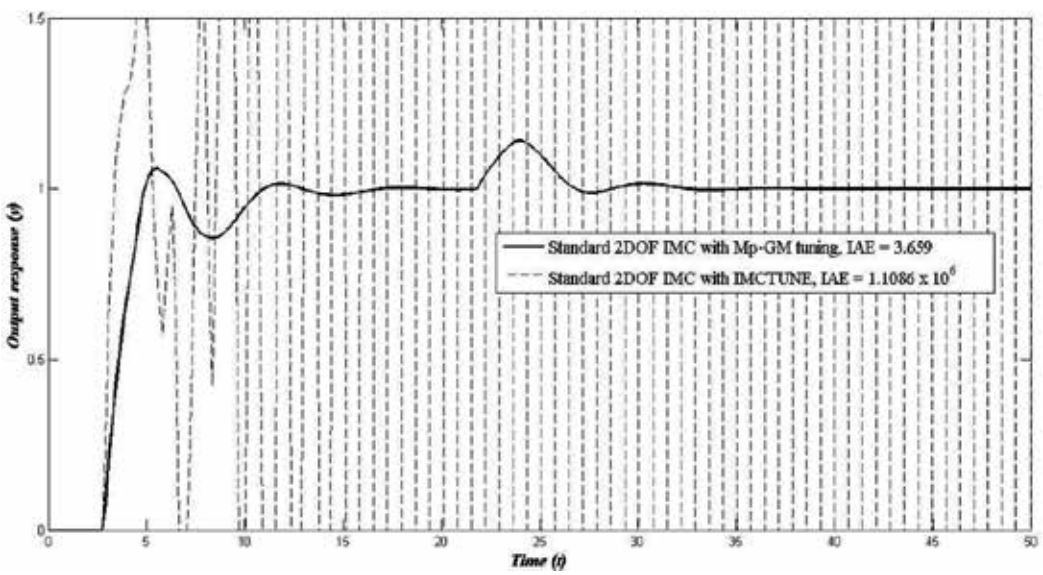

Figure 10. Comparison of responses between Mp-GM and IMCTUNE on 2 DOF-IMC standard.

http://dx.doi.org/10.5772/intechopen.74293

time constant parameter disturbance rejection controller (λ_2) by setting ratio of λ_2 to λ_1 as much as 0.9. This calculation is using Eq. (11) below:

$$G_{c2} = \frac{1}{k}\frac{\tau_p s + 1}{\lambda_1 s + 1}\frac{\alpha s + 1}{\lambda_2 s + 1} \tag{11}$$

where λ_2 and α are the filter time constant parameter and lead parameter at disturbance rejection controller, respectively. The result will be plotted into the Nyquist plot as can be seen in the **Figure 9** [7].

To see the results of Mp-GM tuning, the used IMCTUNE will be required as the comparison. To get parameter controller by IMCTUNE, Mp-tuning software was used [2]. Based on **Figure 10**, it can be seen that this tuning method is able to obtain a good controller parameter when it is even under process uncertainties on standard 2DOF IMC [7].

5. Maximum peak-gain margin tuning method for 2DOF IMC Kaya and 2DOF PID feedback

Four examples of FOPDT cases can be considered to illustrate the use of the Mp-GM tuning method on 2DOF structure control. The examples cover FOPDT cases model with $\frac{\theta}{\tau} < 1$ and $\frac{\theta}{\tau} > 1$ where process time constant or dead time is fixed. The assumption for uncertainty model is the deviation ±20%. As described earlier, the worst case will be determined as the maximum value of the calculation of complementary sensitivity function of 1DOF-IMC controller that was given in Eq. (13), with Eq. (12) as process and model transfer function.

$$G_p = G_{pm} = \frac{ke^{-\theta s}}{\tau s + 1} \tag{12}$$

$$T(j\omega) = \frac{G_{c1}G_p}{1 + G_{c1}\left(G_p - G_{pm}\right)} y_{sp} \tag{13}$$

The first FOPDT case model where the variables are gain and dead time with $\frac{\theta}{\tau} < 1$ is described as below.

$$Gp = \frac{ke^{-\theta s}}{\tau s + 1},\ 0.8 \le k \le 1.2,\ 16 \le \tau \le 24 \ \text{ and } \ 9.6 \le \theta \le 12 \tag{14}$$

$$Gp_m = \frac{e^{-10s}}{20s + 1} \tag{15}$$

$$Gd = \frac{0.5}{2s + 1} \tag{16}$$

By using Mp-GM tuning, it is obtained that the worst case of the plant is the condition with k = 1.2, τ = 16, and θ = 12. The second FOPDT case where the variables are gain and dead time with $\frac{\theta}{\tau} > 1$ is described as below.

$$Gp = \frac{ke^{-\theta s}}{\tau s + 1}, 0.8 \le k \le 1.2, 1.6 \le \tau \le 2.4 \text{ and } 9.6 \le \theta \le 12 \tag{17}$$

$$Gp_m = \frac{e^{-10s}}{2s + 1} \tag{18}$$

where the parameter of the worst case of the plant is the condition with k = 1.2, τ = 2.4, and θ = 12, respectively. The third FOPDT case model where the variables are gain and process time constant with $\frac{\theta}{\tau} < 1$ is described as below.

$$Gp = \frac{ke^{-\theta s}}{\tau s + 1}, 1.6 \le k \le 2.4, 2.4 \le \tau \le 3.6 \text{ and } 1.2 \le \theta \le 1.8 \tag{19}$$

$$Gp_m = \frac{e^{-1.5s}}{3s + 1} \tag{20}$$

The worst case plant is obtained under the condition with k = 2.4, τ = 2.4, and θ = 1.8. The fourth FOPDT case model where the variables are gain and process time constant with $\frac{\theta}{\tau} > 1$ is described as below.

$$Gp = \frac{ke^{-\theta s}}{\tau s + 1}, 1.6 \le k \le 2.4, 2.4 \le \tau \le 3.6 \text{ and } 6.4 \le \theta \le 9.6 \tag{21}$$

$$Gp_m = \frac{e^{-8s}}{3s + 1} \tag{22}$$

The worst case plant is obtained under the condition with k = 2.4, τ = 3.6, and θ = 9.6.

Parameter value of set point tracking (λ_1) of 2DOF-IMC Kaya was also determined by calculation in Eq. (13), so that acquired maximum value of complementary sensitivity function will be 1.05. The implementation of the Mp-GM tuning in 2DOF-PID feedback has been done with the same method as the one of 2DOF-IMC Kaya. Therefore, by using Eq. (23) for approximation of set point tracking, controller form in structure 2DOF-PID feedback was obtained. The value of filter time constant G_{c1} (λ_1) of 2DOF-IMC Kaya was also used to get parameter controller in 2DOF-PID feedback.

$$C_r(s) = \frac{G_{c1}(s)}{1 - G_{pm}G_{c1}(s)} \tag{23}$$

In order to improve the controller's performance, the dead time can be approximated using a first-order Taylor series expansion such as Eq. (24);

$$e^{-\theta s} = 1 - \theta s \tag{24}$$

By substituting Eqs. (10) and (12) into the Eq. (23), Eq. (25) can be obtained. Eq. (25) can be approximated into the proportional integral (PI) controller form as Eq. (26).

$$C_r(s) = \frac{1}{k}\frac{\tau s + 1}{\lambda_1 s + \theta s} \tag{25}$$

$$C_r(s) = k_c\left(1 + \frac{1}{\tau_I s}\right) \tag{26}$$

where:

$$\mathrm{k_c} = \frac{1}{\mathrm{k}}\frac{\tau_\mathrm{p}}{\lambda_1 + \theta}$$

$$\tau_\mathrm{I} = \tau_\mathrm{p}$$

To determine the parameter value of λ_2 and α as parameter disturbance rejection controller in 2DOF-IMC Kaya, the same steps are used. By using Eq. (27), one can obtain parameter disturbance rejection by looping the value of α in calculating transfer function open loop, so that the acquired GM will be 2.4 by setting ratio of λ_2 to λ_1 as much as 0.9.

$$G_{ol} = G_{c2}G_p + G_{c1}\left(G_p - G_{pm}\right) \tag{27}$$

whereas disturbance rejection controller at 2DOF-PID feedback will have same transfer function form with controller that is used in 2DOF-IMC Kaya. The transfer function is given in Eq. (11). As a correction factor, parameter gain of disturbance rejection controller will be multiplied by 0.5 in 2DOF-IMC Kaya and by 0.3 in 2DOF-PID feedback. Parameter values of 2DOF-IMC Kaya and 2DOF-PID feedback are given in **Table 1**.

The implementation of Mp-GM tuning method into 2DOF-PID filter set point and Vilanova structure control has been done with the analogies that of 2DOF-IMC standard, so that one uses Eq. (29) for approximation of set point tracking controller form in structure 2DOF-PID filter set point and Eq. (30) for approximation of set point tracking controller form in structure 2DOF-PID Vilanova. The parameter λ_1 (the filter time constant) was obtained by using Eq. (13) so that acquired maximum value of complementary sensitivity function will be 1.05.

Variation of FOPDT cases that used	**Parameter values of PI for set point tracking controller**		**Parameter values of 2DOF-IMC controller and disturbance rejection in 2DOF-PID feedback controller**		
	$\mathbf{k_c}$	$\boldsymbol{\tau_I}$	$\boldsymbol{\lambda_1}$	$\boldsymbol{\lambda_2}$	$\boldsymbol{\alpha}$
First case	0.7051	20	18.366	16.5294	22.2694
Second case	0.2539	2	14.792	13.3128	16.4128
Third case	0.0807	3	2.776	2.4984	3.3784
Fourth case	0.0759	3	11.772	10.5948	13.0948

Table 1. Parameter values of 2DOF-IMC Kaya and 2DOF-PID feedback.

To get the parameter value of λ_2 and α, one can use Eq. (28) as the open-loop transfer function of 2DOF-IMC standard. By looping the value of α in the calculation of open-loop transfer function, one can get the acquired GM of 2.4 by setting ratio of λ_2 to λ_1 as much as 0.9.

$$G_{ol} = G_{c2}\left(G_p - G_{pm}\right) \tag{28}$$

$$F(s) = \frac{G_{c1}(s)}{G_{c2}(s)} \tag{29}$$

$$C_{sp}(s) = \frac{G_{c1}(s)}{1 - G_{pm}G_{c2}(s)} \tag{30}$$

Substituting Eqs. (10) and (11) into Eq. (29) will give PD controller as set point tracking controller in 2DOF-PID filter set point;

$$F(s) = \frac{\lambda_2 s + 1}{\alpha s + 1} \tag{31}$$

Substituting Eqs. (10) and (12) into Eq. (30), one can obtain Eq. (32). This equation will be used to approximate the function into PID series with derivative filter controller form in Eq. (33) as set point tracking controller in 2DOF-PID Vilanova.

$$C_{sp}(s) = \frac{1}{k}\frac{\lambda_2\tau s^2 + (\lambda_2 + \tau)s + 1}{(\lambda_1\lambda_2 + \alpha\theta)s^2 + (\lambda_1 + \lambda_2 - \alpha + \theta)s} \tag{32}$$

$$C_{sp}(s) = k_C\left(\frac{\tau_I s + 1}{\tau_I s}\right)\left(\frac{\tau_D s + 1}{A\tau_D s + 1}\right) \tag{33}$$

where:

$$\mathrm{k_c} = \frac{0.5 \text{ x } \tau}{\mathrm{k}(\lambda_1 + \lambda_2 + \theta - \alpha)}$$

$$\tau_\mathrm{I} = \tau$$

$$\tau_\mathrm{D} = \lambda_2$$

$$\mathrm{A} = \frac{\lambda_1\lambda_2 + \alpha\theta}{\lambda_2(\lambda_1 + \lambda_2 + \theta - \alpha)}$$

For the disturbance rejection on 2DOF-PID filter set point and Vilanova controller, one can obtain the same controller form like Eqs. (34) and (35).

$$C^{'(s)} = C_{yd}(s) = \frac{G_{c2}(s)}{1 - G_{pm}G_{c2}(s)} \tag{34}$$

$$C'(s) = C_{yd}(s) = \frac{1}{k}\frac{\alpha\tau s^2 + (\alpha + \tau)s + 1}{(\lambda_1\lambda_2 + \alpha\theta)s^2 + (\lambda_1 + \lambda_2 - \alpha + \theta)s} \tag{35}$$

Eq. (35) for disturbance rejection controller will be approximated into PID series with derivative filter form as Eq. (36)

$$C'(s) = k_C\left(\frac{\tau_I s + 1}{\tau_I s}\right)\left(\frac{\tau_D s + 1}{A\tau_D s + 1}\right) \tag{36}$$

where:

$$k_c = \frac{0.5 \text{ x } \tau}{k(\lambda_1 + \lambda_2 + \theta - \alpha)}$$

$$\tau_I = \tau$$

$$\tau_D = \alpha$$

$$A = \frac{\lambda_1\lambda_2 + \alpha\theta}{\alpha(\lambda_1 + \lambda_2 + \theta - \alpha)}$$

The gain parameter controller of PID series with derivative filter that is used on 2DOF-PID filter set point and 2DOF-PID Vilanova will be multiplied with weighting factor equal to 0.5 as factor correction. As a comparison to see performance of Mp-GM tuning, analytical robust tuning (ART) proposed by Vilanova was used [4]. Parameter values of 2DOF-PID filter set point are given in **Table 2** and 2DOF-PID Vilanova is given in **Table 3**.

The response of 2DOF IMC Kaya and 2DOF-PID which had been tuned with Mp-GM in the FOPDT case model with variations of ratio of dead time (θ) and process time constant (τ) for θ fixed is presented in **Figures 11** and **12**, while τ fixed is presented in **Figure 12**. The worst case in FOPDT case with ratio dead time and time constant process lower than 1 was found from the larger (upper limit) steady-state gain process, the larger the (upper limit) time delay, the smaller the (lower limit) process time constant. On the other hand, in FOPDT case with ratio dead time and process time constant more than 1, the worst case was found on the upper limit on all parameters of process model. **Figures 11** and **12** with the control action of 2DOF-IMC Kaya that was tuned by Mp-GM showed that processes with ratio dead time and process time constant more than 1 at fixed dead time gave smaller IAE and faster settling time toward desired set point. On the other hand, processes with ratio less than 1 produce sluggish control

Variation of FOPDT cases that used	**Parameter values of 2DOF-IMC standard**			**Parameter values of PID series with derivative for disturbance rejection controller**			
	λ_1	λ_2	**A**	k_c	τ_I	τ_D	**A**
First case	12.35	11.115	20.295	1.5186	20	20.295	1.2789
Second case	11.365	16.4128	23.7185	0.2539	2	23.7185	1.8922
Third case	1.854	1.6686	3.0486	0.7599	3	3.0486	1.2739
Fourth case	9.543	8.5887	20.1687	0.2516	3	20.1687	2.0231

Table 2. Parameter values of 2DOF-PID filter set point.

Cases	Mp-GM tuning								Parameter values of PI controller using ART method	
	Parameter values of PID series with derivative for set point tracking controller				Parameter values of PID series with derivative for disturbance rejection controller					
	k_c	τ_I	τ_D	A	k_c	τ_I	τ_D	A	k_c	τ_I
1st	1.5186	20	11.115	2.3241	1.5186	20	20.295	1.2728	0.582	19.867
2nd	0.2539	2	10.229	4.3877	0.2539	2	23.719	1.8922	0.116	1.7867
3rd	0.7598	3	1.6686	2.3275	0.7598	3	3.0486	1.2739	0.291	2.98
4th	0.2515	3	8.5887	4.7508	0.2515	3	20.169	2.0231	0.091	2.7055

Table 3. Parameter values of 2DOF-PID Vilanova.

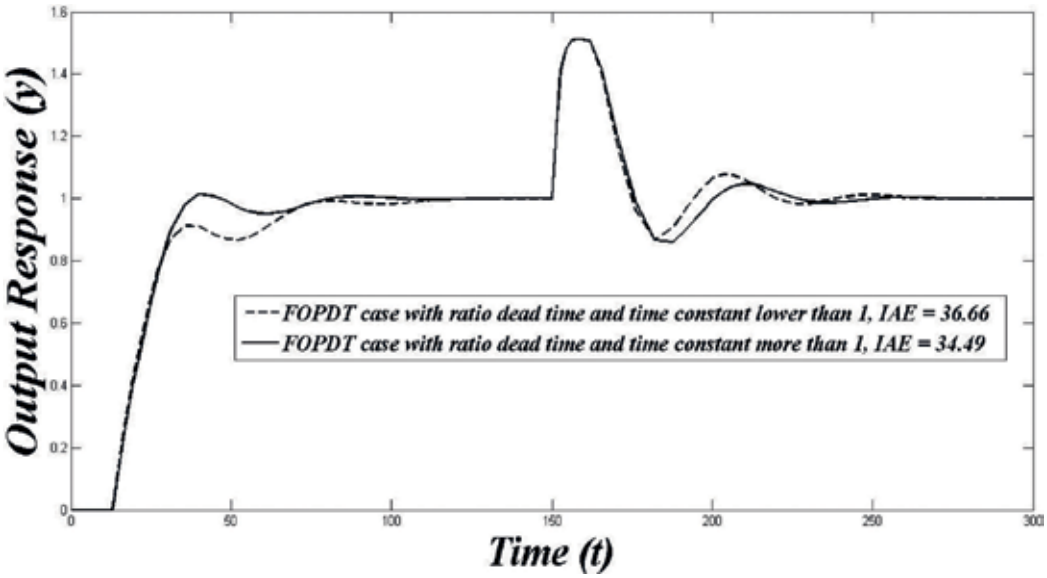

Figure 11. Responses of 2DOF-IMC Kaya with dead time fixed.

action. The reason was that at processes with ratio less than 1, it produced bigger process time constant, so that it gave sluggish control action. While for the case in which process time constant is fixed, then processes with ratio dead time and process time constant greater than 1 produce smaller IAE and faster settling time to reach desired set point. Processes with ratio less than 1 have a smaller dead time so that it can produce faster control action with smaller overshoot. The use of the same transfer function of disturbance rejection cause control action that was produced in 2DOF-PID feedback was almost the same as response that was resulted in 2DOF-IMC Kaya controller.

Using the 2DOF-IMC standard that was tuned by Mp-GM method to be applied for 2DOF-PID filter set point and 2DOF-PID Vilanova causes both of the them to produce somewhat the same response. **Figures 13** and **14** showed that the processes with ratio dead time and process time

http://dx.doi.org/10.5772/intechopen.74293

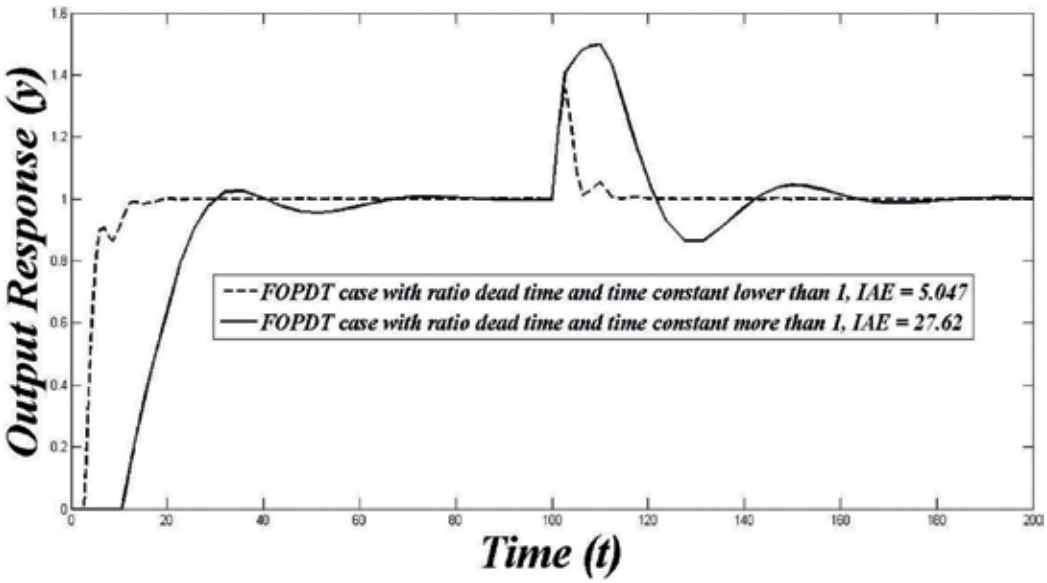

Figure 12. Responses of 2DOF-IMC Kaya with fixed time constant process.

constant more than 1 produce a faster response with smaller IAE and overshoot in either dead time or process time constant is fixed. The output response of 2DOF-PID Vilanova structure which was tuned by Mp-GM tuning and ART method showed that Mp-GM produced control action with smaller overshoot and smoother than ART method even though Mp-GM method gave bigger IAE value with dead time fixed. On the other hand, Mp-GM gives sluggish control action with bigger IAE than ART method in case FOPDT with ratio dead time and process time

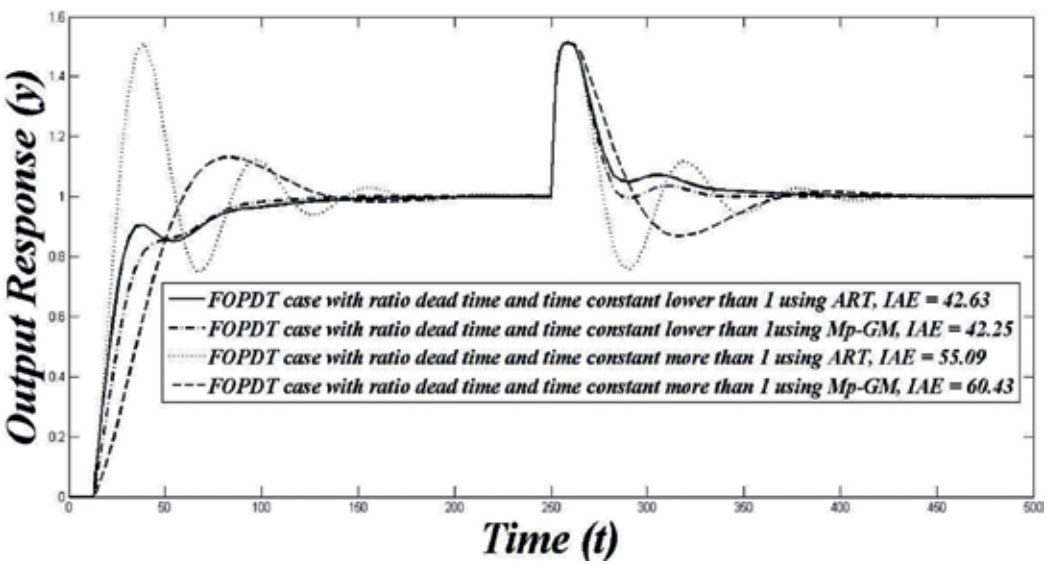

Figure 13. Responses of 2DOF-PID Vilanova with fixed dead time.

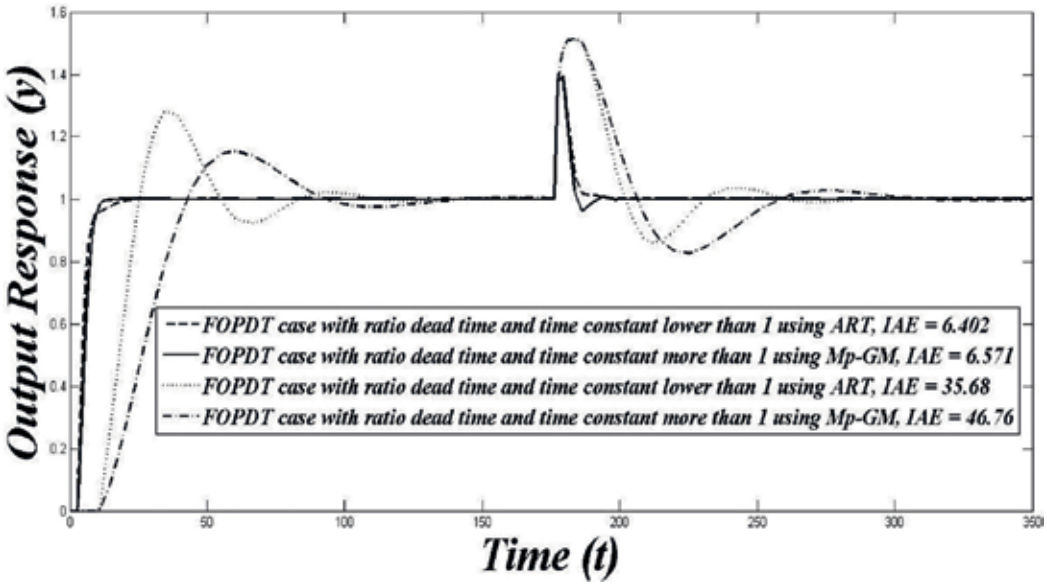

Figure 14. Responses of 2 DOF-PID Vilanova with fixed time constant process.

constant larger than 1 at process time constant fixed. As for the case with ratio less than 1, Mp-GM and ART methods gave somewhat same results. All cases showed that Mp-GM can give same and better response with an easier way than ART method. But in overall, all of the FOPDT cases that are used showed good results for set point tracking and disturbance rejection both on 2DOF-IMC Kaya or all of 2DO-PID controller that used in this research. This can be seen from controller response, which can be returned to its desired condition when there is a change of the set point and the load. The weighting factor which was added as a correction factor at the equation for calculation of parameter gain controller can have faster response, so that it needs less time to reach a desired set point. These results show that Mp-GM tuning method can be implemented in other 2DOF structure controllers.

6. Mp-GM implementation for simulation of temperature control on CSTR reactor using Simulink and HYSYS

In the previous section, the Mp-GM tuning has been proven capable of being implemented on 2DOF controllers to control various processes using Simulink simulation to see the control response. Furthermore, Mp-GM method will also be used for tuning the control of a real process modeling using HYSYS program. The process to be used as a model is the process of hydrolysis of propylene oxide to produce propylene glycol. The hydrolysis reaction is assumed to be of one-order with the expected 50% reaction conversion. Propylene oxide as limiting reactant and water as an excess reactant. This reaction is a type of exothermic reaction, so that a CSTR reactor with coolant is used as a heat absorbing medium generated from the reaction. Design data for the CSTR are provided in **Table 4**.

Based on the derivation of the equation, one can obtain the function transfer equation in the form of second-order Laplace transform for the influence of the feed temperature to the reaction temperature as in Eq. (37)

$$G_p = \frac{1,4582s + 12,249}{s^2 + 3,1937s + 13,1413} \tag{37}$$

To facilitate the implementation of the Mp-GM tuning method, the second-order function transfer equation is approximated by the Skogestad's "Half rule"

$$G_p = \frac{e^{-0,12s}}{0,082s^2 + 0,261s + 1,0728} \tag{38}$$

Furthermore, to obtain the first-order function transfer form, Eq. (38) is then approximated by Panda method so that the Eq. (39)

$$G_p = \frac{0,932e^{-0,202s}}{0,243s + 1} \tag{39}$$

The inconsistency parameter is assumed to be ±20% of the transfer of the process model function in Eq. (39) as $0.7456 \le k_c \le 1.1184$; $0.1616 \le \tau \le 0.2424$ dan $0.1944 \le \theta \le 0.2916$.

	Input	Output		
		Manual	Simulation	Error (%)
The concentration of propylene oxide (lbmol/ft^3)	0.132	0.066	0.06587	0.002
The concentration of propylene glycol (lbmol/ft^3)	—	0.066	0.06613	0.002
Temperature (°F)	60	102.64	102.64	—
Pressure (psia)	16.17	16.17	16.17	—
Energy *Coolant* (Btu/hr)	-7.837×10^5			—

Table 4. The simulation data of input and output of CSTR reactor on propylene oxide hydrolysis process to produce propylene glycol.

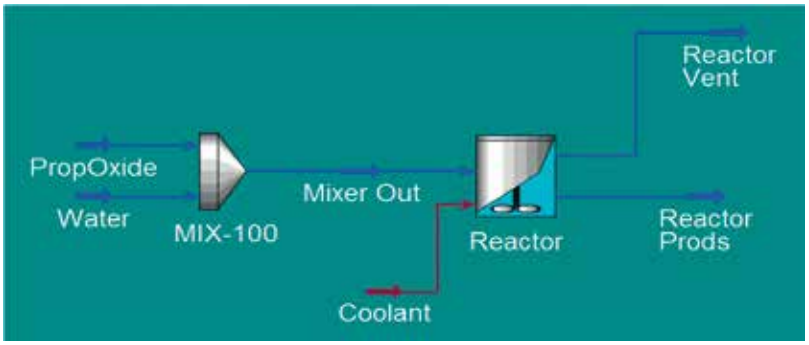

Figure 15. Steady-state simulation of propylene oxide hydrolysis process to produce propylene glycol using CSTR reactor with HYSYS.

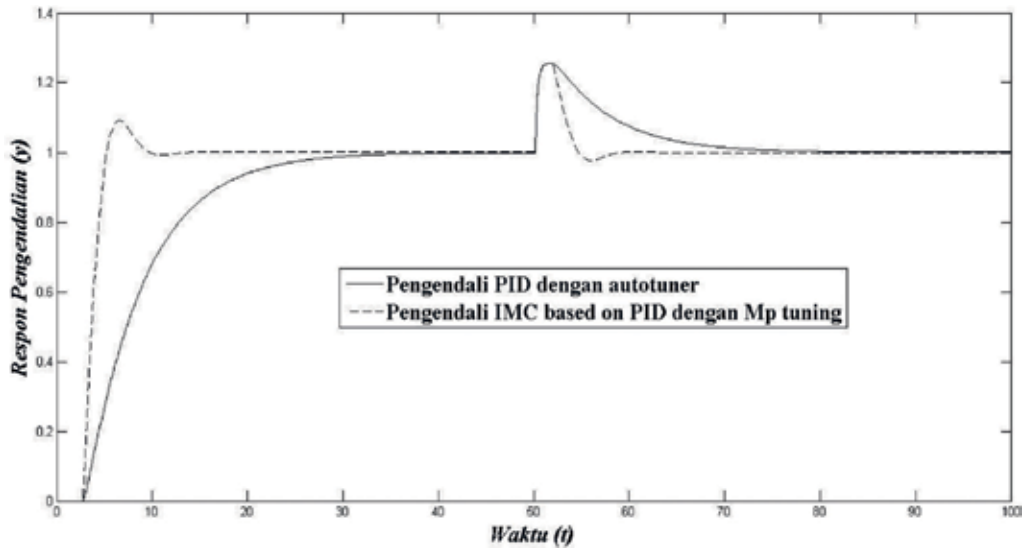

Figure 16. Comparison of temperature control responses in the process of hydrolysis of propylene oxide with CSTR reactor with disturbance +20% change in feed temperature simulation Simulink.

Based on transfer function of process, the value of process model parameters, respectively, for kp, τp, and θ is 3.22, 0.97, and 0.15 was obtained. The parameter values for the worst case process are each of 3.864, 0.776, and 0.18.

Based on the simulation using Simulink and HYSYS software, the control result profile for disturbance change +20% from the propylene oxide feed temperature is given in **Figures 16** and **17**. **Figures 16** and **17** show that the resulting control profile gives almost the same result. From simulation using Simulink and HYSYS, it is shown that the use of Mp-GM tuning gives faster control response to achieve stability with smaller IAE compared with autotuner method.

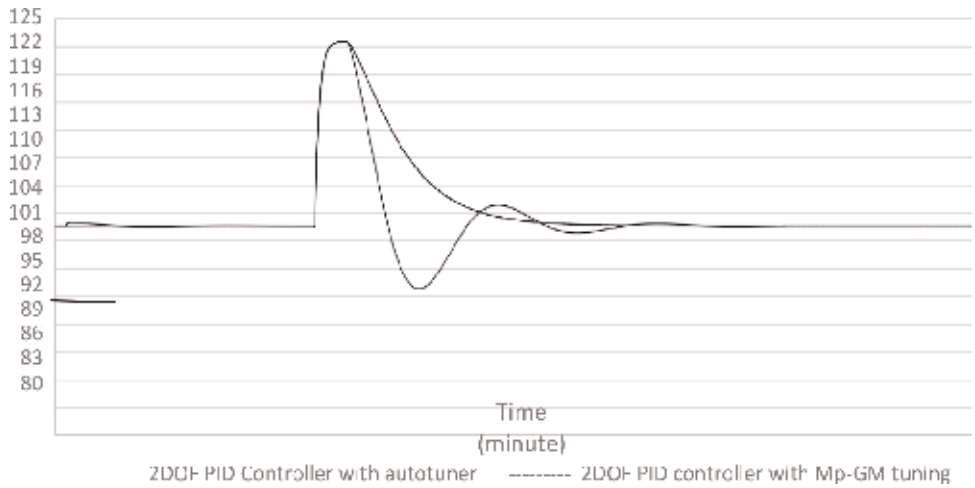

Figure 17. Comparison of temperature control responses in the process of hydrolysis of propylene oxide with CSTR reactor with disturbance +20% change in feed temperature simulation HYSYS.

Based on the calculation with Simpson rule method 1/3 obtained IAE value for 2DoF PID controller with autotuner and 2DoF PID controller with a Mp-GM tuning of 1221.721 and 528.3267. Similar results were obtained from the control response profile with disturbance −20% of the propylene oxide feed temperature as given in **Figures 16** and **17**. The control response with 2DOF PID controller with Mp-GM tuning gives better results when viewed from the control response profile or the resulting IAE value. Where based on Simpson rule method 1/3 obtained IAE value for 2DoF PID controller with autotuner and Mp-GM tuning is equal to 924.2412.

7. Conclusion

A maximum peak-gain margin (Mp-GM) tuning method has been used for 2DOF-IMC Kaya and 2DOF-PID. The simulation results show that the maximum peak gain margin tuning method can give a good target set point tracking, disturbance rejection, and robustness in system 2DOF structure controller with a little addition step. All of the process of FOPDT with different ratio of dead time and process time constant showed good responses. Mp-GM tuning is able to give better response than analytical robust tuning (ART) at the 2DOF-PID Vilanova structure control. The implementations of Mp-GM tuning on another model controller like 2DOF-IMC Kaya follow the similar steps by adding a correction factor of 0.5 multiplied by transfer function disturbance rejection. The implementations of Mp-GM tuning on another 2DOF-PID consist of three ways:

1. Determining the worst case as maximum value of complementary sensitivity function of 1DOF-IMC controller.
2. Determining parameter λ_1 by looping λ_1 in calculating Eq. (13) so that acquired maximum value of complementary sensitivity function will be 1.05 (for first looping, λ_1 will be set equal to θ), while for parameter λ_2 and α will be obtained by looping the value of α in calculating Eq. (27) for 2DOF-PID feedback and Eq. (28) for 2DOF-PID filter set point and Vilanova so that the acquired GM will be 2.4 by setting ratio of λ_2 to λ_1 as much as 0.9.
3. Substituting the value of k, τ, θ, λ_1, λ_2, and α into the previous equations that have been derived to obtain parameter value of PID controller (k_c, τ_I, $\tau_{D,}$ A) that will be used in 2DOF-PID controller.

Author details

Juwari Purwo Sutikno[1]*, Nur Hidayah[2] and Renanto Handogo[1]

*Address all correspondence to: juwari@chem-eng.its.ac.id and joecheits@yahoo.com

1 Department of Chemical Engineering, Institut Teknologi Sepuluh Nopember, Surabaya, Indonesia

2 Department of Industrial Engineering, Sari Mulia University, Banjarmasin, Indonesia

References

[1] Mazzini HM, Santos DFG. Two degree of freedom PID control for integrating process. In: XVIII Congreso Brasilleiro Automatica/12 a 16 Setembro; Bonito-MS, Brasil; 2010

[2] Morari M, Zafiriou E. Robust Process Control. Englewood Cliffs, NJ: Prentice – Hall; 1989. Books

[3] Stryczek K, Laiseca M, Brosilow C, Leitman MG. Tuning and design of single-input, single-output control systems for parametric uncertainty. AICHE Journal. 2000;**46**(8):1616-1631

[4] Tham Ming T. Part of a Set of Lecture Notes on Introduction to Robust Control. Chemical and Process Engineering University of Newcastle Upon Tyne; 2002. Manual in pdf. https://pdfs.semanticscholar.org/9642/e32f84e5e0697f5c2ebc3ad9b86474b24e17.pdf?_ga=2.89823387.1035637983.1531365135-1361555406.1531365135

[5] Seborg DE, Edgar TF, Mellicamp DA. Process Dynamic and Control. 2nd ed. New Jersey: John Wiley & Sons, Inc.; 2004. Books

[6] Araki M, Taguchi H. Two degree of freedom PID controller. International Journal of Control, Automation and Systems. 2003;**1**(4):401-411

[7] Juwari AA, Badhrulhisham CS, Yee MR. A new tuning method for two-degree-of-freedom internal model control under parametric uncertainty. Process systems engineering and process safety. Chinese Journal of Chemical Engineering. 2013;**21**(9):1030-1037

[8] Vilanova R, Alvaro VM, Arrieta O. Analytical robust tuning approach for two degree of freedom. Engineering Letters. 2011;**19**(3):EL_19_3_08

[9] Kaya I. Two-degree-of-freedom IMC structure and controller design for integrating processes based on gain and phase-margin specifications. IEEE Proceedings-Control Theory and Applications. 2004;**151**(4):481-487

[10] Liu T, Gao F. Enhanced IMC-based load disturbance rejection design for integrating processes with slow dynamics. In: Proceedings of the 9th International Symposium on Dynamics and Control of Process Systems; Lueven Belgium; 2010

[11] Marlin TE. Process control: Designing processes and control systems for dynamic performance. In: Chemical Engineering Series. 2nd ed. Boston: McGrawHill; 2000. Books

[12] Viteckova M, Vitecer A. Two degree of freedom controller tuning for integral plus time delays plants. ICIC Express Letters. 2008;**2**(3):225-229

[13] Zhang J, Wang J, Zhao Z. A novel two degree of freedom PID controller for integrator and dead time process. In: Proceedings of the 6th World Congress on Intelligent Control and Automation; Dalian, China. 2006

[14] Brosilow C, Joseph B. Techniques of model-based control. In: Prentice Hall International Series in the Physical and Chemical Engineering Science. New Jersey: Prentice Hall PTR; 2001. Books

Chapter 3

Optimum PI/PID Controllers Tuning via an Evolutionary Algorithm

Jorge-Humberto Urrea-Quintero,
Jesús-Antonio Hernández-Riveros and
Nicolás Muñoz-Galeano

Additional information is available at the end of the chapter

http://dx.doi.org/10.5772/intechopen.74297

Abstract

In this chapter, it is demonstrated that when using advanced evolutionary algorithms, whatever the adopted system model (SOSPD, nonminimum phase, oscillatory or nonlinear), it is possible to find optimal parameters for PID controllers satisfying simultaneously the behavior of the system and a performance index such as absolute integral error (IAE). The Multidynamics Algorithm for Global Optimization (MAGO) is used to solve the control problem with PID controllers. MAGO is an evolutionary algorithm without parameters, with statistical operators, and for the optimization, it does not need the derivatives, what makes it very effective for complex engineering problems. A selection of some representative benchmark systems is carried out, and the respectively two-degree-of-freedom (2DoF) PID controllers are tuned. A power electronic converter is adopted as a case study and based on its nonlinear dynamical model, a PI controller is tuned. In all cases, the control problem is formulated as a constrained optimization problem and solved using MAGO. The results found are outstanding.

Keywords: evolutionary algorithms, PID controller, nonlinear model, MAGO, 2DoF PID-based controllers, SOSPD model, control benchmark, power electronic converters

1. Introduction

It is well known that most of 90% of the closed-loop implemented strategies are PI or PID controllers [1]. Since its introduction in 1940, researchers' interest has been focused on the development on simplistic but effective tuning rules for PID controllers [2]. For any industrial plant without resonant characteristics, a SOSPD model can represent the dominant dynamics

and that a suitable PID tuning can be achieved [3]. Moreover, Åström and Hägglund proposed a collection of systems models with various difficulties of control that are suitable for testing PID controllers. Those models illustrate systems with various difficulties of control. Nevertheless, SOSPD representation is limited, and a wide range of process dynamics can be found, for example, process with a non-minimum phase behavior or oscillations. Therefore, PID control traditional tuning is not well suited for most of the complex problems. The trend remains in the so-called two degree-of-freedom (2DoF) PID controllers [4]. The 2DoF PID control structure has two components: one to tune the controller considering the regulatory closed-loop mode performance and robustness and the second one to improve the servo-control behavior. 2DoF PID tuning could be also based on a system transfer function. A 2DoF PID control structure is the option to achieve simultaneously a good system performance as both regulator and servomechanism modes what is a challenge of control requirements for a traditional PID controller.

Evolutionary algorithms (EA) have been proved to be an effective tool to optimal PID controllers tuning [5]. In general, EA is considered as an optimal algorithm that is able to deal with ill-defined problem domain such as multimodality, discontinuity, time variance, randomness and noise [6]. MAGO as EA does not work with genetic operators. MAGO operators are inspired in numerical derivation applying the Nelder-Mead method, the estimation distribution of the actual population and a statistical quality control technique. Additionally, MAGO has only two tunable parameters: the population size and the number of generations. These two parameters could be removed, but they remain because in real situations they help to understand the context of the problem. Particularly, MAGO has been successfully tested for the tuning of PID controllers based on SOSPD models [7]. MAGO has been used in various fields of engineering [8], LQR tuning [9–11], drivers in tuning PID controllers [12, 13], showing successful solutions in each case applied.

Despite a lot of works in PID controllers tuning, a general concern remains because real processes have multiple operational constraints, and some exhibit high nonlinear dynamics that cannot successfully be captured by transfer functions. This chapter shows that advanced evolutionary algorithms are suitable to solve the control problem with PID controllers when the control system is formulated as an optimization problem. The evolutionary algorithm MAGO is used to solve the control problem with traditional PI and with 2DoF PID controllers. MAGO is an evolutionary algorithm without parameters; it is based on statistical operators and does not need the derivatives of the nonlinear optimization problems. Furthermore, this chapter demonstrates that whatever system model is adopted (SOSPD, non-minimum phase, oscillatory or nonlinear), it is possible to find optimal parameters for PID controllers satisfying the system behavior and a performance index such as absolute integral error (IAE). This chapter is divided into four sections as follows: in Section 2, the general problem statement of PID controllers tuning is introduced and formulated as an optimization problem. In Section 3, the (EA) MAGO is presented and the evolutionary design procedure of a PID controller is established. In Section 4, a selection of some representative benchmark systems from [5] is carried out, and the respectively 2DoF PID controllers are tuned. In Section 5, a power electronic converter (DC-DC buck converter) is adopted as a case study, and based on its nonlinear

http://dx.doi.org/10.5772/intechopen.74297

dynamical model, a PI controller is tuned by MAGO. PI-MAGO controller performance is tested, and a comparison is carried out against a PID controller tuned by the pole placement method. In all cases, the control problem is formulated as a constrained optimization problem and solved using MAGO.

2. Problem statement

2.1. Control system representation

Consider a single-input single-output (SISO) control system depicted in **Figure 1**. In this system, $r(t)$ is the set-point, $u(t)$ is the controller output signal, $d(t)$ is the load-disturbance, and $y(t)$ is the controller process variable.

The system output $y(t)$ simultaneously depends on $r(t)$ and $d(t)$. Two operation modes should be taken into account for the controller design, one as a servomechanism and the other as a regulator. In the first case, the control objective is to track the set-point $r(t)$. In the second case, the control objective is to reject a change in $d(t)$ while $y(t)$ is keeping as close as possible to $r(t)$. However, it is not always possible to specify distinctly performance criteria for both operation modes. Furthermore, a trade-off between servo-regulator modes must be specified as in the traditional PID controller tuning case.

The general form to represent a dynamical system is given by Eqs. (1) and (2), where x is the system state and $\dot{x}$ is the time derivative of the system state; $y(t)$ is the system output and functions g and h are nonlinear and represent the dynamical system evolution.

$$\dot{x}(t) = g(x, u, d) \tag{1}$$

$$y(t) = h(x, u, d) \tag{2}$$

Through Taylor linearization, it is possible to obtain a linear representation of Eqs. (1) and (2) given by Eqs. (3) and (4). Where $A \in \mathcal{R}^{nxn}$ is the system Jacobian, $B \in \mathcal{R}^{nxm}$ is an input matrix, $C \in \mathcal{R}^{kxn}$ is an output matrix and $D \in \mathcal{R}^{kxm}$ is a direct transmission matrix.

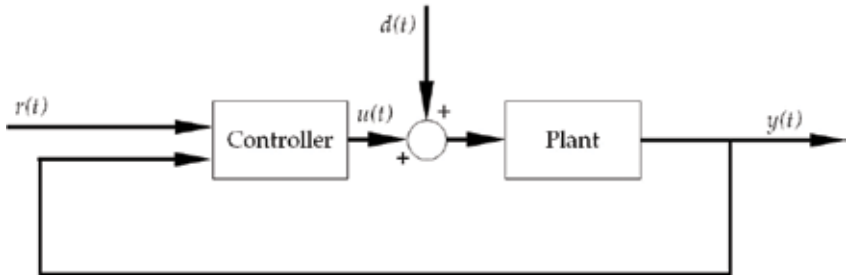

Figure 1. Single-input single-output (SISO) feedback control system.

$$\dot{x} = Ax + Bu \tag{3}$$

$$y = Cx + Du \tag{4}$$

Eqs. (3) and (4) are usually employed in control theory for designing multi-input multi-output (MIMO) control structures. However, transfer functions are a better approximation for designing SISO control structures. The realization given by Eq. (5) is obtained by applying the Laplace transform to Eqs. (3) and (4).

$$G(s) = C\left[\frac{adj(sI - A)^T}{\det(sI - A)}\right]B + D \tag{5}$$

On the other hand, the control policy of an ideal PID controller is expressed by Eq. (6). Where, $e(t) = r(t) - y(t)$, K_p is the proportional gain, T_i is the integral time constant and T_d is the derivative time constant.

$$u(t) = K_p\left\{e(t) + \frac{1}{T_i}\int_0^t e(\tau)d\tau + T_d\frac{de(t)}{dt}\right\} \tag{6}$$

PID frequency domain representation is given by Eq. (7).

$$C(s) = K_p\left(1 + \frac{1}{T_i s} + T_d s\right) \tag{7}$$

The closed-loop transfer function form for the system represented in **Figure 1** considering a PID controller is given by Eq. (8).

$$Y(s) = \frac{C(s)G(s)}{1 + C(s)G(s)}R(s) + \frac{G(s)}{1 + C(s)G(s)}D(s) \tag{8}$$

If the system operates in the servomechanism mode, that is when disturbances are not considered, the output signal can be represented as in Eq. (9).

$$Y_{sp}(s) = \frac{C(s)G(s)}{1 + C(s)G(s)}R(s) \tag{9}$$

If the system operates in the regulation mode, that is when the signal reference is not considered, the output signal can be represented as in Eq. (10).

$$Y_{ld}(s) = \frac{G(s)}{1 + C(s)G(s)}D(s) \tag{10}$$

From Eqs. (9) and (10), both control objectives cannot be optimally achieved because the controller parameters simultaneously affect the servo and regulatory operation modes. At most, a tuning PID controller process can be carried out by establishing a servo-regulatory trade-off to obtain a closed-loop performance that is not optimum for neither servo nor regulatory operation modes, but it has an acceptable performance in both cases.

Controllers of the form given by either Eqs. (6) or (7) are known as one degree of freedom (1DoF) PID controllers. Two degree of freedom (2DoF) PID controllers are an alternative to overcome the 1DoF PID controller operation limitations. The control policy for a 2DoF PID controller is given by Eqs. (11) or (12). Considering the proportional, integral and derivative error, respectively in Eqs. (13), (14) and (15), where K_p is the proportional gain, T_i is the integral time constant and T_d is the derivative time constant, β and γ are the set-point weights. In **Figure 2**, the 2DoF PID controller block diagram is depicted.

$$u(t) = K_p\left\{e_p(t) + \frac{1}{T_i}\int_0^t e_i(\varepsilon)d\varepsilon + T_d\frac{de_d}{dt}\right\} \tag{11}$$

$$C_{2DoF}(s) = K_p\left\{e_p(s) + \frac{1}{T_i s}e_i(s) + T_d e_d(s)\right\} \tag{12}$$

with

$$e_p(s) = \beta R(\mathrm{s}) - \mathrm{Y(s)} \tag{13}$$

$$e_i(s) = R(s) - Y(s) \tag{14}$$

$$e_d(s) = \gamma R(s) - Y(s) \tag{15}$$

The parameter γ is more frequently applied as a derivative mode switch (0 or 1) for $R(s)$. γ is normally set to zero to avoid an extreme instantaneous change in the controller output when a set-point step change occurs. In consequence, Eq. (12) can be arranged as in Eq. (16).

$$C_{2DoF}(s) = K_p\left(\beta + \frac{1}{T_i s}\right)R(S) - K_p\left(1 + \frac{1}{T_i s} + T_d s\right)Y(s) \tag{16}$$

A compact form of Eq. (16) consistent with **Figure 2** is given by Eq. (17). Where $C_r(s)$, is the set-point controller transfer function and $C_y(s)$ is the feedback controller transfer function.

$$C_{2DoF}(s) = C_r(s)R(s) - C_y(s)Y(s) \tag{17}$$

The closed-loop transfer function form for the system represented in **Figure 2** considering a 2DoF PID controller is given by Eq. (18). Where $M_{yr}(s)$ is the transfer function from the set

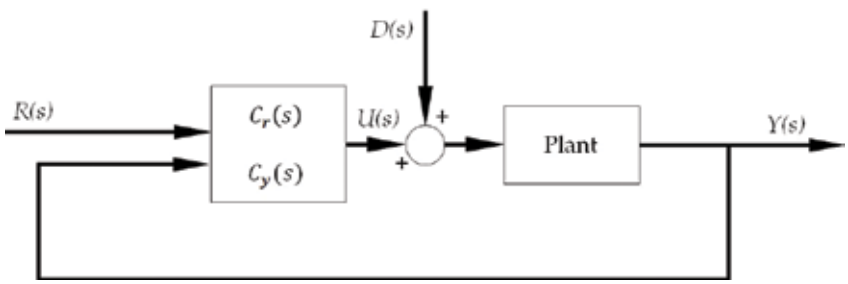

Figure 2. 2DoF closed-loop block diagram.

point to the controlled output (servo-control closed-loop), and $M_{yd}(s)$ is the transfer function from load-disturbance to the controller output (regulatory control closed-loop).

$$Y(s) = M_{yr}(s)R(s) + M_{yd}D(s) \tag{18}$$

With

$$M_{yr}(s) = \frac{C_r(s)G(s)}{1 + C_y(s)G(s)} \tag{19}$$

$$\mathrm{M_{yd}} = \frac{\mathrm{G(s)}}{1 + \mathrm{C_y(s)G(s)}} \tag{20}$$

From Eqs. (19) and (20), both control objectives can be achieved separately because of the possibility of tuning two different controllers, one for each operation mode.

2.2. Optimum control problem formulation

The usual criterion for tuning a controller is directly related to the desired closed-loop system response. Integral performance indexes allow quantifying the closed-loop system performance due to a unit step load disturbance. Most common employed indexes are integral of absolute error (IAE) (see Eq. (21)) and integral of absolute control action $u(t)$ (IAU) (see Eq. (22)).

$$IAE = \int_0^\infty |e(t)|dt \tag{21}$$

$$IAU = \int_0^\infty |e_u(t)|dt \tag{22}$$

For the PID case, $e(t)$ and $e_u(t)$, Eqs. (21) and (22), respectively, can be calculated as $e(t) = r(t) - y(t, \theta)$ and $e_u(t) = u_0 - u(t, \theta)$, where u_0 is the initial condition $\theta = \begin{bmatrix} K_p & T_i & T_d \end{bmatrix}$.

The load disturbance may enter at many different places, and extreme cases occur when it enters at the process input or output. However, when a feedback error appears, integral performance indexes evaluate the controller performance indistinctly, whereas load disturbance appears [14]. The abovementioned fact is the main motivation to adopt integral performance indexes.

The integrated error for a unit step disturbance at the process input is the inverse of the controller integral gain, $IE = 1/k_i$. For a unit step output disturbance, it is instead, $IE = 1/Kk_i$, where K is the static gain of the process. When the closed-loop system is well-damped, $IE \approx IAE$ are approximately the same [1]. The criteria IE and IAE are widely employed to measure controllers performance. IAE and IAU performance indexes are initially adopted in this work because of its interpretability from the PID controller parameters, but other criteria could also been used.

http://dx.doi.org/10.5772/intechopen.74297

The controller tuning process that minimizes an integral performance index can be seen as an optimization problem where the ultimate goal is to find a controller parameters combination such that the value of an Integral Performance Index is minimized.

For the 1DoF PID controller, the optimal tuning problem consists of minimizing the objective function given by Eq. (23), where the minimum is the result of obtaining a suitable combination of the 1DoF PID parameters $\theta = \begin{bmatrix} K_p & T_i & T_d \end{bmatrix}$.

$$\text{Min}_\theta \left\{ J_{IAE} = \sum_{t_k}^{t_{kf}} |e(t_k)| \right\} \tag{23}$$

Subject to a process model (see Eqs. (1)–(5)), a control action (see Eq. 6) and

$$K_{p_{min}} \leq K_p \leq K_{p_{max}}$$

$$T_{i_{min}} \leq T_i \leq T_{i_{max}}$$

$$T_{d_{min}} \leq T_d \leq T_{d_{max}}$$

Similarly, for the 2DoF PID controller, the optimal problem consists of minimizing the objective function given by Eq. (24), where the minimum is the result of obtaining a suitable combination of the 2DoF PID parameters $\theta = \begin{bmatrix} K_p & T_i & T_d & \beta \end{bmatrix}$.

$$\text{Min}_\theta \left\{ J_{IAE+IAU} = \sum_{t_k}^{t_{kf}} |e(t_k)| + \sum_{t_k}^{t_{kf}} |e_u(t_k)| \right\} \tag{24}$$

Subject to a process model (see Eqs. (1)–(5)), a control action (see Eq. 11) and

$$K_{p_{min}} \leq K_p \leq K_{p_{max}}$$

$$T_{i_{min}} \leq T_i \leq T_{i_{max}}$$

$$T_{d_{min}} \leq T_d \leq T_{d_{max}}$$

$$\beta_{min} \leq \beta \leq \beta_{max}$$

3. Tuning of PID controllers using an evolutionary algorithm

From the observation of living beings, we can see that these reproduce, adapt, and evolve in relation to the environment where they develop. Some of the characteristics acquired during life may be inheritable by the next generation. The synthetic theory of evolution has been able to explain these processes and biological variations in detail [15]. This theory bases on genes as units of inheritance transfer, that is, functional units of basic information for the development of an organism. The genetic material of an individual is in its genotype. The genotype consists of an organization of hierarchical structures of genes. The complex information contained in

the genotype is expressed in the phenotype, that is, the visible characteristics and functionality of individuals. In the evolutionary process, the occurrence of small variations in the phenotypes, apparently random and without a clear purpose, is recognized. Such variations which are usually called mutations prove their efficacy in the light of the environment and prevail through the selection of the individual, or otherwise they disappear. The natural needing to produce offspring motivates the selection of individuals. Because of a severe competition for reproduction, which only the fittest individuals achieve, it is assumed that the offspring overcome their parents by inheriting their mixed characteristics. When resources in the environment become insufficient, only the fittest individuals will have a better chance of survival and reproduce. The selective pressure on individuals of a species makes them continually improve with respect to its environment. Evolutionary algorithms (EA) emulate the synthetic theory of evolution.

As natural evolution, an EA begins with an initial set of potential solutions to a specific problem. This set can be composed at random in a delimited searching space or using information of the problem. EA include operators that select and create new individuals. Crossover operator exchange of genetic material among "parents" to generate new "sons," and the mutation operator makes small variations. The new set of possible solutions is evaluated using a "fitness" function. When evaluating, the fittest are favored, leaving them as new "parents." The process is cyclically repeated to find the best solution to the problem in a delimited searching space.

EA encompass different approaches that transfer the behavior of adaptation and evolution of species, giving rise to several methods. Among the most popular approaches are genetic algorithms, genetic programming, evolutionary strategies, and evolutionary programming. Nowadays, EA are not only based in the biological evolution, rather EA are identified as algorithms that search iteratively for a solution through a population in evolution. Some of the main reasons for new optimization heuristics are the need to identify the interrelationships between the variables used to represent individuals according to the coding applied and the need to reduce the own parameters of the classical EA. New EA use operators different to the genetic ones. Some of those algorithms are differential evolution, estimation of distribution algorithms, and the multidynamics algorithm for global optimization.

Differential evolution at first glance is not based on any natural process. The proportional difference of two randomly chosen individuals from the population is added to a third individual, also randomly chosen. From this differential mutation, a fourth individual appears. This individual is compared against its parent, the third one. The best of them is selected to the next generation. The process is repeated until a stop criterion [16].

Estimation of distribution algorithms also bases their search on populations that evolve. The new population is recreated in each generation from the probability distribution obtained from the best individuals of the previous generation. The interrelationships between the variables are expressed explicitly through that distribution. There are no crossing or mutation operators. The process is repeated until a stop criterion [17].

In MAGO, a differential crossover is applied between the target individual and its mutant coming from a numerical derivation. A tournament chooses the best of them. The interrelationships

http://dx.doi.org/10.5772/intechopen.74297

among the variables are explicit through a distribution of the population in each generation. The new population is sampled from a set composed of the best individuals until now, the historical trend and other individuals completely new. Next, this algorithm is explained in detail.

3.1. Multidynamics algorithm for global optimization

EA emulates the mechanisms of natural selection and genetic inheritance inspiring from the Neo-Darwinian theory of biological evolution. EA have evolved themselves to treat with artificial evolution processes. MAGO is a good example of this evolution. MAGO does not work with genetic operators [18]. MAGO starts with a random initial population on a search space bounded by the problem. To guarantee diversity and increase the exploitation of the search space, MAGO creates new individuals by means of three different subgroups of the population simultaneously. Each group has its own dynamics: a normal distribution over the searching space, a conservation mechanism of the best individual, and a strategy for maintaining diversity [19]. Because introducing statistics operators, MAGO provides a strong way to demonstrate the evolution. The mutation based on numerical derivation, generalizes the searching space where MAGO can acts. MAGO takes advantage of the concept of control limits [20] to produce individuals on each generation simultaneously from the three different subgroups. The size of the population is fixed, but the cardinality of each subgroup changes in each generation according to the first, second and third deviation of the actual population, respectively. The exploration is performed creating new individuals from these three subpopulations, individuals that are governed by any of their dynamics, the exploration is performed. For the exploitation, MAGO, looking for the goal, uses a greedy criterion in the first subset.

MAGO is evolutionary in the sense that works with a population of possible solutions randomly distributed throughout the searching space approaching iteratively to the final solution. MAGO is autonomous in the sense that it regulates its own behavior and does not need human intervention. Unlike other EA, MAGO has only two parameters: the population size and the number of generations. These two parameters could be removed, but they remain because in real situations they help to understand the context of the problem.

In each generation, MAGO divides the population into three subgroups. To know how many individuals will belong to each subgroup, the actual entire population is observed as having a normal distribution. The average location, the first, second and third dispersion of the whole population are calculated to form the three groups. To each subgroup is assigned many individuals as the cardinality of each different level of standard deviation. Each group has its own evolution. The cardinality of these subgroups changes autonomously in each generation.

The subgroup named Emerging Dynamics (G_1) creates a subpopulation of individuals around the individual with better characteristics; this group is the evolutionary elite of each generation, that is, the fittest individuals contributing with their genes to the next generation. The Crowd Dynamics (G_2) creates a group of individuals but around the current population mean, configuring the historical trend. This dynamic is applied to the largest portion of the population, and it is always close to the emerging dynamics, but never close enough to be confounded. These two dynamics could be merged within a same territory only until there are

sufficient and necessary conditions to ensure a full exploration of the searching space, usually at the end of the evolutionary process. The Accidental Dynamics (G_3) is a small group created by quantum speciation. It is established in isolation from individuals of the other two dynamics generation after generation. This portion of the population is always formed spontaneously and contains entirely new individuals. MAGO uses the covariance matrix of the population of each generation to establish a distribution of exploration. With the Accidental Dynamics, the main diagonal of the covariance matrix is different from zero, ensuring numerical stability of the evolutionary process. Because in each generation, the population is treated for its division by a normal distribution for its division according to the first, second, and third deviation, the subgroups G_1, G_2, and G_3 not interbreed.

Emerging Dynamics: This subset is created with the N1 fittest individuals in each generation. The N1 fittest individuals within the first standard deviation of the average location of the current population of individuals move in a line toward the best one of the entire population, in a kind of mutation that incorporate information from the best of all. The mutation and selection of individuals who have obtained the best values in their objective function is based on the simplex search method of numerical derivation [21]. MAGO uses only two individuals for this mutation, the best one and the trial one. If this movement generates a better individual, this one passes to the next generation; otherwise, its predecessor passes on with no changes. This method does not require gradient information for the derivation.

The fittest individuals are ordered from the best one. Test individuals are created bringing them closer to the best one, following the rule in Eq. (25):

$$x_T^{(j)} = x_i^{(j)} + F^{(j)} \times \left(x_B^{(j)} - x_i^{(j)}\right) \tag{25}$$

where $x_B^{(j)}$ is the best individual of generation j and $x_i^{(j)}$ is the selected fittest individual. $F^{(j)}$ is a matrix that includes information about the covariance of the problem variables, Eq. (26), including information about the interrelationships of the variables in the actual generation. The covariance matrix of the current population considers the effect of the evolution, and Eq. (25) propagates it on new individuals.

$$F^{(j)} = \frac{S^{(j)}}{\left\|S^{(j)}\right\|} \tag{26}$$

where $S^{(j)}$ is the sample covariance matrix of the individual population in generation j.

Crowd Dynamics: The number of individuals of this subgroup corresponds to the cardinality of the second deviation of the normal distribution of the actual population. This subgroup has the role of exploring the searching space in a neighborhood close to the population mean. If the population mean and dispersion matrix for generation j are $x_M^{(j)}$ and $S^{(j)}$, then the Crowd Dynamics individuals are created from a uniform distribution on the hyper-rectangle-$\left[LB^{(j)}, UB^{(j)}\right]$, see Eqs. (27) and (28). The diagonal of the population dispersion matrix of the generation j, described by Eq. (29).

$$LB^{(j)} = x_M^{(j)} - \sqrt{\text{diag}\left(S^{(j)}\right)} \tag{27}$$

$$UB^{(j)} = x_M^{(j)} + \sqrt{\text{diag}\left(S^{(j)}\right)} \tag{28}$$

$$\text{diag}\left(S^{(j)}\right) = \left[S_{11}^{(j)} \quad S_{22}^{(j)} \quad \ldots \quad S_m^{(j)}\right]^T \tag{29}$$

Initially, the neighborhood around the mean may be large, but as evolution proceeds, this neighborhood is reduced, and the population mean is getting closer to the optimal but following on another path.

Accidental Dynamics: This group is a smaller one in relation to its impacts on the population. N3 new individuals are created from a uniform distribution over the whole search space, as in the initial population. The two dynamics mentioned above concentrate the population around their local optima. To maintain diversity, MAGO introduces new individuals in each generation with the accidental dynamic, sampling a uniform distribution throughout the search space. This dynamic also ensures the numerical stability of the covariance dispersion matrix. The accidental dynamics always guarantees the diversity and dispersion of the population, even if the other two groups already have converged. Following, the pseudo code of MAGO is presented.

MAGO Pseudo Code.

1: $j = 0$. Initial Generation.
2: Random initial population generation uniformly distributed over the searching space.
3: repeat
4: Evaluate each individual with the objective function.
5: Calculate the population covariance matrix and the first, second and third dispersion.
6: Calculate the cardinalities N1, N2 and N3 of the groups G_1, G_2 and G_3.
7: Select N1 fittest individuals, modify them according to Eq. (25), translate the winners toward the best one and make them compete. Pass the fittest to the next generation $j + 1$.
8: Sample N2 individuals from a uniform distribution in hyper rectangle $\left[LB^{(j)}, UB^{(j)}\right]$ and pass them to generation $j + 1$.
9: Sample N3 individuals from a uniform distribution over the whole search space and pass them to generation $j + 1$.
10: $j = j + 1$
11: until an ending criterion is satisfied

Cardinalities. For control tables, if the process is outside the control limits, then it is assumed that the process is out of order. The next step in MAGO is a type of variance decomposition, inspired by the well-known variance analysis (ANOVA). Consider the population dispersion matrix of generation j, $S^{(j)}$ and its diagonal $\text{diag}\left(S^{(j)}\right)$. If $Pob^{(j)}$ is the set of possible solutions in generation j, then three groups can be defined as in Eqs (30), (31), and (32). If N1, N2, and N3 are the cardinalities of the sets G_1, G_2, and G_3, then the cardinality of the Emerging Dynamics, Crowd Dynamics and Accidental Dynamics are set, respectively.

$$G_1 = \left\{ \boldsymbol{x} \in Pob^{(j)} / x_M^{(j)} - \sqrt{\text{diag}\left(S^{(j)}\right)} \leq \boldsymbol{x} \geq x_M^{(j)} + \sqrt{\text{diag}\left(S^{(j)}\right)} \right\} \tag{30}$$

$$G_2 = \left\{ \boldsymbol{x} \in Pob^{(j)} / x_M^{(j)} - 2\sqrt{\text{diag}\left(S^{(j)}\right)} \leq \boldsymbol{x} \geq x_M^{(j)} + \sqrt{\text{diag}\left(S^{(j)}\right)} \right\} \tag{31}$$

$$G_3 = \left\{ \boldsymbol{x} \in Pob^{(j)} / x \leq x_M^{(j)} - 2\sqrt{\text{diag}\left(S^{(j)}\right)}; \boldsymbol{x} \geq x_M^{(j)} + 2\sqrt{\text{diag}\left(S^{(j)}\right)} \right\} \tag{32}$$

where, $XM^{(j)}$ is the mean of the actual population and $Pob^{(j)} = G1 \bigcup G2 \bigcup G3$.

This way of defining the elements of each group is dynamical in nature and autonomous in MAGO. Cardinalities depend on the dispersion of the whole population in generation j.

3.2. Design of PI/PID controllers via an evolutionary algorithm

A feedback controller is a device that automatically manipulates a predetermined variable to ensure the balance of the system around an operating point. It compares the actual value of the controlled variable to its desired value (feedback) obtaining an error signal to calculate the control action so that it maintains or returns the system to the point of operation [9].

The output, $u(t)$, (control action) is a composite of three effects, K_p, the proportional action, T_i, the integral time and, T_d, the derivative time, which are calculated based on the error. An optimal PID controller consists of adjusting its parameters K_p, T_i, and T_d so that a performance criterion (error between the actual output of the plant regarding the desired value and/or effort control) is minimized. MAGO is a real-valued evolutionary algorithm, very efficient and effective instrument to solve problems in continuous domain. It has been chosen as a tool for estimating the parameters of a controller that minimizes an integral performance index. The representation of the evolutionary individual is a vector containing the controller parameters, as positive values in a continuous domain. See **Table 1**.

The fitness function for the optimization problem of a 1DoF PID controller is defined in Eq. (33). The error is calculated for each point of time, t_k, throughout the measurement horizon as the difference between the system output and the reference signal.

$$J(\theta) = J\left(K_p, T_i, T_d\right) = \text{Min}_\theta \left\{ J_{IAE} = \sum_{t_k}^{t_{kf}} |e(t_k)| \right\} \tag{33}$$

A complete analysis of the methods of tuning controllers based on SOSPD was made in [23, 24]. Each tuning rule for PID controllers has restrictions on the behavior of the plant, expressed

$K_p \in \boldsymbol{\mathcal{R}}$	$T_i \in \boldsymbol{\mathcal{R}}$	$T_d \in \boldsymbol{\mathcal{R}}$	$\beta \in \boldsymbol{\mathcal{R}}$

Table 1. Structure of the evolutionary individual.

in the range of validity, and has only been applied to a certain group of processes. In general, those rules are based on several relationships and/or conditions of the parameters defining the process model. Most methods for optimal tuning of SOSPD systems require, from experiments carried out directly on the plant, additional critical system information. Readers are referred to [25] for a good compilation of the PID tuning rules and [26] for a complete analysis of the different tuning rules characteristics and features. It is not always possible to perform experiments such as reaction curves and closed-loop tests because the extreme stress and oscillations may create instability and damage to the system. This scenario shows that a general rule for tuning PID controllers must be sought. A tuning method that best satisfies the operation requirements of each problem and ensures optimal values for the controller parameters according to the 2DoF PID chosen criterion. This situation could be reduced to an optimization problem consisting of minimizing an objective function. A suitable combination of the three parameters required by the PID controller will be the result of minimizing a performance criterion. This is the approach taken in this chapter.

MAGO has shown a great capacity to optimize nonlinear dynamical problems in the continuous domain. Because that, it has been selected for tuning several optimal 2DoF PID controllers. Next section is concerned to optimal 2DoF PID controllers satisfying an integral performance index and not requiring additional system information coming from experiments on the plant.

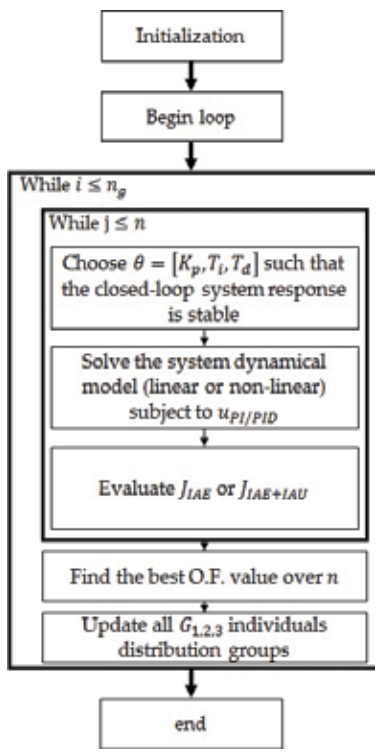

Figure 3. Flowchart of the MAGO algorithm for PI/PID controllers tuning.

With MAGO, the optimization of 2DoF PID controllers is made in only one stage and simultaneously for the regulator and servomechanism modes. The flowchart for tuning of PID controller using MAGO is shown in **Figure 3**. In this chapter, it is not included a convergence analysis of the MAGO; however, its convergence has been previously demonstrated in [18, 19].

4. 2DoF PID controllers tuning on benchmark plants

A 2DoF PID controller attempts simultaneously achieve good closed-loop servo-regulatory dynamical responses. Most of the recent literature working on 2DoF PID controllers had been based on both First Order Systems plus Time Delay (FOSPD) and Second Order plus Time Delay (SOSPD) models with satisfactory results [27–30].

In [22], a set of system models as a benchmark suitable for testing PID controllers was proposed. FOSPD and SOSPD were included in the benchmark. This set of system models presents different challenges of control because PID controllers are not well suited for all of them. From the best of our knowledge, none of the PID controller tuning rules applies to obtain suitable values for its parameters for all the systems in that benchmark.

In this chapter, nine different system models are taken from the benchmark and 2DoF PID controllers are designed, one for each system model. The 2DoF PID controller parameters obtained here are compared with parameters reported in [22] for the same system models. The 2DoF PID controller-tuning problem is formulated as a constrained optimization problem based on IAE and IAU performance indexes. Then, MAGO is employed to solve the optimization problem. Consider the system models given by Eqs. (34)–(42).

Multiple equals poles:

$$G_1(s) = \frac{1}{(s+1)^8} \tag{34}$$

Fourth-order system:

$$G_2 = \frac{1}{(s+1)(0.5s+1)(0.25s+1)(0.125s+1)} \tag{35}$$

Right half plane zero (non-minimum phase):

$$G_3 = \frac{1-5s}{(s+1)^3} \tag{36}$$

Time delay and lag: (FOSPD):

$$G_4 = \frac{1}{0.1s+1}e^{-s} \tag{37}$$

http://dx.doi.org/10.5772/intechopen.74297

Time delay and double lag (SOSPD):

$$G_5 = \frac{1}{(0.1s+1)^2} e^{-s} \tag{38}$$

Fast and slow modes:

$$G_6 = \frac{100}{(s+10)^2} \left(\frac{1}{s+1} + \frac{0.5}{s+0.05} \right) \tag{39}$$

Conditionally stable system:

$$G_7 = \frac{(s+6)^2}{s(s+1)^2(s+36)} \tag{40}$$

Oscillatory system:

$$G_8 = \frac{25}{(s+1)(s^2+s+25)} \tag{41}$$

Unstable pole:

$$G_9 = \frac{1}{s^2-1} \tag{42}$$

In [22], the control problem was solved as an optimization process where the objective function was a combination of the IAE and IAU performance indexes. The main features of the procedure used in to solve the control problem were: (1) not only IAE but also IAU are included in the objective function establishing a kind of trade-off between the system performance and robustness due to the restriction imposed in the controller action effort through the IAU index. (2) Four 2DoF PID controller parameters were simultaneously optimized to take the full advantage of the control structure qualities. Traditionally, the tuning process for a 2DoF PID controller is carried out in two stages as follows: firstly, values of K_p, T_i, and T_d are found such that closed-loop system achieves some dynamical behavior. Secondly, the value of β is settled such that the closed-loop dynamical response of the system is improved when the system operates as servomechanism. These two stages tuning process imply that the closed-loop system responses are not optimal for any of the system operation modes. (3) The optimization process simultaneously considers both system operation modes, that is, optimum 2DoF PID controller parameters were found such that the closed-loop system response is optimal for both servo and regulatory modes. MATLAB functions `fminsearh` and `fmincon` were employed to solve the optimization problem. `Fminsearch` function was used to find a set of initial conditions for the controller parameters. Next, `fmincon` function was used trying to find the overall optimal controller parameters. The authors highlight that with this optimization strategy exists the possibility that the problem solution is not the global optimum of the objective function although the closed-loop systems performance was satisfactory in all cases.

In this chapter, a similar procedure for solving the optimization is adopted to facilitate the comparison of results. However, MAGO is adopted as optimizer instead of using native MATLAB functions `fminsearh` and `fmincon`. The objective function to be optimized is given by Eq. (43), where r and s refer to regulation-servo operation modes.

$$\mathrm{Min}_{\theta}\left\{\left(\sum_{t_k}^{t_{kf}}|e(t_k)|+\sum_{t_k}^{t_{kf}}|e_u(t_k)|\right)_s+\left(\sum_{t_k}^{t_{kf}}|e(t_k)|+\sum_{t_k}^{t_{kf}}|e_u(t_k)|\right)_r\right\} \tag{43}$$

Subject to $G_{1,2,\ldots,9}$ (see Eqs. (34)–(42))

$$U(s)=K_p\left(\beta+\frac{1}{T_i s}\right)R(S)-K_p\left(1+\frac{1}{T_i s}+T_d s\right)Y(s)$$

$$K_{p_{min}} \le K_p \le K_{p_{max}}$$

$$T_{i_{min}} \le T_i \le T_{i_{max}}$$

$$T_{d_{min}} \le T_d \le T_{d_{max}}$$

$$\beta_{min} \le \beta \le \beta_{max}$$

Table 2 summarizes results obtained with MAGO and in [22] for 2DoF PID controller parameters. **Table 3** summarizes results obtained with MAGO and in [22] for each of the IAE and IAU performance indexes.

From **Table 2**, it is seen that parameters obtained with MAGO for 2DoF PID controllers are different in all cases, although they have similar magnitude scales. This implies that MAGO found a different minimum for the objective function (see Eq. (43)).

From **Table 3**, it is seen that MAGO found a better minimum value for the integral performance indexes except for the performance index IAU_s for G_6, G_8, and G_9 systems. In [22], an

System model	K_p		T_i		T_d		β	
	[22]	**MAGO**	**[22]**	**MAGO**	**[22]**	**MAGO**	**[22]**	**MAGO**
G_1	0.890	0.9544	5.147	5.4354	1.999	1.8095	0.661	0.4453
G_2	3.637	3.2947	1.334	1.2791	0.420	0.4270	0.222	0.3096
G_3	0.335	0.3515	2.665	2.6949	0.774	0.7941	0.844	0.5355
G_4	0.423	0.5278	0.538	0.5765	0.137	0.1557	1.000	0.2593
G_5	0.367	0.5013	0.497	0.6117	0.103	0.2380	1.000	0.7687
G_6	0.626	1.8491	0.441	0.8014	0.000	0.1580	0.000	0.9654
G_7	65	68.4154	1.736	1.2209	0.632	0.3924	0.141	0.0228
G_8	0.596	0.6238	0.424	0.3392	0.172	0.1877	1.000	0.4617
G_9	40	33.7561	1.430	0.7854	0.297	0.3159	0.231	0.0486

Table 2. 2DoF PID controller parameters.

System model	IAE_s		IAU_s		IAE_r		IAU_r		Total	
	[22]	MAGO	[22]	MAGO	[22]	MAGO	[22]	MAGO	[22]	MAGO
G_1	8.420	8.9159	2.878	1.9858	5.999	5.8509	7.643	6.8976	24.943	23.6502
G_2	1.460	1.3676	1.511	0.6211	0.375	0.4045	1.692	0.6923	5.039	3.0855
G_3	8.575	9.0000	1.969	1.1623	16.912	17.0410	9.005	7.8505	36.462	35.0539
G_4	1.396	1.5763	1.318	0.4935	1.300	1.3516	2.338	1.4282	6.353	4.8496
G_5	1.464	1.5213	1.351	0.3665	1.431	1.3194	2.415	1.3957	6.610	4.6029
G_6	1.543	0.7787	1.734	7.8872	1.205	0.4895	2.311	0.5851	6.793	9.7405
G_7	1.555	1.2055	1.212	11.187	0.027	0.0180	1.121	0.1752	3.915	12.5855
G_8	1.176	1.2154	1.593	0.7958	1.003	0.9138	2.112	1.0807	5.883	4.0057
G_9	1.064	0.7669	2.087	16.310	0.036	0.0242	1.173	0.2073	4.360	17.3089

Table 3. 2DoF PID controller IAE and IAU performance indexes.

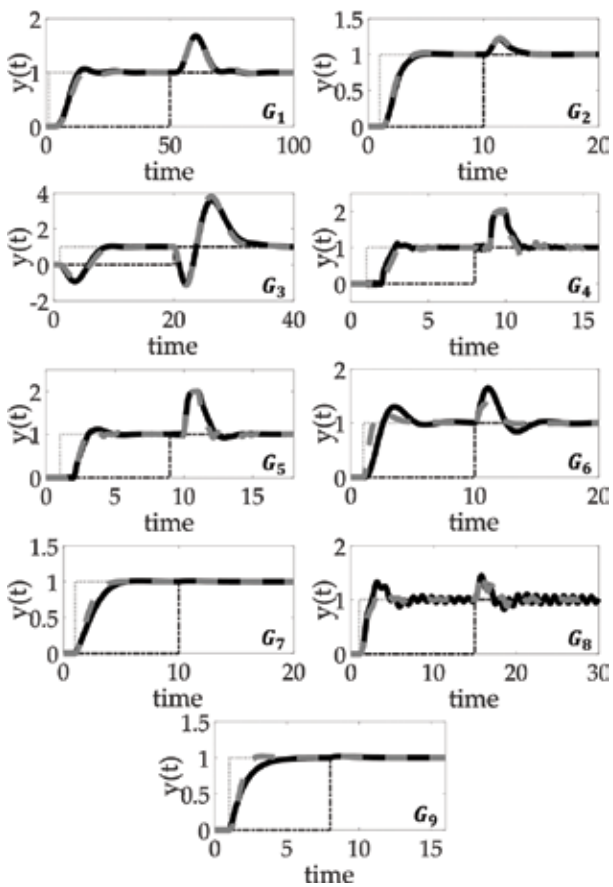

Figure 4. Simulation results for 2DoF PID controllers applied to the benchmark. Closed-loop system dynamical response comparison: 2DoF PID controller tuned with parameters reported in [22] (solid line) and results from MAGO (dashed line).

additional optimization constraint was imposed for systems G_6, G_8, and G_9 to avoid changes larger than 10 times the steady-state value of the control action, that is, $\Delta u < u_{ss}$, where u_{ss} is the steady-state of u. In this chapter, this additional constraint was not included. This constraint could be incorporated as follows: $\Delta u = K_p \beta \Delta r < 10 u_{ss}$.

Figure 4 shows the closed-loop dynamical response for systems given by Eqs. (34)–(42). To test the 2DoF PID controllers' performance, a step change in $r(t)$ at $t = 0$ (dotted line) and a step change in $d(t)$ at $t = 50$ (dash-dot line) were applied. Results by MAGO (dashed line) are compared with results in [22] (solid line). PID controllers tuned by MAGO perform similar but faster for G_6, G_8, and G_9 systems.

Figure 5 shows control actions for systems given by Eqs. (34)–(42). In **Figure 5**, results obtained by MAGO (dashed line) and in [22] (solid line) are contrasted. From **Figure 5**, it is seen that the control action effort is similar for most cases except for G_6, G_8, and G_9 systems, for which an

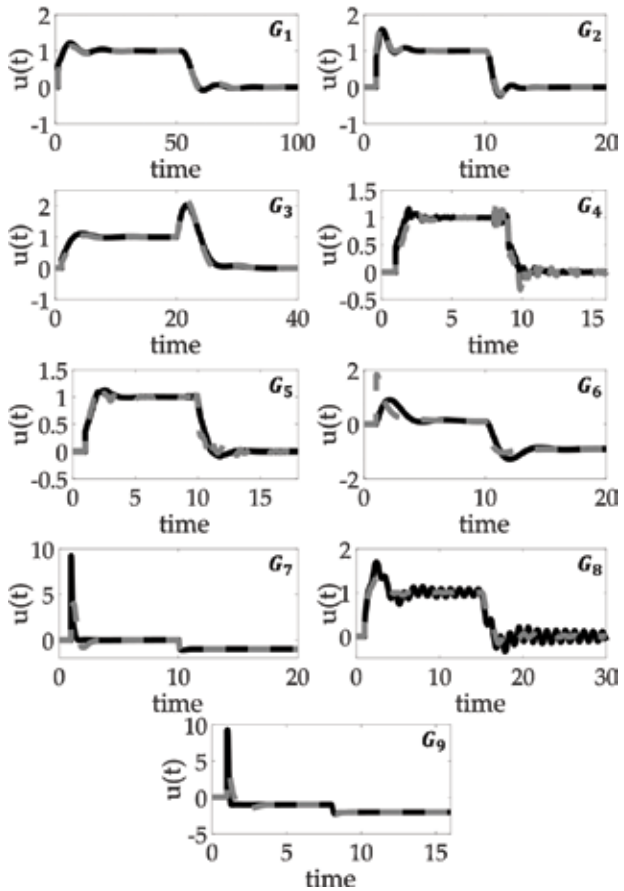

Figure 5. Simulation results for 2DoF PID controllers applied to the benchmark. Closed-loop dynamical response of the control action: 2DoF PID controllers tuned with parameters in [22] (solid line) and results from MAGO (dashed line).

additional optimization constrain was included in [22] to avoid control action changes larger than 10 times u_{ss}.

From **Figures 4** and **5**, it is seen that MAGO solves the optimization problem satisfactorily because the control objective is achieved for all systems. For instance, MAGO is not only suitable to solve the 1DoF PID control problem based on SOSPD [6], but also to solve the 2DoF PID control problem based on a wide range of systems, each one of them with different dynamical characteristics and challenges from the control point of view.

5. Case study: Evolutionary PI controller tuning for a buck DC-DC converter based on its nonlinear model

Power electronic converters (PEC) are electronic circuits that are commonly designed to regulate the voltage in their output when the input is a nonregulated current or voltage source. A PEC is highly efficient, highly reliable, negligible maintenance and very small. A PEC is usually composed of switches (Q IGBT or Mosfets and D diodes). Because switches a PEC is nonlinear dispositive with an interesting behavior, so a DC-DC buck converter is chosen in this chapter as a case of study.

DC-DC buck converters are nonlinear systems which analysis and control could be difficult. Linear techniques based on classical controller have problems related to the stability around the operation point [31]. Nonlinear controllers can be implemented to improve the stability of the converter, but such techniques could be complex [32, 33]. Control techniques-based artificial intelligence simplifies the design and implementation, not requiring the mathematical model; nonetheless, they are designed based on expert knowledge of the converter [34–36]. Sliding mode control technique has the advantage to reject easily perturbations, but variable frequency of switching may be handled [37]. There are many articles dealing with control for the DC-DC buck converter but is still no consensus on the control strategy should be implemented. This is another reason to choose a DC-DC buck converter as a study case.

DC-DC buck converter, or step-down converter, is a power converter that steps down the voltage from its supply (input) to its load (output). **Figure 5** shows the equivalent circuit of the DC-DC buck converter. It is composed of an inductor (L), a capacitor (C), a diode (D), and a switch (Q) (IGBT is considered as the switch for the analysis). The converter is supplied by a DC input voltage (v_g) and feeds in its output (v_o) a resistive load (R). **Figure 6** also depicts the reference currents and voltages of the circuit, using passive sign convention. In this chapter, it is assumed that the converter operates in continuous condition mode (CCM).

The converter has two states per switching cycle (T_s) according to the position of the switch Q when CCM operation is considered. The on state is when Q is on (closed) and D is inversely polarized (open), while the off state is when Q (open) is off and D is directly polarized (closed). Dynamical model and steady-state analysis can be done if Kirchhoff laws are applied, see Eqs. (44) and (45). Step-by-step DC-DC buck converter dynamical model deduction can be

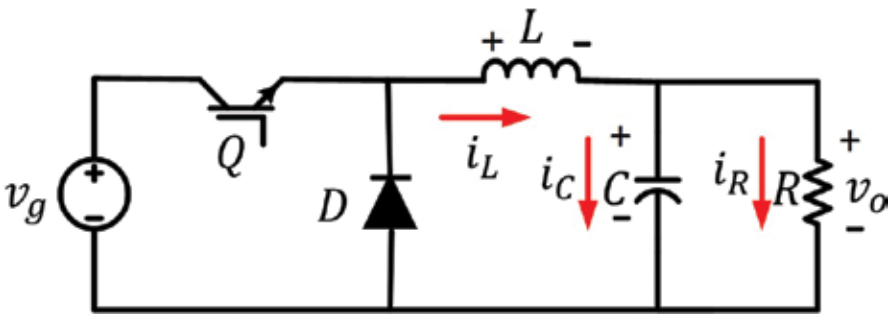

Figure 6. DC-DC buck converter equivalent circuit schematic.

found in [38]; where u is the switching function ($u = 1$ for on-state and $u = 0$ for off-state). The nonlinearity is because the product between v_g and u.

$$L\frac{di_L}{dt} = v_g u - v_c \tag{44}$$

$$C\frac{dv_c}{dt} = \left(i_L - \frac{v_c}{R}\right) \tag{45}$$

The DC-DC buck converter model given by Eqs. (44) and (45) describes the nonlinear dynamical evolution of the system. From the control point of view, a model given by Eqs. (44) and (45) is inconvenient, and a linear approximation is preferred. The linear DC-DC buck converter state-space representation is given by Eqs. (46) and (47). Where d is an input control (duty cycle) and correspond with $\langle u \rangle = d$, $d \in [0, 1]$, the average value of u. V_g is the average value of v_g (state in its rated value) and D is d in an operation point (D is also defined as the reason between the on-time and the switching-time $D = t_{on}/T_s$). Note that v_g is chosen as a system input, and it represents a system disturbance.

$$\begin{bmatrix} i_L \\ \dot{v_c} \end{bmatrix} = \begin{bmatrix} 0 & -\frac{1}{L} \\ \frac{1}{C} & -\frac{1}{RC} \end{bmatrix} \begin{bmatrix} i_L \\ v_c \end{bmatrix} + \begin{bmatrix} \frac{V_g}{L} & \frac{D}{L} \\ 0 & 0 \end{bmatrix} \begin{bmatrix} d \\ v_g \end{bmatrix} \tag{46}$$

$$\begin{bmatrix} i_L \\ v_o \end{bmatrix} = \begin{bmatrix} 1 & 0 \\ 0 & 1 \end{bmatrix} \begin{bmatrix} i_L \\ v_c \end{bmatrix} + \begin{bmatrix} 0 & 0 \\ 0 & 0 \end{bmatrix} \begin{bmatrix} d \\ v_g \end{bmatrix} \tag{47}$$

Transfer functions ($G_{i_L d}$, $G_{i_L v_g}$, $G_{v_c d}$ and $G_{v_c v_g}$) can be obtained by applying the realization of Eq. (5). Transfer functions are shown by Eq. (48).

$$\begin{bmatrix} G_{\frac{i_L}{d}} & G_{\frac{i_L}{v_g}} \\ G_{\frac{v_C}{d}} & G_{\frac{v_C}{v_g}} \end{bmatrix} = \begin{bmatrix} \frac{CV_g Rs + V_g}{RLCs^2 + Ls + R} & \frac{RCDs + D}{RLCs^2 + Ls + R} \\ \frac{V_g R}{RLCs^2 + Ls + R} & \frac{DR}{RLCs^2 + Ls + R} \end{bmatrix} \tag{48}$$

Transfer function $G_{v_c d}$ can be used for controlling the output voltage by means of the change of d; similarly, $G_{i_L d}$ can be used for controlling the inductor current. $G_{v_c v_g}$ and $G_{i_L v_g}$ can be used to determine the change on v_c and i_L when v_g is considered as a perturbation. Narrowing this chapter to controlling v_c, $G_{v_c d}$ and $G_{v_c v_g}$ are the transfer functions that we are focus on; similarly, $G_{i_L d}$ and $G_{i_L v_g}$ should also be used for the explanation. Classic control commonly uses $G_{v_c d}$ to regulate v_c; nevertheless, $G_{v_c v_g}$ also affects v_c and must be taken into account if the implementation of a robust control strategy is desired. For controlling purposes, v_g is a perturbation while d is the control input that allows the control of the system, both v_g and d affect v_c (see **Figure 7**).

From the control point of view, the DC-DC buck converter can operate in two modes, as regulator and servomechanism. Regulation mode objective is to maintain constant the converter output voltage against any system disturbance. Servomechanism mode objective is to track an output voltage reference. Both operation modes can be combined at any moment. For instance, the selected control strategy for the DC-DC buck converter should assure a good performance for both operation modes. In this chapter, a PI/PID-based control structure fulfills both DC-DC buck converter control objectives. A DC-DC buck converter is parameterized as follows: $C = 22\ \mu F$, $L = 0.5$ mH, $R = 10\ \Omega$, $V_g = 12\ V$, $V_o = 6\ V$, $D = 0.5$, $R_L = R_c = 1\ \Omega$.

A rigorous way to tune PI controllers for DC-DC buck converters is through the pole placement method [36]. As PI controller tune requirements, wide accepted specifications are a bandwidth $BW \geq \frac{1}{5} f_{sw}$, where f_{sw} is the converter switching frequency, and a damping factor $\zeta = 1/\sqrt{2}$. These closed-loop requirements are settled to establish a trade-off between DC-DC buck closed-loop performance and robustness.

Sisotool is a friendly MATLAB environment to tune PI/PID controller parameters. **Figure 8** shows the DC-DC buck converter root locus diagram for the PI and PID controllers. In **Figure 8**, points represented as cruces correspond to poles and circles correspond to zeros, the diagonal line from the origin corresponds to $\zeta = 1/\sqrt{2}$. In consequence, shaded area is for $\zeta < /\sqrt{2}$, while non-shaded area is for $\zeta > 1/\sqrt{2}$. From **Figure 8a**, it is possible to observe that $\zeta = 1/\sqrt{2}$ cannot be achieved no matter how large the value of the PI controller real zero is. On the other hand, in **Figure 8b**, it is possible to observe that $\zeta = 1/\sqrt{2}$ can be achieved with a PID controller. **Figure 8** shows the DC-DC buck converter closed-loop bode diagram. From **Figure 9**, it is possible to observe that $BW = \frac{1}{5} f_{sw} = 4$ kHz. PID parameters are $K_p = 0.1624$,

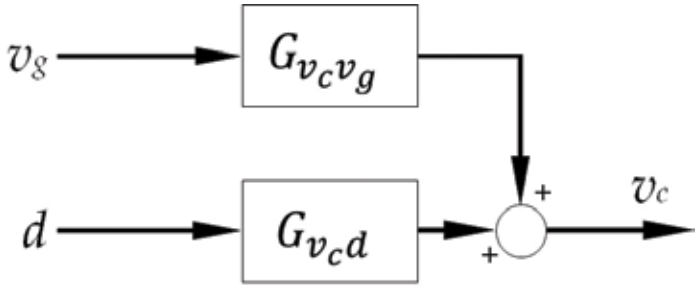

Figure 7. DC-DC buck converter open-loop block diagram.

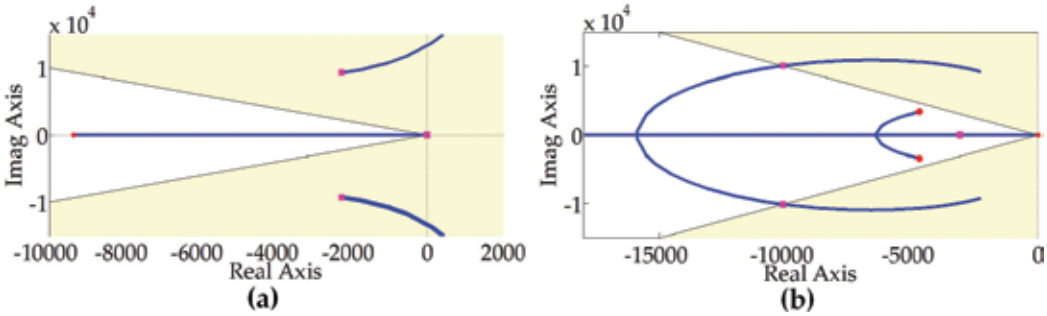

Figure 8. DC-DC buck converter root locus: (a) PI controller and (b) PID controller.

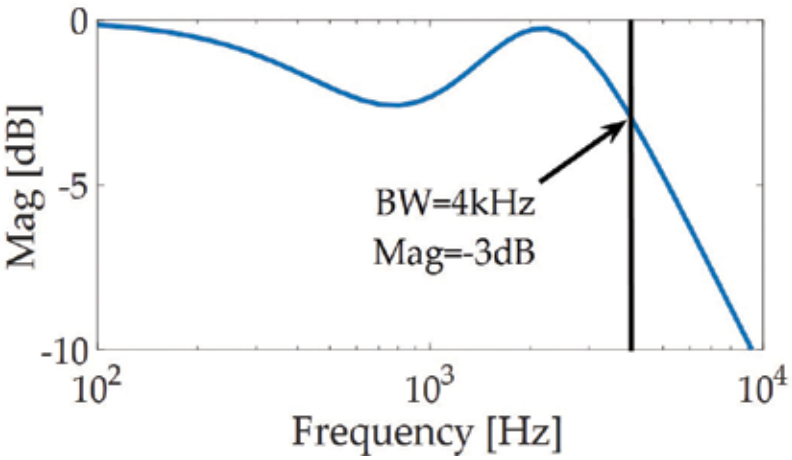

Figure 9. DC-DC buck converter closed-loop bode diagram for the PID controller.

$T_i = 1.7240\,e-3\,[s]$ and $T_d = 1.6763\,e-5\,[s]$. Furthermore, the tuned PID controller fulfills the desired closed-loop requirements for the DC-DC buck converter, while a PI controller cannot be tuned to fulfill the closed-loop requirements for the DC-DC buck converter.

PI rather than PID control structures are preferred in PECs applications because PI-based control structures significantly reduce the feedback induced noise. In this chapter is proposed an alternative way to tune PI controllers for DC-DC buck converters in order to overcome the limitations with the pole placement method. PI controller tuning problem is formulated as a constrained optimization problem and solved using MAGO as in Eq. (49). $\theta = \begin{bmatrix} K_p & T_i \end{bmatrix}$ are the PI controller parameters, α and γ are tuneable weighs establishing a trade-off between IAE and IAU performance indexes and $t_{s_{max}}$ is the maximum allowed closed-loop setting time.

$$\text{Min}_\theta \left\{ \alpha \left(\sum_{t_k}^{t_{kf}} |e(t_k)| \right) + \gamma \left(\sum_{t_k}^{t_{kf}} |e_u(t_k)| \right) \right\} \tag{49}$$

Subject to *Buck DC-DC nonlinear dynamical model* Eqs. (43) and (45)

http://dx.doi.org/10.5772/intechopen.74297

$$u(t) = K_p\left\{e(t) + \frac{1}{T_i}\sum_{t_k}^{t_{kf}} |e(t_k)|\right\}$$

$$0 \le K_p \le 5$$

$$0 \le T_i \le 1e-3$$

$$\alpha = 1$$

$$\gamma = 0.5$$

Main features of the formulated optimization problem are: (1) DC-DC buck nonlinear dynamical model is incorporated instead of duty to output voltage transfer function. Using the nonlinear dynamical model of the DC-DC buck converter, it is possible to solve the optimization problem simultaneously considering regulation and servomechanism operation modes. (2) Objective function includes simultaneously IAE and IAU performance indexes. The inclusion of the IAU gives a kind of closed-loop robustness because it limits the maximum control action effort avoiding system oscillations and actuator saturations. (3) The optimization process is carried out based on the temporal dynamical response of the DC-DC buck converter operating in closed-loop. For each MAGO iteration, it is necessary to solve the DC-DC buck converter nonlinear dynamical model in the closed-loop mode. To solve the nonlinear dynamical model in the closed-loop mode, it is necessary to define an experiment such that multiple set-point changes and disturbances appear through the simulation time. The solution of the optimization problem is the set of PI controller parameters that minimize both IAE and IAU indexes for the experiment setup.

The total simulation time for the DC-DC buck converter is 25 min. The experiment setup for the optimization process is as follows: for the time interval $t \in [0, 5]$ ms, the system is at the nominal conditions. For $t \in (5, 10]$ ms, the set-point for the output voltage is settled in 8 V. For $t \in (10, 15]$ ms, the input voltage is settled in 14 V, while the output voltage remains in 8 V. For $t \in (15, 20]$ ms, output and input voltages are settled in 4 V and 10 V, respectively. For $t \in (20, 25]$ ms, output and input voltages are returned to their nominal values. Both adjustable MAGO parameters n and ng were settled in 100. The optimization problem solution using MAGO is: objective function value equals 0.1066, PI controller parameters values are $K_p = 0.0382$ and $T_i = 1.5364\, e - 4\ [s]$.

PSIM is a recognized platform to simulate and validate the control system performance for PEC. A PSIM simulation is carried out for the DC-DC buck converter to validate MAGO optimization results. A DC-DC buck converter simulation is implemented on PSIM including parasitic losses in their passive elements as equivalent series resistances (ESR). Simulation aims to test the real closed-loop system performance. Therefore, two DC-DC buck converter closed-loop simulations are carried out as follows: (1) PID controller obtained by the pole placement method is implemented and its performance is tested. (2) PI controller obtained by MAGO is implemented and its performance is tested. In both cases, the experiment setup used in MAGO optimization is applied to test PID and PI controllers' performance.

$G_{v_c d}$ and $G_{v_c v_g}$ were deduced in this chapter without including losses in the inductor and capacitor; switching losses which includes the losses in the IGBT and the diode neither were considered. A comparison between a DC-DC buck converter including resistive losses (PSIM simulation) and a DC-DC buck converter which does not include them (MATLAB simulation) are presented in **Figure 10**. For this purpose, pointed line diagrams correspond to PSIM bode diagrams (nonlinear model), while continuous line diagrams correspond to MATLAB bode diagrams of transfer functions $G_{v_c d}$ and $G_{v_c v_g}$ (linear model). PSIM simulation corresponds to the most realistic approximation of the system due to it is the nonlinear representation which includes the resistive losses. In **Figure 10**, there is a big difference between MATLAB and PSIM bode diagrams. This chapter uses the linear model (Eqs. 46 and 47) to implement the control strategy, while the DC-DC buck converter to be controlled includes the resistive losses.

Figure 11 shows the DC-DC buck converter closed-loop dynamical response for both PI controller tuned by MAGO (PI-MAGO) and PID controller tuned by the pole placement method. **Figure 10a** shows both v_g and $v_{o_{Ref}}$ time trajectories. From **Figure 11a**, it is seen that these time trajectories agree with the experiment setup proposed for the optimization problem. Multiple set-point changes ($v_{o_{Ref}}$) and disturbances (v_g) are applied to test the closed-loop dynamical response of the DC-DC buck converter.

Figure 11b shows the dynamical closed-loop response for the DC-DC buck converter output (v_o). From **Figure 11b**, it is seen that the converter control objective is achieved satisfactorily. DC-DC buck converter in closed-loop mode can simultaneously track the set point and reject the disturbance. Both faster than 2.5 ms and with an approximated over-shoot of 12 and 2.5% for the PI and PID controllers, respectively. A remarkable issue is that the converter control objective is achieved when the PSIM DC-DC buck converter model includes the parasitic losses in their passive elements. This implies that both controllers are robust to the model

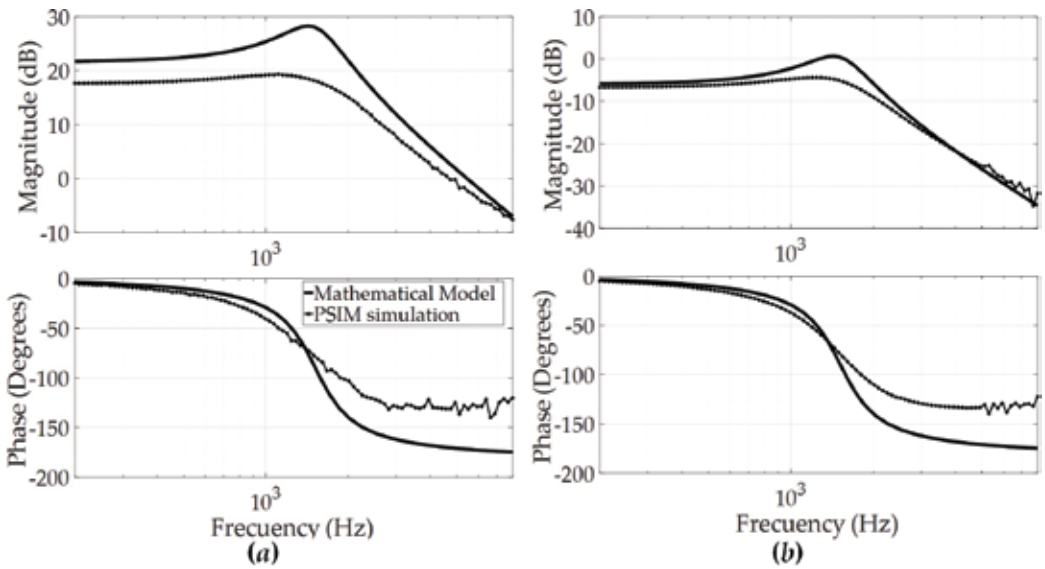

Figure 10. PSIM simulation and nonlinear mathematical model comparison: (a) $G_{v_c d}$ and (b) $G_{v_c v_g}$.

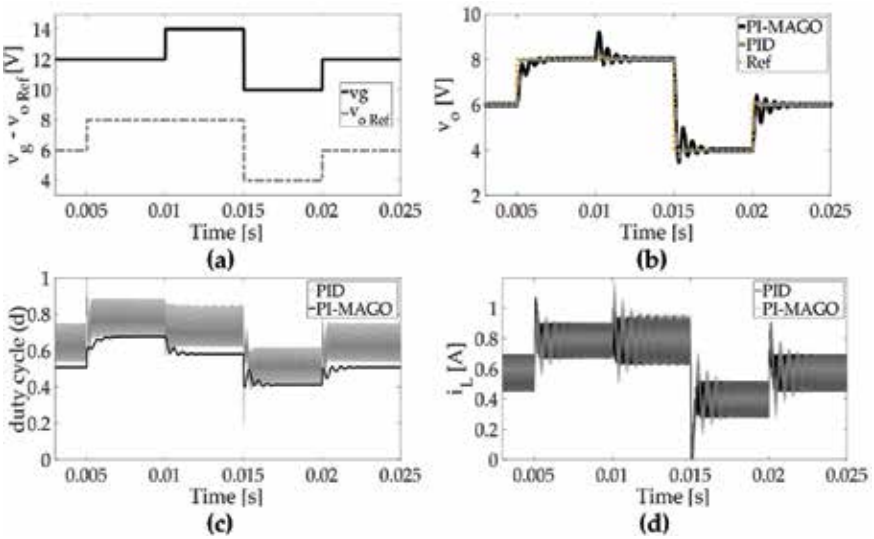

Figure 11. DC-DC buck converter closed-loop PSIM simulation.

mismatch. From **Figure 11b**, it is seen that PID controller performs better than PI controller does; however, the PI performance, it is also acceptable.

Figure 11c shows the control action (d) dynamical response for both PI and PID controllers. From **Figure 11c**, it is seen that d has significant oscillations for PID controller compared with PI controller. The most probable reason for these oscillations is the induced noise caused by the time derivative constant (T_d) in the PID controller. For instance, the PI controller is preferred in PEC applications because the closed-loop induced noise is smaller than in the PID controller case, although the PI controller has a poor dynamical performance than PID controller. An important issue related with d behavior is that never reaches its maximum or minimum value, implying that for the selected setup the actuator does not saturates.

Figure 11d shows the inductor current (i_L) dynamical response for both PI and PID controller. From **Figure 10d**, DC-DC buck converter operates in the CCM overall simulation time.

In summary, both PI and PID controllers achieve the DC-DC buck converter control objective. PID controller performs better than PI controller, but the last one has a smaller induced noise in d, which is a desired characteristic in PEC applications. In consequence, MAGO solution improves the solution obtained by the pole placement method, where a PI controller was not possible to tune because the root locus limitations (see **Figure 8**).

6. Conclusions

A method of tuning optimal controllers on nonlinear systems through the evolutionary algorithm MAGO has been successfully developed and implemented. The MAGO resolves the tuning as a constrained nonlinear optimization problem for both 1DoF and 2DoF PI/PID

controllers on several types of plants running on different modes of operation. To ensure the desired performance of the control loop, everything is reduced to the characterization and adjusting of the value of a set of tuning parameters whatever the chosen control structure is. The usual tuning controller procedures involve uncertainty and time to obtain the right parameters, generally by trial and proof by trained personal depending of the method used. This chapter showed a way to reduce these challenges. MAGO straightforwardly assesses the controller's parameters penalizing the error between the reference value and the output of the plant and minimizing the IAE and IAU performance criteria.

Traditional PID controller tuning rules are restricted to certain values on the behavior of the system and are limited to an only one type of operation. Most methods require experiments to be carried out directly on the plant to get additional necessary system information to apply them; these activities are not always possible to achieve because the triggering of extreme stresses and oscillations of the plant which may create instability and damages on the system, so that, they are not recommended. For benchmark models, the PID controller tuning was made by the MAGO without additional knowledge of the plant. The evolutionary solution obtained with the MAGO covers all those restrictions, extends their maximum and minimum limits, and it does not need additional experimental information from the plants and is suitable for both servo and regulator operating modes. The results showed that regardless of both the plant or controller models used, MAGO gets a satisfactory closed-loop system performance in agreement with the literature reported.

A linear model without losses for the DC-DC buck converter was used to implement the control strategy while a nonlinear system which includes parasitic losses was simulated as a most realistic system in PSIM. There was a big difference between the bode diagrams of the linear model and the nonlinear system; nevertheless, the controllers tuned by MAGO have a successfully behavior in terms of performance and robustness. MAGO controllers let overcome the limitations of traditional PI controllers.

The challenge of rely on a single method to assess the controller for different kinds of plants has been solved applying the evolutionary algorithm MAGO as a tool of optimization. The MAGO was applied to a set of benchmark plants, represented in both transfer functions and differential equation systems, with a control loop operating on both servo and regulator modes. The optimal tuning values of the K_p, T_i and T_d parameters for the optimal PID controller found by the evolutionary method achieved successful results for each of the cases studied. Noticeable results tuning with the algorithm MAGO were obtained when comparing the performance of the traditional PID controller performance for the DC-DC buck converter against the PI-MAGO controller. PI-MAGO controller has a comparable performance with the PID controller tuned by pole placement method. Moreover, PI-MAGO controller minimized the induced closed-loop noise.

This chapter showed that, although there would be options in the traditional rules of controllers tuning, the use of heuristic algorithms is indeed easy than using the classic methods of optimal tuning. The evolutionary algorithm MAGO was used as a tool to optimize the controller parameters for optimal 2DoF PID controllers working on benchmark plants and to optimize the PI controller parameters in a DC-DC buck converter application. Regardless of

the operating mode of the controller and the representation type of the plant used, better results are yielded when optimization is made with the MAGO algorithm than with the traditional methods for optimal tuning.

Acknowledgements

The authors gratefully acknowledge the University of Antioquia (UdeA) for the support of the project CODI 2015-7747. This work was partially supported by COLCIENCIAS (Fondo Nacional de Financiamiento para la Ciencia, la Tecnología y la Innovación Francisco José de Caldas) with the doctoral scholarship 727-2015.

Author details

Jorge-Humberto Urrea-Quintero[1]*, Jesús-Antonio Hernández-Riveros[2] and Nicolás Muñoz-Galeano[1]

*Address all correspondence to: jhurreaq@unal.edu.co

1 Faculty of Engineering, Universidad de Antioquia, Medellín, Colombia

2 Department of Electrical Energy and Automatics, Universidad Nacional de Colombia, Sede Medellín, Colombia

References

[1] Åström KJ, Hägglund T. Advanced PID Control. Systems and Automation Society: ISA-The Instrumentation; 2006 http://lup.lub.lu.se/record/535630

[2] O'Dwyer A. Handbook of PI and PID Controller Tuning Rules. 3rd edition. Imperial College Press; 2009. 608 p. ISBN: 978-1-908978-77-6

[3] Alcántara S, Vilanova R, Pedret C. PID control in terms of robustness/performance and servo/regulator trade-offs: A unifying approach to balanced autotuning. Journal of Process Control. 2013;**23**(4):527-542. DOI: 10.1016/j.jprocont.2013.01.003

[4] Alfaro VM, Vilanova R. Model-Reference Robust Tuning Design Methodology. In: Model-Reference Robust Tuning of PID Controllers. Springer International Publishing; 2016. pp. 29-34. DOI: 10.1007/978-3-319-28213-8_4

[5] Reynoso-Meza G, Sanchis J, Blasco X, Freire RZ. Evolutionary multi-objective optimisation with preferences for multivariable PI controller tuning. Expert Systems with Applications. 2016;**51**(1):120-133. DOI: 10.1016/j.eswa.2015.11.028

[6] Willjuice Iruthayarajan M, Baskar S. Evolutionary algorithms based design of multivariable PID controller. Expert Systems with Applications. 2009;**36**(5):9159-9167. DOI: 10.1016/j.eswa.2008.12.033

[7] Hernández-Riveros JA, Urrea-Quintero JH, Carmona-Cadavid CV. Evolutionary tuning of optimal PID controllers for second order systems plus time delay. In: Computational Intelligence. Cham: Springer; 2016. pp. 3-20. DOI: 10.1007/978-3-319-26393-9_1

[8] Fleming PJ, Purshouse RC. Evolutionary algorithms in control systems engineering: A survey. Control engineering practice. 2002;**10**(11):1223-1241. DOI: 10.1016/S0967-0661(02)00081-3

[9] Ghoreishi SA, Mohammad AN, Basiri SO. Optimal design of LQR weighting matrices based on intelligent optimization methods. International Journal of Intelligent Information Processing. 2011;**2**(1). DOI:10.4156/ijiip.vol2

[10] Tijani IB, Akmeliawati R, Abdullateef AI. Control of an inverted pendulum using MODE-based optimized LQR controller. In: Industrial Electronics and Applications (ICIEA), 8th IEEE Conference on; June 2013. p. 1759-1764. DOI:10.1109/ICIEA.2013.6566653

[11] Hassani K, Lee, WS. Optimal tuning of linear quadratic regulators using quantum particle swarm optimization. In: Proceedings of the International Conference of Control, Dynamics and Robotics; May 2014. p. 1-8

[12] Li Y, Ang KH, Chong GC. PID control system analysis and design. IEEE Control Systems magazine. 2006;**26**(1):32-41. DOI: 10.1109/MCS.2006.1580152

[13] Hernández-Riveros JA, Urrea-Quintero JH. SOSPD controllers tuning by means of an evolutionary algorithm. International Journal of Natural Computing Research (IJNCR). 2014;**4**(2):40-58. DOI:10.4018/978-1-4666-7456-1.ch038

[14] Garpinger O, Hägglund T, Åström KJ. Performance and robustness trade-offs in PID control. Journal of Process Control. 2014;**24**(5):568-577. DOI: 10.1016/j.jprocont.2014.02.020

[15] Freeman Scott, Herron Jon C. Evolutionary Analysis. 5th ed. Pearson; 2014. 848 p. ISBN-13: 9780321868992.

[16] Chakraborty U, editor. Advances in differential evolution. Springer; 2008. DOI:10.1007/978-3-540-68830-3

[17] Hansen, N. Towards a new evolutionary computation advances in the estimation of distribution algorithms, vol. 192 de. Studies in Fuzziness and Soft Computing, Springer; 2006. pp. 75-102. ISBN 978-3-33 540-32494-2

[18] Hernández JA, Ospina JD. A multi dynamics algorithm for global optimization. International Journal of Mathematical and Computer Modelling. Elsevier. 2010;**52**(7-8):1271-1278. DOI: 10.1016/j.mcm.2010.03.024

[19] Hernández-Riveros JA, Villada-Cano D. Sensitivity analysis of an autonomous evolutionary algorithm. Advances in Artificial Intelligence-IBERAMIA; 2012. p. 271-280. DOI: 10.1007/978-3-642-34654-5_28

[20] Montgomery DC. Introduction to Statistical Quality Control. 6th edition. John Wiley & Sons; 2007. 734 p. ISSN: 978-0-470-16992-6

[21] Nelder JA, Mead R. A simplex method for function minimization. The Computer Journal. 1965;**7**(4):308-313. DOI: 10.1093/comjnl/7.4.308

[22] Alfaro VM, Arrieta O, Vilanova R. Control de Dos-Grados-de-Libertad (2-GdL) aplicados al "Benchmark" de Sistemas para Controladores PID. Revista Iberoamericana de Automatica e Informatica Industrial RIAI. 2009;**6**(2):59-67. DOI: 10.1016/S1697-7912(09)70093-7

[23] Comparación del desempeño de los controladores PI y PID [Internet]. 2004. Available from: http://eie.ucr.ac.cr/uploads/file/proybach/pb0431t.pdf [Accessed: 2018-03-07]

[24] Sintonización de controladores PI/PID con los criterios IAE e ITAE, para plantas de polo doble [Internet]. 2005. Available from: http://eie.ucr.ac.cr/uploads/file/proybach/pb0508t.pdf [Accessed: 2018-03-07]

[25] Åström KJ, Hägglund T. Benchmark systems for PID control. IFAC Proceedings Volumes. Elsevier. 2000;**33**(4):165-166. DOI: 10.1016/S1474-6670(17)38238-1

[26] Desanti J. Robustness of Tuning Methods of Based on Models of First-Order plus Dead Time PI and PID Controllers. Escuela de Ingeniería Eléctrica: Universidad de Costa Rica; 2004

[27] Alfaro VM, Vilanova R, Arrieta O. Maximum sensitivity based robust tuning for two-degree-of-freedom proportional−integral controllers. Industrial & Engineering Chemistry Research. 2010;**49**(11):5415-5423. DOI: 10.1021/ie901617y

[28] Alfaro VM, Vilanova R. Model reference based robust tuning of five-parameter 2DoF PID controllers for first-order plus dead-time models. In: Control Conference (ECC), 3931-3936 July 2013. European: IEEE; 2013. pp. 3931-3936

[29] Kumar M, Patel V. Tuning of two degree of freedom PID controller for second order processes. International Journal of Science, Engineering and Technology Research. 2015; **4**(5):1543-1546 ISSN: 2278-7798

[30] Moliner R, Tanda R. Herramienta para la sintonía robusta de controladores PI/PID de dos grados de libertad. Revista Iberoamericana de Automática e Informática Industrial RIAI. 2016;**13**(1):22-31. DOI: 10.1016/j.riai.2015.05.003

[31] Guesmi K, Essounbouli N, Hamzaoui A. Systematic design approach of fuzzy PID stabilizer for DC-DC converters. Energy Conversion and Management. 2008;**49**(10):2880-2889. DOI: 10.1016/j.enconman.2008.03.012

[32] Wen Y, Trescases O. Non-linear control of current-mode buck converter with an optimally scaled auxiliary phase. In: Industrial Technology (ICIT), IEEE International Conference on; March 2010. p. 783-788. DOI:10.1109/ICIT.2010.5472628

[33] Barrado A, Lazaro A, Pleite J, Vazquez R, Vazquez J, Olias E. Linear-non-linear control (LnLc) for DC-DC buck converters: Stability and transient response analysis. In: Applied Power Electronics Conference and Exposition (APEC'04), Nineteenth Annual IEEE; February 2004. p. 1329-1335. DOI:10.1109/APEC.2004.1295995

[34] Eker I, Torun Y. Fuzzy logic control to be conventional method. Energy conversion and management. 2006;**47**(4):377-394. DOI: 10.1016/j.enconman.2005.05.008

[35] Gao D, Jin Z, Lu Q. Energy management strategy based on fuzzy logic for a fuel cell hybrid bus. Journal of Power Sources. 2008;**185**(1):311-317. DOI: 10.1016/j.jpowsour.2008.06.083

[36] Qi W, Li S, Tan SC, Hui SR. Parabolic-modulated sliding mode voltage control of buck converter. IEEE Transactions on Industrial Electronics. 2017;**65**(1):844-854. DOI: 10.1109/TIE.2017.2716859

[37] Trejos A, Gonzalez D, Ramos-Paja CA. Modeling of step-up grid-connected photovoltaic systems for control purposes. Energies. 2012;**5**(6):1900-1926. DOI: 10.3390/en5061900

[38] Bacha S, Munteanu I, Bratcu AI. Power electronic converters modeling and control. Adv. Textb. Control Signal Process. 2014;**454**:454. DOI: 10.1007/978-1-4471-5478-5

Chapter 4

Advanced Methods of PID Controller Tuning for Specified Performance

Štefan Bucz and Alena Kozáková

Additional information is available at the end of the chapter

http://dx.doi.org/10.5772/intechopen.76069

Abstract

This chapter provides a concise survey, classification and historical perspective of practice-oriented methods for designing proportional-integral-derivative (PID) controllers and autotuners showing the persistent demand for PID tuning algorithms that integrate performance requirements into the tuning algorithm. The proposed frequency-domain PID controller design method guarantees closed-loop performance in terms of commonly used time-domain specifications. One of its major benefits is universal applicability for both slow and fast-controlled plants with unknown mathematical model. Special charts called B-parabolas were developed as a practical design tool that enables consistent and systematic shaping of the closed-loop step response with regard to specified performance and dynamics of the uncertain controlled plant.

Keywords: PID controller tuning, robust performance indices, B-parabolas, closed-loop, performance assessment, robust performance

1. Introduction

How to tune a controller for any control application quickly and appropriately? This question raised in 1942 is still up to date and constantly occupies the automation community worldwide. The answer is very intricate; its intricacy is comparable with the open hitherto unresolved Hilbert problems known from mathematics.

Will the PID controllers, historically the oldest but currently still the most used ones, control industrial processes in the near and far future? Based on the increase of the number of PID tuning methods from 258 to 408 during 2000–2005, a positive response can be assumed [23].

The remarkably simple ability of the PID controller to generate a difference equation using the present, past and future values of the control error is often projected into the philosophical understanding [1] and forecast this controller a long-term perspective.

Beginnings of PID controllers date back to 1935 when the Taylor Instruments Companies launched their pneumatic controller with a derivative channel [1]. Owing to rapid developments in the control theory, it was supposed that the conventional PID controllers would be gradually replaced by advanced ones; however, this did not come to pass mainly due to the simple PID structure and its commercial usability in practice. For 83 years, control loop designers preferred the PID controllers for their outstanding ability to eliminate the control error using the integrator, their ability to improve the performance using the "trend" of the controlled variable through the derivative channel and for many other benefits. PID controllers are important parts of distributed control systems, predictive control structures; their coefficients are often adapted by means of fuzzy and neural control and set by genetic algorithms [20, 21, 35]. In multiloop control structures, they are able to stabilize unstable objects and difficult-to-control systems. The 46 existing PID variants and reported 408 diverse tuning methods are a good prerequisite for achieving a satisfactory performance in simple as well as demanding industrial applications [23, 25].

PID controllers are widely applied in technological processes of heavy and light industries, for example in control of tension in the roll during paper winding, boiler temperature, chemical reactor pressure, lathe spindle position in metalworking, and so on; they can be found in modern cars controlling combustion control or vehicle dynamics [9], valve opening and robotic arm position. In the interconnected power system, they are used to control turbine power and speed in both primary and secondary regulation of active power and network frequency. Being easy to implement on both Arduino and Raspberry Pi platforms allows them to be used in mobile "unplugged" applications as well.

Commercial applicability of PID controllers is confirmed by studies referring that more than 90% out of all installed controllers in industrial control loops are PID controllers [36]. The alarming fact, however, is that only 20% of them are tuned correctly, and in 30% of all PID applications, the regulation is unsuitable due to an incorrect selection of synthesis method. Another 30% of poor performance is due to ignorance of nonlinear properties of actuators, and the remaining 20% represent an inadequate choice of sampling period or poor signal filtering [5]. Some controllers not only do not provide the required performance yet often even stability of the control loop being operated only in open loop and manually switched off by the service staff when approaching the setpoint [9]. According to other statistics, 30% of controllers operate in manual mode and require continuous fine-tuning and supervising by the process technologist. A 25% of PID applications use coefficients pre-set by the manufacturer with no update of their values with respect to the particular process [47].

Therefore, a natural requirement for innovative PID tuning methods has come up to ensure the specified performance [19, 22] in terms of the maximum overshoot and settling time not only for processes with constant parameters but for their perturbed types. In this chapter, a novel original robust PID tuning method is presented; hopefully, it will help reverse the above mentioned unfavorable statistics of incorrectly tuned PID controllers.

http://dx.doi.org/10.5772/intechopen.76069

2. PID controller design for industrial processes for performance

Despite the fact that there are more than 11,000 PID controllers in 46 variants operating in industrial processes [23], mostly three basic forms are used to control industrial processes: the ideal (textbook) PID controller, the real PID controller with derivative filter, and the ideal PID controller in series with the first-order filter given by the following transfer functions, respectively.

$$G_R(s) = K\left(1 + \frac{1}{T_i s} + T_d s\right), \quad G_R(s) = K\left(1 + \frac{1}{T_i s} + \frac{T_d s}{1 + \frac{T_d}{N} s}\right), \quad G_R(s) = K\left(1 + \frac{1}{T_i s} + T_d s\right)\left(\frac{1}{T_f s + 1}\right), \quad (1)$$

where K is the proportional gain, T_i and T_d are the integral and the derivative time constants, respectively, T_f is the filter time constant and N∈<8,16> in practical applications [37, 38]. The PID controller design objectives are:

1. tracking of setpoint or reference variable w(t) by y(t),
2. rejection of disturbance d(t) and noise n(t) influence on the controlled variable y(t).

Time response of the controlled variable y(t) is modifiable by parameters K, T_i and T_d, respectively; the objective is to achieve a zero steady-state control error e(t) irrespective if caused by changes in the reference w(t) or the disturbance d(t). This section presents practice-oriented PID controller design methods based on various performance criteria.

Consider the control loop in **Figure 1** with control action u(t) generated by the PID controller (switch SW in position "1").

A controller design is a two-step procedure consisting of controller structure selection (P, PI, PD or PID) followed by tuning coefficients of the selected controller type.

2.1. PID controller structure selection

An appropriate structure of the controller $G_R(s)$ is usually selected with respect to:

- zero steady-state error condition (e(∞) = 0),
- type of the controlled plant,
- parameters of the controlled plant.

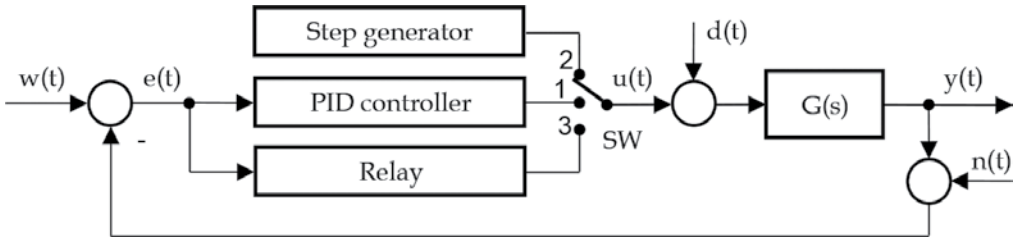

Figure 1. Feedback control loop with load disturbance d(t) and measurement noise n(t).

2.1.1. PID controller structure selection based on zero steady-state error condition

Consider the unity feedback control loop (**Figure 1**), where G(s) is the controlled system. According to the final value theorem, the steady-state error

$$e(\infty) = \lim_{s\to 0} sE(s) = \lim_{s\to 0} s\frac{1}{1+L(s)}W(s) = q!w_q \lim_{s\to 0}\frac{s^{\nu-q}}{s^{\nu}+K_L} \tag{2}$$

is zero if the integrator orders $\nu_L = \nu_S + \nu_R$ in the open-loop $L(s) = G(s)G_R(s)$ is greater than the order q of the reference signal $w(t) = w_q t^q$, i.e.,

$$\nu_L > q, \tag{3}$$

where ν_S and ν_R are integrator orders of the plant and the controller, respectively, K_L is the open-loop gain and w_q is a positive constant [46].

2.1.2. PID controller structure selection based on the plant type

Industrial process variables (e.g., position, speed, current, temperature, pressure, humidity, level) are commonly controlled using PI controllers; in practice, the derivative part is usually switched off due to measurement noise. For pressure and level control in gas tanks, using a P-controller is sufficient [3]. However, adding the derivative part improves closed-loop stability and steepens the step response rise time.

2.1.3. PID controller structure selection based on plant parameters

Consider the FOPDT (j = 1) and FOLIPDT (j = 3) plant models, respectively given as $G_{FOPDT} = K_1 e^{-D_1 s}/[T_1 s + 1]$ and $G_{FOLIPDT} = K_3 e^{-D_3 s}/\{s[T_3 s + 1]\}$ with the parameters given as follows:

$$\mu_1 = \frac{D_1}{T_1}; \quad \vartheta_1 = K_1 K_c; \quad \mu_3 = \frac{D_3}{T_3}; \quad \vartheta_3 = \frac{\lim_{s\to 0} sG(s)}{\omega_c |G(j\omega_c)|} = \frac{T_c K_3 K_c}{2\pi}; \quad \mu_3 = \frac{\frac{2}{\pi} + arctg\sqrt{\vartheta_3^2 - 1}}{\sqrt{\vartheta_3^2 - 1}}, \tag{4}$$

where K_c and ω_c are critical gain and critical frequency of the plant, respectively, the normalized time delay μ_j and the parameter ϑ_j can be used to select appropriate PID control strategy. According to **Table 1** [46], the derivative part is not used in presence of intense noise and a PID controller is not appropriate for plants with large time delays.

2.2. Performance measures in PID controller design

Performance measures for industrial control loops can be expressed both in the time and the frequency domains. The time-domain performance indicators allow to directly expressing the desired process parameter, whereas the frequency-domain performance indicators can be used as PID tuning parameters.

Ranges for μ and ϑ	Control strategy			
	No precise control necessary	Precise control needed		
		High noise	Low saturation	Low measurement noise
$\mu_1 > 1$; $\vartheta_1 < 1.5$	I	I + B + C	PI +B + C	PI +B + C
$0.6 < \mu_1 < 1$; $1.5 < \vartheta_1 < 2.25$	I or PI	I + A	PI + A	(PI or PID) + A + C
$0.15 < \mu_1 < 0.6$; $2.25 < \vartheta_1 < 15$	PI	PI	PI or PID	PID
$\mu_1 < 0.15$; $\vartheta_1 > 15$ or $\mu_3 > 0.3$; $\vartheta_3 < 2$	P or PI	PI	PI or PID	PI or PID
$\mu_3 < 0.3$; $\vartheta_3 > 2$	PD + E	F	PD + E	PD + E

A: forward compensation suggested, B: forward compensation necessary, C: dead-time compensation suggested, D: dead-time compensation necessary, E: set-point weighting necessary, F: pole-placement.

Table 1. Controller structure selection with respect to plant model parameters.

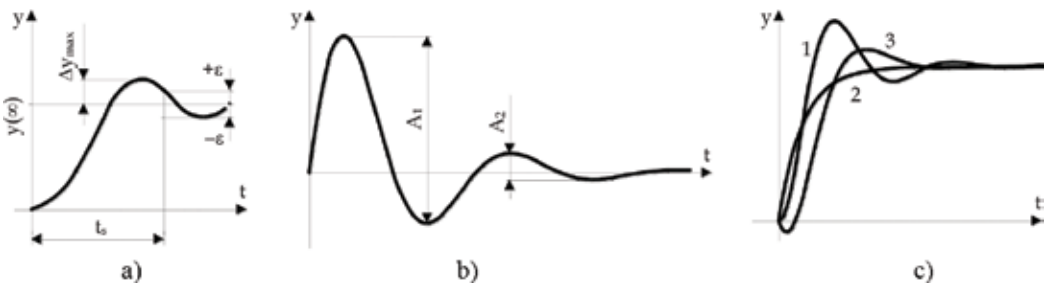

Figure 2. Performance measures: δ_{DR}, t_s, η_{max} and e(∞); (a) setpoint step response; (b) load disturbance step response; (c) over-, critically- and underdamped closed-loop step-responses.

2.2.1. Performance measures in the time-domain

In the time-domain, satisfactory setpoint tracking (**Figure 2a**) and disturbance rejection (**Figure 2b**) are indicated by small values of maximum overshoot and a decay ratio, respectively, given as

$$\eta_{\max} = 100\frac{\left|y_{\max} - y(\infty)\right|}{y(\infty)}\ [\%]; \delta_{DR} = \frac{A_{i+1}}{A_i}, \tag{5}$$

where y(∞) denotes the steady-state value of y(t) [4]. A measure of the y(t) response decay is the ratio of two successive amplitudes A_{i+1}/A_i, where i = 1…N, and N is half the number of points of intersections of y(∞) and y(t). The settling time t_s is the time after which the output y(t) remains within ±ε% of its final value (**Figure 2b**); typically ε = [1%÷5%]y(∞), $\delta_{DR} \in (1:4;1:2)$,

$\eta_{max} \in (0\%;50\%)$. **Figure 2c** depicts underdamped (plot 1), overdamped (plot 2) and critically damped (plot 3) closed-loop step responses.

2.2.2. Performance measures in the frequency-domain

The most frequent parameters for PID tuning are the following performance measures [1]:

- ϕ_M and G_M: phase and gain margins, respectively,
- M_s and M_t: maximum peaks of magnitudes of the sensitivity function S(jω) and complementary sensitivity function T(jω), respectively,
- λ: required closed-loop time constant.

If a designed controller $G_R(j\omega)$ guarantees, that $|S(j\omega)|$ or $|T(j\omega)|$ do not exceed prespecified values M_s or M_t, respectively, defined by

$$M_s = \sup_{\omega} |S(j\omega)| = \sup_{\omega} \left| \frac{1}{1 + L(j\omega)} \right|; \quad M_t = \sup_{\omega} |T(j\omega)| = \sup_{\omega} \left| \frac{L(j\omega)}{1 + L(j\omega)} \right| \tag{6}$$

for $\omega \in \langle 0,\infty)$, then the Nyquist plot of the open-loop transfer function $L(s) = G(s)G_R(s)$ avoids the respective circles M_S or M_T each given by its center and radius as follows:

$$C_S = [-1, j0], R_S = \frac{1}{M_s}; C_T = \left[-\frac{M_t^2}{M_t^2 - 1}, j0 \right], R_T = -\frac{M_t}{|1 - M_t^2|}. \tag{7}$$

By avoiding the Nyquist plot of L(s) to enter the circles corresponding to M_S or M_T, a safe distance from the critical point is kept (**Figure 3a**). Typical $|S(j\omega)|$ and $|T(j\omega)|$ plots for properly designed controller are in **Figure 3b**. The disturbance d(t) is sufficiently rejected if

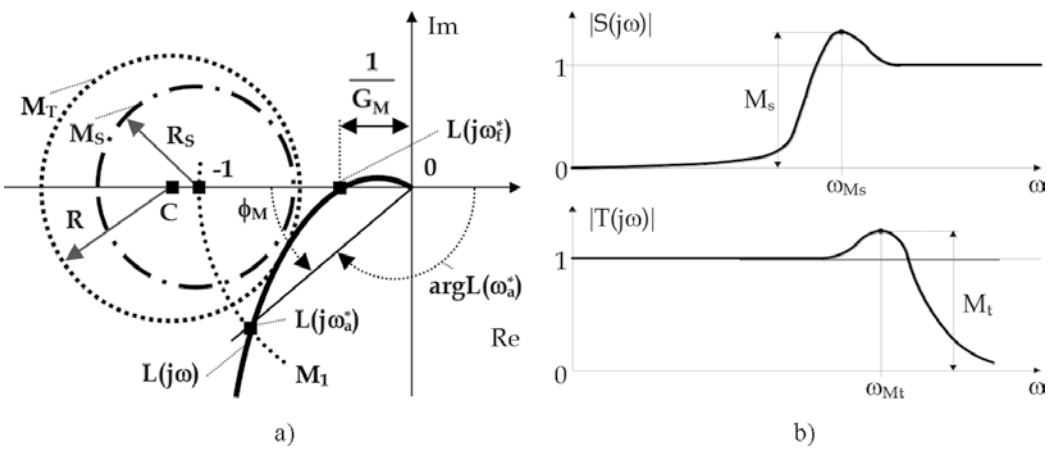

Figure 3. (a) Definition and geometrical interpretation of ϕ_M and G_M in the complex plane; (b) sensitivity and complementary sensitivity magnitudes $|S(j\omega)|$, $|T(j\omega)|$ and performance measures M_s, M_t.

$M_s \in (1.2;2)$. The reference w(t) is properly tracked by the process output y(t) if $M_t \in (1.3;2.5)$. With further increasing of M_t the closed-loop tends to be oscillatory.

From **Figure 3a** results, that by increasing open-loop phase margin ϕ_M the gain crossover $L(j\omega_a^*)$ on the unit circle M_1 moves away from the critical point $(-1,j0)$; similarly by increasing open-loop gain margin G_M the phase crossover $L(j\omega_f^*)$ moves away from $(-1,j0)$. Therefore, the stability margins ϕ_M or G_M given by

$$\varphi_M = 180^\circ + \arg L(\omega_a^*); \quad G_M = \frac{1}{\left|L\left(j\omega_f^*\right)\right|} \tag{8}$$

are frequently used performance measures, their typical values are $\phi_M \in (20^\circ;90^\circ)$, $G_M \in (2;5)$. Relations between individual stability margins and respective magnitude peaks are given by the following inequalities

$$\varphi_M \geq 2\arcsin\left(\frac{1}{2M_s}\right); \quad \varphi_M \geq 2\arcsin\left(\frac{1}{2M_t}\right); \quad G_M \geq \frac{M_s}{M_s - 1}; \quad G_M \geq 1 + \frac{1}{M_t}. \tag{9}$$

The point in which the Nyquist plot $L(j\omega)$ touches the M_T circle defines the closed-loop resonance frequency ω_{Mt}.

2.3. PID controller design methodologies for performance

When synthesizing a control loop, if the controller type is already known and the designer has just to select a suitable method to appropriately adjust its coefficients, we speak about *PID controller tuning methods*. *Controller design* is a more complex problem which includes determining controller structure and then calculating its parameters. When setting coefficients of industrial PID controllers $\{K, T_i, T_d\}$, basically the following procedures are applied:

1. *Trial-and-error methods* are based on closed-loop experiments [1]. Controller parameters settings are based on observation of the response to reference or disturbance changes with the assistance of an expert, or the design is driven by empirical rules. The control-loop synthesis is time-consuming and its success is not guaranteed.

2. *Analytical methods* are used to generate a control law based on the mathematical model of the plant; the plant model is obtained from first principles or via experimental identification. The success of these methods depends on the accuracy of the mathematical model of the plant, and is not always achievable in practical cases (e.g., for a cement kiln).

3. *Classical tuning* methods use only a limited number of characteristic parameters of the plant obtained from the step response or critical system parameters [11, 27, 31]. Their main advantage is a simple and short calculation of controller parameters. The control objective is to provide a satisfactory response to reference change, or disturbance rejection and often their combination. The main drawback is that the designer cannot influence the performance by means of the adjustable parameters of the algorithm. Also, the resulting closed-loop response may not be satisfactory if the step response of the plant is nonmonotonic, or

when the plant has nonminimum-phase dynamics or large time delay. Most of these methods are implemented in autotuners of industrial PID controllers [1].

4. *Autotuners* are a modern and convenient means for adjusting coefficients of industrial controllers [33, 34, 49]. They implement a two-step algorithm of automatic acquisition of characteristic parameters of the controlled process followed by automatic calculation and adjustment of the controller coefficients. After activating the autotuning function on the industrial controller, the control-loop synthesis is performed automatically in a very short time. The ABB, Emerson, Fischer-Rosemont, Foxboro, Honeywell, Siemens, Yokogava, or ZPA controllers have a built-in PID autotuning function implemented on a microcomputer [47]. In many situations, however, these methods are unreliable because of the imperfection of the plant identification algorithm and the subsequent controller design.

5. *Robust PID controller tuning methods for specified performance* represent a modern area of industrial control-loop synthesis. They improve the PID tuning methods by providing stability and required performance also for processes with variable parameters. The controller tuned only by conventional method is just "intuitively" invariant against perturbations of the controlled plant; robust operation of the control loop is usually possible only for small changes of plant parameters. The major disadvantage of these methods is that the control law is not based on the knowledge of uncertainties of the controlled object and a further research on their possible expansion is needed. The proposed original method which eliminates this drawback, its theoretical analysis and verification on benchmark examples are the core of the chapter.

2.4. PID controller tuning methods for performance

Tuning methods are commonly used engineering tool for the synthesis of industrial control loops as they do not require a full knowledge of the mathematical description of the controlled plant. This differentiates them from analytical methods which, on the contrary are based on a precise knowledge of the mathematical model of the controlled system. In the tuning methods, the controlled process is considered as a black-box ① which is to be revealed only to such extent that the controller synthesis is successful and the control objectives ② are achieved. Thus, only those characteristic parameters ③ of the unknown plant have to be acquired via appropriate identification ④ that are inevitable for the PID controller design. In this way, the PID controller ⑤ coefficients can be obtained in a relatively short time. The implicit knowledge about the controlled system ⑥ and the ambient influences affect the choice of the PID coefficients calculation method ⑦. According to the way of using the identified data of the controlled plant, the tuning methods are classified into as follows:

a. model-free PID controller tuning methods,

b. model-based PID controller tuning methods.

Percentage proportions of commonly used PID controller tuning methods are presented in **Figure 4**.

Approximately 12% out of all tuning methods are model-free methods, 88% (app. seven times more) are model-based ones. A 37% portion belongs to PID controllers of FOLPDT (first order

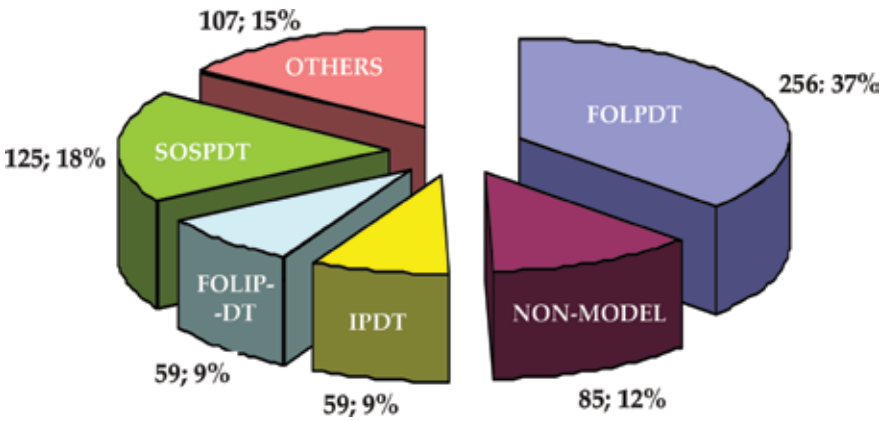

Figure 4. Percentages of commonly used PID controller tuning methods.

lag plus dead time) system models which are the most commonly used approximation of plant dynamics in industries (thermal plants, chemical and woodworking industries). Equal 9% shares belong to IPDT (integral plus dead time) and FOLIPDT (first order lag integral plus dead time) models with integral behavior encountered mainly in drives and power industry in modeling mechanical subsystems of rotating machines, valves and servo-systems and 18% of algorithms are used to control plants with SOSPDT (second order system plus dead time) models [26]. Controllers for other system types are tuned by methods from the 15% portion.

2.4.1. Model-free PID controller tuning with guaranteed performance

There are such PID tuning algorithms, which can be applied without any knowledge about the unknown plant model. These methods yielding PID coefficients for systems with a general, unknown model are known as "Non-Model Specific", "Model-Free" or "Rule-Based" Methods. Their basic feature is that the identified characteristic parameters of the unknown system appear directly in the PID coefficient tuning rules. They are very popular among practitioners due to a high flexibility and ability to control a wide class of systems. The respective algorithms have been tested on benchmark examples, the control objectives can be expressed by empirical rules. They are simply algorithmizable for application in industrial autotuners. A seven-step flow diagram of a direct tuning method is depicted in **Figure 5**.

The oldest direct-type engineering method is the well-known Ziegler-Nichols frequency method (1942) [48]. The control objective ⑦ is a rapid disturbance rejection so that each amplitude of the oscillatory response to disturbance step change is only a quarter of the previous amplitude. The method is based on two identified ② characteristic parameters ① of the unknown plant : the critical frequency $\omega_c = 2\pi/T_c$ and the critical gain K_c used for calculation of the coefficients of P, PI and PID controllers ⑦. The first characteristic parameter provides basic information on plant dynamics, while the value of the second parameter indicates the degree-of-stability of the plant. PID controller parameters according to the Ziegler-Nichols method are calculated using the algorithm ⑥ $P_{ZN} = 0.6K_c$, $T_{iZN} = 0.5T_c = \pi/\omega_c$, $T_{dZN} = 0.125T_c = 0.25\pi/\omega_c$, in which the characteristic parameters $\{K_c, \omega_c\}$ are directly included.

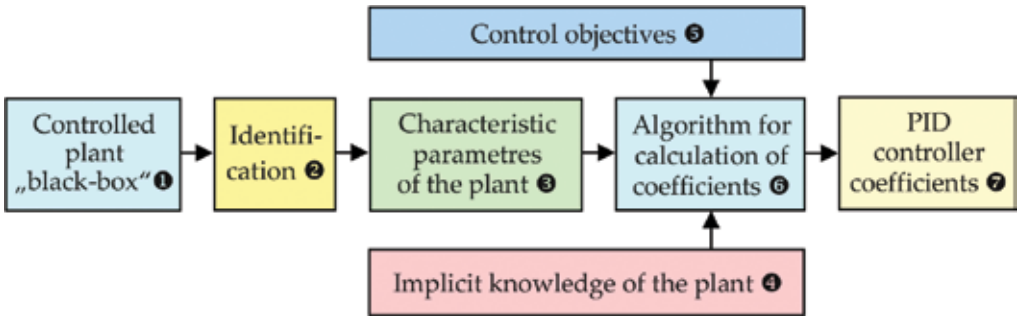

Figure 5. Flow chart of the direct engineering PID tuning method.

2.4.1.1. Trial-and-error tuning methods

When first PID controllers were developed in the period 1935–1942, no tuning methods were available at the market. The controller "design" consisted in experimenting with control loops without considering any relationship between plant parameters and controller coefficients. Acquired experience, however, was generalized giving rise to empirical trial-and-error tuning method that consist of three main steps:

1. Turning off the integral and derivative parts of the PID controller and increasing the gain until the closed-loop oscillates with constant amplitudes, then adjusting the gain at half of this value.
2. Decreasing the integral time until oscillations with constant amplitude are obtained, then adjusting the integral time at a treble of this value.
3. Increasing the derivative time until oscillations with constant amplitude are obtained, then adjusting the derivative time at a third of this value.

The set of these rules of thumb is still being used in practice to roughly tune industrial PID controllers and is considered as a predecessor of all engineering tuning methods. In 1942, two direct tuning methods were published and authored by Ziegler and Nichols [48], employees of the Taylor Instrument Companies producing PID controllers. The first one is *time-domain method*; according to it, the PID coefficients are calculated using the effective time delay and the effective time constant of the step response of the industrial plant. The *frequency-domain* method uses the critical gain K_c and the period of critical oscillations T_c to calculate the PID coefficients according to the relations $\Theta_{PID} = (P, T_i, T_d) = (\alpha_1 K_c, \alpha_2 T_c, \alpha_3 T_c)$, where the weights of critical parameters are $(\alpha_1, \alpha_2, \alpha_3) = (0.6, 0.5, 0.125)$.

2.4.1.2. Tuning rules based on ultimate parameters of the industrial process

Due to its simplicity, the Ziegler-Nichols frequency-domain methods are still used in industrial autotuners in the original version, although they have undergone various modifications during the last 70 years of its existence. Due to the technological development after the industrial revolution and major electrification, PID tuning for stability was no more sufficient because a fast setpoint attainment could bring about important savings of time and money and

accelerate the entire production process. More and more demanding requirements on control performance were formulated, and an intense demand for effective tuning methods guaranteeing required performance has arisen.

As a rule, application of Ziegler-Nichols methods usually leads to oscillatory closed-loop responses; hence, many scientists have become interested in their possible improvement. Forty-two modifications of the Ziegler-Nichols frequency method were developed in the period from 1967 to 2010. They differ from the classical algorithm in using various other combinations of the weights (α_1, α_2, α_3). An overview of selected model-free methods is given in **Table 2**.

Tuning rules No. 1–3 are the well-known Ziegler-Nichols frequency-domain method which objective is a fast rejection of the disturbance d(t) and δ_{DR} = 1:4. In the complex plane interpretation (**Figure 6**), the method corresponds to shifting the critical point C = [−1/K_c + j0], into the points C_P = [−0.5 + j0], C_{PI} = [−0.45 + j0.0896] and C_{PID} = [−0.6-j0.28] using respectively P, PI and PID controllers tuned according to **Table 2**. Put simply, the open-loop Nyquist plot is shaped into a sufficient distance from the limit of instability specified by the point (−1.j0).

No.	Design method, year	Controller	K	T_i	T_d	Performance
1.	Ziegler and Nichols, 1942 [48]	P	$0.5K_c$	—	—	Quarter decay ratio
2.	Ziegler and Nichols, 1942 [48]	PI	$0.45K_c$	$0.8T_c$	—	Quarter decay ratio
3.	Ziegler and Nichols, 1942 [48]	PID	$0.6K_c$	$0.5T_c$	$0.125T_c$	Quarter decay ratio
4.	Pettit and Carr, 1987 [27]	PID	K_c	$0.5T_c$	$0.125T_c$	Underdamped
5.	Pettit and Carr, 1987 [27]	PID	$0.67K_c$	T_c	$0.167T_c$	Critically damped
6.	Pettit and Carr, 1987 [27]	PID	$0.5K_c$	$1.5T_c$	$0.167T_c$	Overdamped
7.	Chau, 2002 [16]	PID	$0.33K_c$	$0.5T_c$	$0.333T_c$	Small overshoot
8.	Chau, 2002 [16]	PID	$0.2K_c$	$0.55T_c$	$0.333T_c$	No overshoot
9.	Bucz, 2011 [6]	PID	$0.54K_c$	$0.79T_c$	$0.199T_c$	Overshoot $\eta_{max} \leq 20\%$
10.	Bucz, 2011 [6]	PID	$0.28K_c$	$1.44T_c$	$0.359T_c$	Settling time $t_s \leq 13/\omega_c$

Table 2. Model-free PID controller tuning rules based on critical plant parameters.

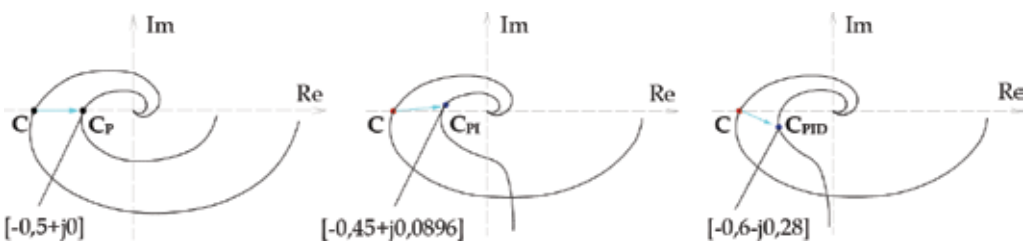

Figure 6. Moving the critical point C = [−1/K_c + j0] of the plant using P, PI and PID controllers designed by Ziegler-Nichols frequency-domain method for critical frequency ω_c of the plant.

Related methods (No. 4–10) use various weighting of critical parameters thus allowing to vary the closed-loop performance requirements (see the last column in **Table 2**). All presented methods (No. 1–10) are applicable for various plant types, easy-to-use and time efficient.

2.4.1.3. Specification of critical parameters of the plant using relay experiment

In autotuners of industrial controllers, a relay test [29] using an ideal relay (IR) or a hysteresis relay (HR) is used to quickly determine the plant critical parameters K_c and T_c. In the manual mode, after setting the nominal setpoint w(t) and switching the SW to position "3", a stable limit cycle around the nominal working point y(t) arises in the control loop in **Figure 1**. As a result of switching between the −M, +M relay levels, the controlled system G(s) is excited by a rectangular periodic signal u(t) (**Figure 7a**). The critical frequency ω_c and the critical gain K_c are calculated as follows:

$$\omega_c = \frac{2\pi}{T_c}; \quad K_{c\_IR} = \frac{4M}{\pi A_c}; \quad K_{c\_HR} = \frac{4(M - 0.5\Delta_{DB})}{\pi A_c}, \tag{10}$$

where the period T_c and the amplitude A_c of critical oscillations are read off from y(t) of the recorded limit cycle (**Figure 7b**); Δ_{DB} is the width of the hysteresis plot, the relay amplitude M is chosen as (3÷10)% of the control u(t) limits. A typical limit cycle is depicted in **Figure 7b**. A hysteresis relay is used if y(t) corrupted by a noise n(t) [47].

The advantage of these methods is their applicability for different types of systems, simplicity and the short time needed for the controller design of the—approx. (3÷4)T_c.

2.4.2. Model-based PID controller tuning with guaranteed performance

In these methods, the identified characteristics of the unknown system are used to create its typical model, and the controller design algorithm is derived for this particular model. Formulas for calculation of the controller coefficients include process model parameters that are function of the identified process data. Each method works perfectly for the system whose model has been used in the design algorithm. However, if the system is approximated differently, the achieved performance may be impaired or even insufficient. The advantage is that control objectives can be clearly defined and expressed using analytical relationships (e.g., it is possible to derive the relationship for maximum overshoot of the step response). A small flexibility due to the "tailor-made" design for one type of model limits the widespread application of these methods in autotuners of industrial controllers.

PID tuning algorithms of indirect tuning methods have two more steps compared with direct methods, as shown in the flow chart in **Figure 8**. When choosing the procedure for creating a

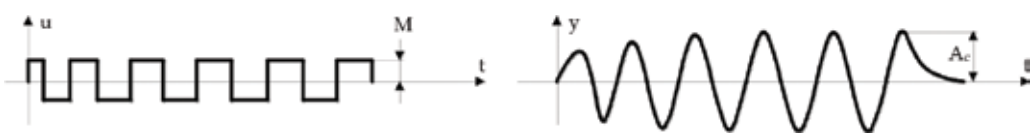

Figure 7. Determination of critical parameters K_c and T_c of the controlled plant from the limit cycle.

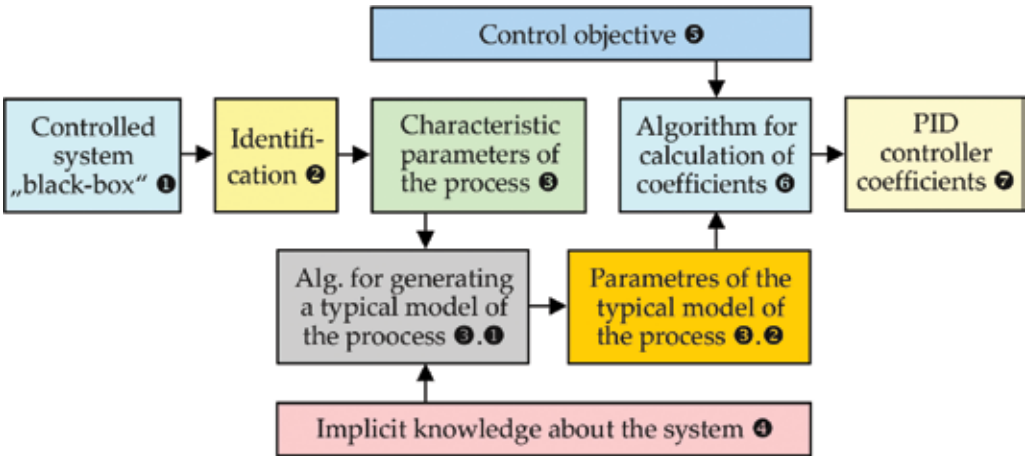

Figure 8. Flow chart of the indirect engineering method for PID tuning.

typical model ③.①, it is important how the implicit information about the controlled system is considered (if we deal with a driving system, a thermal process, a mechanical or pneumatic system, etc.). If the typical model for the given controlled system has already been selected, the model parameters are calculated in step ③.② and subsequently used in calculation of the PID coefficients.

2.4.2.1. Specification of FOLPDT, IPDT and FOLIPDT plant model parameters

The static and dynamic properties of most technological processes can be expressed by one of the FOLPDT, IPDT, FOLIPDT, or SOSPDT models. Model parameters are identified from the recorded step response of the controlled system (**Figure 9**) and are further used in calculation of PID controller coefficients. According to **Figure 1**, step response of the controlled process is obtained by switching SW into position "2" and performing step change in u(t).

Transfer functions of the model are found from the step response parameters according to **Figure 9**.

$$G_{FOLPDT}(s) = \frac{K_1 e^{-D_1 s}}{T_1 s + 1}; \quad G_{IPDT}(s) = \frac{K_2 e^{-D_2 s}}{s}; \quad G_{FOLIPDT}(s) = \frac{K_3 e^{-D_3 s}}{s(T_3 s + 1)}. \tag{11}$$

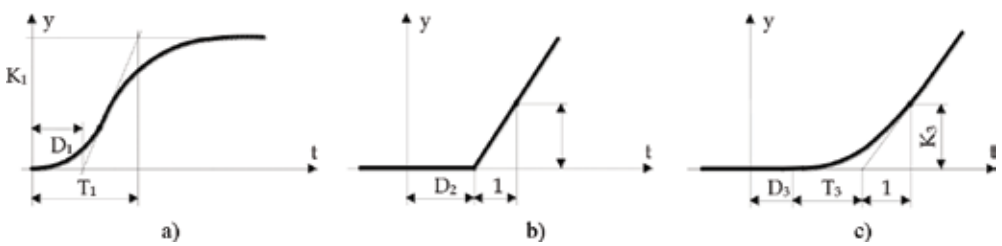

Figure 9. Typical step responses of (a) FOLPDT; (b) IPDT and (c) FOLIPDT models.

No.	Design method, year, control purpose	Controller	K	T_i	T_d	Performance
11.	Ziegler and Nichols, 1942 [48]	P	$1/\vartheta_1$	—	—	Quarter decay ratio
12.	Ziegler and Nichols, 1942 [48]	PI	$0.9/\vartheta_1$	$3D_1$	—	
13.	Ziegler and Nichols, 1942 [48]	PID	$1.2/\vartheta_1$	$2D_1$	$0.5D_1$	
14.	Chien et al., 1952, regulator tuning [18]	PI	$0.6/\kappa_1$	$4D_1$	—	η_{max} = 0%, $D_1/T_1 \in (0.1;1)$
15.	Chien et al., 1952, regulator tuning [18]	PID	$0.95/\vartheta_1$	$2.38D_1$	$0.42D_1$	
16.	Chien et al., 1952, regulator tuning [18]	PI	$0.77/\vartheta_1$	$2.33D_1$	—	η_{max} = 20%, $D_1/T_1 \in (0.1;1)$
17.	Chien et al., 1952, regulator tuning [18]	PID	$1.2/\vartheta_1$	$2D_1$	$0.42D_1$	
18.	Chien et al., 1952, servo tuning [18]	PI	$0.35/\vartheta_1$	$1.17D_1$	—	η_{max} = 0%, $D_1/T_1 \in (0.1;1)$
19.	Chien et al., 1952, servo tuning [18]	PID	$0.6/\vartheta_1$	D_1	$0.5D_1$	
20.	Chien et al., 1952, servo tuning [18]	PI	$0.6/\vartheta_1$	D_1	—	η_{max} = 20%, $D_1/T_1 \in (0.1;1)$
21.	Chien et al., 1952, servo tuning [18]	PID	$0.95/\vartheta_1$	$1.36D_1$	$0.47D_1$	
22.	ControlSoft Inc., 2005 [23]	PID	$2/K_1$	$T_1 + D_1$	$\max(D_1/3;T_1/6)$	Slow loop
23.	ControlSoft Inc., 2005 [23]	PID	$2/K_1$	$T_1 + D_1$	$\min(D_1/3;T_1/6)$	Fast loop

Table 3. PID tuning rules based on FOPDT model, $\vartheta_1 = K_1D_1/T_1$ is the normalized process gain.

2.4.2.2. PID controller tuning formulas for FOLPDT models

The FOPDT model (11a) is used to approximate dynamics of chemical processes, thermal plants, production processes, and so on. To calculate the P, PI and PID controller, coefficients based on the parameters of the FOLPDT model of the controlled system, the tuning formulas in **Table 3** can be used.

2.4.2.3. PID controller tuning formulas for IPDT and FOLIPDT models

While dynamics of slow technological processes (polymer production, heat exchange, etc.) can be approximated by an IPDT model (11b), electromechanical subsystem of rotating machines and servo drive objects are typical examples for using a FOLIPTD model [42] (11c) (**Table 4**).

The gain K in the rule No. 27 is variable with respect to the normalized time delay $\upsilon_3 = D_3/T_3$ of the FOLIPDT model; for the corresponding pairs holds: $(\upsilon_3;x_3)$ = {(0.02;5), (0.053;4); (0.11;3); (0.25;2.2); (0.43;1.7); (1;1.3); (4;1.1)}.

No.	Design method, year, model	Controller	K	T_i	T_d	Performance
24.	Haalman, 1965, IPDT model [12]	P	$0.66/(K_2D_2)$	—	—	M_s = 1.9
25.	Ziegler and Nichols, 1942, IPDT model [48]	PI	$0.9/(K_2D_2)$	$3.33D_2$	—	Quarter decay ratio
26.	Ford, 1953, IPDT model [10]	PID	$1.48/(K_2D_2)$	$2D_2$	$0.37D_2$	Decay ratio 1:2.7
27.	Coon, 1956, FOLIPDT model [8]	P	$\frac{x_3}{K_3(T_3+D_3)}$	—	—	Quarter decay ratio
28.	Haalman, 1965, FOLIPDT model [12]	PD	$0.66/(K_3D_3)$	—	T_3	M_s = 1.9

Table 4. PID tuning rules based on IPDT and FOLIPDT model parameters.

2.4.2.4. PID controller tuning formulas for SOSPDT plant models

Flexible systems in wood processing industry, automotive industry, robotics, shocks and vibrations damping are often modeled by SOSPDT models with transfer functions

$$G_{SOSPDT}(s) = \frac{K_4 e^{-D_4 s}}{(T_4 s + 1)(T_5 s + 1)}; \quad G_{SOSPDT}(s) = \frac{K_6 e^{-D_6 s}}{T_6^2 s^2 + 2\xi_6 T_6 s + 1}, \tag{12}$$

where for SOSPDT model (12b) the relative damping $\xi_6 \in (0;1)$ indicates oscillatory step response.

If $\xi_4 > 1$, SOSPDT model (12a) is used; its parameters are found from the nonoscillatory step response in **Figure 10a** using the following relations

$$T_{4.5} = \frac{1}{2}\left(C_2 \pm \sqrt{C_2^2 - 4C_1^2}\right); \quad D_4 = \frac{t_{0.33}}{0.516} - \frac{t_{0.7}}{1.067}; \quad C_1 = \frac{(t_{0.33} - t_{0.7})}{1.529}; \quad C_2 = \frac{S}{y(\infty)}, \tag{13}$$

where $S = K_4(T_4 + T_5 + D_4)$ is the area above the step response of the process output y(t), and y(∞) is its steady-state value.

Parameters of the SOSPDT model (12b) can be found from evaluation of 2–4 periods of step response oscillations (**Figure 10b**) using following rules [39]

$$\xi_6 = \frac{-\ln \frac{a_{i+1}}{a_i}}{\sqrt{\pi^2 + \ln^2 \frac{a_{i+1}}{a_i}}}; \quad T_6 = \frac{\sqrt{1 - \zeta_6^2}}{\pi N}(t_{N+1} - t_1); \quad D_6 = \frac{1}{N}\left[\sum_{i=1}^{N} t_i - \frac{N+1}{2}(t_{N+1} - t_1)\right]. \tag{14}$$

Quality of identification improves with increasing number N of read-off amplitudes. If N > 2 several values ξ_6, T_6 and D_6 are obtained, and their average is taken for further calculations. **Table 5** summarizes useful tuning formulas for both oscillatory and nonoscillatory systems with SOSPDT model properties.

Using tuning methods shown in **Tables 2–5**, achieved performance is a priori given by the particular method (e.g., quarter decay ratio when using Ziegler-Nichols methods No. 11–13 in **Table 3**) or guarantees performance however not specified by the designer (e.g., in Chen

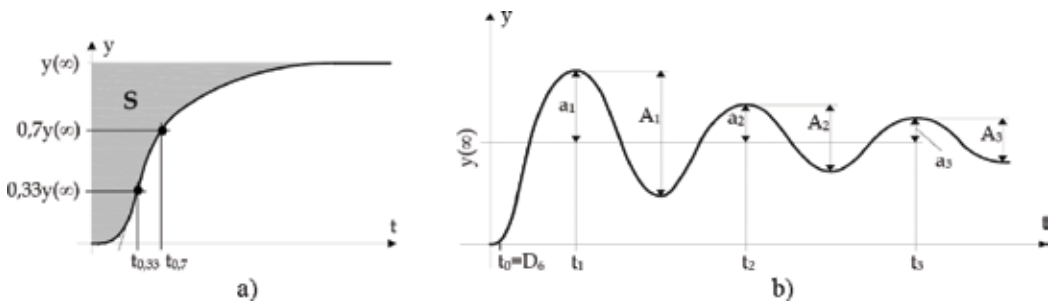

Figure 10. Step response of (a) nonoscillatory, (b) oscillatory SOSPDT model.

No.	Method, year	Controller	K	T_i	T_d	Performance for
29.	Suyama, 1992 [30]	PID	$\frac{T_4+T_5}{2K_4D_4}$	$T_4 + T_5$	$\frac{T_4T_5}{T_4+T_5}$	Closed-loop step response overshoot $\eta_{max} = 10\%$
30.	Vítečková, (1999) [40], Vítečková et al. (2000) [41]	PID	$x_4 \frac{T_4+T_5}{K_4D_4}$	$T_4 + T_5$	$\frac{T_4T_5}{T_4+T_5}$	Overdamped plants; $T_5 > T_4$ $\eta_{max} = 0\%$: $x_4 = 0.368$; $\eta_{max} = 30\%$: $x_4 = 0.801$
31.	Vítečková, (1999) [40], Vítečková et al. (2000) [41]	PID	$\frac{x_6\zeta_6T_6}{K_6D_6}$	$2\zeta_6T_6$	$\frac{T_6}{2\zeta_6}$	Underdamped plants ($0.5<\xi_6\leq1$) $\eta_{max} = 0\%$: $x_6 = 0.736$; $\eta_{max} = 30\%$: $x_6 = 1.602$
32.	Wang and Shao (1999) [43]	PID	$\frac{x_6\zeta_6T_6}{K_6D_6}$	$2\xi_6T_6$	$\frac{T_6}{2\xi_6}$	$[G_M = 2, \phi_M = 45°]$: $x_6 = 1.571$ $[G_M = 5, \phi_M = 72°]$: $x_6 = 0.628$
33.	Chen et al., 1999 [17]	PID	$\frac{x_6\zeta_6T_6}{K_6D_6}$	$2\xi_6T_6$	$\frac{D_6}{2\xi_6}$	$[G_M;\phi_M;M_s] = [3.14;61.4°;1]$: $x_6 = 1.0$ $[G_M;\phi_M;M_s] = [1.96;44.1°;1.5]$: $x_6 = 1.6$

Table 5. Tuning rules based on SOSPDT model parameters.

No.	Method, year	K	T_i	T_d	T_f	Performance
34.	Visioli, 2001, Regulator tuning [36]	$1.37\nu_1/K_1$	$2.42T_1\nu_1^{1.18}$	$0.60T_1$	—	Minimum ISE
35.	Visioli, 2001, Regulator tuning [36]	$1.37\nu_1/K_1$	$4.12T_1\nu_1^{0.90}$	$0.55T_1$	—	Minimum ISTE
36.	Visioli, 2001, Regulator tuning [36]	$1.70\nu_1/K_1$	$4.52T_1\nu_1^{1.13}$	$0.50T_1$	—	Minimum IST^2E
37.	Chandrashekar et al., 2002 [15]	$10.3662/K_1$	$0.3874T_1$	$0.0435T_1$	$0.0134T_1$	$t_s = 0.1\ T_1$: $\nu_1 = 0.1$
38.	Chandrashekar et al., 2002 [15]	$2.0217/K_1$	$4.65T_1$	$0.2366T_1$	$0.0696T_1$	$t_s = 0.8\ T_1$: $\nu_1 = 0.5$

Table 6. Tuning rules for unstable FOPDT model.

method No. 33 in **Table 5** gain margin $G_M = 1.96$, phase margin $\phi_M = 44.1°$ and maximum peak $M_s = 1.5$ of the sensitivity to disturbance d(t)).

2.4.2.5. PID controller tuning formulas for unstable FOLPDT models

Minimization of performance indices can be applied also for unstable FOLPDT models

$$G_{FOLPDT\_US}(s) = \frac{K_1 e^{-D_1 s}}{T_1 s - 1} \tag{15}$$

leading to simple tuning rules for PID controller (1a) (No. 34–38 in **Table 6**). Tuning rules No. 37 and 38 for PID controller (1c) show that settling time t_s increases with growing normalized time delay $\nu_1 = D_1/T_1$ of the FOLPDT model (15).

2.5. PID controller design for specified performance

The main benefit of these methods consists of that all tuning rules are based on a single tuning parameter that enables to systematically affect the closed-loop performance by step response shaping [32].

No.	Design method, year, model	K	T_i	T_d
39.	Hang and Åström, 1988, Nonmodel [13]	$K_c \sin\varphi_M$	$\frac{T_c(1-\cos\varphi_M)}{\pi\sin\varphi_M}$	$\frac{T_c(1-\cos\varphi_M)}{4\pi\sin\varphi_M}$
40.	Rotach, 1994, Nonmodel [28]	$\frac{M_t\lvert G(j\omega_{Mt})\rvert}{\sqrt{M_t^2-1}}$	$\frac{-2}{\omega_{Mt}^2\left(\frac{d[\arg G(\omega_{Mt})]}{d\omega_{Mt}}\right)}$	$-\frac{1}{2}\frac{d[\arg G(\omega_{Mt})]}{d\omega_{Mt}}$
41.	Wojsznis et al., 1999, FOPDT [45]	$\frac{K_c\cos\varphi_M}{G_M}$	$\frac{T_c}{\pi}\left(tg\,\varphi_M+\sqrt{1+tg^2\varphi_M}\right)$	$\frac{T_c}{4\pi}\left(tg\,\varphi_M+\sqrt{1+tg^2\varphi_M}\right)$
42.	Morari and Zafiriou, 1989, FOPDT [22]	$\frac{T_1+0,5D_1}{K_1(\lambda+D_1)}$	$T_1+\frac{1}{2}D_1$	$\frac{T_1D_1}{2T_1+D_1}$
43.	Chen and Seborg, 2002, FOPDT [17]	$\frac{T_1^2+T_1D_1-(\lambda-T_1)^2}{(\lambda+L)^2}$	$\frac{T_1^2+T_1D_1-(\lambda-T_1)^2}{T_1+L_1}$	-

Table 7. PID design for specified performance based on tuning parameters ϕ_M, G_M, M_t and λ.

2.5.1. PID controller tuning formulas with performance specification

Table 7 shows open formulas for PID controller design; their tuning is carried out with respect to closed-loop performance specification.

Rules No. 39–43 consider tuning of ideal PID controller (1a). To apply the Rotach method [29], knowledge of the plant magnitude $|G(j\omega)|$ is supposed as well as of the roll-off of the phase plot $\arg G(\omega)$ at $\omega = \omega_{Mt}$, where the maximum peak M_t of the complementary sensitivity is required. Method No. 42 is based on the so-called λ-tuning, where the resulting closed-loop is expressed as a 1st order system with time constant λ; this rule considers real PID controller (1b) with filtering constant in the derivative part $T_f = 0.5\lambda D_1/(1 + D_1)$, where λ is to be chosen so as to meet following conditions: $\lambda > 0.25D_1$; $\lambda > 0.25T_1$ [22]. The λ-tuning technique is used also in the rule No. 43 to design interaction PI controller.

2.5.2. Closed-loop performance evaluation under PID controller tuning

Phase margin ϕ_M is the most widespread performance measure in PID controller design. Maximum overshoot η_{max} and settling time t_s of the closed-loop step response are related with ϕ_M according to Reinisch relations

$$\eta_{\max} = \begin{cases} -0.91\varphi_M + 64.55 & for\ \ \varphi_M \in \langle 38^\circ, 71^\circ \rangle \\ -1.53\varphi_M + 88.46 & for\ \ \varphi_M \in \langle 12^\circ, 38^\circ \rangle \end{cases}; \quad \eta_{\max} = 100e^{-2\pi b^2 M_t}; \quad t_s \in \left(\frac{\pi}{\omega_a^*}, \frac{4\pi}{\omega_a^*}\right) \tag{16}$$

valid for second-order closed-loop with relative damping $\omega_a^* \in (0.25;0.65)$ where ω_a^* is the gain crossover frequency [14]. Relations

$$\eta_{\max} \le 100\frac{1.18M_t - |T(0)|}{|T(0)|}[\%]; \quad t_s \approx \frac{3}{\omega_a^*}\ for M_t \in (1.3, 1.5) \tag{17}$$

are general for any order of the closed-loop T(s); if the controller has the integral part then $|T(0)| = |T(\omega = 0)| = 1$ [14].

The engineering practice is persistently demanding for PID controller design methods that simultaneously guarantee several performance criteria [24], especially the maximum

overshoot η_{max} and the settling time t_s. However, we ask the question: how to suitably transform the abovementioned engineering requirements into frequency-domain specifications applicable for PID controller coefficients tuning? The response can be found in Section 3 in which a novel original PID controller design method is presented.

3. PID controller design for specified performance based on harmonic excitation

The proposed original method [6] enables to guarantee required closed-loop performance for a whole family of plants specified by the uncertainty description. The core of it is the recently developed PID controller design method based on external harmonic excitation [7]—a two-step PID tuning method for performance specified in terms of maximum overshoot η_{max} and settling time t_s.

In the first step, the plant is identified using external harmonic excitation signal (a sinusoid) with the frequency ω_n. In the second step, two developed PID controller design approaches can be applied:

1. the approach based on guaranteed phase margin ϕ_M suitable for nonintegrating systems with/without time delay and for integrating systems as well;
2. the approach based on guaranteed gain margin G_M suitable for nonintegrating systems with unstable zero.

For the ϕ_M–based approach, the specified performance is achieved by means of developed quadratic dependences $\eta_{max} = f(\phi_M,\omega_n)$ and $t_s = f(\phi_M,\omega_n)$ parameterized by ω_n; the corresponding plots are called B-parabolas. For the G_M–based approach similar quadratic dependences for both the maximum overshoot $\eta_{max} = f(G_M,\omega_n)$ and the settling time $t_s = f(G_M,\omega_n)$ were constructed. These approaches enable to achieve fulfillment of the following performance measures (ω_c is the plant ultimate frequency):

- for plants without integration behavior: $\eta_{max} \in \langle 0\%, 90\% \rangle$ and $t_s \in \langle 6.5/\omega_c, 45/\omega_c \rangle$,
- for plants with integration behavior: $\eta_{max} \in \langle 9.5\%, 90\% \rangle$ and $t_s \in \langle 11.5/\omega_c, 45/\omega_c \rangle$,
- for plants with unstable zero: $\eta_{max} \in \langle 0\%, 90\% \rangle$ and $t_s \in \langle 8.5/\omega_c, 45/\omega_c \rangle$.

A setup for the proposed harmonic excitation based method [7] is in **Figure 11**, where G(s) is a transfer function of the controlled plant with unknown mathematical model, $G_R(s)$ is a PID controller transfer function, and SW is a switch.

3.1. Process identification using external harmonic excitation

A sinusoidal excitation signal $u(t) = U_n \sin(\omega_n t)$ is injected into the plant G(s) when the switch is in the position SW = 4. The plant output y(t) is sinusoidal as well with the same frequency ω_n, magnitude Y_n and a phase lag φ, that is $y(t) = Y_n \sin(\omega_n t + \varphi)$, where $\varphi = \arg G(\omega_n)$ (**Figure 12**).

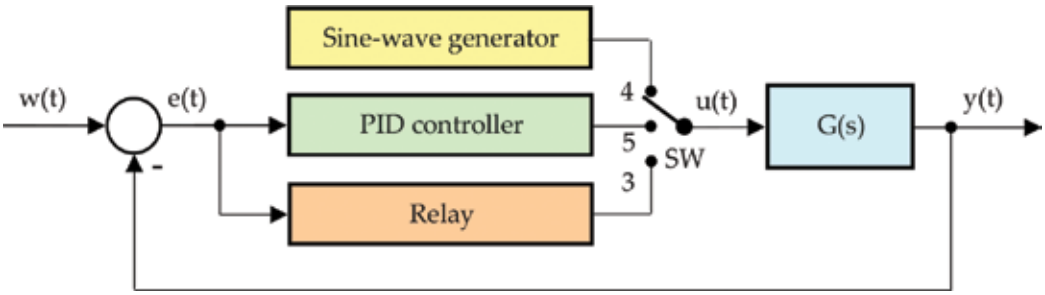

Figure 11. A setup for implementation of the external harmonic excitation based method.

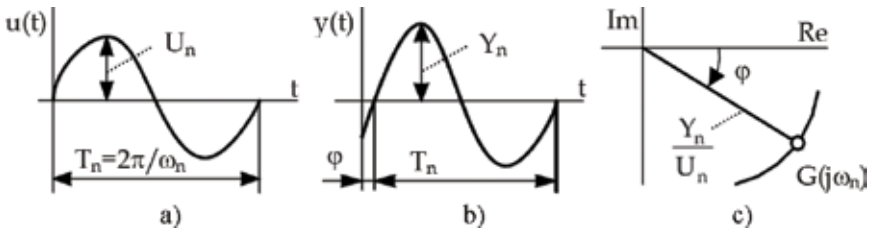

Figure 12. Time responses of (a) u(t); (b) y(t), and (c) location of $G(j\omega_n)$ in the complex plane.

After obtaining Y_n and φ from the recorded time responses u(t) and y(t), one point of the (unknown) plant frequency characteristics related with the excitation frequency ω_n can be plotted in the complex plane (**Figure 12**)

$$G(j\omega_n) = |G(j\omega_n)|e^{j\arg G(\omega_n)} = \frac{Y_n(\omega_n)}{U_n(\omega_n)}e^{j\varphi(\omega_n)}. \tag{18}$$

It is recommended to choose $U_n = (3\div7)\%u_{max}$ [7]. Identified plant parameters are described by the triple $\{\omega_n, Y_n/U_n, \varphi\}$. Note that if SW = 4, the identification is performed in open-loop, hence this approach is applicable for stable plants only.

3.2. PID controller tuning rules based on harmonic excitation

Based on identified plant parameters, PID controller can be tuned using the phase margin and/or gain margin approaches. In the control loop in **Figure 11**, switch SW in "5" and the PID controller in manual mode. To guarantee a specified phase margin ϕ_M at the gain crossover frequency ω_a^*, the closed-loop characteristic equation under a PID controller $1 + L(j\omega) = 1 + G(j\omega)G_R(j\omega) = 0$ can be easily broken down into the magnitude and phase conditions ($\omega_a^* = \omega_n$, and ϕ_M is the required phase margin, $L(j\omega)$ is the loop transfer function)

$$|G(j\omega_n)||G_R(j\omega_n)| = 1, \arg G(\omega_n) + \arg G_R(\omega_n) = -180^\circ + \varphi_M. \tag{19}$$

To guarantee a specified gain margin G_M at the phase crossover frequency ω_p^*, the closed-loop characteristic equation can be expressed by the magnitude and phase conditions [6] as follows ($\omega_p^* = \omega_n$)

$$|G(j\omega_n)||G_R(j\omega_n)| = 1/G_M, \arg G(\omega_n) + \arg G_R(\omega_n) = -180^\circ. \tag{20}$$

Graphical interpretation of (19), (20) is shown in **Figure 13**. Let us denote $\varphi = argG(\omega_n)$, $\Theta = argG_R(\omega_n)$, and consider the ideal PID controller (1a), where K is proportional gain, and T_i, T_d are the integral and the derivative time constants, respectively. Substituting for $s = j\omega_n$ into (1a) we obtain

$$G_R(j\omega_n) = K + jK\left[T_d\omega_n - \frac{1}{T_i\omega_n}\right]. \tag{21}$$

Comparison of (21) with its polar form

$$G_R(j\omega_n) = |G_R(j\omega_n)|e^{j\Theta} = |G_R(j\omega_n)|[\cos\Theta + j\sin\Theta] \tag{22}$$

yields a complex Eq. (23) for phase margin approach and (24) for gain margin approach

$$K + jK\left[T_d\omega_n - \frac{1}{T_i\omega_n}\right] = \frac{\cos\Theta}{|G(j\omega_n)|} + j\frac{\sin\Theta}{|G(j\omega_n)|}, \tag{23}$$

$$K + jK\left[T_d\omega_n - \frac{1}{T_i\omega_n}\right] = \frac{\cos\Theta}{G_M|G(j\omega_n)|} + j\frac{\sin\Theta}{G_M|G(j\omega_n)|}. \tag{24}$$

Finally, PID controller parameters are obtained from (23), (24) using the substitution $|G_R(j\omega_n)| = 1/|G(j\omega_n)|$ for the phase margin approach and $|G_R(j\omega_n)| = 1/[G_M|G(j\omega_n)|]$ for the gain

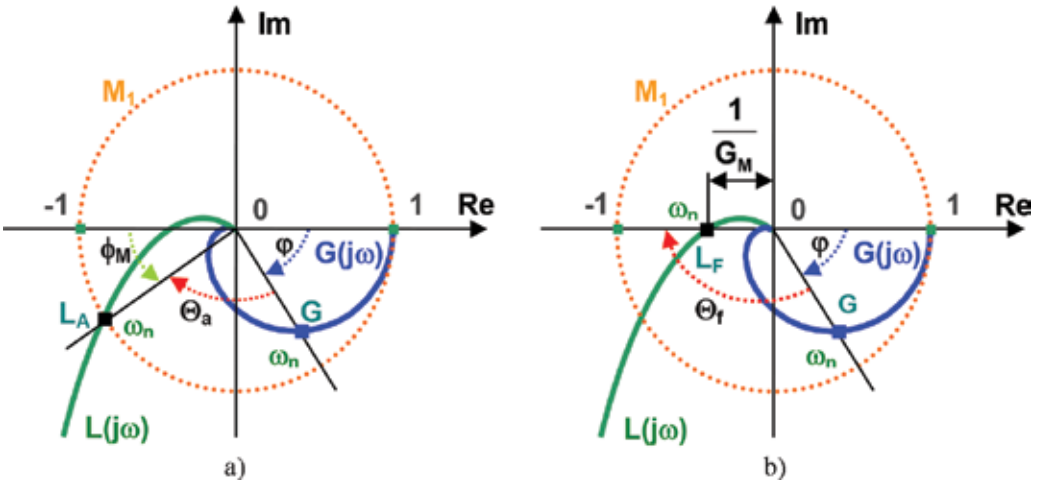

Figure 13. Graphical interpretation of (a) ϕ_M, ω_a^* and shifting G into L_A at $\omega_a^* = \omega_n$; (b) G_M, ω_f^* and shifting G into L_F at $\omega_f^* = \omega_n$.

margin approach resulting from (24). The complex equations (23), (24) are solved as a set of two real equations (25) for the phase margin or (26) for the gain margin approaches, respectively

$$K = \frac{\cos\Theta}{|G(j\omega_n)|}, K\left[T_d\omega_n - \frac{1}{\beta T_d\omega_n}\right] = \frac{\sin\Theta}{|G(j\omega_n)|}, \tag{25}$$

$$K = \frac{\cos\Theta}{G_M|G(j\omega_n)|}, K\left[T_d\omega_n - \frac{1}{\beta T_d\omega_n}\right] = \frac{\sin\Theta}{G_M|G(j\omega_n)|}, \tag{26}$$

where (25a, 26a) represent general rules for calculating the controller gain K. After substituting (25a), (26a) and the ratio $\beta = T_i/T_d$ into (25b), (26b), after some manipulations we obtain a quadratic equation in T_d for both approaches

$$T_d^2\omega_n^2\beta - T_d\omega_n\beta tg\Theta - 1 = 0. \tag{27}$$

Expression for calculating T_d is the positive solution of (27)

$$T_d = \frac{tg\,\Theta}{2\omega_n} + \frac{1}{\omega_n}\sqrt{\frac{tg^2\Theta}{4} + \frac{1}{\beta}}. \tag{28}$$

Hence, the PID controller parameters are calculated using the expressions (25a), (26a), $T_i = \beta T_d$ and (28); Θ is obtained from (19b) using (29) for the phase margin approach and (20b) for the gain margin approach

$$\Theta = -180^\circ + \phi_M - \arg G(\omega_n) = -180^\circ + \phi_M - \varphi, \tag{29}$$

$$\Theta = -180^\circ - \arg G(\omega_n) = -180^\circ - \varphi. \tag{30}$$

Using the PID controller designed for the phase margin ϕ_M, the identified point G of the plant Nyquist plot G(jω) with co-ordinates (1) is moved into the point L_A of the open-loop Nyquist plot located on the unit circle M_1 (**Figure 13a**). In this way, the gain crossover L_A of the open-loop L(jω) is specified

$$L_A \equiv L(j\omega_n) = [|L(j\omega_n)|, \arg L(\omega_n)] = \left[1, \phi_M\right], \tag{31}$$

for which the designed PID controller guarantees the required phase margin ϕ_M; so for ω_n is $|L(j\omega_n)| = 1$. In case of PID controller design for gain margin G_M, the identified point G of the plant Nyquist plot G(jω) with co-ordinates (1) is moved into the open-loop frequency response point L_F lying on the negative real half-axis of the complex plane (**Figure 13b**). In this way, the phase crossover L_F of the open-loop L(jω) is specified

$$L_F \equiv L\left(j\omega_f^* \equiv \omega_n\right) = [|L(j\omega_n)|, \arg L(\omega_n)] = \left[\frac{1}{G_M}, -180^\circ\right]. \tag{32}$$

Location of the points $G(j\omega_n)$ and $L(j\omega_n)$ in the complex plane is shown in **Figure 13**.

No.	Design method, year	Controller	K	T_i	T_d	Range of Θ
44.	Ext. sinusoidal excitation method, Phase-margin approach 2017, $\Theta = -180^{\circ} + \phi_M - \varphi$	PI	$\frac{\cos\Theta}{\lvert G(j\omega_n)\rvert}$	$\frac{-1}{\omega_n tg\Theta}$	–	$\left(-\frac{\pi}{2};0\right)$
45.	Ext. sinusoidal excitation method, Phase-margin approach 2017, $\Theta = -180^{\circ} + \phi_M - \varphi$	PD	$\frac{\cos\Theta}{\lvert G(j\omega_n)\rvert}$	–	$\frac{1}{\omega_n} tg\Theta$	$\left(0;\frac{\pi}{2}\right)$
46.	Ext. sinusoidal excitation method, Phase-margin approach 2017, $\Theta = -180^{\circ} + \phi_M - \varphi$	PID	$\frac{\cos\Theta}{\lvert G(j\omega_n)\rvert}$	βT_d	$\frac{tg\Theta}{2\omega_n} + \frac{1}{\omega_n}\sqrt{\frac{tg^2\Theta}{4} + \frac{1}{\beta}}$	$\left(-\frac{\pi}{2};\frac{\pi}{2}\right)$
47.	Ext. sinusoidal excitation method, Gain-margin approach 2017, $\Theta = -180^{\circ} - \varphi$	PI	$\frac{\cos\Theta}{G_M\lvert G(j\omega_n)\rvert}$	$\frac{-1}{\omega_n tg\Theta}$	–	$\left(-\frac{\pi}{2};0\right)$
48.	Ext. sinusoidal excitation method, Gain-margin approach 2017, $\Theta = -180^{\circ} - \varphi$	PD	$\frac{\cos\Theta}{G_M\lvert G(j\omega_n)\rvert}$	–	$\frac{1}{\omega_n} tg\Theta$	$\left(0;\frac{\pi}{2}\right)$
49.	Ext. sinusoidal excitation method, Gain-margin approach 2017, $\Theta = -180^{\circ} - \varphi$	PID	$\frac{\cos\Theta}{G_M\lvert G(j\omega_n)\rvert}$	βT_d	$\frac{tg\Theta}{2\omega_n} + \frac{1}{\omega_n}\sqrt{\frac{tg^2\Theta}{4} + \frac{1}{\beta}}$	$\left(-\frac{\pi}{2};\frac{\pi}{2}\right)$

Table 8. PI, PD and PID controller tuning rules using the harmonic excitation method.

PI, PD and PID tuning formulas for both approaches (ϕ_M and G_M) are summed up in **Table 8**.

The excitation frequency can be adjusted according to the empirical relations [6].

$$\omega_n \in \underset{\phi_M - approach}{\langle 0.2\omega_c, 0.95\omega_c\rangle}; \omega_n \in \underset{G_M - approach}{\langle 0.5\omega_c, 1.25\omega_c\rangle}. \tag{33}$$

3.3. Controller structure selection using the "triangle ruler" rule

The argument Θ in the tuning rules in **Table 8** indicates the angle to be contributed to the identified phase φ at ω_n by the controller to obtain the resulting open-loop phase ($-180^{\circ}+\phi_M$) necessary to guarantee the required phase margin ϕ_M (or the gain margin G_M). Working range of the PID controller argument is given by the union of PI and PD controllers phase ranges

$$\Theta_{PID} \in \Theta_{PI} \cup \Theta_{PD} = \left(-90^{\circ}, 0^{\circ}\right) \cup \left(0^{\circ}, +90^{\circ}\right) = \left(-90^{\circ}, +90^{\circ}\right), \tag{34}$$

which is symmetric with respect to 0° and due to frequency properties of PI, PD and PID controllers also upper- and lower-bounded. The working range (34) can be interpreted using a pretended transparent triangular ruler turned according to **Figure 14**; its segments to the left and right of the axis of symmetry represent the PD and PI working ranges, respectively.

Figure 14a shows the situation, when the identified point G is situated in the 1st quadrant of the complex plane. In case of phase-margin approach, put this ruler on **Figure 14a**, the middle of the hypotenuse on the origin of the complex plane and turn it so that its axis of symmetry merges with the ray (0,G). Thus, the ruler determines in the complex plane the cross-hatched area representing the full working range of the PID controller argument. The controller type is chosen depending on the situation of the ray (0,L_A) forming with the negative real half-axis the angle ϕ_M: situation of the ray (0,L_A) in the left-hand sector suggests a PD controller, and in the

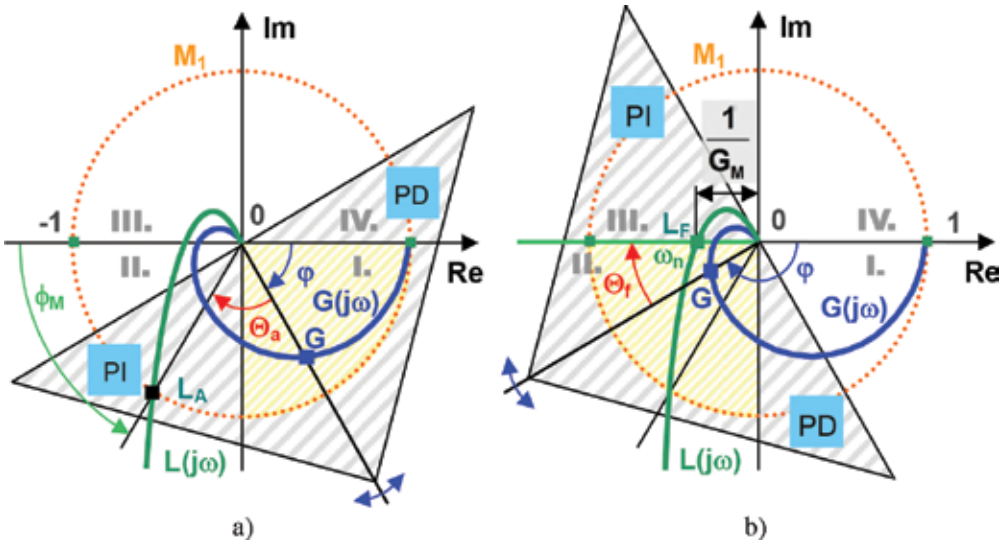

Figure 14. Controller structure selection using the "triangle ruler" rule with respect to the situation of (a) G and L_A; (b) G and L_F.

right-hand sector the PI controller. **Figure 14a** shows the case, when the phase margin ϕ_M is achievable using both PI or PID controller. According to **Figure 14b**, the identified point G is placed in 2nd quadrant of the complex plane. Applying the gain-margin approach, the ruler is to be put on **Figure 14b** according to the similar setup than in case of phase-margin approach. The controller type is chosen depending on the situation of the ray $(0,L_F)$ lying on the border of the second and third quadrants of the complex plane; in this case, PI or PID controller type has to be chosen.

3.4. Closed-loop performance

This subsection answers the following question: how to transform the practical performance requirements in terms of maximum overshoot η_{max} and settling time t_s into the couple of frequency-domain parameters (ω_n,ϕ_M) needed for identification and PID controller coefficients tuning?

3.4.1. Systems without integrator

Looking for an appropriate transformation $\Re$: $(\eta_{max},t_s)\rightarrow(\omega_n,\phi_M)$ we will consider typical phase margins ϕ_M given by the set

$$\left\{\varphi_{Mj}\right\} = \left\{20^\circ, 30^\circ, 40^\circ, 50^\circ, 60^\circ, 70^\circ, 80^\circ, 90^\circ\right\}, \tag{35}$$

j = 1…8. Let us split (33a) into 5 equidistant sections $\Delta\omega_n = 0.15\omega_c$, and generate the set of excitation frequencies

$$\{\omega_{nk}\} = \{(0.2, 0.35, 0.5, 0.65, 0.8, 0.95)\omega_c\} = \{\sigma_k \omega_c\}, \tag{36}$$

k = 1…6. Its elements divided by the plant critical frequency ω_c determine the set of so-called excitation levels

$$\{\sigma_k\} = \{0.2, 0.35, 0.5, 0.65, 0.8, 0.95\}, \tag{37}$$

k = 1…6. Let us demonstrate the qualitative effect of ω_{nk} and ϕ_{Mj} on closed-loop step response for the plant

$$G_3(s) = \frac{1}{(s+1)(0.5s+1)(0.25s+1)(0.125s+1)} \tag{38}$$

under PID controllers designed for three phase margins ϕ_M = 40°, 60°, 80° on three excitation levels $\sigma_1 = \omega_{n1}/\omega_c$ = 0.2; $\sigma_3 = \omega_{n3}/\omega_c$ = 0.5 and $\sigma_5 = \omega_{n5}/\omega_c$ = 0.8. Related closed-loop step responses are shown in **Figure 15**.

Achieving required t_s and η_{max} was tested by designing PID controller for a vast set of benchmark examples [2] at excitation frequencies and phase margins expressed by a Cartesian product $\phi_{Mj} \times \omega_{nk}$ of the sets (35) and (36) for j = 1…8, k = 1…6. Resulting dependences $\eta_{max} = f(\phi_M, \omega_n)$ and $t_s = (\phi_M, \omega_n)$ are plotted in **Figure 16** [6].

Considering the frequencies $\omega_a^* = \omega_n$ are equal which results from the assumptions of the sinusoidal excitation method, the settling time can be expressed by the relation

$$t_s = \frac{\gamma\pi}{\omega_n} \tag{39}$$

similar to (16c) [6], where γ is the curve factor of the step response; in the relation (16c) for the 2nd order closed-loop, γ is from the interval (1;4) and depends on the relative damping [14]. In case of the proposed sinusoid excitation based method γ varies over a considerably broader interval (0.5;16) found empirically and depends strongly on ϕ_M, that is $\gamma = f(\phi_M)$ at the given excitation frequency ω_n. To examine closed-loop settling times for plants with different dynamics, it is advantageous to define the relative settling time [7]

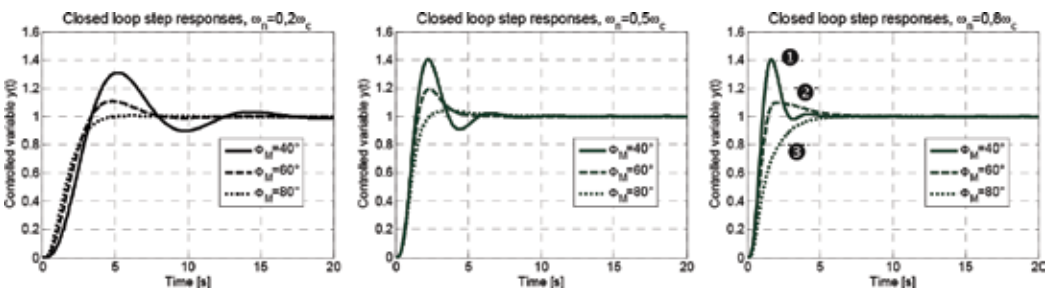

Figure 15. Closed-loop step responses of $G_3(s)$ for various ϕ_M and ω_n.

$$\tau_s = t_s \omega_c. \tag{40}$$

Substituting for $\omega_n = \sigma\omega_c$ into (39) and (40), we obtain a relation for the relative settling time

$$\tau_s = \frac{\pi}{\sigma}\gamma, \tag{41}$$

where t_s is related to the critical frequency ω_c. Due to introducing ω_c the right-hand side in (41) is constant for the given plant and independent of ω_n. The dependency (41) obtained empirically for different excitation frequencies ω_{nk} is depicted in **Figure 16b**; it is evident that at every excitation level σ_k with increasing phase margin ϕ_M the relative settling time τ_s first decreases and after achieving its minimum τ_{s_min} it increases again. The empirical dependences in **Figure 16** have been approximated by quadratic regression curves, thus they are called B-parabolas [7].

3.4.1.1. Discussion

When choosing $\phi_M = 40^\circ$ on the B-parabola corresponding to the excitation level $\sigma_5 = \omega_{n5}/\omega_c = 0.8$ (further denoted as $B_{0.8}$ parabola), maximum overshoot $\eta_{max} = 40\%$ and relative settling time $\tau_s \approx 10$ are expected (see **Figure 16**). Point ❶ corresponding to these parameters and is located on the left (falling) portion of $B_{0.8}$ yielding oscillatory step response (see response ❶ in **Figure 15c**). If the phase margin to $\phi_M = 60^\circ$ increases, the relative settling time decreases into the point ❷ on the right (rising) portion of the $B_{0.8}$ parabola; the corresponding step response ❷ in **Figure 15c** is weakly aperiodic. For the phase margin $\phi_M = 80^\circ$, the $B_{0.8}$ parabola indicates a zero maximum overshoot, the relative settling time $\tau_s = 20$ corresponds to the position ❸ on the $B_{0.8}$ parabola with aperiodic step response ❸ (**Figure 15c**). If the maximum overshoot $\eta_{max} = 20\%$ is acceptable, then $\phi_M = 53^\circ$ yields the least possible relative settling time $\tau_s = 6.5$ on the given level $\sigma_5 = 0.8$ ("at the bottom" of $B_{0.8}$).

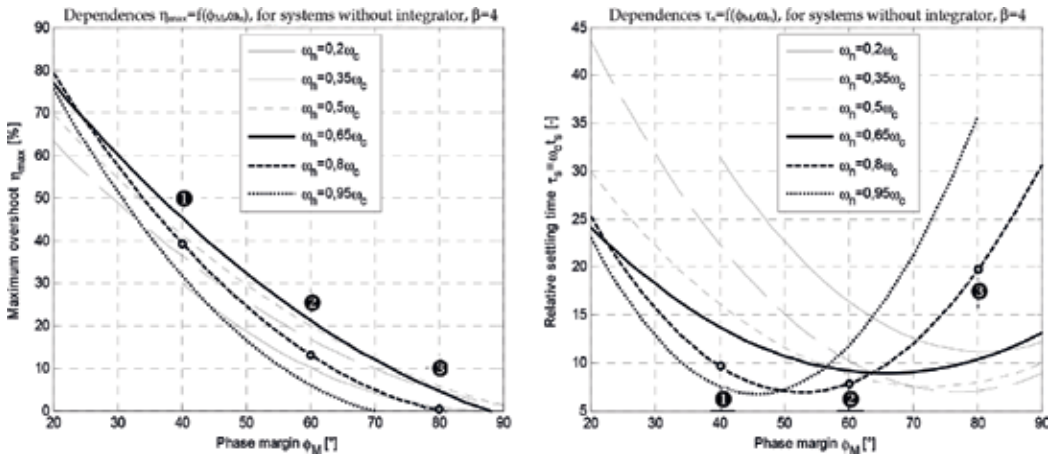

Figure 16. Dependences: (a) $\eta_{max} = f(\phi_M, \omega_n)$; (b) $\tau_s = \omega_c t_s = f(\phi_M, \omega_n)$ for $\phi_{Mj} \times \omega_{nk}$, j = 1…8, k = 1…6 (relative settling time $\tau_s = t_s\omega_c$).

3.4.1.2. Example 1

Using the sinusoid excitation method, design ideal PID controllers (1a) for an operating amplifier modeled by the transfer function $G_A(s)$

$$G_A(s) = \frac{1}{(T_A s + 1)^3} = \frac{1}{(0,01s + 1)^3}. \tag{42}$$

The control objective is to guarantee maximum overshoots η_{max1} = 30%, η_{max2} = 5% and a maximum relative settling time τ_s = 12 in both cases.

3.4.1.3. Solution

1. Critical frequency of the plant identified by the Rotach test is ω_c = 173.216[rad/s] (the process is "fast"). The prescribed settling time is $t_s = \tau_s/\omega_c$ = 12/173.216[s] = 69.3[ms].
2. For the expected performance $(\eta_{max1};\tau_s)$ = (30%;12) (Design No. 1) a satisfactory choice is $(\phi_{M1};\omega_{n1}) = (50^\circ;0.5\omega_c)$ resulting from the $B_{0.5}$ parabola in **Figure 16**. The performance in terms of $(\eta_{max2};\tau_s)$ = (5%;12) (Design No. 2) can be achieved by choosing $(\phi_{M2};\omega_{n2}) = (70^\circ;0.8\omega_c)$ resulting from the $B_{0.8}$ parabola in **Figure 16**.
3. Identified points for the first and second designs are $G_A(j0.5\omega_c) = 0.43e^{-j120^\circ}$ and $G_A(j0.8\omega_c) = 0.19e^{-j165^\circ}$, respectively. According to **Figure 17a**, both points are located in the quadrant II of the complex plane, on the Nyquist plot $G_A(j\omega)$ (continuous curve) which verifies the identification.

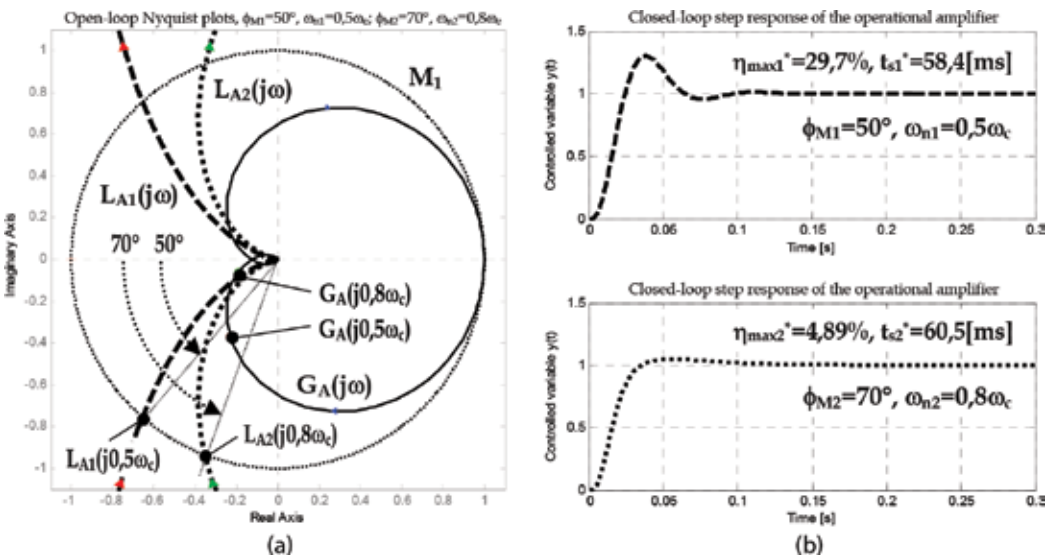

Figure 17. (a) Open-loop Nyquist plots; (b) closed-loop step responses of the operational amplifier, required performance η_{max1} = 30%, η_{max2} = 5% and τ_s = 12.

4. Using the PID controller designed for $(\phi_{M1};\omega_{n1}) = (50°;0.5\omega_c)$, the point $G_A(j0.5\omega_c)$ is moved into the gain crossover $L_{A1}(j0.5\omega_c) = 1e^{-j130°}$ on the unit circle M_1, which verifies achieving the phase margin $\phi_{M1} = 180° - 130° = 50°$ (dashed Nyquist plot). The point $G_A(j0.8\omega_c)$ has been moved by the PID controller designed for $(\phi_{M2};\omega_{n2}) = (80°;0.8\omega_c)$ into $L_{A2}(j0.8\omega_c) = 1e^{-j110°}$ yielding a phase margin $\phi_{M2} = 180° - 110° = 70°$ (dotted Nyquist plot).

5. Achieved performance read-off from the closed-loop step response in **Figure 17b** (dashed line) is $\eta_{max1}^* = 29.7\%$, $t_{s1}^* = 58.4$[ms]. Performance in terms of $\eta_{max2}^* = 4.89\%$, $t_{s2}^* = 60.5$ [ms] identified from the closed-loop step response in **Figure 17b** (dashed line) complies with the required performance.

3.4.2. Systems with time delay

The sinusoid excitation method is applicable also for plants with time delay commonly considered as difficult-to-control systems [1]. It is a well-known fact that at each frequency $\omega_n \in \langle 0,\infty)$ the time delay D turns the phase by $\omega_n D$ with respect to the delay-free system [44]. For time-delayed systems, the phase condition (29) is extended by an additional phase $\varphi_D = -\omega_n D$

$$(\varphi' + \varphi) + \Theta = -180^\circ + \phi_M, \tag{43}$$

where φ' is the phase of the delay-free system and

$$\varphi = \varphi' + \varphi_D \tag{44}$$

is the identified phase of the plant including the time delay.

The added phase $\varphi_D = -\omega_n D$ is associated with the required phase margin ϕ_M according to

$$\varphi' + \Theta = -180^\circ + (\phi_M + \omega_n D). \tag{45}$$

The only modification in using the PID tuning rules in **Table 9** is that an increased required phase margin is to be specified.

Model	η_{max},τ_s	ω_c [rad/s]	t_s [s]	B-par.	ϕ_M/G_M	ω_n/ω_c	$G(j\omega_n)$	$G_R(j\omega_n)$	η_{max}^*	t_s^* [s]
$G_A(s)$	30%,12	173.2	0.069	**Figure 16**	50°	0.5	$0.43e^{-j120°}$	$2.31e^{-j10°}$	29.7%	0.058
$G_A(s)$	5%,12	173.2	0.069	**Figure 16**	70°	0.8	$0.19e^{-j165°}$	$5.20e^{j55°}$	4.89%	0.061
$G_B(s)$	30%,12	0.352	34.1	**Figure 16**	55 + 45.9°	0.35	$1.03e^{-j23°}$	$0.97e^{-j56°}$	18.6%	24.78
$G_B(s)$	5%,12	0.352	34.1	**Figure 16**	70 + 26.2°	0.2	$1.09e^{-j13°}$	$0.92e^{-j71°}$	0.15%	28.69
$G_C(s)$	30%,20	0.241	83.1	**Figure 21**	53 + 10.1°	0.35	$12.7e^{-j122°}$	$0.08e^{j5.8°}$	29.6%	81.73
$G_C(s)$	20%,20	0.241	83.1	**Figure 21**	62 + 14.5°	0.5	$8.10e^{-j129°}$	$0.12e^{-j28°}$	19.7%	82.44
$G_D(s)$	30%,12	0.049	245.9	**Figure 25**	15 dB	1.25	$0.14e^{-j204°}$	$1.47e^{j24°}$	24.5%	241.9
$G_D(s)$	5%,12	0.049	245.9	**Figure 25**	18 dB	0.65	$0.38e^{-j136°}$	$0.38e^{-j44°}$	4.55%	243.4

Table 9. PID controller design parameters, required and achieved performance, identified plant parameters for $G_A(s)$, $G_B(s)$, $G_C(s)$ and $G_D(s)$.

$$\phi'_{\mathrm{M}} = \phi_{\mathrm{M}} + \omega_{\mathrm{n}}\mathrm{D} \tag{46}$$

and the controller working angle Θ is to be computed using the relation

$$\Theta = -180^{\circ} - \varphi' + \left(\phi_M + \omega_n D\right). \tag{47}$$

The phase delay ω_nD increases with increasing frequency ω_n of the sinusoidal excitation signal. It is recommended to use the smallest possible added phase $\varphi_D = -\omega_n D$ to lessen the impact of time delay on closed-loop dynamics.

3.4.2.1. Discussion

The time delay D can be easily specified during identification of the critical frequency as a time $D = T_y - T_u$, that elapses since the start of the test at time T_u until time T_y, when the system output starts responding to the excitation signal u(t). A small added phase $\varphi_D = -\omega_n D$ due to time delay can be achieved by choosing the smallest possible ω_n attenuating the effect of D in (47) and subsequently in the PID controller design. Therefore when designing a PID controller for time delayed systems, it is recommended to choose the lowest possible excitation level when using B-parabolas (most frequently $\omega_n/\omega_c = 0.2$ resp. 0.35) and corresponding couples of B-parabolas in **Figure 16**. From the given couple $(\eta_{max};t_s)$, ϕ_M is specified using the chosen couple of B-parabolas, however its increased value $\phi_{M'}$ given by (46) is to be supplied in the design algorithm thus minimizing effect of the time delay on closed-loop dynamics.

3.4.2.2. Example 2

Using the sinusoid excitation method, design ideal PID controllers (1a) for a distillation column model given by the transfer function $G_B(s)$

$$G_B(s) = \frac{K_B e^{-D_B s}}{T_B s + 1} = \frac{1.11 e^{-6,5s}}{3.25s + 1}. \tag{48}$$

Control objectives are the same as in Example 1.

3.4.2.3. Solution and discussion

1. Critical frequency of the plant is $\omega_c = 0.3521$[rad/s]. Based on comparison of critical frequencies, $G_B(s)$ is 500-times slower than $G_A(s)$. Required settling time is $t_s = \tau_s/\omega_c = 12/0.3521$[s] = 34.08[s].
2. Because $D_B/T_B = 2 > 1$, the plant is a so-called "dead-time dominant system." Due to a large time delay, it is necessary to choose the lowest possible excitation frequency ω_n to minimize the added phase $\omega_n D_B$ in (47). Hence, for the required performance $(\eta_{max2};\tau_s) = (5\%;12)$ (Design No. 2) we choose the $B_{0.2}$ parabolas in **Figure 16** at the lowest possible level $\omega_n/\omega_c = 0.2$ to find $(\phi_{M2};\omega_{n2}) = (70^{\circ};0.2\omega_c)$. The added phase value is $\omega_{n2}D_B = 0.2\omega_c D_B = 0.2 \cdot 0.3521 \cdot 6.5 \cdot 180/\pi = 26.2^{\circ}$, hence the phase supplied to the PID design algorithm

is $\phi'_{M2} = \phi_{M2} + \omega_{n2}D_B = 70° + 26.2° = 96.2°$ (instead of $\phi_{M2} = 70°$ for a delay-free system). The required performance $(\eta_{max1};\tau_s) = (30\%;12)$ (Design No. 1) can be achieved by choosing $(\phi_{M1};\omega_{n1}) = (55°;0.35\omega_c)$ from the $B_{0.35}$ parabolas in **Figure 16** (i.e., $\omega_n/\omega_c = 0.35$). The phase margin $\phi'_{M1} = 55° + 45.9°$ supplied into the design algorithm was increased by $\omega_{n1}D_B = 0.35\omega_c D_B = 0.35 \cdot 0.3521 \cdot 6.5 \cdot 180/\pi = 45.9°$ compared with $\phi_{M1} = 55°$ in case of delay-free system.

3. **Figure 18a** shows that identified points $G_B(j0.35\omega_c) = 1.03e^{-j23°}$ and $G_B(j0.2\omega_c) = 1.09e^{-j13°}$ are located in the quadrant I of the complex plane at the beginning of the frequency response $G_B(j\omega)$ (continuous curve).

4. The point $G_B(j0.2\omega_c)$ (Design No. 2) was shifted by the PID controllers to the open-loop amplitude crossover $L_{B2}(j0.2\omega_c) = 1e^{-j110°}$ (dotted Nyquist plot in **Figure 18a**). Note that L_{B2} has the same position in the complex plane as L_{A2} in **Figure 17a**, however at a considerably lower frequency $\omega_{n2B} = 0.2 \cdot 0.3521 = 0.07$[rad/s] compared to $\omega_{n2A} = 0.8 \cdot 173.216 = 138.6$[rad/s] ($t_{s2\_B}^* = 28.69$[s] is almost 500 times larger than $t_{s2\_A}^* = 0.0584$[s] which demonstrates the key role of ω_n in achieving required closed-loop dynamics). The identified point $G_B(j0.35\omega_c)$ (Design No. 1) was moved by the designed PID controller into the amplitude crossover $L_{B1}(j0.35\omega_c) = 1e^{-j125°}$ (dashed Nyquist plot in **Figure 18a**).

5. Achieved performances ($\eta_{max1}^* = 18.6\%$, $t_{s1}^* = 24.78$[s], dashed line), ($\eta_{max2}^* = 0.15\%$, $t_{s2}^* = 28.69$[s], dotted line) in terms of the closed-loop step responses in **Figure 18b** comply with the required performance specification.

3.4.3. Systems with 1st order integrator

Corresponding B-parabolas in **Figures 19–21** were obtained by applying the sinusoid excitation method on a set of benchmark systems with first-order integrator (for a Cartesian product

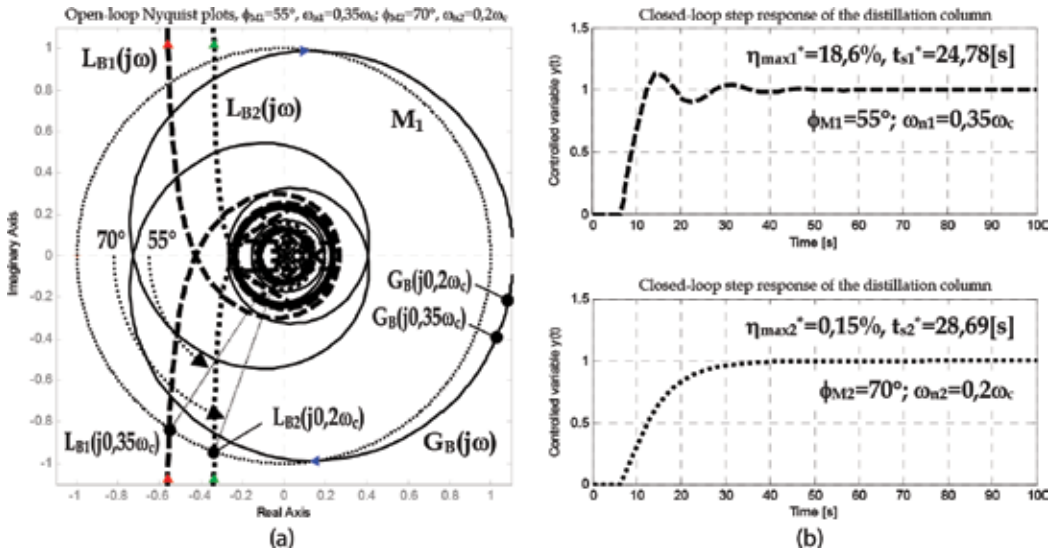

Figure 18. (a) Open-loop Nyquist plots; (b) closed-loop step responses of the distillation column, required performance $\eta_{max1} = 30\%$, $\eta_{max2} = 5\%$ and $\tau_s = 12$.

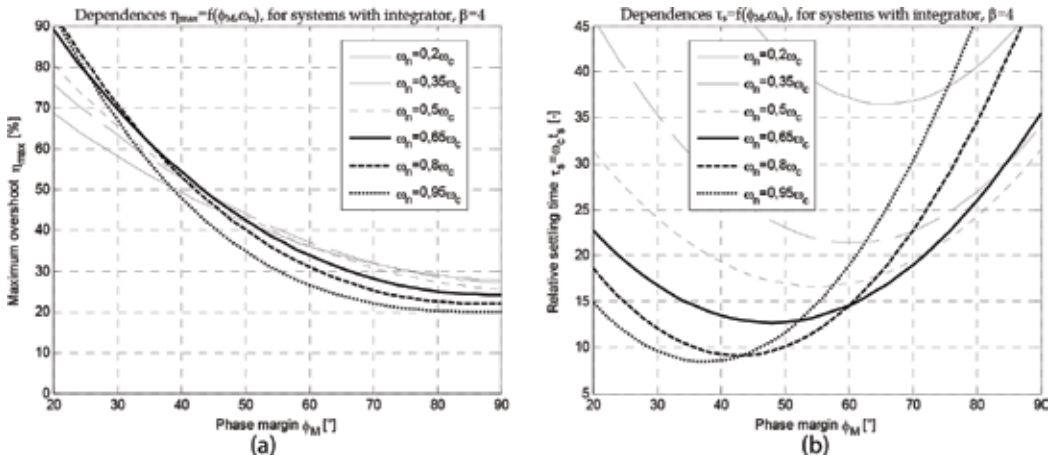

Figure 19. B-parabolas: (a) $\eta_{max} = f(\phi_M,\omega_n)$; (b) $\tau_s = \omega_c t_s = f(\phi_M,\omega_n)$ for systems with integrator $\beta = 4$.

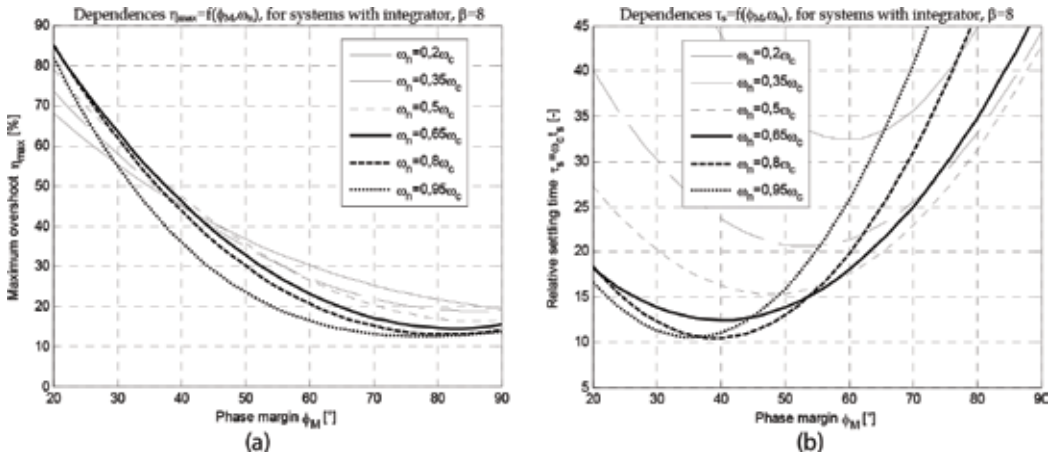

Figure 20. B-parabolas: (a) $\eta_{max} = f(\phi_M,\omega_n)$; (b) $\tau_s = \omega_c t_s = f(\phi_M,\omega_n)$ for systems with integrator $\beta = 8$.

$\phi_{Mj} \times \omega_{nk}$ of the sets (35) and (36), j = 1…8, k = 1…6 and three various ratios T_i/T_d: β = 4, 8 and 12).

3.4.3.1. Discussion

Inspection of **Figures 19a, 20a** and **21a** reveals that increasing β results in decreasing of the maximum overshoot η_{max}, narrowing of the B-parabolas of relative settling times $\tau_s = f(\phi_M,\omega_n)$ for each identification level ω_n/ω_c and consequently increasing the settling time.

Consider for example, the $B_{0.95}$ parabolas in **Figures 19b, 20b** and **21b**: if $\phi_M = 70°$ and $\beta = 4$ the relative settling time is $\tau_s = 30$, for $\beta = 8$ it grows up to $\tau_s = 40$, and for $\beta = 12$ even to $\tau_s = 45$. If a 10% maximum overshoot is acceptable for the given system with integrator, then the standard

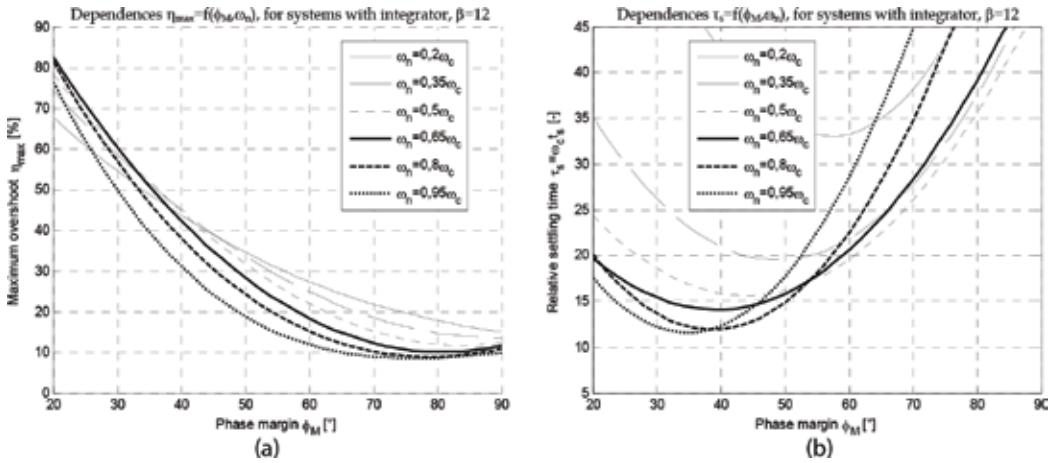

Figure 21. B-parabolas: (a) $\eta_{max} = f(\phi_M,\omega_n)$; (b) $\tau_s = \omega_c t_s = f(\phi_M,\omega_n)$ for systems with integrator $\beta = 12$.

interaction PID controller can be used with no need to use the setpoint filter; however a larger settling time is expected.

3.4.3.2. Example 3

Using the sinusoidal excitation method, let us design ideal PID controllers for a flow valve modeled by the transfer function $G_C(s)$ (system with an integrator and a time delay)

$$G_C(s) = \frac{K_C e^{-D_C s}}{s(T_C s + 1)} = \frac{1.3e^{-2.1s}}{s(7.51s + 1)}. \tag{49}$$

The control objective is to guarantee a maximum overshoot of the closed-loop step response $\eta_{max1} = 30\%$, $\eta_{max2} = 20\%$ and a maximum relative settling time $\tau_s = 20$.

3.4.3.3. Solution and discussion

1. Critical frequency of the plant identified by the Rotach test is $\omega_c = 0.2407$[rad/s]. Then, the required settling time is $t_s = \tau_s/\omega_c = 20/0.2407$[s] = 83.09[s].
2. For $G_C(s)$ the time delay/time constant ratio is $D_C/T_C = 2.1/7.51 = 0.28 < 1$, hence, the influence of the time constant prevails—$G_C(s)$ is a so-called "lag-dominant system" with integrator, therefore B-parabolas are to be chosen carefully. From one side, due to time delay it would be desirable to choose B-parabolas from **Figures 19, 20** or **21** with the lowest identification level $\omega_n/\omega_c = 0.2$. However, the minima of $B_{0.2}$ parabolas in **Figure 19b** (for $\beta = 4$), **Figure 20b** (for $\beta = 8$) and **Figure 21b** (for $\beta = 12$) indicate that the smallest feasible relative settling time $\tau_s = 36.5$ (for $\beta = 4$), $\tau_s = 33$ (for $\beta = 8$) and $\tau_s = 34$ (for $\beta = 12$), which do not satisfy the required value $\tau_s = 20$.

3. The first performance specification $(\eta_{max1};\tau_s) = (30\%;20)$ can be provided using the $B_{0.35}$ parabolas for $\beta = 12$ (**Figure 21b**) at the level $\omega_n/\omega_c = 0.35$ and for parameters $(\phi_{M1};\omega_{n1}) = (53^\circ;0.35\omega_c)$ (Design No. 1), supplying the augmented open-loop phase margin $\phi'_{M1} = \phi_{M1} + \omega_{n1}D_C = 53^\circ + 10.1^\circ = 63.1^\circ$ into the PID controller design algorithm. The second performance specification $(\eta_{max2};\tau_s) = (20\%,20)$ can be achieved using the $B_{0.5}$ parabolas in **Figure 21** for $\beta = 12$ and $\omega_n/\omega_c = 0.5$ and parameters $(\phi_{M2};\omega_{n2}) = (62^\circ;0.5\omega_c)$ (Design No. 2). To reject the influence of D_C, instead of $\phi_{M2} = 62^\circ$ the augmented open-loop phase margin $\phi'_{M2} = \phi_{M2} + \omega_{n1}D_C = 62^\circ + 14.5^\circ = 76.5^\circ$ was supplied into the PID controller design algorithm.

4. Identified points $G_C(j0.35\omega_c) = 12.7e^{-j122^\circ}$ and $G_C(j0.5\omega_c) = 8.10e^{-j129^\circ}$ are located on the plant frequency response $G_C(j\omega)$ (continuous curve) in **Figure 22a** verifying correctness of the identification.

5. Using the PID controller, the first identified point $G_C(j0.35\omega_c)$ (Design No. 1) was moved into the gain crossover $L_{C1}(j0.35\omega_c) = 1e^{-j127^\circ}$ located on the unit circle M_1; this verifies achieving the phase margin $\phi_{M1} = 180^\circ - 127^\circ = 53^\circ$ (dashed Nyquist plot in **Figure 22a**). Achieved performance in terms of the closed-loop step response in **Figure 22b** is $\eta_{max1}^* = 29.6\%$, $t_{s1}^* = 81.73$[s] (dashed line).

6. The second identified point $G_C(j0.5\omega_c)$ (Design No. 2) was moved into $L_{C2}(j0.5\omega_c) = 1e^{-j118^\circ}$ achieving the phase margin $\phi_{M2} = 180^\circ - 118^\circ = 62^\circ$ (dotted Nyquist plot in **Figure 22a**). Achieved performance in terms of the closed-loop step response parameters (**Figure 22b**) $\eta_{max2}^* = 19.7\%$, $t_{s2}^* = 82.44$[s] (dotted line) meets the required specification. Frequency characteristics $L_{C1}(j\omega)$, $L_{C2}(j\omega)$ begin near the negative real half-axis of the complex plane because both open-loops contain a 2nd order integrator.

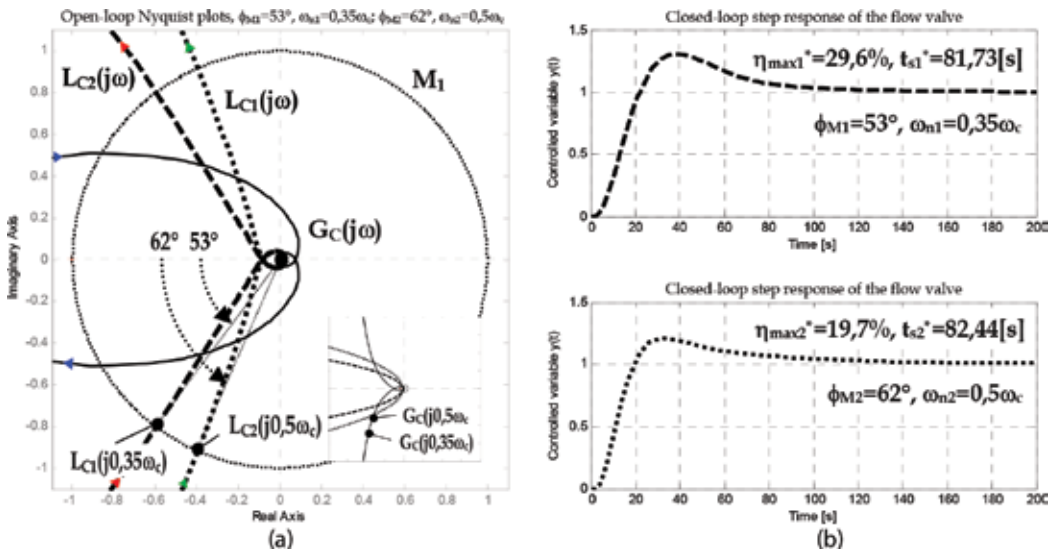

Figure 22. (a) Open-loop Nyquist plots; (b) closed-loop step responses of the flow valve, required performance $\eta_{max1} = 30\%$, $\eta_{max2} = 20\%$ and $\tau_s = 20$.

3.4.4. Systems with unstable zero

Consider typical gain margins G_M given by the set

$$\{G_{Mj}\} = \{3dB, 5dB, 7dB, 9dB, 11dB, 13dB, 15dB, 17dB\} \tag{50}$$

for j = 1…8. Let us split (33b) into five equal sections and generate the set of excitation frequencies

$$\{\omega_{nk}\} = \{0.5\omega_c, 0.65\omega_c, 0.8\omega_c, 0.95\omega_c, 1.1\omega_c, 1.25\omega_c\} \tag{51}$$

for k = 1…6. Its elements divided by the plant critical frequency ω_c determine excitation levels

$$\{\sigma_k = \omega_{nk}/\omega_c\} \Rightarrow \{\sigma_k\} = \{0.5, 0.65, 0.8, 0.95, 1.1, 1.25\} \tag{52}$$

for k = 1…6. **Figure 23** shows closed-loop step response shaping using different G_M and ω_n in the PID tuning for the plant (53b) with parameters $T_3 = 0.75$, $\alpha_3 = 1.3$, for four required gain margins $G_M = 5$ dB, 9 dB, 11 dB and 13 dB, and three different excitation levels $\sigma_1 = \omega_{n1}/\omega_c = 0.5$, $\sigma_3 = \omega_{n3}/\omega_c = 0.8$ and $\sigma_5 = \omega_{n5}/\omega_c = 1.1$.

Consider the following benchmark plants

$$G_2(s) = \frac{-\alpha_2 s + 1}{(T_2 s + 1)^{n_2}}, G_3(s) = \frac{-\alpha_3 s + 1}{(s+1)(T_3 s + 1)\left(T_3^2 s + 1\right)\left(T_3^3 s + 1\right)}. \tag{53}$$

The proposed method has been applied for each element of the Cartesian product $\omega_{nk} \times G_{Mj}$ of the sets (51) and (50). Significant differences between dynamics of individual control loops under designed PID controllers can be observed for the benchmark systems (53).

Consider the benchmark plants $G_2(s)$ and $G_3(s)$ with following parameters: $G_{2.1}(s)$: (T_2, n_2,α_2) = (0.75,8,0.2); $G_{2.2}(s)$: (1,3,0.1); $G_{2.3}(s)$: (0.5,5,1); $G_3(s)$: $T_3 = 0.5$, $\alpha_3 = 1.3$.

Couples of examined plants [$G_3(s)$, $G_{2.3}(s)$] and [$G_{2.2}(s)$, $G_{2.1}(s)$] differ principally by the ratio α/T, which is significant for the closed-loop performance assessment for plants with an unstable zero (for the 1st couple [$\alpha_3/T_3 = 2.6$, $\alpha_{2.3}/T_{2.3} = 2$], for the 2nd couple [$\alpha_{2.2}/T_{2.2} = 0.1$, $\alpha_{2.1}/T_{2.1} = 0.27$]).

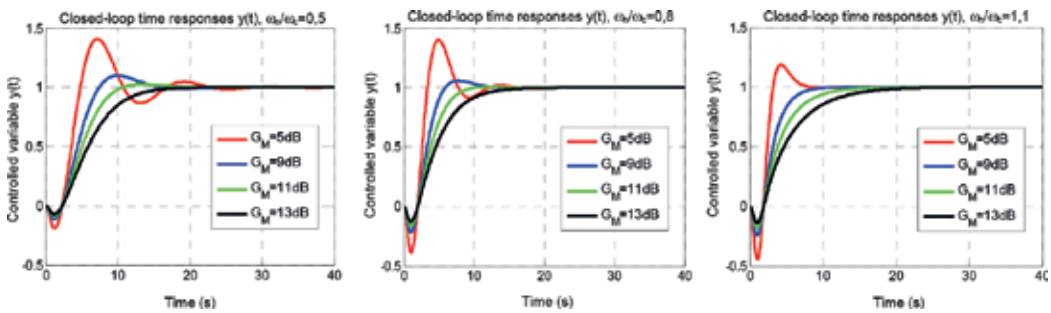

Figure 23. Closed-loop step responses of the plant $G_3(s)$ under PID controllers designed for various G_M and ω_n.

According to the ratio α/T unknown plants with an unstable zero can be classified in following two groups [7]:

1. plants with $\alpha/T < 0.3$;
2. plants with $\alpha/T > 0.3$.

With respect to this classification, B-parabolas $\eta_{max} = f(G_M,\omega_n)$, $\tau_s = f(G_M,\omega_n)$ for nonminimum phase systems with an unstable zero constructed for different open-loop gain margins G_M and excitation levels σ are depicted in **Figure 24** (for $\alpha/T > 0.3$) and in **Figure 25** (for $\alpha/T < 0.3$).

3.4.4.1. Example 4

Using the sinusoid excitation method, ideal PID controllers are to be designed for a heating plant described by the transfer function $G_D(s)$ (a system with an unstable zero)

$$G_D(s) = \frac{K_D(-T_z s + 1)}{(T_D s + 1)^3} = \frac{0.8(-7.5s + 1)}{(27.5s + 1)^3}. \tag{54}$$

The control objective is to guarantee a maximum overshoot η_{max1} = 30%, η_{max2} = 5% and maximum relative settling time τ_s = 12.

3.4.4.2. Solution and discussion

1. Critical frequency of the plant identified by the Rotach test is $\omega_c = 0.0467$[rad/s], the system is "slow". The required settling time is $t_s = \tau_s/\omega_c = 12/0.0488 = 245.90$[s].
2. Because $\alpha/T_D = 7.5/27.5 = 0.27 < 0.3$, the gain margin G_M and the excitation frequency ω_n of the controlled object $G_D(s)$ will be determined using B-parabolas in **Figure 25**. For the required performance (η_{max1},τ_s) = (30%,12) the appropriate values of gain margin and

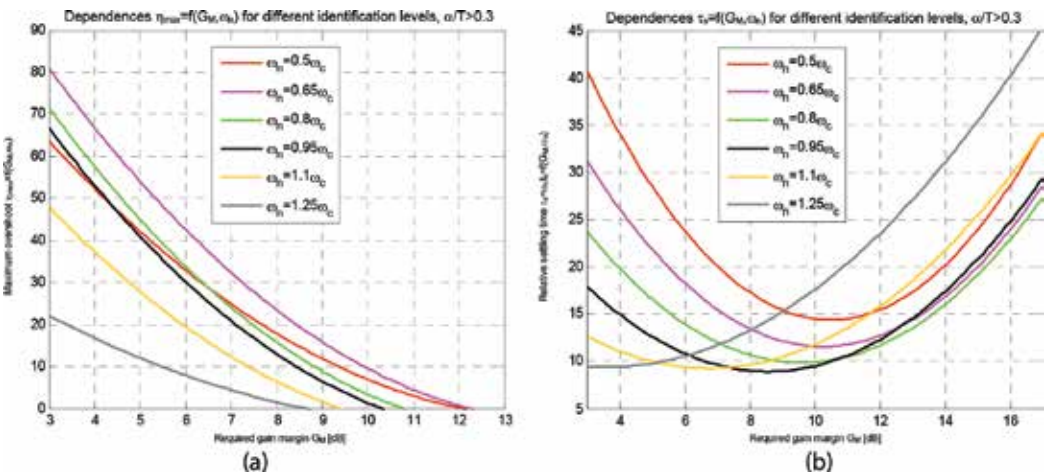

Figure 24. B-parabolas: (a) $\eta_{max} = f(G_M,\omega_n)$; (b) $\tau_s = \omega_c t_s = f(G_M,\omega_n)$ for nonminimum phase systems, $\alpha/T > 0.3$.

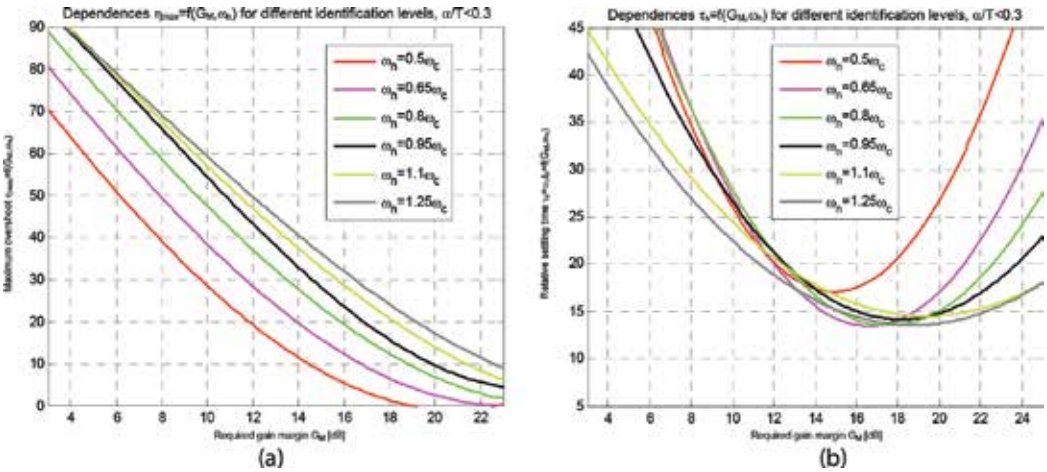

Figure 25. B-parabolas: (a) $\eta_{max} = f(G_M,\omega_n)$; (b) $\tau_s = \omega_c t_s = f(G_M,\omega_n)$ for nonminimum phase systems, $\alpha/T < 0.3$.

excitation frequency are $(G_{M1},\omega_{n1}) = (15\text{ dB},1.25\omega_c)$, that is "gray parabolas" in **Figure 25**. Similarly, the performance $(\eta_{max2},\tau_s) = (5\%,12)$ can be achieved by choosing $(G_{M2},\omega_{n2}) = (18\text{ dB},0.65\omega_c)$ according to "violet" B-parabolas in **Figure 25**.

3. Examination of the Nyquist plots of the controlled object $G_D(j\omega)$ and the open-loops $L_{D1}(j\omega)$, $L_{D2}(j\omega)$ in **Figure 26a** reveals that the first identified point $G_D(j1.25\omega_c)$ is located in the quadrant III of the complex plane, and its identification is carried out under a relatively low frequency $1.25\omega_c = 1.25\cdot0.0467 = 0.0584$[rad/s], hence no high-frequency

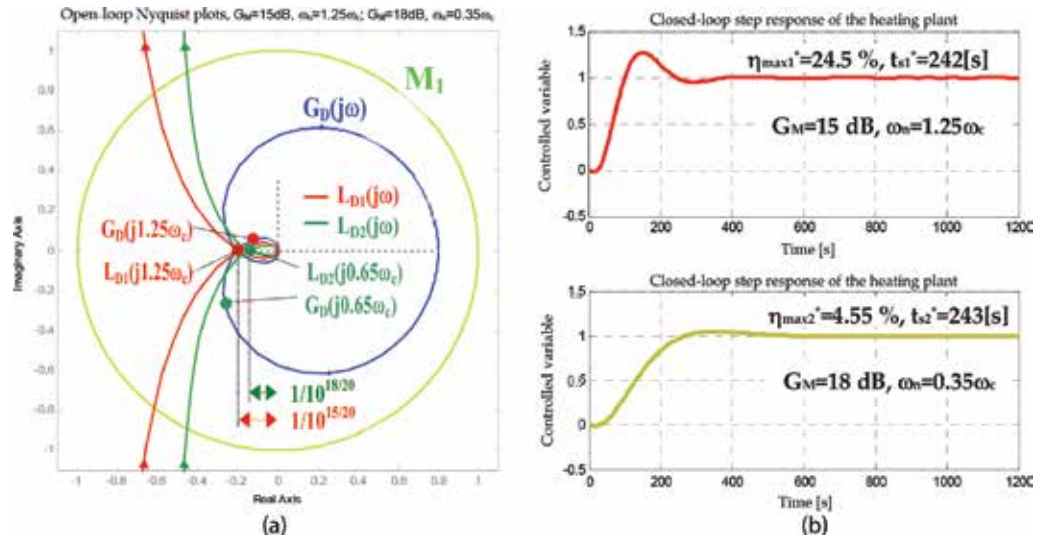

Figure 26. (a) Open-loop Nyquist plots; (b) closed-loop step responses of the heating system, required performance $\eta_{max1} = 30\%$, $\eta_{max2} = 5\%$ and $\tau_s = 12$.

noise corrupting the excitation and output signals u(t) and y(t), respectively, is expected during identification. If, however, the identification at the excitation level $\omega_n = 1.25\omega_c$ were carried out for a "fast" object with a high value of ω_c, it would be necessary to choose the lowest possible excitation level in order to reject the identification noise. The second identified point $G_D(j0.65\omega_c)$ is placed in the quadrant II of the complex plane.

4. Using the PID controller designed for $(G_{M1},\omega_{n1}) = (15\text{ dB},1.25\omega_c)$ the point $G_D(j1.25\omega_c)$ was compensated into the target point $L_{D1}(j1.25\omega_c) = \left[1/10^{GM_1/20}\right]e^{-j180^\circ}$ located on the negative real half-axis where the gain margin G_{M1} of the open-loop $L_{D1}(j\omega)$ (red Nyquist plot) is satisfied. The achieved performance evaluated from the closed-loop step response in **Figure 26b** is $\eta_{max1}^* = 24.5\%$, $t_{s1}^* = 241.88$[s].

5. Using the PID controller designed for $(G_{M2},\omega_{n2}) = (18\text{ dB},0.65\omega_c)$, the point $G_D(j0.65\omega_c)$ was moved to the target point $L_{D2}(j0.65\omega_c) = \left[1/10^{GM_2/20}\right]e^{-j180^\circ}$ where the gain margin G_{M2} of the open-loop $L_{D2}(j\omega)$ (green Nyquist plot) is satisfied. The achieved performance $\eta_{max2}^* = 4.55\%$, $t_{s2}^* = 243.42$[s] evaluated from the closed-loop step response in **Figure 26b** satisfies the control objective.

Time-domain performance requirements specified by the process technologist, identified plant parameters needed for PID controller tuning (for two PID controllers of all four plants $G_A(s)$, $G_B(s)$, $G_C(s)$ and $G_D(s)$) along with specified and achieved performance measure values are summarized in **Table 9**. The asterisk "*" indicates closed-loop performance complying with the required one.

3.5. Robust PID controller design for specified performance

When identifying an uncertain plant, the sinusoidal excitation with the frequency ω_n is repeated for individual parameter changes to obtain a set of points G_i from the set of frequency responses of the uncertain plant

$$G_i(j\omega_n) = |G_i(j\omega_n)|e^{j\arg G_i(\omega_n)} = a_i + jb_i, \tag{55}$$

i = 1,2…N. Plant parameter changes are reflected in changes of the magnitude and the phase $|G_i(j\omega_n)|$ and $\arg G_i(\omega_n)$, respectively; i = 1…N; $N = 2^p$ is the number of identification experiments and p is the number of varying technological quantities of the plant. The nominal model $G_0(j\omega_n)$ is obtained from mean values of the real and imaginary parts of $G_i(j\omega_n)$

$$G_0(j\omega_n) = a_0 + jb_0 = \frac{1}{N}\sum_{i=1}^{N} a_i + j\frac{1}{N}\sum_{i=1}^{N} b_i, \tag{56}$$

i = 1,2…N. Obviously

$$|G_0(j\omega_n)| = \sqrt{a_0^2 + b_0^2} = \frac{1}{N}\sqrt{\left(\left[\sum_{i=1}^{N} a_i\right]^2 + \left[\sum_{i=1}^{N} b_i\right]^2\right)}; \quad \arg G_0(j\omega_n) = \operatorname{arctg}\frac{b_0}{a_0} = arctg\frac{\sum_{i=1}^{N} b_i}{\sum_{i=1}^{N} a_i}, \tag{57}$$

where $\varphi_0(\omega_n) = \arg\{G_0(j\omega_n)\}$. The points G_i represent some elements of the family of plants and can be enclosed by a circle M_G centered in $G_0(j\omega_n)$ with the radius $R_G \equiv R_G(\omega_n)$ corresponding to the maximum distance between $G_i(j\omega_n)$ and $G_0(j\omega_n)$

$$R_G = \max_i \left\{ \sqrt{(a_i - a_0)^2 + (b_i - b_0)^2} \right\}, \tag{58}$$

i = 1,2…N. Actually, the control law generated by the robust controller $G_{Rrob}(s)$ designed for the nominal point $G_0(j\omega_n)$ performs the mapping

$$\wp : \{R_G \rightarrow R_L : R_L = |G_{Rrob}|R_G\} \tag{59}$$

of the set of identified points $G_i(j\omega_n)$ encircled by M_G with the radius R_G onto the set of points $L_i(j\omega_n)$ delineated by M_L and calculates the radius $R_L \equiv R_L(\omega_n)$ of the dispersion circle M_L which encloses the points $L_i(j\omega_n)$ of the Nyquist plot so as to guarantee fulfillment of the robust performance condition.

A robust PID controller is designed using the sinusoidal excitation method with input data for the nominal model $G_0(j\omega_n)$: $\{|G_0(j\omega_n)|; \varphi_0 = \arg G_0(\omega_n)\}$. Substituting them into (25a), (26a), (29) and (30), the expressions for calculating robust PID controller parameters according to **Table 8** are obtained. Obviously, the phase and gain margins ϕ_M and G_M, respectively, are robust PID controller tuning parameters and at the same time attractive robustness measures [6].

3.5.1. Robust performance condition

Theorem 1 *(Sufficient condition for robust performance under a PID controller).*

Consider an uncertain continuous-time stable dynamic system described by a nominal model and unstructured uncertainty. The PID controller $G_R(s)$ tuned according to the rules in **Table 8** guarantees robust closed-loop performance if the following conditions are satisfied

$$\varphi_M > \arccos\left(1 - \frac{1}{2}\left(\frac{\chi_L R_G(\omega_n)}{|G_0(j\omega_n)|} + \chi_S \sin\varphi_S\right)^2\right), \quad G_M > \frac{1 + \chi_L\left[\frac{R_G(\omega_n)}{|G_0(j\omega_n)|}\right]}{1 - \chi_S\left[\frac{G_S - 1}{G_S}\right]}, \tag{60}$$

where ϕ_M and G_M are the required phase and gain margins, respectively, ω_n is the excitation frequency, $\chi_L = R_L^+/R_L$ and $\chi_S = R_S^+/R_S$ are safety factors of radii of the dispersion circles M_L and M_S, respectively, delineating prohibited areas; $R_G(\omega_n)$ is the radius of the dispersion circle at the Nyquist plot of the plant at ω_n, and $G_0(\omega_n)$ is a point at the Nyquist plot of the nominal plant at ω_n. The prohibited area M_S can be defined in terms of ϕ_M or G_M using the expressions $\phi_S = \arcsin(R_S)$ or $G_S = 1/(1-R_S)$, respectively.

Proof:

The proof is straightforward using **Figures 27** and **28**. If the nominal open-loop $L_0(s) = G_0(s)$ $G_R(s)$ is stable, then according to the Nyquist stability criterion the closed-loop with the uncertain plant will be stable if the distance between L_0 and $(-1, j0)$, that is $|1 + L_0(j\omega_n)|$ is

greater than the sum of the radii $R_L(\omega_n)$ of the circle M_L centered in L_0, and $R_S(\omega_n)$ of the circle M_S centered in (−1.0j), that is

$$R_L + R_S < |1 + L_0(j\omega_n)|. \tag{61}$$

3.5.1.1. Robust performance condition: phase margin approach

According to **Figure 27**, the distance between (−1.0j) and the open-loop Nyquist plot $L_0(j\omega_n)$ at ω_n, that is $|1 + L_0(j\omega_n)|$ can be calculated by applying the cosine rule to the triangle given by the vertices $(-1.0, L_0)$ (ϕ_M is the phase margin)

$$|1 + L_0| = \sqrt{1 + |L_0|^2 - 2|L_0| \cos \varphi_M}. \tag{62}$$

From the principles of the sinusoidal excitation PID controller tuning method results that the robust controller shifts the nominal point of the plant frequency response G_0 to the point L_0 situated on the unit circle. Thus, ω_n becomes the gain crossover frequency. As the point L_0 is situated on the unit circle M_1, the magnitude $|L_0(j\omega_n)|$ equals one, that is $|L_0| = |G_0||G_R| = 1$, yielding the transformation ratio $|G_R| = |G_0|^{-1}$ between the radii R_G and R_L of the circles M_G and M_L, respectively. The radius R_L of the dispersion circle M_L can be expressed as

$$R_L = R_G|G_R| = \frac{R_G}{|G_0|}. \tag{63}$$

Substituting (62) and (63) in (61) yields the robust performance condition

$$\left(\frac{\chi_L R_G(\omega_n)}{|G_0(j\omega_n)|} + \chi_S R_S\right)^2 < 2 - 2\cos\varphi_M, \tag{64}$$

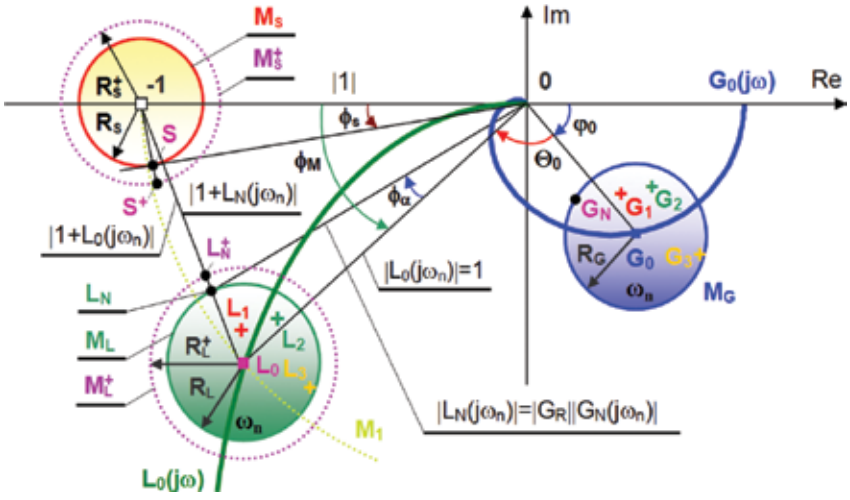

Figure 27. Dispersion circles M_G and M_L and the prohibited area delineated by the circle M_S for the phase-margin approach.

which after some manipulations is identical to the proven condition (60a). Typical values of safety factors are χ_L = 1.1 and χ_S = 1.2. The value of ϕ_M chosen according to the robust performance condition used in the tuning rules in **Table 1** yields robust PID controller coefficients. The design procedure is illustrated in Section 3.5.1.3.

3.5.1.2. Robust performance condition: gain margin approach

According to **Figure 28**, $|1 + L_0(j\omega_n)|$ is a complement of $|0,L_0| = |L_0|$ to the unit value. Thus

$$|L_0(j\omega_n)| + |1 + L_0(j\omega_n)| = 1 \Rightarrow |1 + L_0(j\omega_n)| = 1 - |L_0(j\omega_n)|. \tag{65}$$

From the principles of the proposed PID tuning method results that the robust controller shifts the point $G_0(\omega_n)$ of the plant nominal frequency response to L_0 situated on the negative real half-axis of the complex plane. From the relation $|L_0(j\omega_n)| = |G_0(j\omega_n)||G_R(j\omega_n)| = 1/G_M$ results the ratio $|G_R(j\omega_n)| = 1/[G_M|G_0(j\omega_n)|]$ between the radii R_G and $R_L = |G_R|R_G$ of the circles M_G and M_L, respectively. The radius R_L of the dispersion circle M_L is calculated as follows

$$R_L = R_G|G_R| = \frac{R_G}{G_M|G_0(j\omega_n)|}. \tag{66}$$

Substituting (65) and (66) into the general robust performance condition (61) and considering the safety factors χ_L and χ_S, the following inequality is obtained

$$\frac{G_M - 1}{G_M} > \frac{\chi_L R_G}{G_M|G_0(j\omega_n)|} + \chi_S R_S, \tag{67}$$

which after some manipulations is identical to the proven condition (60b). According to the robust performance condition, the chosen value G_M is substituted into (26a) and robust PID controller parameters are obtained from **Table 8**. ϕ_S and G_S are found from the B-parabolas (**Figures 16, 19–21, 24, 25**) considering η_{maxN} and τ_{sN} of the worst-case plant.

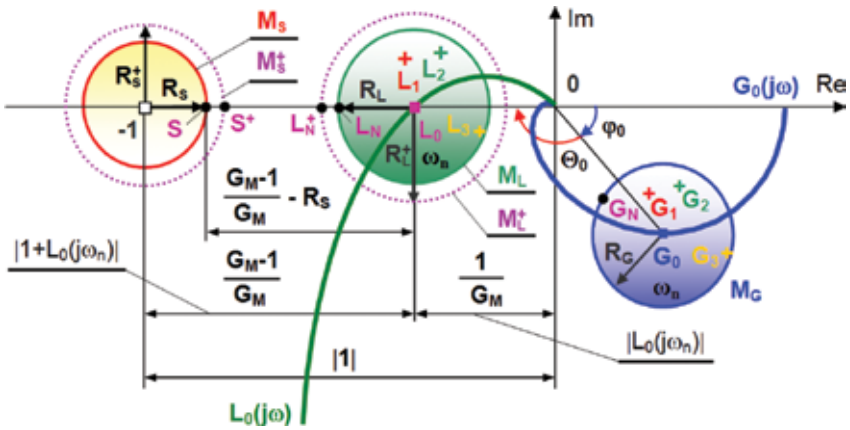

Figure 28. Dispersion circles M_G and M_L and the prohibited area delineated by the circle M_S for gain-margin approach.

3.5.1.3. Examples

3.5.1.3.1. Example 5

Consider the plant model $G_A(s)$ from Subsection 3.4

$$G_{A0}(s) = \frac{K_{A0}}{(T_{A0}s+1)^3} = \frac{1}{(0.01s+1)^3} \tag{68}$$

to be the nominal model of an uncertain system where K_A and T_A are uncertain parameters varying within ±15% from their nominal values K_{A0} and T_{A0} (i.e., the total dispersion is κ = 30%). Let us design a robust PID controller to guarantee η_{maxN} = 30% and a relative settling time τ_{sN} = 12 for the worst-case model of $G_A(s)$.

3.5.1.3.2. Robust PID controller design for the uncertain plant $G_A(s)$—solution and discussion

1. The measured ultimate frequency of the nominal model is ω_{c0} = 173.216[rad/s]. From the robust performance condition results $t_{sN} = \tau_{sN}/\omega_c$ = 12/173.216 = 69.3[ms].

2. For the required performance (η_{maxN},τ_{sN}) = (30%,12) the corresponding values of phase margin and excitation frequency have been selected (ϕ_M,ω_{n0}) = (50°,0.5ω_{c0}) using the pair of "red" B-parabolas in **Figure 16**. As there are two uncertainties in $G_A(s)$ (K_A and T_A), the number of identification experiments is $N = 2^2 = 4$.

3. For ω_{n0} = 0.5,ω_{c0} = 0.5·173.21 = 86.61[rad/s], four points of the family of Nyquist plots corresponding to the uncertain plant model were identified using the sinusoidal excitation: $G_{A1}(j\omega_{n0})$, $G_{A2}(j\omega_{n0})$, $G_{A3}(j\omega_{n0})$ and $G_{A4}(j\omega_{n0})$ (blue "x "in **Figure 29a**). The nominal point $G_{A0}(j\omega_{n0})$ calculated from the coordinates of all identified points $G_{Ai}(j\omega_{n0})$, i = 1, 2, 3, 4 is

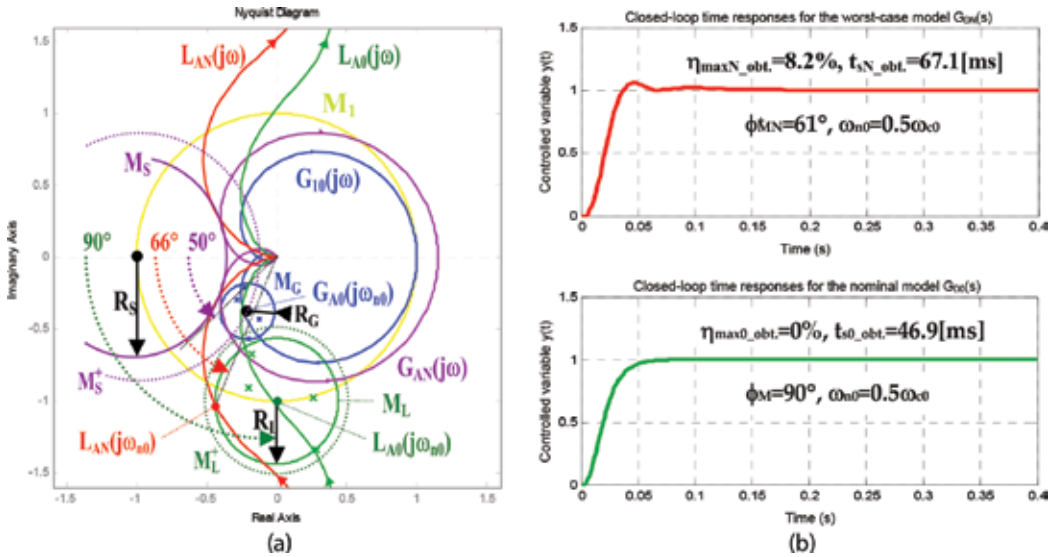

Figure 29. (a) Nyquist plots for $G_A(s)$, η_{maxN} = 30% and τ_{sN} = 12; (b) closed-loop step responses satisfy the required performance η_{maxN} = 30% and τ_{sN} = 12 (upper plot: worst-case plant model; lower plot: nominal plant model).

located on the "blue" Nyquist plot of the nominal model $G_{A0}(j\omega_n)$. The dispersion circle M_G is centered in $G_{A0}(j\omega_{n0})$ with the radius $R_G = 0.199$.

4. The desired robust performance $\eta_{maxN} = 30\%$, $\tau_{sN} = 12$ can be achieved using $\phi_S = 50^\circ$ at the excitation level $\omega_{n0} = 0.5\omega_{c0}$.

5. R.H.S. of the robust performance condition (60a) is $\delta_{0\_RP} = 89.39^\circ$, thus the robust performance condition (60a) $\phi_M > \delta_{0\_RP}$ will be satisfied if choosing for example $\phi_M = 90^\circ$.

6. Using the designed PID controller, the nominal point $G_{A0}(j\omega_{n0})$ is shifted to $L_{A0}(j\omega_{n0}) = G_{A0}(j\omega_{n0})G_{R\_rob}(j\omega_{n0}) = 1e^{-j90^\circ}$ on the unit circle M_1 (**Figure 29a**).

7. The smallest phase margin estimated from the location of the worst-case point $L_{AN} = 1.13e^{-j114^\circ}$ is $\phi_{MN} = 66.2^\circ$. The achieved smallest phase margin $\phi^+_{MN} = 61^\circ$ is given by the intersection of the "red" Nyquist plot and the unit circle M_1 (closest to the negative real half-axis).

8. Radius of the prohibited area $R_S = \sin\phi_S = \sin(50 \cdot 3.14/180) = 0.766/\chi_S = 0.6383$ multiplied by the expansion coefficient $\chi_S = 1.2$, as well as the $\chi_S = 1.1$-times enlarged radius R_L of the dispersion circle M_L guarantee that none of the open-loop Nyquist plots enters the prohibited area delineated by the M_S circle. The enlarged circles $M_L{}^+$ and $M_S{}^+$ (dotted plots in **Figure 29a**) are touching, which indicates fulfillment of the robust performance condition.

9. From the closed-loop step response of the worst-case plant model (**Figure 29b**, red plot) results $\eta_{maxN\_obtained} = 8.2\%$ and the relative settling time $\tau_{sN\_obtained} = \omega_{c0}t_{sN\_obtained} = 173.216 \cdot 0.0671 = 11.62$, which proves achievement of the specified performance. Using the phase margin $\phi_M = 90^\circ$ at the identification level $\omega_{n0} = 0.5\omega_{c0}$ ("red" B-parabolas in **Figure 16a**) corresponds to the nominal performance $\eta_{max0} = 2\%$ and $\tau_{s0} = 10$. The closed-loop step response in **Figure 29b** (green plot) corresponding to the nominal model satisfies $\eta_{max0\_obtained} = 0\%$ and $\tau_{s0\_obtained} = 173.216 \cdot 0.0469 = 8.12$ as expected.

3.5.1.3.3. Example 6

Consider the plant model from the Subsection 3.4

$$G_{D0}(s) = \frac{K_{D0}(-\alpha_D s + 1)}{(T_{D0}s + 1)^3} = \frac{0.8(-7.5s + 1)}{(27.5s + 1)^3} \tag{69}$$

to be the nominal model of the uncertain plant $G_D(s)$ with parameters K_D, T_D and α_D varying within ±15% from their nominal values K_{S0}, T_{S0} and α_{D0} (the total dispersion is $\kappa = 30\%$). A robust PID controller is to be designed to guarantee specified performance in terms of a maximum overshoot $\eta_{maxN} = 5\%$ and a relative settling time $\tau_{sN} = 12$ for the worst-case model of $G_D(s)$.

3.5.1.3.4. Robust PID controller design for the uncertain plant $G_D(s)$—solution and discussion

1. The measured ultimate frequency of the nominal model is $\omega_{c0} = 0.0488$[rad/s]. From the requirements on the nominal closed-loop performance results: $t_s = \tau_{s0}/\omega_c = 12/0.0488 = 245.9$[s].

2. For the required performance $(\eta_{maxN},\tau_{sN}) = (5\%,12)$ the corresponding values of gain margin and excitation frequency have been selected $(G_M,\omega_n) = (18\text{ dB},0.65\omega_{c0})$ using the pair of "red" B-parabolas in **Figure 25**. As there are three uncertain parameters in $G_D(s)$ (K_D, T_D and α_D), the number of identification experiments is $N = 2^3 = 8$.

3. For $\omega_{n0} = 0.65\omega_{c0} = 0.65 \cdot 0.04880 = 0.03172$[rad/s], eight points of the family of Nyquist plots corresponding to the uncertain plant model were identified using the sinusoidal excitation: $G_{D1}(j\omega_n)\ldots G_{D8}(j\omega_n)$ (depicted by blue "x" in **Figure 30**). The nominal point $G_{D0}(j\omega_n)$ calculated from the coordinates of all identified points $G_{Di}(j\omega_n)$, i = 1…8 is located on the Nyquist plot of the nominal model $G_{D0}(j\omega_n)$ (blue curve) thus proving correctness of the identification. Radius of the dispersion circle M_G centered in the nominal point $G_{D0}(j\omega_{n0})$ with the radius $R_G = 0.164$.

4. The desired robust performance $\eta_{maxN} = 30\%$, $\tau_{sN} = 12$ can be achieved using $\phi_S = 50^\circ$ at the excitation level $\omega_{n0} = 0.5\omega_{c0}$.

5. Using the designed robust PID controller, the nominal point $G_{D0}(j\omega_{n0})$ of the plant is shifted to the point $L_{D0}(j\omega_{n0}) = G_{D0}(j\omega_{n0})G_{R\_rob}(j\omega_{n0}) = 0.0841e^{-j180^\circ}$ located on the unit circle. The nominal open-loop Nyquist plot (green plot) crosses $L_{D0}(j\omega_{n0})$ (**Figure 14**), the radius of the circle M_L is $R_L = 0.0400$.

6. The smallest gain margin $G^+_{MN} = 18.8$ dB is estimated from the position of the worst-case point $L_{DN}(j\omega_{n0}) = 0.112e^{-j197^\circ}$. The achieved smallest gain margin is given by the intersection point of the red Nyquist plot with the negative real half-axis of the complex plane $G^+_{MN} = 16.9$ dB.

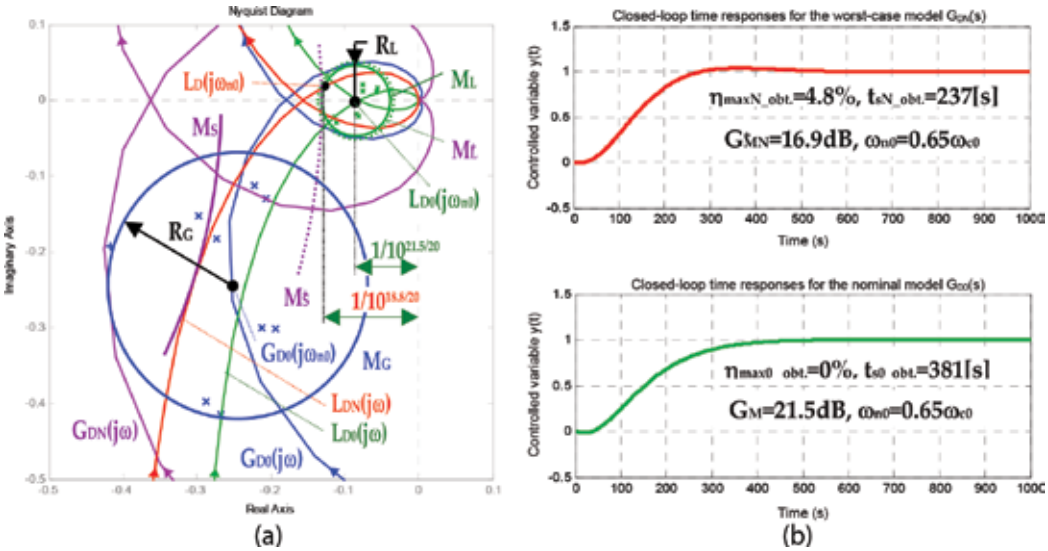

Figure 30. (a) Nyquist plots for $G_D(s)$, $\eta_{maxN} = 5\%$ and $\tau_{sN} = 12$; (b) closed-loop step responses with $G_D(s)$ for the required performance $\eta_{maxN} = 5\%$ and $\tau_{sN} = 12$ (upper plot: worst-case plant model; lower plot: nominal plant model).

7. Both the radius of the prohibited area $R_S = (G_S-1)/G_S = (10^{18/20}-1)/10^{18/20} = 0.8741/\chi_S = 0.699$ multiplied by the expansion coefficient $\chi_S = 1.2$, as well as the radius R_L of the dispersion circle M_L enlarged $\chi_S = 1.1$-times guarantee that none of the open-loop Nyquist plots enters the prohibited area delineated by the M_S circle. The enlarged circles M_L^+ a M_S^+ in **Figure 30a** (dotted curves) touch, which indicates fulfillment of the robust performance condition.

8. As $G_M = 21.5$ dB at the excitation level $\omega_{n0} = 0.65\omega_{c0}$ has been considered, according to "pink "B-parabolas in **Figure 25a** nominal performance $\eta_{max0} = 1.5\%$ and $\tau_{s0} = 21$ is expected. The nominal closed-loop step response in **Figure 30b** (green plot) shows the nominal performance in terms of $\eta_{max0\_obtained} = 0\%$ and $\tau_{s0\_obtained} = 0.0488 \cdot 381 = 18.59$ as expected.

9. From the closed-loop step response of the worst-case plant model (**Figure 30b**, red plot) results $\eta_{maxN\_obtained} = 4.8\%$ and the relative settling time $\tau_{sN\_obtained} = \omega_{c0}t_{sN\_obtained} = 0.0488 \cdot 237 = 11.57$ which proves achievement of the specified performance. Using the gain margin $G_M = 21.5$ dB at the excitation level $\omega_{n0} = 0.65\omega_{c0}$ ("pink" B-parabolas in **Figure 25a**) indicates the expected nominal performance $\eta_{max0} = 1.5\%$ and $\tau_{s0} = 21$. The closed-loop step response in **Figure 30b** (green plot) corresponding to the nominal model satisfies $\eta_{max0\_obtained} = 0\%$ and $\tau_{s0\_obtained} = 0.0488 \cdot 381 = 18.59$ as expected.

4. Conclusion

A novel frequency-domain PID design method for performance specified in terms of maximum overshoot and settling time is presented applicable for uncertain systems with parametric uncertainties. One of the main results is developed empirical charts called B-parabolas; this insightful graphical tool is used to transform engineering time-domain performance specifications (maximum overshoot and settling time) into frequency-domain performance measures (phase margin and gain margin). The developed PID design method is based on shaping the closed-loop step response using various combinations of excitation signal frequencies and required phase and gain margins. Using B-parabolas, it is possible to shape time responses of processes with various types of dynamics. By applying appropriate PID controller design methods including the above presented, it is possible to achieve cost-effective control of processes with uncertainties. The presented advanced external harmonic excitation-based design method contributes to improve the unfavorable statistical ratio between the properly tuned to all implemented PID controllers in industrial control loops.

Author details

Štefan Bucz* and Alena Kozáková

*Address all correspondence to: stefan.bucz@stuba.sk

Faculty of Electrical Engineering and Information Technology, Slovak University of Technology, Bratislava, Slovak Republic

References

[1] Åström KJ, Hägglund T. PID Controllers: Theory, Design and Tuning. 2nd ed. Research Triangle Park: Instrument Society of America; 1995. ISBN 1-55617-516-7

[2] Åström KJ, Hägglund T. Benchmark Systems for PID Control. In: IFAC Workshop on Digital Control PID'00; 5-7 April 2000; Terrassa, Spain. 2000. pp. 181-182

[3] Bakošová M, Fikar M. *Riadenie procesov*, Edícia vysokoškolských učebníc, Slovenská technická univerzita v Bratislave, Vydavateľstvo STU v Bratislave. Bratislava, Slovenská republika; 2008. ISBN 978-80-227-2841-6 (in Slovak)

[4] Balátě J. Automatické řízení. 2. přepracované vydání. Nakladatelství BEN—technická literatúra. Praha, Česká republika; 2004. ISBN 80-7300-148-9

[5] Bialkowski WL. Dreams versus reality: A view from both sides of the gap. Pulp and Paper Canada. 1993;**94**(11):19-27

[6] Bucz Š. Engineering methods of PID controller tuning for specified performance [doctoral thesis]. Bratislava, Slovenská Republika: Slovenská Technická Univerzita v Bratislave; 2011 (in Slovak)

[7] Bucz Š, Veselý V, Kozáková A, Kozák Š. A novel PID controller design methodology for specified performance using ultimate plant parameters. In: Proceedings of the 19th World Congress of the International Federation of Automatic Control. IFAC; 2014. pp. 4909-4914. ISBN 978-3-902823-62-5

[8] Coon GA. How to find controller settings from process characteristics. Control Engineering. May 1956;**3**(5):66-76

[9] Crolla D, Foster DE, Kobayashi T, Vaughan N. Encyclopedia of Automotive Engineering. United Kingdom: John Wiley and Sons Ltd.; 2015

[10] Ford RL. The determination of the optimum process-controller settings and their confirmation by means of an electronic simulator. Proceedings of the IEE, Part 2. 1953;**101**(80): pp. 141-155 and pp. 173-177

[11] Grabbe EM, Ramo S, Wooldrige DE. Handbook of Automation Computation and Control. Vol. 1, 2, 3. New York; 1959–61

[12] Haalman A. Adjusting controllers for a deadtime process. Control Engineering. 1965; (July):71-73

[13] Hang CC, Åström KJ. Practical aspects of PID auto-tuners based on relay feedback. In: Proceedings of the IFAC Adaptive control of Chemical Processes Conference, Copenhagen, Denmark; 1988. pp. 153-158

[14] Harsányi L, Murgaš J, Rosinová D, Kozáková A. Teória automatického riadenia, Edícia skrípt. Slovenská Technická Univerzita v Bratislave. 1998 (in Slovak)

[15] Chandrashekar R, Sree RP, Chidambaram M. Design of PI/PID controllers for unstable systems with time delay by synthesis method. Indian Chemical Engineer Section A. 2002; **44**(2):82-88

[16] Chau PC. Process Control—A First Course with MATLAB. 1st ed. New York: Cambridge University Press; 2002. ISBN 978-0521002554

[17] Chen D, Seborg DE. PI/PID controller design based on direct synthesis and disturbance rejection. Industrial and Engineering Chemistry Research. 2002;**41**:4807-4822

[18] Chien KL, Hrones JA, Reswick JB. On the automatic control of generalised passive systems. Transactions of the ASME. 1952;**74**(February):175-185

[19] Kozáková A, Veselý V, Osuský J. Decentralized digital PID design for performance. In: 12th IFAC Symposium on Large Scale Systems: Theory and Applications; 12-14 July 2010; Lille, France. Ecole Centrale de Lille; 2010. ISBN 978-2-915-913-26-2

[20] Leva A, Maggio M. A systematic way to extend ideal pid tuning rules to the real structure. Journal of Process Control. 2011;**21**:130-136

[21] Leva A, Negro S, Papadopoulos AV. PI/PID autotuning with contextual model parametrisation. Journal of Process Control. 2010;**20**:452-463

[22] Morari M, Zafiriou E. Robust Processs Control. Englewood Cliffs, New Jersey, USA: Prentice-Hall Inc.; 1989. ISBN 0137821530, 07632

[23] O'Dwyer A. Handbook of PI and PID Controllers Tuning Rules. 2nd ed. London: Imperial College Press; 2006. ISBN 1860946224

[24] Osuský J, Veselý V, Kozáková A. Robust Decentralized Controller Design with Performance Specification, Vol. 4(1). Kumamoto, Japan: ICIC Express Letters; 2010. pp. 71-76. ISSN 1881-803X

[25] Padula F, Visioli A. Tuning rules for optimal PID and fractional-order PID controllers. Journal of Process Control. 2011;**21**:69-81

[26] Padula F, Visioli A. On the stabilizing PID controllers for integral processes. IEEE Transactions on Automatic Control. 2012;**57**:494-499

[27] Pettit JW, Carr DM. Self-tuning controller. US Patent No. 4669040; 1987

[28] Rotach V. Avtomatizacija nastrojki system upravlenija. Moskva, Russia: Energoatomizdat; 1984 (in Russian)

[29] Rotach V. Calculation of the Robust Settings of Automatic Controllers, Vol. 41(10). Moscow, Russia: Thermal Engineering (Russia); 1994. pp. 764-769

[30] Suyama K. A simple design method for sampled-data PID control systems with adequate step responses. Proceedings of the International Conference on Industrial Electronics, Control, Instrumentation and Automation. 1992:1117-1122

[31] Veronesi M, Visioli A. Performance assessment and retuning of PID controllers. Industrial and Engineering Chemistry Research. 2009;**48**:2616-2623

[32] Veronesi M, Visioli A. An industrial application of a performance assessment and retuning technique for PI controllers. ISA Transactions. 2010;**49**:244-248

[33] Veselý V. Easy tuning of PID controller. Journal of Electrical Engineering. 2003;**54**(5–6): 136-139, Bratislava, Slovak Republic. ISSN 1335-3632

[34] Vilanova R. IMC based robust PID design: Tuning guidelines and automatic tuning. Journal of Process Control. 2008;**18**:61-70

[35] Visioli A. Fuzzy logic based set-point weight tuning of PID controllers. IEEE Transactions on Systems, Man, and Cybernetics—Part A. 1999;**29**:587-592

[36] Visioli A. Tuning of PID controllers with fuzzy logic. IEE Proceedings—Control Theory and Applications. 2001;**148**(1):180-184

[37] Visioli A. Practical PID control. Advances in industrial control. Springer-Verlag London Limited; 2006. ISBN 1-84628-585-2

[38] Visioli A. Research trends for PID controllers. Acta Polytechnica. 2012;**52**(5/2012)

[39] Vítečková M. Seřízení regulátorů metodou požadovaného modelu. Ostrava: Skriptum Vysoká škola báňska, Technická univerzita; 1998. ISBN 80-7078-628-0 (in Czech)

[40] Vítečková M. Seřízení číslicových i analogových regulátorů pro regulované soustavy s dopravním zpožděním (Digital and analog controller tuning for processes with time delay). Automatizace. 1999;**42**(2):106-111 (in Czech)

[41] Vítečková M, Víteček A, Smutný L. Controller tuning for controlled plants with time delay. In: Preprints of Proceedings of PID'00: IFAC Workshop on Digital Control; 5-7 April 2000; Terrassa, Spain. 2000. pp. 83-288

[42] Wang L, Cluett WR. Tuning PID controllers for integrating processes. IEE Proceedings—Control Theory and Applications. 1997;**144**(5):385-392

[43] Wang Y-G, Shao H-H. PID autotuner based on gain- and phase-margin specification. Industrial and Engineering Chemistry Research. 1999;**38**:3007-3012

[44] Wittenmark B. A sample-induced delays in synchronous multirate systems. In: European Control Conference; Porto, Portugal. 2001. pp. 3276-3281

[45] Wojsznis WK, Blevins TL, Thiele D. Neural network assisted control loop tuner. In: Proceedings of the IEEE International Conference on Control Applications, Vol. 1; USA: 1999. pp. 427-431

[46] Xue D, Chen Y, Atherton DP. Linear Feedback Control: Analysis and Design with MATLAB. SIAM Press; 2007. ISBN 978-0-898716-38-2

[47] Yu C-C. Autotuning of PID Controllers. A Relay Feedback Approach. 2nd ed. Springer-Verlag London Limited; 2006. ISBN 1-84628-036-2

[48] Ziegler JG, Nichols NB. Optimum settings for automatic controllers. ASME Transactions. 1942;**64**:759-768

[49] Zhuang M, Atherton DP. Automatic tuning of optimum PID controllers. IEE Proceedings Part D: Control Theory and Applications. 1993;**140**(3):216-224. ISSN 0143-7054

Chapter 5

PID Control for Takagi-Sugeno Fuzzy Model

Taieb Adel and Chaari Abdelkader

Additional information is available at the end of the chapter

http://dx.doi.org/10.5772/intechopen.74295

Abstract

In this chapter, we deal with the problem of controlling Takagi-Sugeno (TS) fuzzy model by PID controllers using the particle swarm optimization (PSO). Therefore, a new algorithm is proposed. This algorithm relies on the use of a new objective function taking into account both the performance indices and the error signal. The advantages of this approach are discussed through simulations on a numerical example.

Keywords: nonlinear system, TS fuzzy model, PID, self-tuning of PID controller, PSO

1. T-S fuzzy model

The theory of modeling based on multiple models has evolved greatly. Indeed, several techniques have been developed in the literature. The common feature of all these modeling techniques is the decomposition of the dynamic behavior of the system into a number of operating zones. Each zone is characterized by a local linear model. Fuzzy logic based on the use of linguistic rules, heuristic strategies and the operator's know-how. Subsequently, it has undergone a major evolution mainly in Japan where it has been applied in several industrial applications. This type of model proposed by Takagi and Sugeno (1985) makes it possible to express a nonlinear system in several locally linear subsystems. The validity of each local model is defined by a weighting function with bounded support.

The TS model is built on a set of rules of type:

- R^i: "IF premises THEN consequence"

where the premises are obtained from the linguistic propositions allowing the evaluation of the weighting functions and where the consequences corresponding to the local models.

We consider a class of nonlinear systems defined by:

$$y(t+1) = f(X(t)) \tag{1}$$

with the regressor vector $X(t)$ is:

$$X(t) = [y(t), y(t-1), \ldots, y(t-m, u(t), u(t-1), \ldots, u(t-m)] \tag{2}$$

where k represents the discrete time, n and m denote, respectively, the number of delayed output and the number of delayed input. The function $f(x(t))$ is approximated by a TS fuzzy model which is charities by consequent rules that are local linear function of the input variables [1]. The fuzzy rules of the TS model take the following general form:

$$R^i : \text{if } X_1 \text{ is } A_1^i \text{ and if } X_z \text{ is } A_z^i \text{ Then } y_i(t) = [X(t)\,1]\theta_i^T \tag{3}$$

where R^i denotes the ith IF-THEN rule, r is the number of rules, $A_j^i\,(j = 1, \ldots, z)$ is the fuzzy subset, $u(t)$ is the system input variable, $y(t)$ is the system output, $\theta_i = [a_{i1}, a_{i2}, \ldots, a_{iz}, b_{i0}]$ is the parameter vector of the corresponding local linear model. Let $\mu_i(X(t))$ is the normalized membership function of the inferred fuzzy set A^i, where $A^i = \Pi_{j=1}^z A_j^i$. The final output is calculated as the average of the outputs corresponding to the rules R^i, weighted by the normalized degree of completion (membership), according to the following expression:

$$\widehat{y} = \sum_{i=1}^{r} \mu_{it} y_i \tag{4}$$

The membership values μ_{it} have to satisfy the following conditions:

$$\mu_{it} \in [0\,1] \;\; i = 1, \ldots, r \tag{5}$$

$$\sum_{i=1}^{r} \mu_{it} = 1 \;\; t = 1, \ldots, N \tag{6}$$

$$0 < \sum_{k=1}^{N} \mu_{it} < N \quad i = 1, \ldots, r \tag{7}$$

Once the parameters of the premises are fixed, the parameters of the consequent for each rule can be obtained using the recursive weighted least squares technique, using the values of the membership degrees of the fuzzy partition matrix of the classification process as weights [2]:

The steps of the WRLS method are summarized in the following algorithm:

Initialize: $\boldsymbol{\theta}_{ig(0)} = 0$ and $\mathbf{P}_{i(0)} = \alpha_i I$.

for $g = 1, \;\; \ldots, \;\; c_i$

$$\boldsymbol{\theta}_{ig(t)} = \boldsymbol{\theta}_{ig(t-1)} + \mathbf{L}_{i(t)}\left(y_{i(t)} - \left[\mathbf{x}_{i(t)}\ 1\right]\boldsymbol{\theta}_{ig(t-1)}^{T}\right) \tag{8}$$

$$\mathbf{L}_{i(t)} = \frac{\mathbf{P}_{i(t-1)}\left[\mathbf{x}_{i(t)}\ 1\right]^{T}}{1/\mu_{igt} + \left[\mathbf{x}_{i(t)}\ 1\right]\mathbf{P}_{i(t-1)}\left[\mathbf{x}_{i(t)}\ 1\right]^{T}} \tag{9}$$

$$\mathbf{P}_{i(t)} = \mathbf{P}_{i(t-1)} - \mathbf{L}_{i(t)}\left[\mathbf{x}_{i(t)}\ 1\right]\mathbf{P}_{i(t-1)} \tag{10}$$

with $k = 1, \ldots, N$, $\mathbf{P}_{i(t-1)} \in \Re^{(M_i+1)\times(M_i+1)}$ and $\mathbf{L}_{i(t)} \in \Re^{(M_i+1)}$.

end for

2. PID control by pole placement

This section is intended to model the digital PID controller in a new form RST. The control structure RST is the establishment of three polynomials $R(q^{-1})$, $S(q^{-1})$ and $T(q^{-1})$. According to the first section, the local linear systems can be represented by:

$$Y(q^{-1})A(q^{-1}) = B(q^{-1})u(q^{-1}) \tag{11}$$

Indeed, the vector x_k takes the following form: $x_k = [-y(k-1) - y(k-2)\ldots - y(k-n)\,u(k-1)\ldots u(k-m)]$. This form is heard when determining PID controller parameters by the method of poles placement. **Figure 1** shows the standard form of RST controller.

In this chapter, we consider only two branches R and S, as shown in **Figure 2**, that is to say:

$$T(q^{-1}) = R(q^{-1}) \tag{12}$$

The transfer function in a closed loop is given by:

$$H_{bf} = \frac{B(q^{-1})}{A(q^{-1})S(q^{-1}) + B(q^{-1})R(q^{-1})} \tag{13}$$

again:

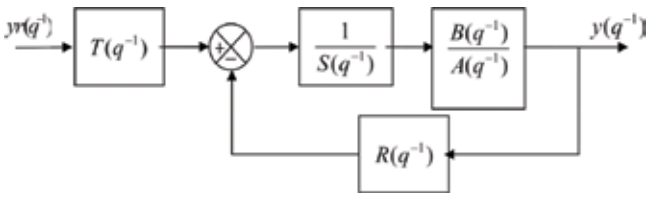

Figure 1. Standard form of RST.

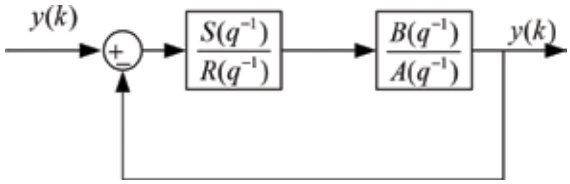

Figure 2. RST structure.

$$H_{bf} = \frac{B(q^{-1})}{P'(q^{-1})} \tag{14}$$

with:

$$\begin{aligned} &e(k) = yr(k) - y(k) \\ &B(q^{-1}) = b_1 q^{-1} + b_2 q^{-2} \\ &A(q^{-1}) = 1 + a_1 q^{-1} + a_2 q^{-2} \\ &R(q^{-1}) = r_0 + r_1(q^{-1}) + r_2(q^{-2}) \\ &S(q^{-1}) = (1 - q^{-1})(1 + s_1(q^{-1})) \end{aligned} \tag{15}$$

For a characteristic polynomial $P^1(q^{-1})$, the poles of the closed loop transfer function are imposed to arrive at the performances required by the follow-up of the specifications.

This problem boils down to solving the following equation:

$$P'(q^{-1}) = A(q^{-1})S(q^{-1}) + B(q^{-1})R(q^{-1}) \tag{16}$$

From the after Scheme 4, the equation of regulator is written by:

$$C(q^{-1}) = K_P \left(1 + \frac{1}{T_I(1 - q^{-1})} + \frac{\frac{N_f T_d}{T_d + N_f Te}(1 - q^{-1})}{1 - \frac{T_d}{T_d + N_f Te} q^{-1}} \right) \tag{17}$$

To simplify Eq. (17), we substitute:

$$a = \frac{Te}{T_I} \tag{18}$$

$$b = \frac{T_d}{T_d + N_f Te} \tag{19}$$

from which we obtain the following standard form:

$$C(q^{-1}) = K_p \left(1 + \frac{a}{1 - q^{-1}} + N_f b \frac{1 - q^{-1}}{1 - bq^{-1}} \right) \tag{20}$$

http://dx.doi.org/10.5772/intechopen.74295

The parameters of the digital PID regulator (r_0, r_1, r_2 and s_1) are chosen according to the desired poles defined by the polynomial $P(q^{-1})$.

The characteristic polynomial can be in the following form:

$$P'(q^{-1}) = 1 + p_1 q^{-1} + p_2 q^{-2} \tag{21}$$

The values of p_1 and p_2 are chosen from the specifications imposed by the specifications (rise time, damping, overshoot, etc.) defined in general by comparing the behavior of the process to that of continuous system of second order.

$$\begin{cases} p_1 = -2e^{\zeta} w_n Te cos\left(w_n Te\sqrt{1-\zeta^2}\right) \\ p_1 = e^{-2\zeta w_n Te} \end{cases} \tag{22}$$

where *zeta* is a damping coefficient and w_n is a pulsation. We wrote:

$$P(q^{-1}) = A(q^{-1})S(q^{-1}) + B(q^{-1})R(q^{-1}) \tag{23}$$

By identification, we find:

$$\begin{cases} b_1 r_0 + s_1 = p_1 + 1 - a_1 \\ b_2 r_0 + b_1 r_1 + (a_1 - 1)s_1 = p_2 + a_1 - a_2 \\ b_2 r_1 + b_1 r_2 + (a_2 - a_1)s_1 = a_2 \\ b_2 r_2 - a_2 s_1 = 0 \end{cases} \tag{24}$$

The control law is:

$$u(q^{-1}) = \frac{R(q^{-1})}{S(q^{-1})} e(q^{-1}) \tag{25}$$

From where:

$$u(k) = r_0 e(k) + r_1 e(k-1) + r_2 e(k-2) + (1 - s_1)u(k-1) + s_1 u(k-2) \tag{26}$$

The structure of the corrector is the standard structure discretized by the approximation upper rectangles, and to find the values of the PID parameters will take the following expression:

$$\begin{cases} K_p = \dfrac{r_0 s_1 - r_1 - (2 + s_1)r_2}{(1 + s_1)^2} \\ T_i = \dfrac{TeK_p(1 + s_1)}{r_0 + r_1 + r_2} \\ T_d = \dfrac{Te\left(s_1^2 r_0 - s_1 r_1 + r_2\right)}{K_p(1 + s_1)^3} \end{cases} \tag{27}$$

3. PID controller based on PSO

3.1. PSO algorithm

Particle swarm optimization (PSO) is a stochastic technique based on collective intelligence, inspired by nature. It was developed by Kennedy and Eberhart [3]. The PSO algorithm is inspired by collective behavior in certain social animals such as fish and migratory birds. This algorithm shares many similarities with evolutionary computational techniques such as genetic algorithms. Indeed, the latter are initialized with random solutions and search for optimums by updating generations involved. However, the PSO has no evolutionary operator such as the crossing and the mutation in the image of genetic algorithms.

In the PSO, each individual of the population is called particle, while the population is known as swarm. It should be noted that a particle can benefit from the movements of other particles in the same population to adjust its position and velocity during the optimization process. Each individual uses local information to which he can access the movement of his nearest neighbors to decide his own move. Very simple rules like "staying close to other people," "going in the same direction" and "going at the same speed" are enough to maintain the cohesion of the whole group. At each displacement, the performance of each particle is measured by its position and velocity by minimizing a performance function called fitness [4].

The PSO's basic algorithm works on a population called a swarm of possible solutions, which are called particles. These particles are placed randomly in the search space of the objective function. At each iteration, the particles move, taking into account their best position (selfish displacement) but also the best position of its vicinity. In fact, the new speed is calculated from the following formula [3]:

$$V_{id}(t+1) = wV_{id}(t) + c_1 r_1 \left(p_{id}(t) - x_{id}(t)\right) + c_2 r_2 \left(p_{gd}(t) - x_{id}(t)\right) \tag{28}$$

In this equality, t is the number of iteration, $V_{id}(t)$ and $x_{id}(t)$ stand for separately the speed of the particle i at its t times and the d-dimension quantity of its position, c_1 and c_2 are the acceleration coefficients, r_1 and r_2 are two random numbers drawn uniformly in $[01]$. p_{id} and p_{gd} are, respectively, the best position reached and the best position of the vicinity reached of the particle i and w is an inertial coefficient defined by:

$$w = w_{\max}\left(\frac{w_{\max} - w_{\min}}{iter_{\max}}\right) iter \tag{29}$$

where $iter_{max}$ is the maximum of iteration in evolution process, $w_{\min}$ and $w_{\max}$ are the minimum and maximum values of w, respectively, and $iter$ is the current value of iteration. The position of the particle can then be determined by the speed that we have just calculated:

$$x_{id} = x_{id} + V_{id} \tag{30}$$

We generate $V_{id}(0)$ and $x_{id}(0)$ at the beginning of our algorithm. The PSO algorithm stops if one of these convergence criteria is reached:

http://dx.doi.org/10.5772/intechopen.74295

- the maximum number of iterations t_{max} is reached;
- the speed variation tends to zero; and
- the fitness function is satisfied.

3.2. Tuning of PID using PSO optimization

The PSO optimization module complete the self-tuning of PID parameters with a microprocessor that achieves the optimum of PID parameters. These parameters are used to retune the PID controller in PID controller module. To seek the optimum parameters *kp*, *ki* and *kd* of PID controller, PSO program should search in D-dimensional search space. The function optimization problem can be viewed as a 3-dimensional space in this chapter. That is, tuning of PID controller parameters is to search optimization value in *kp*, *ki* and *kd*, the 3-dimensionsal search spaces. With the optimized parameters based on PSO algorithm, the PID controller can achieve the optimal properties, that is, a fast system with a minimum of overrun, there is a compromise between performance and minimum energy [5].

In most cases, PID controller work with an error signal (e) that is calculated from the process variable (y) and setpoint (y_r). The error represents the deviation of the process variable from the setpoint. Then, the error signal is described as:

$$e(t) = y_r(t) - y(t) \tag{31}$$

A PID controller optimized with PSO algorithm was developed for a TS Fuzzy system. It was also called the PSO-PID controller. PSO algorithm is mainly utilized to determine three optimal PID gains.

Adjusting the parameters of a PID controller can be considered as an optimization problem where it is a matter of finding the optimal solution of the gains of the controller in a predefined search space in order to allow the system to have certain desired performances. In this context, the PSO algorithm can be applied to find the optimal combination of the proportional, integral and derivative gains of the PID controller. During the application of the PSO, the initial population will be created randomly with Np individuals containing three decision variables: *kp*, *ki* and *kd*. To evaluate the individuals, we inject these gains into the PID controller and measure the parameters of the corresponding system output using the parameters of the TS model. The choice of the cost function is determined by the objective to be achieved. These objectives are determined by the performance defined in the specifications. Typically, this is static error, rise time, stabilization time and maximum allowed exceedance.

In the literature, we can find a multitude of performance indices. Most of these indices are based on the optimization error. The integrated square error (ISE) is given by:

$$J = \int_0^\infty |e^2(t)| dt \tag{32}$$

Another fitness function is integrated time weight square error (ITSE), which is given as follows:

$$J = \int_0^\infty t|e^2(t)|dt \tag{33}$$

It seems simpler, yet it is hard to get the ideal time response too. Another widely used fitness function is:

$$J = \int_0^\infty \left(w_1|e(t)| + w_2u^2(t)\right)dt \tag{34}$$

where $e(t)$ and $u(t)$ represent, respectively, the system error and the output of controller, the utilization of this second item is to limited energy (**Figure 3**).

Since, more than the error signal, the performance indices in the time domain are also the overshoot ($D\%$), steady-state error (Ess) the settling time (T_s) and the rise time (T_r). The performance criteria must include all these performances. Therefore, we proposed a new objective function and it is described by the following equation:

$$J = \left(1 - \exp(-\beta)\right)(D\% + Ess) + \exp(-\beta)(T_s - T_r) \times \int_0^\infty t|e^2(t)|dt \tag{35}$$

The framework of online parameter self-tuning for nonlinear system based on TS Fuzzy model is depicted in **Figure 3**.

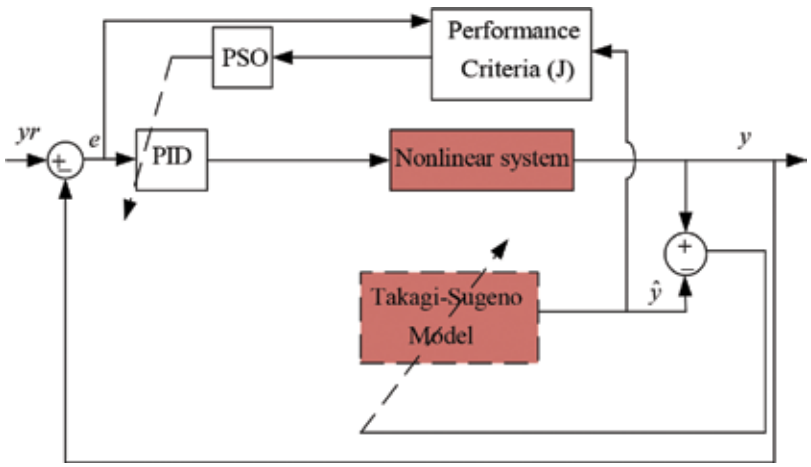

Figure 3. Block diagram of a PID-PSO algorithm.

http://dx.doi.org/10.5772/intechopen.74295

4. Simulation results

This section presents a simulation example to show an application of the proposed control algorithm and its satisfactory performance.

The nonlinear system is characterized by this equation [6]:

$$y(k) = a1^* \sin\left(y(k-1)\right) + a2^* y(k-2) + a3^* u(k-2)^* y(k-3) + b1^* u(k-1) + b2^* \left(\tanh(0.7^* u(k-3))^2\right) \tag{36}$$

with $a1 = 0.4$; $a2 = 0.3$; $a3 = 0.1$; $b1 = 0.6$; and $b2 = 1.8$. Here, $y(k)$ is the output and $u(k)$ is the input which is uniformly bounded in the region $[-2, 2]$.

We choose $[-y(k-1), -y(k-2), u(k-1), u(k-2)]$ as inputs variables, and the number of fuzzy rules is four. The setup applied in this work was the following: the population size was 20, the stopping criterion was 30 generations, $w_{min} = 0.5$, $w_{max} = 0.9$ and $c_1 = c_2 = 2$.

We simulated two experimental cases. In case 1, the simulation result of the control pole placement for the nonlinear system is shown in **Figure 4**.

It can be seen from **Figure 4**, we note that the output of command has an important overshooting. In case 2, the PSO algorithm is adding to PID control. **Figure 5** shows simulation results of the output signal of the control system.

We make a comparative study of PID control by pole placement method and the optimization algorithm of PSO (**Table 1**).

We note though, the advantage of optimizing the parameters of PID controller by PSO compared with the method of pole placement quality control, we observed that the overshoot decreases and the algorithm converges in minimum time.

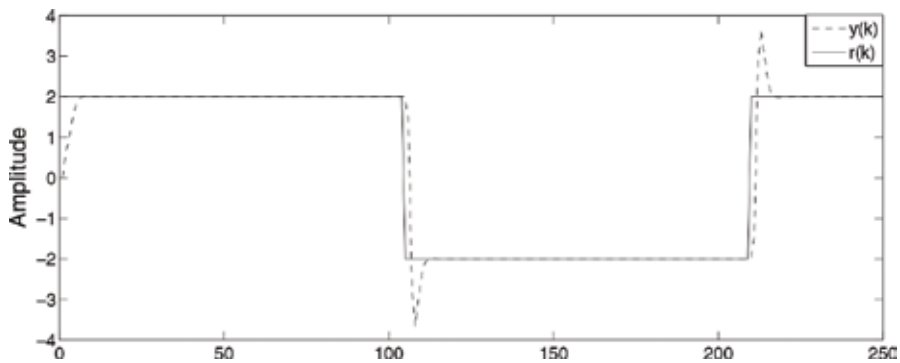

Figure 4. Output signal: PID-pole placement method.

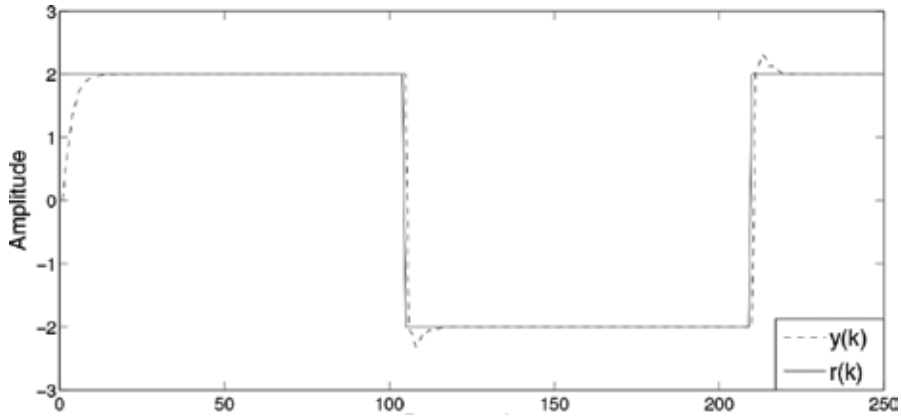

Figure 5. Output signal: PID-optimization of PSO.

	Pole placement method	**Optimization of PSO**
$D(\%)$	64	15
$T_s(s)$	13.568	8.568
$T_r(s)$	10	8

Table 1. Result of PID parameters and PID-PSO.

5. Conclusion

We studied the PID control of a nonlinear system of Takagi-Sugeno for a square input signal using pole placement technique. With this method, we obtain results with an important overshooting. To solve this problem, we have compiled the PID control algorithm with PSO optimization algorithm that it has given good results.

Author details

Taieb Adel* and Chaari Abdelkader

*Address all correspondence to: taeibadel@live.fr

Laboratory of Engineering of Industrial Systems and Renewable Energy, National High School of Engineers of Tunis (ENSIT), Tunis, Tunisia

References

[1] Lagrat I, Ouakka H, Boumhidi I. Adaptive control of a class of nonlinear systems based on Takagi-Sugeno fuzzy model. In: Information and Communication Technologies International Symposium (ICTIS'07); Fez, Morocco. 2007. pp. 3-5

[2] Kung CC, Su JY. Affine Takagi-Sugeno fuzzy modelling algorithm by fuzzy cregression models clustering with a novel cluster validity criterion. IET Control Theory Application. 2007;**1**(5):1255-1265

[3] Kennedy J, Eberhart RC. Particle swarm optimization. In: Proceedings of IEEE International Conference on Neural Networks; Perth, Australia. 1995. pp. 1942-1948

[4] Clerc M, Kennedy J. The particle swarm: Explosion, stability, and convergence in multidimension complex space. IEEE Transactions on Evolutionary Computation. 2002;**16**(1):58-73

[5] Aggarwal V, Mao M, O'Reilly U-M. A self-tuning analog proportional-integral-derivative (PID) controller. In: Adaptive Hardware and Systems. 2006. pp. 12-19

[6] Gomm JB, Yu DL, Williams D. A new model structure selection method for non-linear systems in neural modeling. International Conference in Control IEEE Transaction. 1996; **4**(27):752-757

Chapter 6

Distillation Column

Nasser Mohamed Ramli

Additional information is available at the end of the chapter

http://dx.doi.org/10.5772/intechopen.74656

Abstract

Dynamic simulations are used to model systems that are in transition from a steady state to dynamic state. The dynamic model is used to evaluate different basic control schemes and later to evaluate and test the control strategy. In this chapter, a steady-state simulation and dynamic simulation for debutanizer column are performed using a plant process simulator, HYSYS™. The objective of this chapter is to study the process variables of each controller at the column by using different tuning relations and identify the best tuning methods for the controllers in order to optimise the performance of the column. Two tuning methods are used in determining the controller settings for each controller. The process variable for each controller are used by using two different tuning methods are being studied. Furthermore, the effect on the process variables of each controller when using the controller settings based on real plant data and calculated using the PID equation is also being analysed. As for conclusion, the different tuning methods could give the different results on the behaviour of the response for each controller and the optimum response for each controller could be determined by considering the behaviour of the response and the value of integral square of the error (ISE) and integral of absolute value of error (IAE). All the research and findings obtained will be used to improve the overall performance of the plant as well as to improve the quality of the product and maximise profitability. The successful outcome of this chapter will be a great helping hand for industrial application.

Keywords: distillation column, steady state, dynamic state, PID controller, tuning

1. Introduction

The process industries are dynamic in nature. Process plants rarely run at a steady-state condition on dynamic. Feed and environmental disturbances, equipment vibrations, changes in

ambient conditions, heat exchanger fouling and degrading equipment performance that will effect smooth running of a process operation [1]. The transient behaviour of the process system is best studied using a dynamic simulation tool like HYSYS™. HYSYS™ contains a wide variety of property packages which provide accurate thermodynamic, physical and transport property predictions for hydrocarbon, non-hydrocarbon, petrochemical and chemical fluids. This powerful simulation program provides an environment for exploration of thermodynamic model behaviour, proper determination and tuning of interaction parameters and physical properties, as well as alternative designs for distillation systems.

Through dynamic simulation analyses, users are able to effectively study the impacts that change operating conditions and design modifications have on the operation of a process [2]. Process configurations and control system designs can be evaluated to ensure that they will meet corporate manufacturing objectives regardless of changing process and market conditions. The optimization and design of a process involves both steady-state and dynamic behaviour. Steady-state models consist of steady-state material and energy balances in order to evaluate different plant scenarios. The process engineer can use steady-state model to optimise the process industry by reducing equipment costs and capital while production maximising. Dynamic models allow the design engineer to design and compare alternative control strategies, examine the dynamic response to system disturbances and optimise the tuning of controllers in order to improve the overall performance of the plant [3, 4].

2. Literature review

2.1. Modelling under steady state

Steady-state simulations are widely used in process design, optimization and provide information for process flow sheets in terms of material and energy balances. It is also used for process design equipment such as heat exchangers, reactors and distillation columns. These simulations consist blocks of unit operations connected together and physical property data for the input streams chemical components specified by the user.

Steady-state models can perform steady-state energy and material balances and evaluate different plant scenarios. The design engineer can use steady-state simulation to optimise the process by reducing capital and equipment costs while maximising production.

However, the one obvious limitation of steady-state modelling is that it tells us nothing about the dynamic response, making it difficult to compare the dynamic disturbance rejection capability of alternative control schemes [6].

2.2. Dynamic modelling

Dynamic models are used to predict how to control a process and respond to various upsets in terms of function of time. They are widely used to evaluate equipment configurations, control schemes and determine the reliability and safety of a certain design before capital is committed to the implementation of a process. For an optimum process, dynamic simulation

can be used to assess transient conditions that could determine the process design pressures and temperatures. In many cases, unnecessary capital expenditures can be neglected using dynamic simulation.

Dynamic simulation during process design could lead to profit during plant start-up. Expensive field changes and impact schedule can be minimised if the control system and equipment are validated using dynamic simulation. Shutdown and start-up can be tested using dynamic simulation [7].

During start-up dynamic simulation could also provide controller-tuning parameters. In a lot of cases, accurate tuning controller settings can prevent expensive shutdowns and accelerate plant start-up. Dynamic simulation models used for process design are not based on transfer functions that are run from operator training simulators, but on actual physical equations governing the process and fundamental engineering principles [8].

Dynamic simulation models that are used for process design include:

- From differential balances for equipment models that include mass and energy inventory.
- Rigorous thermodynamics based on property correlations, steam tables and equations of state.
- Actual valve, piping, distillation tray, equipment hydraulics for both incompressible and compressible and lastly critical flow.

These models are so detailed that the results can influence engineering design decisions and ensure a realistic prediction of the process and the control system's interaction to assess control system stability [11].

2.3. PID controller

A proportional-integral-derivative controller (PID controller) is a general control loop feedback mechanism (controller) widely used in industry. A PID controller attempts to correct the error between a desired setpoint and a measured process variable by calculating it and then a corrective action that can adjust the process accordingly to keep the error minimal.

The PID controller involves three important parameters: which are proportional, integral and derivative. The *proportional* controller determines the reaction to the error calculated, the *integral* determines the reaction based on the sum of recent errors and the *derivative* determines the reaction based on the rate at which the error that has been changed. The weighted sum of these three actions is used to adjust the process control element such as the opening of a control valve (manipulated variable) or the power supply of a heating element [9].

The three constants are tuned in the PID controller equation; the controller can provide control action designed for specific requirements. The response of the controller could be decided in terms of the responsiveness of the controller to the required error, the degree to which the controller overshoots the setpoint and the degree of oscillation. The use of the PID algorithm for control does not guarantee optimal control of the system and stability.

To some extent, the applications may require using only one or two mode to provide the appropriate control. This could be achieved by setting the gain of the control outputs to zero. A PID controller will be called a PI, PID, PD, or P controller in the absence of the respective control actions. PI controllers are particularly widely used, since derivative action is sensitive to measurement noise and the absence of an integral value may prevent the system from reaching its setpoint value due to the control action [10].

The PID control scheme is named after its three correcting terms, whose sum constitutes the manipulated variable (MV). Hence:

$$\mathrm{MV(t)} = P_{\mathrm{out}} + I_{\mathrm{out}} + D_{\mathrm{out}} \tag{1}$$

Once the process gain, time constant time delay calculated for first-order response in the open loop tuning, the values are used in the Cohen Coon formula and input in HYSYS to peform the closed loop tuning in the PID equation. The first-order model of different loops are as follows; Temp 1 is controlled by regulating the heat duty of the reboiler using feedback control. Flow 3 is controlled by regulating the bottom liquid flowrate of the column. Pressure 1 is controlled using split range control of the vapour flowrate of the column and outlet vapour of the condenser. Flow 2 is controlled regulated using the distillate flowrate of the column.

3. Methodology

3.1. Data collection

The relevant data are identified and gathered after the problem is clearly defined. The steady-state and dynamic simulation by using HYSYS was performed in order to determine which data are needed for the simulation. The data collected from the plant information (PI) systems with the helping of an engineer in oil refinery industry [12].

3.1.1. Debutanizer column

Table 1 shows the debutanizer column description. The column plant data tabulated in **Table 1** are important in order for the HYSYS simulation to run.

3.1.2. Composition in the feed in mass fraction including components in the feed

Table 2 shows the composition of the feed debutanizer column which is important to analyse as the column consists of multicomponent.

3.1.3. Hypothetical components properties

Table 3 shows the important properties of the hypothetical components that are used for the simulation and the component not available therefore need to input the information in HYSYS.

Number of tray of the column	35
Feed tray-stage number	23
Type of tray used	Valve
Column diameter	1.3 m
Column height	23.95 m
Type of condenser	Partial
Feed mass flowrate	44,106 kg/h
Feed temperature	113°C
Feed pressure	823.8 kPa
Overhead vapour mass flowrate	11,286 kg/h
Overhead liquid mass flowrate	5040 kg/h
Pressure condenser	823.8 kPa
Pressure reboiler	853.2 kPa

Table 1. Debutanizer column plant data.

Composition	**Mass fraction**
Propane	0037
i-Butane	0093
n-Butane	0062
i-Pentane	0082
n-Pentane	0110
Hypo50_13*	0017
Hypo60_13*	0191
Hypo70_13*	0245
Hypo80_13*	0063
Hypo90_13*	0070
Hypo100_13*	0029
Hypo110_13*	0003
Hypo120_13*	0001

Table 2. Composition at the feed.

3.1.4. Operational parameters

3.1.4.1. Temp 1, Flow 3, Pressure 1 and Flow 2

Table 4 shows the operational parameters for Temp 1, Flow 3, Pressure 1 and Flow 2 that are obtained in industry input in the simulation.

Component	Boiling temp (°C)	Critical P (kPa)	Critical T (°C)	Critical volume (m^3/kgmol)	Molecular weight	SG	Viscosity 50°C (cSt)	TVP (kPa)
Hypo40_13*	38	3363	2017	03171	7134	6422	0	0
Hypo50_13*	45	4545	221	02483	7013	7603	021	6845
Hypo60_13*	55	3162	221	03475	8598	666	021	4781
Hypo70_13*	65	3053	2322	03658	8569	6818	021	4431
Hypo80_13*	75	3957	261,7	0,303	83,83	774,9	0,21	26,61
Hypo90_13*	85	2907	2559	03983	9902	7047	021	172
Hypo100_13*	95	3141	2741	03813	9844	7368	021	1463
Hypo110_13*	105	3262	290	0377	105	7582	02114	8582
Hypo120_13*	115	2739	2934	04474	1117	7372	02213	6168

Table 3. Properties of the hypothetical components.

	Temp 1	Flow 3	Pressure 1	Flow 2
Mode	Auto	Auto	Auto	Cascade
Action	Reverse	Reverse	Reverse	Reverse
SP	140.7°C	19.37 m^3/h	823.8 kPa	8.8206 m^3/h
OP	52.00%	74.20%	25.30%	54.30%
Kc	250	0.1	0.5	0.2
Ti	1.33 min	0.5 min	0.7 min	0.2 min
Td	0.333 min	—	—	—
PV Minimum	125.15°C	19.37 m^3/h	552.60 kPa	0.00 m^3/h
PV Maximum	145.55°C	56.40 m^3/h	903.58 kPa	15.80 m^3/h

Table 4. Operational parameter Temp 1, Flow 3, Pressure 1 and Flow 2.

3.1.4.2. Temp 1, Flow 3, Pressure 1 and Flow 2

Table 5 shows the PID controller for Temp 1, Flow 3, Pressure 1 and Flow 2 that are obtained in industry input in the simulation.

3.1.4.3. Temp 1, Flow 3, Pressure 1 and Flow 2

Table 6 shows the ISE and IAE values for Temp 1, Flow 3, Pressure 1 and Flow 2 that are calculated using Microsoft Excel.

3.2. Steady-state modelling using HYSYS

HYSYS™ is widely used for designing a steady-state model for the Debutanizer column before the steady state is transitioned to the dynamic model. Within HYSYS™, steady-state

http://dx.doi.org/10.5772/intechopen.74656

	Temp 1		Flow 3		Pressure 1		Flow 2	
Controller settings	**Real plant data**	**PID equation**	**Real plant data**	**PID equation**	**Real plant data**	**PID equation**	**Real plant data**	**PID equation**
Kc	250	250	0.1	0.1	0.5	0.5	0.2	0.2
Ti (s)	80	3.125	30	0.003	42	0.012	12	0.0167
Td (s)	20	5000	—	—	—	—	—	—

Table 5. PID controller for Temp 1, Flow 3, Pressure 1 and Flow 2.

	Temp 1		Flow 3		Pressure 1		Flow 2	
Controller settings	**Real plant data**	**PID equation**	**Real plant data**	**PID equation**	**Real plant data**	**PID equation**	**Real plant data**	**PID equation**
ISE	2863.68	12099.97	8058.76	8108.98	1,380,285	1,313,971	892.9	2072.93
IAE	771.49	2863.68	560.32	596.14	19749.54	19406.04	193.9	394.55

Table 6. ISE and IAE for Temp 1, Flow 3, Pressure 1 and Flow 2.

simulations can be easily converted into dynamic simulations by specifying pressure/flow relationships, additional engineering details and equipment dimensions. The HYSYS™ environment consists of the basic environment and the simulation environment. The basic environment is used to select the chemical components that are involved in the simulation, as well as the thermodynamic property suitable for the components.

The simulation environment consists of the process flow diagram (PFD) and worksheet. The worksheet contains the information on every heat and flow stream which are involved in

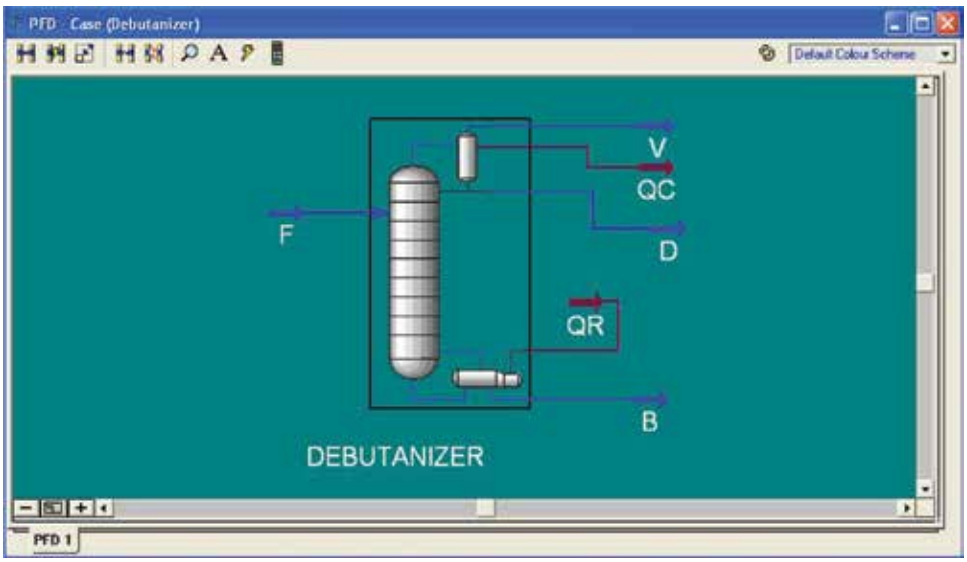

Figure 1. Process flow diagram (PFD) of debutanizer column in steady state.

the simulation. Most of the streams require inputs while HYSYS™, depend on the degree of freedom, will calculate the output streams automatically. The PFD will graphically show the unit's operation streams that are involved. The necessary information such as feed conditions, feed compositions, reflux ratio, pressure condenser, pressure reboiler and so on have to be provided for the chosen unit operation in order to be able to design the unit automatically.

3.3. Dynamic modelling using HYSYS

Figure 1 shows the process flow diagram of debutanizer column and **Figure 2** shows the process flow diagram of debutanizer column in dynamic state. The setpoint that is used in

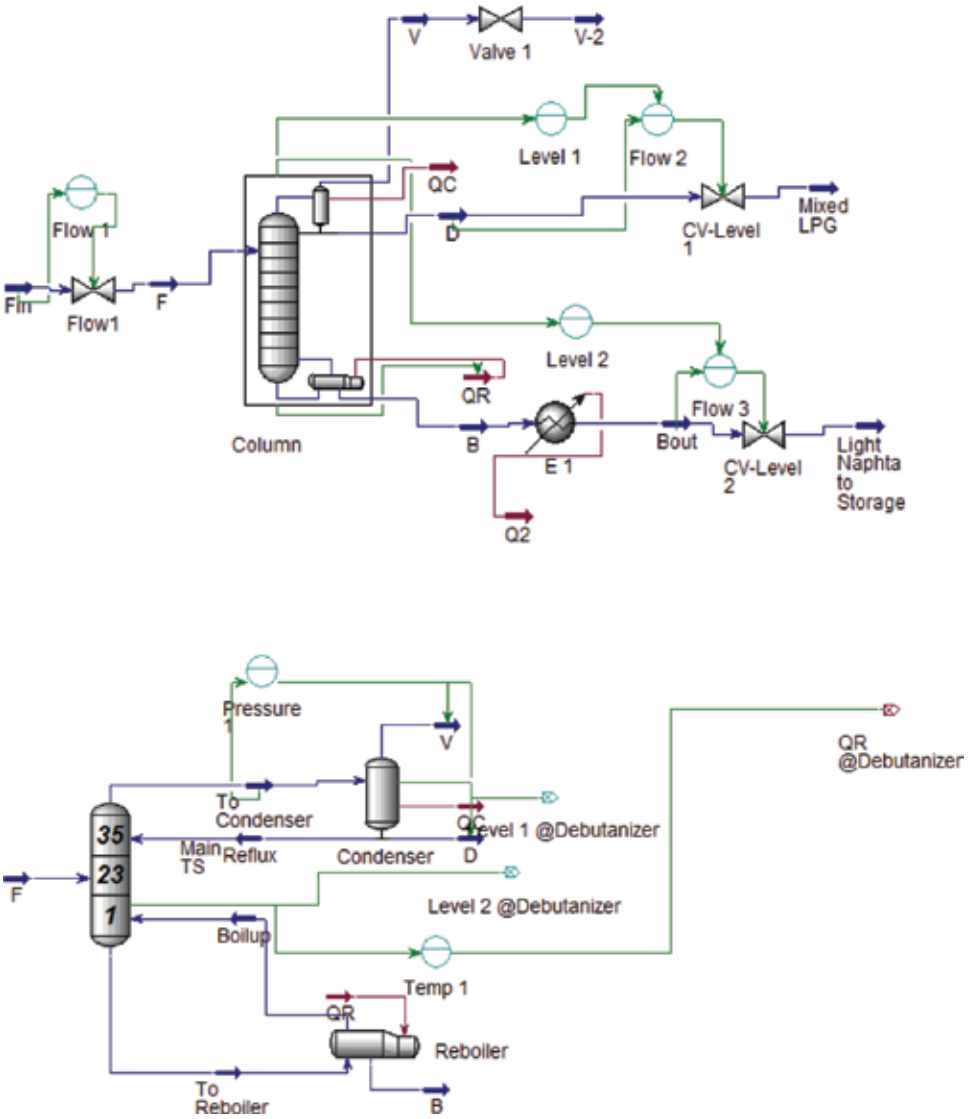

Figure 2. Process flow diagram (PFD) of debutanizer column in dynamic state.

http://dx.doi.org/10.5772/intechopen.74656

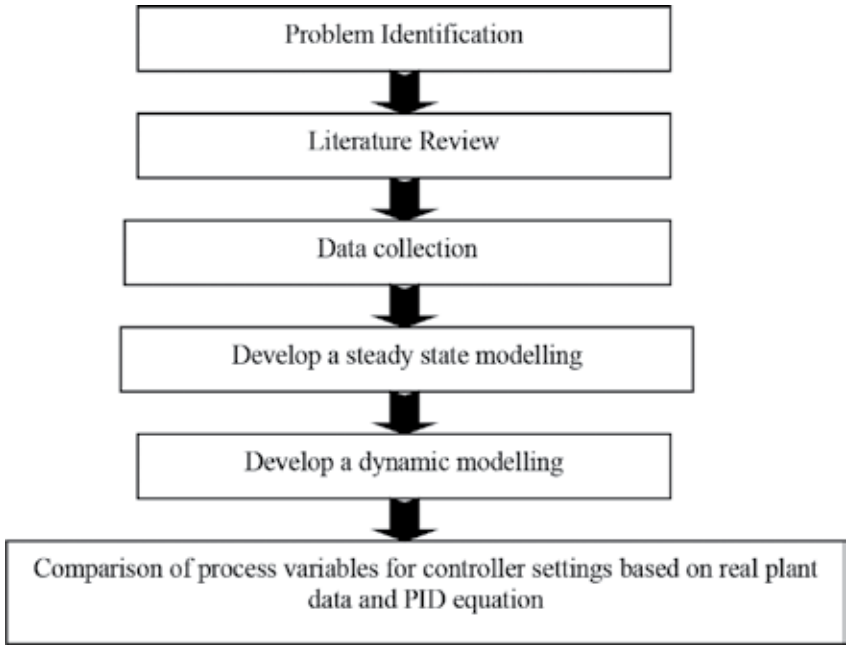

Figure 3. Flow of Modelling.

the simulation is used based on the parameter in **Table 4**. The setpoint value is fixed and then once the transition from steady state to dynamic state the change of setpoint is increased slight about 5% change from the actual setpoint in each controller in the dynamic state.

3.4. Approach methodology

The block diagram in **Figure 3** shows the approach that has been conducted in this chapter. Each step has been done thoroughly in order to fulfil the objective of this chapter. Furthermore, it can be done smoothly by constructing this approach.

4. Results and discussion

4.1. Comparison of process variable for controller settings based on real plant data and PID

Process variables for controller settings are based on real plant data are compared with the controller settings that are calculated using the PID equation.

PID equation

$$G_c(s) = K_c\left(1 + \frac{1}{T_i s} + T_d s\right) \tag{2}$$

The controller variable response for all controllers are also compared with using the integral square of the error (ISE) and integral of absolute value of error (IAE) [5], where

$$ISE = \sum_{i=0} (y_{sp} - y_i)^2 \; IAE = \sum_{i=0} | \; (y_{sp} - y_i) \; | \tag{3}$$

4.1.1. Temp 1

Figure 4 represents the process variables of reboiler outlet temperature to column for controller settings based on real plant data and PID equation. Plant data show optimum response as it fluctuates within the set point and takes a shorter time to settle. Meanwhile, PID equation response decreases dramatically and exceeds the lower limit at 1300 s. Plant data response gives the smallest value of ISE and IAE which are 2863.68 and 771.49, respectively.

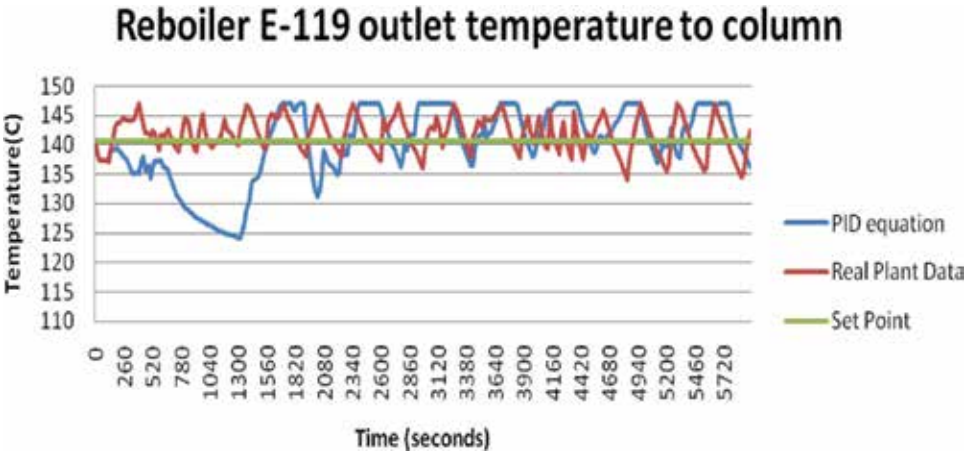

Figure 4. Process variables of Temp 1 for controller settings based on real plant data and PID equation.

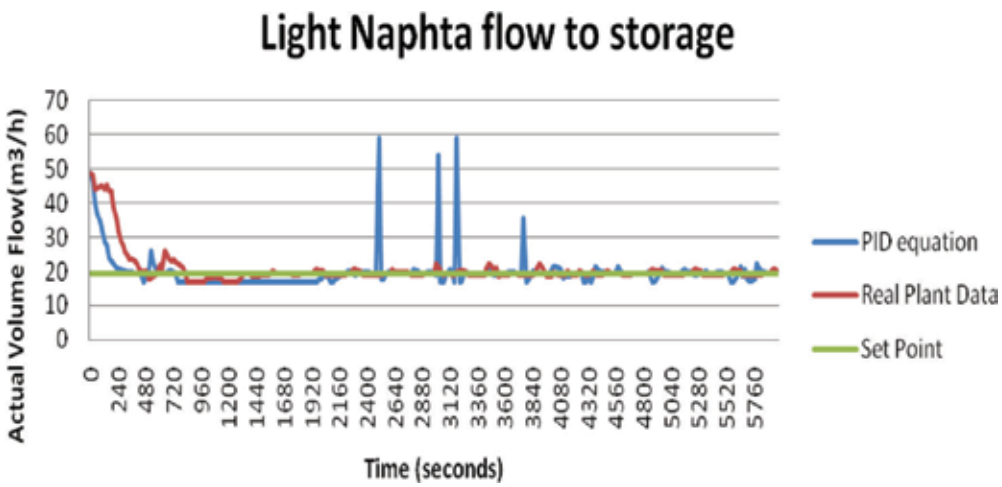

Figure 5. Process variables of Flow 3 for controller settings based on real plant data and PID equation.

http://dx.doi.org/10.5772/intechopen.74656

4.1.2. Flow 3

Figure 5 represents the process variables of light naphta flow to storage for controller settings based on real plant data and PID equation. The response of real plant data reaches the settling time faster than PID equation and exhibits the more stable response with no large oscillation and fluctuates within its set point. Meanwhile, PID equation response shows the large overshoot and exceeds the high limit at 2500 and 3180 s. Plant data response gives the smallest value of ISE and IAE which are 8058.76 and 560.32, respectively.

4.1.3. Pressure 1

Figure 6 represents the process variables of debutanizer overhead pressure for controller settings based on real plant data and PID equation. The responses shows a different trend where the real plant data exhibit the larger overshoot and take a longer settling time compared to

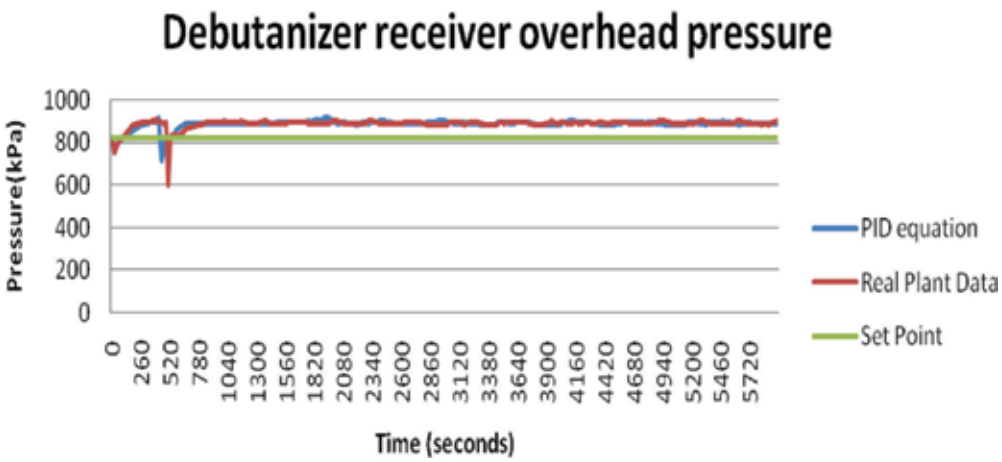

Figure 6. Process variables of Pressure 1 for controller settings based on real plant data and PID equation.

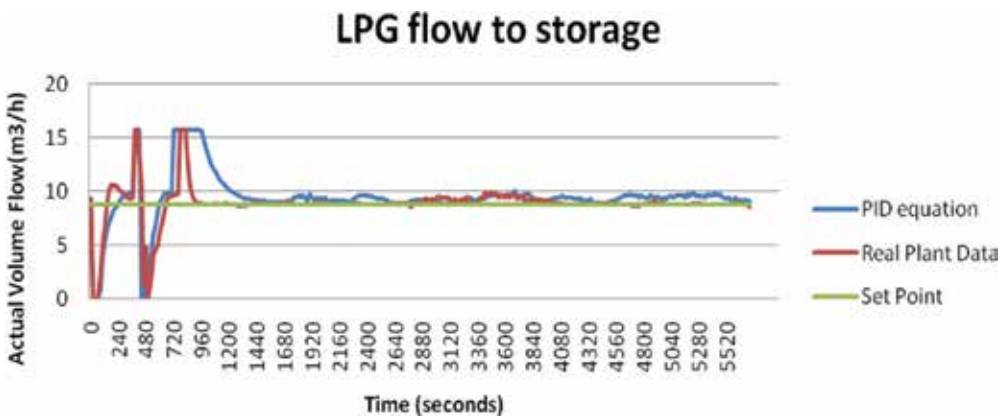

Figure 7. Process variables of Flow 2 for controller settings based on real plant data and PID equation.

PID equation. After both responses had settled, the responses were almost similar to the rapid and smooth response but slightly deviate from the set point. PID equation response gives the smallest value of ISE and IAE which are 1,313,971 and 19406.04, respectively.

4.1.4. Flow 2

Figure 7 represents the process variables of LPG flow to storage for controller settings based on real plant data and PID equation. The response of real plant data reaches the settling time faster than PID equation and exhibits the more rapid and smooth response compared to PID equation. Plant data response gives the smallest value of ISE and IAE which are 892.99 and 193.98, respectively.

5. Conclusion

This chapter is mainly about modelling a steady-state and dynamic model for debutanizer column in order to optimise the performance of the column and to identify the best tuning methods for each controller at the column. Debutanizer column in Crude Distillation Unit (CDU) of oil refinery has been chosen as a model for this chapter.

From results and discussion, it is concluded that the different tuning methods could give the different results on the behaviour of the response for each controller. The optimum response for each controller has been chosen by considering the behaviour of the response and the value of integral square of the error (ISE) and integral of absolute value of error (IAE).

All the findings obtained will be used to improve the overall performance of the plant as well as to improve the quality of the product and maximise profitability. The successful outcome of this chapter will be a great helping hand for industrial application.

5.1. Recommendation

1. Determine the second-order approximation of the transfer function and the process model for each controller.
2. Calculate the controller settings for PI and PID controller by using the process model that determined from the second-order approximation of the transfer function.
3. Implement the model predictive control (MPC) for each controller.

Acknowledgements

The authors would like to acknowledge PETRONAS for providing the required data and information for the research. I would like to acknowledge University Malaya for providing the grant for the research (PS107/2010B).

Author details

Nasser Mohamed Ramli

Address all correspondence to: nasser_mramli@utp.edu.my

Chemical Engineering Department, Faculty of Engineering, Universiti Teknologi Petronas, Bandar Seri Iskandar, Perak, Malaysia

References

[1] Liptak Bela G. Instrument Engineers' Handbook: Process Control. 4th ed. United State of America: CRC Taylor and Francis; 1995

[2] Mohammad AW, Takriff MS. Using Professional Simulation Software for Better Integration in the Chemical Engineering Undergraduate Curriculum. Selangor: Universiti Kebangsaan Malaysia (UKM); 2003

[3] Mohutsiwa Donald A. PID Controller Tuning using Internal Model Control Method [thesis]. University of Southern Queensland; 2006

[4] Aidan O'D. Handbook of PI and PID Controller Tuning Rules. 1st ed. United Kingdom: World Scientific Publishing Co, Imperial College Press; 2003

[5] Karacan S, Hapoglu H, Aplbaz M. Multivariable system identification and generic model control of a laboratory scale packed distillation column. Applied Thermal Engineering. 2007;**27**:1017-1028. DOI: 10.1016/j.applthermaleng.2006.07.032

[6] Available from: http://www.separationprocesses.com/CourseWare/Experiments/DT_Prac05a.htm [Accessed: June 01, 2003]

[7] Available from: http://www.aspentech.com/publication_files/ertc2004_alsop_ferrer.pdf [Accessed: August 01, 2003]

[8] Available from: http://www. cheresources.com/invision/lofiversion/index.php/t5568.html [Accessed: October 1, 2003]

[9] Available from: http://en.wikipedia.org/wiki/Liquified_petroleum_gas [Accessed: December 01, 2003]

[10] Available from: http://en.wikipedia.org/wiki/PID_controller [Accessed: January 01, 2004]

[11] Muda TZT. SKG16: Advance Simulation Inc. Dynamic–Level 3. Malaysia: Institute of Science PETRONAS; 2006

[12] Training Manual for Crude Distillation Unit of Oil Refinery. Malaysia: Institute of Science PETRONAS; 2006

Chapter 7

Constraint Handling Optimal PI Controller Design for Integrating Processes: Optimization-Based Approach for Analytical Design

Rodrigue Tchamna and Moonyong Lee

Additional information is available at the end of the chapter

http://dx.doi.org/10.5772/intechopen.74301

Abstract

This chapter introduces the closed-form analytical design of proportional-integral (PI) controller parameters for the optimal control subjected to operational constraints. The main idea of the design is not only to minimize the control performance index but also to cope with the constraints in the process variable, controller output, and its rate of change. The proposed optimization-based approach is examined to regulatory and servo control of integrating processes with three typical operation constraints. To derive an analytical design formula, the constrained optimal control problem in the time domain was transformed to an unconstrained optimization in a new parameter space associated with closed-loop dynamics. By taking the advantage of the proposed analytical approach, the optimal PI parameters can be found quickly based on the graphical analysis without complex numerical optimization. The resulting optimal PI controller guarantees the globally optimal closed-loop response and handles the operational constraints precisely.

Keywords: constrained optimal control, industrial PI controller, analytical design, constraint handling, integrating process, optimal servo and regulatory control

1. Introduction

Many units used in the chemical process industry, such as heating boilers, batch chemical reactors, liquid storage tanks, or liquid level systems, are integrating processes in which the dynamic response is very slow with a large dominant time constant. In modern control, the integrating process also appears in many applications including space telescope control systems, lightweight robotic arms, and pilot crane control systems. Constraints are inherent in

any industrial control systems, either implicitly or explicitly. They are generally associated with both the process variable and controller output. Indeed, typical operational constraints usually include the actuator magnitude and its rate saturation, process/output variable, and internal state variables. The objective of constrained optimal control is to minimize the control cost subjected to constraints on state variables and/or output variables. The importance of taking constraints into account during the design stage of the controller is no more questioned. In fact, a well-designed optimal control would fail in a real-life situation if the constraints are not taken into account while designing the controller. However, optimal control of a process with multiple constraints is still challenging even for a process with simple dynamics. In a popular approach using Pontryagin's principle or the Hamilton-Jacobi-Bellman equation for a classical optimal control framework [1, 2], the optimal controller parameters are obtained via numerical solution of the nonlinear constrained optimization. However, the existing numerical methods neither guarantee a global optimal solution nor provide useful insights and physical interpretations of the complex relationships existing between the process parameters and control performance. To address this issue, the analytical solutions of optimal proportional-integral (PI) controller under constraints were previously proposed using the optimization-based approach for integrating systems [3–7] and extended to first-order systems [8–11]. This chapter introduces the optimization-based approach for the analytical design of optimal PI controller parameters for integrating processes without violating the operational constraints under a unified framework.

2. Formulation of constrained optimal PI control problem

Figure 1 presents the schematic diagram of an integrating process considered in this chapter. It is a type-C PI controller, also called I-P controller, which is a modified type of PID controller where the set point is removed from the proportional term in order to avoid the initial quick on the manipulated variable for a step change in the set point.

The major resulting transfer functions of this closed-loop system are expressed as

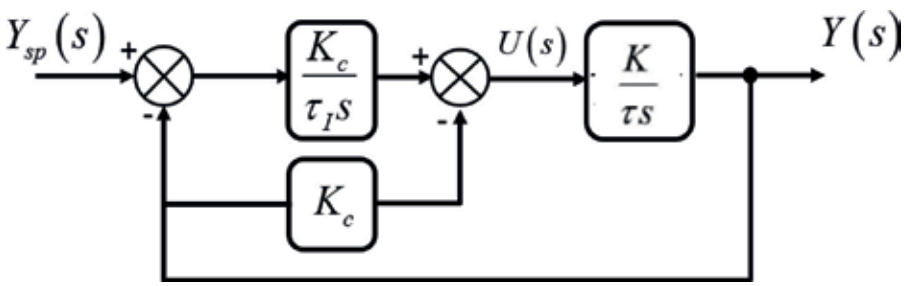

Figure 1. Block diagram of the feedback control of integrating process.

$$Y(s) = \frac{1}{\tau_c \tau_I s^2 + \tau_I s + 1} Y_{sp}(s) + \frac{K_p \tau_c \tau_I s}{\tau_c \tau_I s^2 + \tau_I s + 1} D(s) \tag{1}$$

$$U(s) = \frac{1}{K_p} \frac{s}{\tau_c \tau_I s^2 + \tau_I s + 1} Y_{sp}(s) - \frac{\tau_I s + 1}{\tau_c \tau_I s^2 + \tau_I s + 1} D(s) \tag{2}$$

where

$$\tau_c = \frac{1}{K_p K_c};\ K_p = \frac{K}{\tau} \tag{3}$$

The closed-loop damping ratio of the above system becomes

$$\zeta = \frac{1}{2}\sqrt{\frac{\tau_I}{\tau_c}} \tag{4}$$

The goal of a constrained optimal problem is to minimize the weighted sum of the process variable error, e(t), and the rate of change in the manipulated variable, u′(t), for a given step change, $\Delta D/s$, in disturbance (i.e., optimal regulatory control) or that, $\Delta Y_{sp}/s$, in set point (i.e., optimal servo control) subjected to the following three typical operational constraints: the maximum allowable limit in (1) the controlled variable, $y_{\max}$, (2) the rate of change in the manipulated variable, $u'_{\max}$, and (3) the manipulated variable, $u_{\max}$.

Consequently, the constrained optimal control problem is formulated as

$$\min\Phi = \int_0^\infty \left[\omega_y \left(y(t) - y_{sp}(t)\right)^2 + \omega_{u'}(u'(t))^2\right] dt \tag{5a}$$

subject to

$$|y(t)| \le y_{\max} \tag{5b}$$

$$|u'(t)| \le u'_{\max} \tag{5c}$$

$$|u(t)| \le u_{\max} \tag{5d}$$

Through some mathematical operations, the above optimal control problem formulated in the time domain can be transformed to the form with the two new design parameters ζ and τ_c as expressed in **Table 1**. As shown in **Table 1**, the three constraints are also expressed as only a function of ζ and τ_c. Then, a simple graphical examination of the contour of the objective function and the constraints in (ζ, τ_c) space allows to find the location of global optimal solution without complex numerical optimization process.

	Regulatory control	**Servo control**
Objective function	$\min\Phi_r(\zeta,\tau_c)=\alpha\tau_c^3\zeta^2+\frac{\beta}{\tau_c}\left(\frac{1}{4\zeta^2}+1\right)$	$\min\Phi_s(\zeta,\tau_c)=\alpha\tau_c(4\zeta^2+1)+\frac{\beta}{\tau_c^3\zeta^4}$
Constraints	$\tau_c g_r(\zeta)\le\gamma_g$ $h_r(\zeta,\tau_c)\le\gamma_h$ $f_r(\zeta,\tau_c)\le\gamma_f$	$g_s(\zeta)\le\gamma_g$ $h_s(\zeta)\le\tau_c^2\gamma_h$ $f_s(\zeta,\tau_c)\le\gamma_f$
Parameters	$\alpha=2\omega_y(K_p\Delta D)^2;\beta=\frac{\omega_{u'}}{2}(\Delta D)^2;$ $\gamma_g=\left\lvert\frac{y_{max}}{K_p\Delta D}\right\rvert;\gamma_h=\left\lvert\frac{u'_{max}}{\Delta D}\right\rvert;\gamma_f=\left\lvert\frac{u_{max}}{\Delta D}\right\rvert$	$\alpha=\frac{\omega_y\Delta Y_{sp}^2}{2};\ \beta=\frac{\omega_{u'}}{32}\left(\frac{\Delta Y_{sp}}{K_p}\right)^2;$ $\gamma_g=\left\lvert\frac{y_{max}}{\Delta Y_{sp}}\right\rvert;\gamma_h=\left\lvert\frac{K_p u'_{max}}{\Delta Y_{sp}}\right\rvert;\gamma_f=\left\lvert\frac{K_p\tau_c u_{max}}{\Delta Y_{sp}}\right\rvert$
Functions g,h,f	$g_r(\zeta)=\frac{2}{\sqrt{1+x^2}}\exp\left(-\frac{\tan^{-1}x}{x}\right)$ for $0<\zeta<1$ $=2\exp(-1)$ for $\zeta=1$ $=\frac{2}{\sqrt{1-x^2}}\exp\left(-\frac{\tanh^{-1}x}{x}\right)$ for $\zeta>1$	$g_s(\zeta)=1+\exp\left(-\frac{\pi}{x}\right)$ for $0<\zeta<1$ $=1$ for $\zeta\ge1$ where $x=\frac{\sqrt{1-\zeta^2}}{\zeta}$ for $0<\zeta\le1$ $=\frac{\sqrt{\zeta^2-1}}{\zeta}$ for $\zeta>1$
	$h_r(\zeta,\tau_c)=\frac{1}{2\tau_c\zeta}\exp\left[-\frac{1}{x}\tan^{-1}\left(\frac{4\zeta^2-1}{4\zeta^2-3}x\right)\right]$ for $\zeta<\frac{1}{2}$ $=\left\lvert\frac{u'(0)}{\Delta D}\right\rvert=\frac{1}{\tau_c}$ for $\zeta\ge\frac{1}{2}$	$h_s(\zeta)=\frac{1}{4\zeta^2}$ for $\zeta>0$
	$f_r(\zeta,\tau_c)=1+\exp\left\{-\frac{1}{x}\tan^{-1}\left[\frac{2\zeta^2}{2\zeta^2-1}x\right]-\frac{\pi}{x}\right\}$ for $0<\zeta<\frac{1}{\sqrt{2}}$ $=1+\exp\left\{-\frac{1}{x}\tan^{-1}\left[\frac{2\zeta^2}{2\zeta^2-1}x\right]\right\}$ for $\frac{1}{\sqrt{2}}\le\zeta<1$ $=1+\exp(-2)$ for $\zeta=1$ $=1+\exp\left\{-\frac{1}{x}\tanh^{-1}\left[\frac{2\zeta^2}{2\zeta^2-1}x\right]\right\}$ for $\zeta>1$	$f_s(\zeta,\tau_c)=\frac{1}{2\zeta}\exp\left(-\frac{1}{x}\tan^{-1}x\right)$ for $0<\zeta<1$ $=\frac{1}{2}\exp(-1)$ for $\zeta=1$ $=\frac{1}{2\zeta}\exp\left(-\frac{1}{x}\tanh^{-1}x\right)$ for $\zeta>1$

Table 1. Objective function and constraints of the optimal control problem in (ζ,τ_c) space.

3. PI controller design

3.1. Optimal regulatory control

Applying the Lagrangian multiplier [12], it converts the constrained optimization problem in **Table 1** to an equivalent unconstrained problem. In regulatory control, the constrained problem can be converted as

$$\begin{aligned}\min \mathrm{L}(\zeta, \tau_{\mathrm{c}}, \varpi, \sigma) = \Phi_r(\zeta, \tau_{\mathrm{c}}) + \varpi_1\left(\gamma_{\mathrm{h}} - h_r(\zeta, \tau_{\mathrm{c}}) - \sigma_1^2\right) \\ + \varpi_2\left(\gamma_{\mathrm{g}} - g_r(\zeta)\tau_c - \sigma_2^2\right) + \varpi_3\left(\gamma_{\mathrm{f}} - f_r(\zeta, \tau_{\mathrm{c}}) - \sigma_3^2\right)\end{aligned} \tag{6}$$

where ϖ_i and σ_i are the Lagrange multiplier and the slack variable, respectively.

The necessary conditions for an optimal solution are then

$$\frac{\partial L}{\partial \tau_{\mathrm{c}}} = \frac{\partial \Phi_r}{\partial \tau_{\mathrm{c}}} + \varpi_1\left[-\frac{\partial h_r(\zeta, \tau_{\mathrm{c}})}{\partial \tau_{\mathrm{c}}}\right] + \varpi_2\left[-g_r(\zeta)\right] + \varpi_3\left[-\frac{\partial f_r(\zeta, \tau_{\mathrm{c}})}{\partial \tau_{\mathrm{c}}}\right] = 0 \tag{7a}$$

$$\frac{\partial L}{\partial \zeta} = \frac{\partial \Phi_r}{\partial \zeta} - \varpi_1 \frac{\partial h_r(\zeta, \tau_{\mathrm{c}})}{\partial \zeta} - \varpi_2 \tau_c \frac{\partial g_r(\zeta)}{\partial \zeta} - \varpi_3 \frac{\partial f_r(\zeta, \tau_{\mathrm{c}})}{\partial \zeta} = 0 \tag{7b}$$

$$\frac{\partial L}{\partial \varpi_1} = \gamma_{\mathrm{h}} - h_r(\zeta, \tau_{\mathrm{c}}) - \sigma_1^2 = 0;\ \frac{\partial L}{\partial \varpi_2} = \gamma_g - \tau_{\mathrm{c}} g_r(\zeta) - \sigma_2^2 = 0;\ \frac{\partial L}{\partial \varpi_3} = \gamma_{\mathrm{f}} - f_r(\zeta, \tau_c) - \sigma_3^2 = 0 \tag{7c}$$

$$\frac{\partial L}{\partial \sigma_1} = -2\varpi_1\sigma_1 = 0;\ \frac{\partial L}{\partial \sigma_2} = -2\varpi_2\sigma_2 = 0;\ \frac{\partial L}{\partial \sigma_3} = -2\varpi_3\sigma_3 = 0 \tag{7d}$$

The simultaneous solutions of Eqs. (7a)–(7d) for possible combinations of $\sigma_i = 0$, $\sigma_i \neq 0$, $\varpi_i = 0$, and $\varpi_i \neq 0$ are associated with the corresponding optimal cases. Note that instead of introducing the slack variables, Karush-Kuhn-Tucker conditions [13] can also be utilized for solving the constrained optimization problem, which finds the same optimal PI parameters by the Lagrangian multiplier method.

Figure 2 presents seven possible cases for the location of global optima: the global optimum can be found inside the feasible region (case A), or on the boundary of one constraint (cases B, C, and E), or on the intersection point of two constraints (cases D, F, and G).

The global optima of the seven cases can be evaluated by inspecting their geometrical characteristics in (ζ, τ_c) space as well as the corresponding conditions of the Lagrange multipliers and slack variables as follows:

Case A ($\varpi_1 = \varpi_2 = \varpi_3 = 0$): The extreme point, $\left(\zeta^{\dagger}, \tau_c^{\dagger}\right)$, which is located inside the feasible region, is therefore the global optimum. Solving Eqs. (7a) and (7b) simultaneously, the global optimum can be determined in explicit form as

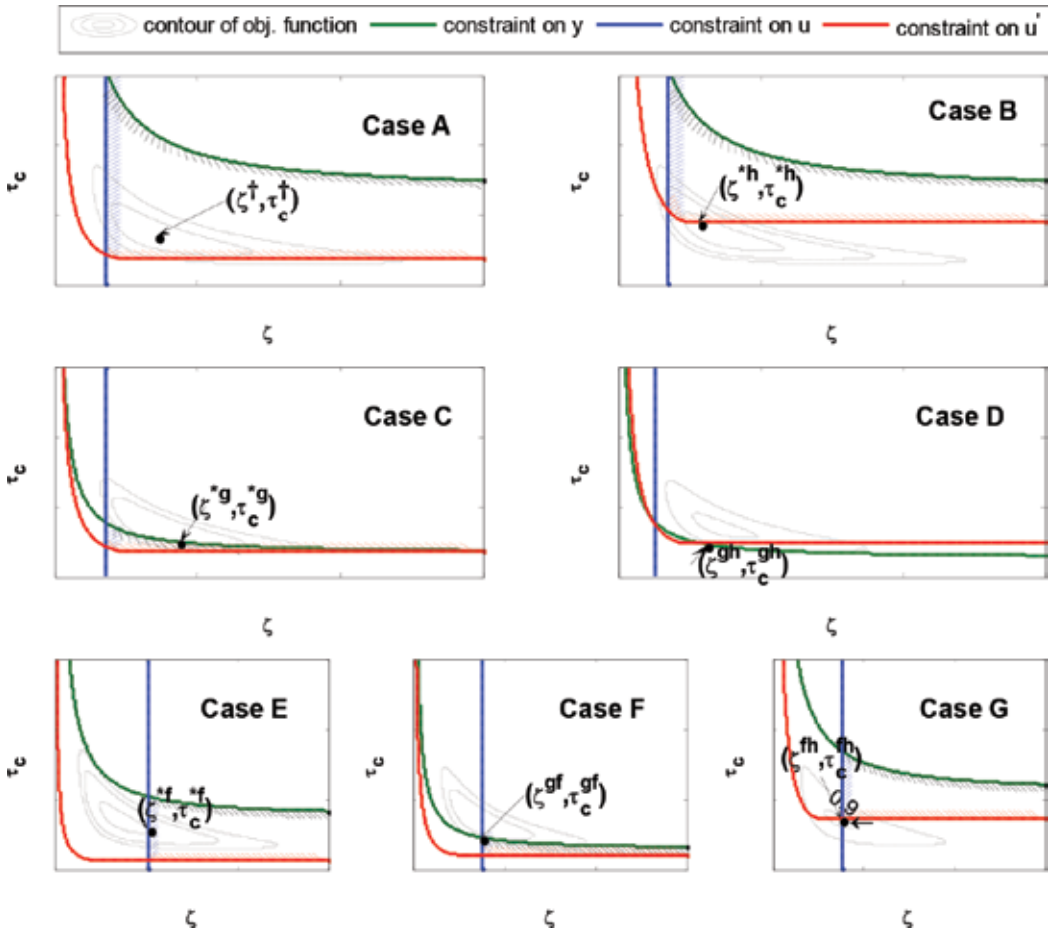

Figure 2. Contours, constraints, and possible locations of the global optimum in regulatory control case.

$$\zeta^{\dagger} = \sqrt{\frac{1}{2}} \tag{8a}$$

$$\tau_c^{\dagger} = \left(\frac{\beta}{\alpha}\right)^{1/4} \tag{8b}$$

Case B ($\sigma_1 = \varpi_2 = \varpi_3 = 0$): The global optimum, symbolized as $\left(\zeta^{*\mathrm{h}}, \tau_{\mathrm{c}}^{*\mathrm{h}}\right)$, is positioned on the constraint, $\gamma_{\mathrm{h}} = h_r(\zeta, \tau_{\mathrm{c}})$. $\zeta^{*\mathrm{h}}$ and $\tau_{\mathrm{c}}^{*\mathrm{h}}$ can be obtained by substituting $\sigma_1 = \varpi_2 = \varpi_3 = 0$ into the equation of necessary conditions, thus solving the following system of equations:

$$\gamma_{\mathrm{h}} - h_r(\zeta, \tau_c) = 0 \tag{9a}$$

$$\frac{\partial \Phi_r}{\partial \zeta} - \frac{\partial \Phi_r}{\partial \tau_c}\left[\frac{\partial h_r}{\partial \tau_c}\right]^{-1}\frac{\partial h_r}{\partial \zeta} = 0 \tag{9b}$$

Case C ($\varpi_1 = \sigma_2 = \varpi_3 = 0$): The global optimum, $\left(\zeta^{*g}, \tau_c^{*g}\right)$, is located on the constraint, $\gamma_g = \tau_c g_r(\zeta)$, and obtained by solving the following system of equations:

$$\gamma_g - g_r(\zeta)\tau_c = 0 \tag{10a}$$

$$\frac{\partial \Phi_r}{\partial \zeta} g_r - \tau_c \frac{\partial \Phi_r}{\partial \tau_c} \frac{\partial g_r}{\partial \zeta} = 0 \tag{10b}$$

Case D ($\sigma_1 = \sigma_2 = \varpi_3 = 0$): The global optimum represented by $\left(\zeta^{gh}, \tau_c^{gh}\right)$ is located on the intersection point by $\gamma_h = h_r(\zeta, \tau_c)$ and $\gamma_g = \tau_c g_r(\zeta)$, thus can be calculated by solving

$$\gamma_g - \tau_c g_r(\zeta) = 0 \tag{11a}$$

$$\gamma_h - h_r(\zeta, \tau_c) = 0 \tag{11b}$$

Case E ($\varpi_1 = \varpi_2 = \sigma_3 = 0$): The global optimum, $\left(\zeta^{*f}, \tau_c^{*f}\right)$, is located on the constraint, $\gamma_f = f_r(\zeta, \tau_c)$, and can be found by solving

$$\gamma_f - f_r(\zeta, \tau_c) = 0 \tag{12a}$$

$$\frac{\partial f_r}{\partial \tau_c} \frac{\partial \Phi_r}{\partial \zeta} - \frac{\partial f_r}{\partial \zeta} \frac{\partial \Phi_r}{\partial \tau_c} = 0 \tag{12b}$$

Case F ($\varpi_1 = \sigma_2 = \sigma_3 = 0$): The global optimum, $\left(\zeta^{gf}, \tau_c^{gf}\right)$, which is on the intersection point created by $\gamma_f = f_r(\zeta, \tau_c)$ and $\gamma_g = \tau_c g_r(\zeta)$, is calculated by solving

$$\gamma_f - f_r(\zeta, \tau_c) = 0 \tag{13a}$$

$$\gamma_g - \tau_c g_r(\zeta) = 0 \tag{13b}$$

Case G ($\sigma_1 = \varpi_2 = \sigma_3 = 0$): The global optimum, $\left(\zeta^{fh}, \tau_c^{fh}\right)$, is located on the intersection point of the constraints $\gamma_f = f_r(\zeta, \tau_c)$ and $\gamma_h = h_r(\zeta, \tau_c)$, and calculated by solving

$$\gamma_f - f_r(\zeta, \tau_c) = 0 \tag{14a}$$

$$\gamma_h - h_r(\zeta, \tau_c) = 0 \tag{14b}$$

After the global optimum is determined in (ζ, τ_c) space, the optimal PI parameters corresponding to each case can then be calculated from Eqs. (3) and (4) as

$$K_c^{opt} = \frac{1}{K_p \tau_c^{opt}}; \tau_I^{opt} = 4\left(\zeta^{opt}\right)^2 \tau_c^{opt} \tag{15}$$

One of main advantages of the optimization-based graphical approach is that the conditions for the seven possible cases can be directly evaluated based on a meticulous analysis of the

graphical shape of the constraints and contours in (ζ, τ_c) space. The concept of the relative locations between the extreme point and its projections to the constraints is used mainly to develop the conditions to discriminate each case associated with the corresponding global optimum. **Figure 3** shows an example of the projection of the extreme point and its notation rule used in this graphical analysis for the optimal PI design. The notation, $\zeta^{\dagger f}$, represents the abscissa of the projection of the extreme point on the constraint curve by *f*. Similarly, $\tau_c^{\dagger h}$ and $\tau_c^{\dagger g}$ indicate the ordinate of the projection of the extreme point on the constraint curves by *h* and *g*, respectively. If $\tau_c^{\dagger}$ is such that $\tau_c^{\dagger h} \le \tau_c^{\dagger} \le \tau_c^{\dagger g}$, then the global optimum is above the constraint, *h*, and below the constraint, *g*. Referring to **Figure 2**, this corresponds to cases A, E, or possibly G. In this case, it is apparent from **Figure 2** that if $\zeta^{\dagger f} < \zeta^{\dagger}$, it belongs to case A (i.e., the extreme point is the global optimum), otherwise it belongs to either case E or G. Cases E and G can be distinguished simply by comparing τ_c^{*f} and τ_c^{fh}, where τ_c^{fh} is the ordinate of the intersection of the constraints by *f* and *h*. As seen in **Figure 2**, if $\tau_c^{*f} > \tau_c^{fh}$, the global optimum case belongs to case E, otherwise case G.

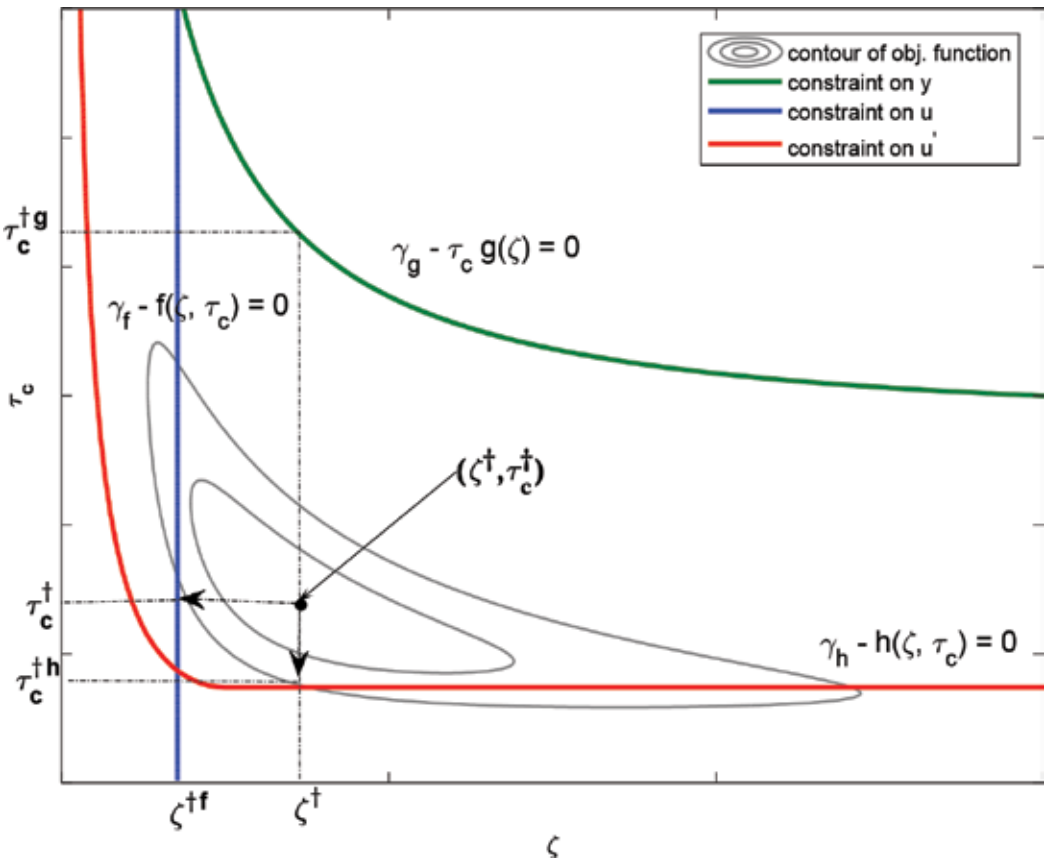

Figure 3. Projection of the extreme point on the constraints in (ζ, τ_c) space.

Using similar reasoning, the conditions to discriminate each of seven cases associated with the global optimum can be established according to the relative locations between the extreme point and its projections to the constraints. **Table 2** lists the results for the conditions and characteristics of the global optima.

3.2. Optimal servo control

The constrained optimization problem in **Table 1** can be converted into an equivalent unconstrained problem by applying the Lagrangian multiplier [12] as follows:

$$\begin{aligned}\min L(\tau_c, \zeta, \varpi, \sigma) = \alpha\tau_c\left(4\zeta^2+1\right) + \frac{\beta\left(4\tau_c^2\zeta^2+\tau^2\right)}{\tau^2\tau_c^3\zeta^4} + \varpi_1\left(\tau_c^2\gamma_h - h_s(\zeta) - \sigma_1^2\right) \\ + \varpi_2\left(\gamma_g - g_s(\zeta) - \sigma_2^2\right) + \varpi_3\left(\gamma_f - f_s(\zeta,\tau_c) - \sigma_3^2\right)\end{aligned} \tag{16}$$

where ϖ_i and σ_i are the Lagrange multiplier and the slack variable, respectively.

Applying the same way used in the regulatory control case, the seven optimal cases can be found by solving the necessary conditions of the above unconstrained problem for the corresponding combination of slack variable and Lagrange multiplier. **Figure 4** illustrates the seven possible locations of the global optimum.

After obtaining the global optimum for a particular case, the optimal parameters of the PI controller can be calculated using Eq. (15), i.e., $K_c = 1/K_p\tau_c^{opt}; \tau_I = 4\left(\zeta^{opt}\right)^2\tau_c^{opt}$. **Table 3** summarizes the conditions that lead to each global optimal location.

4. Design and evaluation of feasible constraints

The optimal solutions in **Tables 2** and **3** are only true if the constraint set is such that a solution exists. Indeed, depending on the constraint set, the optimal solution may not have a feasible solution. Therefore, before applying the constrained optimal control formulation, either any given constraint set should first be screened quickly to determine its basic feasibility or a constraint set should be designed to be feasible.

4.1. Optimal regulatory control

Conditions for a feasible $\left(y_{max}, u'_{max}\right)$: For a given y_{max}, there is a minimum available u'_{max} value below which the optimal control problem is not feasible. **Figure 5** demonstrates the effects of the constraint specifications on the feasible region in (ζ, τ_c) space. The constraint imposed by Eq. (5d) lies on a vertical line that shifts and bends rightward as u_{max} decreases. The constraint given in Eq. (5c) shifts upward as u'_{max} decreases, whereas the constraint in Eq. (5b) shifts downward as y_{max} decreases. Note that the feasible region only exists when the constraint curve of u'_{max} is below that of y_{max}.

Case	Constraint specification	Condition	Global optimum	Location of global optimum	Calculation of global optimum
A	Mild $y_{\max}$ Mild $u'_{\max}$ Mild $u_{\max}$	$\left[\zeta^{\dagger f} \le \zeta^{\dagger}\right] \cap \left[\tau_c^{\dagger h} \le \tau_c^{\dagger} \le \frac{\gamma_g}{g_r(\zeta^{\dagger})}\right]$	$(\zeta^{\dagger}, \tau_c^{\dagger})$	In the interior of the feasible region	$\zeta^{\dagger} = \sqrt{\frac{1}{2}}$ $\tau_c^{\dagger} = \left(\frac{\beta}{\alpha}\right)^{1/4}$
B	Mild $y_{\max}$ Tight $u'_{\max}$ Mild $u_{\max}$	$\left[\zeta^{\dagger f} \le \zeta^{*h} \le \zeta^{gh}\right] \cap \left[\tau_c^{\dagger} < \tau_c^{\dagger} h\right]$	$(\zeta^{*h}, \tau_c^{*h})$	On $\gamma_h = h_r(\zeta, \tau_c)$	$\gamma_{\mathrm{h}} - h_r(\zeta, \tau_c) = 0$ $\frac{\partial \Phi_r}{\partial \zeta} - \frac{\partial \Phi_r}{\partial \tau_c}\left[\frac{\partial h_r}{\partial \tau_c}\right]^{-1} \frac{\partial h_r}{\partial \zeta} = 0$
C	Tight $y_{\max}$ Mild $u'_{\max}$ Mild $u_{\max}$	$\left[\zeta^{\dagger f} \le \zeta^{*g} \le \zeta^{gh}\right] \cap \left[\tau_c^{*f} \le \tau_c^{gf}\right] \cap \left[\tau_c^{\dagger} \ge \frac{\gamma_g}{g_r(\zeta^{\dagger})}\right]$	$(\zeta^{*g}, \tau_c^{*g})$	On $\tau_c = \frac{\gamma_g}{g_r(\zeta)}$	$\gamma_{\mathrm{g}} - g_r(\zeta)\tau_c = 0$ $\frac{\partial \Phi_r}{\partial \zeta} g_r - \tau_c \frac{\partial \Phi_r}{\partial \tau_c} \frac{\partial g_r}{\partial \zeta} = 0$
D	Tight $y_{\max}$ Tight $u'_{\max}$ Mild $u_{\max}$	$\left[\left(\zeta^{*h} \ge \zeta^{gh}\right) \cap \left(\tau_c^{\dagger} < \tau_c^{\dagger h}\right)\right]$ or $\left[\left(\zeta^{*g} > \zeta^{gh}\right) \cap \left(\tau_c^{\dagger} \ge \frac{\gamma_g}{g_r(\zeta^{\dagger})}\right)\right]$	$\left(\zeta^{gh}, \tau_c^{gh}\right)$	On the vertex by $\tau_c = \frac{\gamma_g}{g_r(\zeta)}$ and $\gamma_h = h_r(\zeta, \tau_c)$	$\gamma_g - \tau_c g_r(\zeta) = 0$ $\gamma_{\mathrm{h}} - h_r(\zeta, \tau_c) = 0$
E	Mild $y_{\max}$ Mild $u'_{\max}$ Tight $u_{\max}$	$\left[\left(\zeta^{\dagger} < \zeta^{\dagger f}\right) \cap \left(\tau_c^{fh} \le \tau_c^{*f}\right)\right]$ or $\left[\left(\zeta^{gh} > \zeta^{*g}\right) \cap \left(\tau_c^{gf} \ge \tau_c^{*f} \ge \tau_c^{fh}\right)\right]$	$\left(\zeta^{*f}, \tau_c^{*f}\right)$	On $\gamma_f = f_r(\zeta, \tau_c)$	$\gamma_{\mathrm{f}} - f_r(\zeta, \tau_c) = 0$ $\frac{\partial f_r}{\partial \tau_c}\frac{\partial \Phi_r}{\partial \zeta} - \frac{\partial f_r}{\partial \zeta}\frac{\partial \Phi_r}{\partial \tau_c} = 0$
F	Tight $y_{\max}$ Mild $u'_{\max}$ Tight $u_{\max}$	$\left[\zeta^{\dagger f} > \zeta^{*g} > \zeta^{gh}\right] \cap \left[\tau_c^{*f} > \tau_c^{gf}\right]$	$\left(\zeta^{gf}, \tau_c^{gf}\right)$	On the vertex by $\gamma_f = f_r(\zeta, \tau_c)$ and $\tau_c = \frac{\gamma_g}{g_r(\zeta)}$	$\gamma_{\mathrm{f}} - f_r(\zeta, \tau_c) = 0$ $\gamma_{\mathrm{g}} - \tau_c g_r(\zeta) = 0$
G	Mild $y_{\max}$ Tight $u'_{\max}$ Tight $u_{\max}$	$\left[\left(\zeta^{\dagger} < \zeta^{\dagger f}\right) \cap \left(\tau_c^{*f} \le \tau_c^{fh}\right)\right]$ or $\left[\left(\zeta^{gh} \ge \zeta^{*h} \ge \zeta^{\dagger f}\right) \cap \left(\tau_c^{\dagger} < \tau_c^{\dagger h}\right)\right]$	$\left(\zeta^{fh}, \tau_c^{fh}\right)$	On the vertex by $\gamma_f = f_r(\zeta, \tau_c)$ and $\gamma_h = h_r(\zeta, \tau_c)$	$\gamma_{\mathrm{f}} - f(\zeta, \tau_c) = 0$ $\gamma_{\mathrm{h}} - h(\zeta, \tau_c) = 0$

Table 2. Global optima of the constrained optimal regulatory control problem.

http://dx.doi.org/10.5772/intechopen.74301

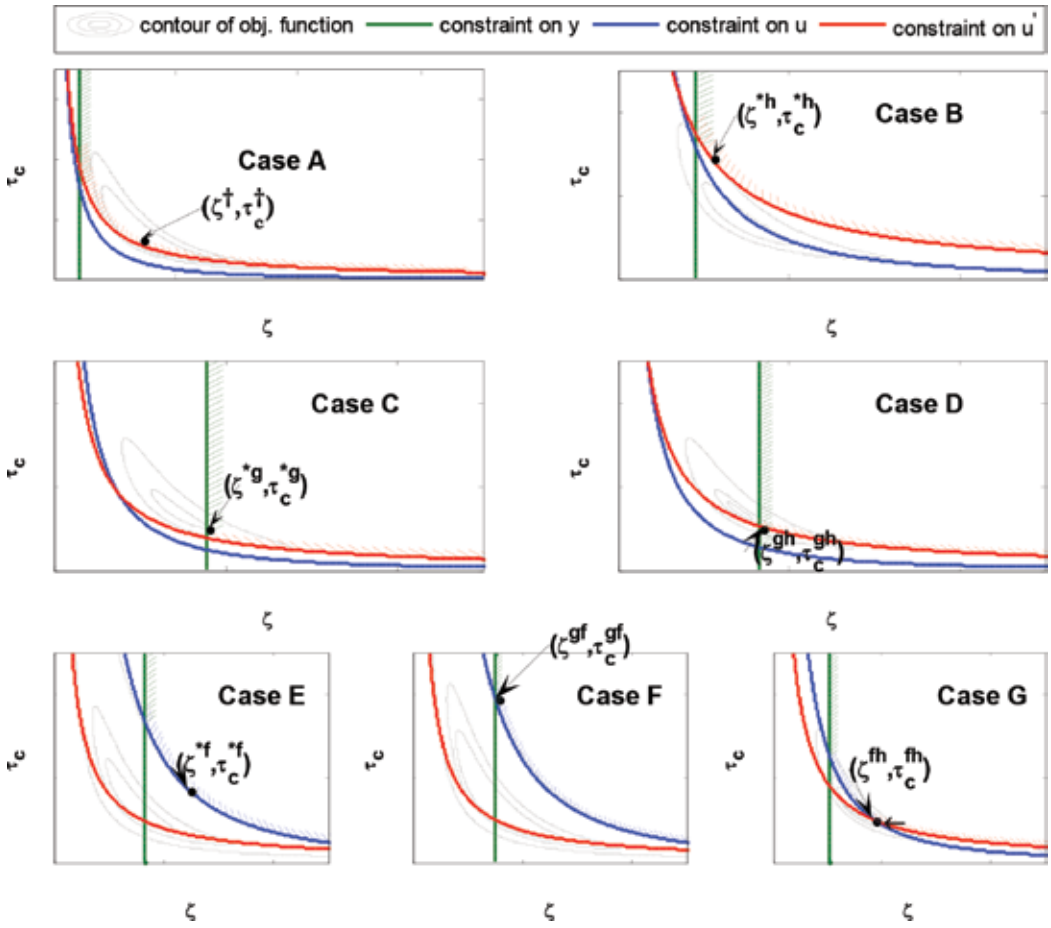

Figure 4. Contours, constraints, and possible locations of the global optimum in servo control case.

As indicated in **Figure 5**, the feasible region reduces in size as $u'_{\max}$ and $y_{\max}$decrease, exhibiting continued reduction until ceasing to exist if the constraints are lower than some minimum allowable values. Therefore, there exists a tangent point (ζ^t, τ_c^t) in (ζ, τ_c) space, where the two constraint curves of $u'_{\max}$ and $y_{\max}$ meet at a single point; this point equates to the smallest feasible $u'_{\max}$ for a given $y_{\max}$ (or the smallest feasible $y_{\max}$ for a given $u'_{\max}$) for different specifications of $u'_{\max}$ and $y_{\max}$.

Let ${u'}^t{}_{\max}$ be the smallest possible value of $u'_{\max}$. ${u'}^t{}_{\max}$ can be obtained when $\zeta = \zeta^t$. ζ^t can be calculated by solving the following equation:

$$\frac{dh_r(\zeta, \tau_c)}{d\zeta} = \frac{dh_r\left(\zeta, \gamma_g g_r^{-1}\right)}{d\zeta} = 0 \tag{17}$$

Case	Constraint specification	Condition	Global optimum	Location of global optimum	Calculation of global optimum
A	Mild $y_{\max}$ Mild $u'_{\max}$ Mild $u_{\max}$	$\left[\zeta_{\min} \le \zeta^{\dagger}\right] \cap \left[\tau_c^{\dagger} \ge \max\left(\tau_c^{*\mathrm{h}}, \tau_c^{*f}\right)\right]$ where $\zeta_{\min}$ is the minimum allowable damping factor by solving $g(\zeta_{\min}) = \gamma_{\mathrm{g}}$	$(\zeta^{\dagger}, \tau_c^{\dagger})$	In the interior of the feasible region	$\zeta^{\dagger} = \sqrt{\frac{1}{2}}$ $\tau_c^{\dagger} = \left(\frac{4\beta}{\alpha}\right)^{1/4}$
B	Mild $y_{\max}$ Tight $u'_{\max}$ Mild $u_{\max}$	$\left[\zeta^{*h} > \max\left(\zeta^{hf}, \zeta_{\min}\right)\right] \cap \left[\tau_c^{\dagger} < \max\left(\tau_c^{*h}, \tau_c^{*f}\right)\right]$	$(\zeta^{*h}, \tau_c^{*h})$	On $\tau_{\mathrm{c}}^2 = \gamma_h^{-1} h_s(\zeta)$	$\zeta^{*\mathrm{h}} = \left(\frac{4\beta\gamma_h^2}{\alpha} + \frac{1}{4}\right)^{1/2} \tau_{\mathrm{c}}^{*\mathrm{h}} = \left(\gamma_h^{-1} h_s\left(\zeta^{*\mathrm{h}}\right)\right)^{\frac{1}{2}}$
C	Tight $y_{\max}$ Mild $u'_{\max}$ Mild $u_{\max}$	$\left[\zeta_{\min} > \zeta^{\dagger}\right] \cap \left[\tau_c^{*g} > \max\left(\tau_c^{gh}, \tau_c^{\mathrm{gf}}\right)\right]$	$(\zeta^{*\mathrm{g}}, \tau_c^{*\mathrm{g}})$	On $g_s(\zeta) = \gamma_{\mathrm{g}}$	$g_s(\zeta^{*g}) = \gamma_g$ $\tau_c^{*g} = \frac{1}{\zeta^{*g}} \left(\frac{3\beta}{\alpha\left(4(\zeta^{*g})^2 + 1\right)}\right)^{1/4}$
D	Tight $y_{\max}$ Tight $u'_{\max}$ Mild $u_{\max}$	$\left[\tau_c^{\dagger} \ge \max\left(\tau_c^{*\mathrm{h}}, \tau_c^{*f}\right) \cap \zeta_{\min} > \zeta^{\dagger} \cap \tau_c^{gh} > \max\left(\tau_c^{*\mathrm{g}}, \tau_c^{\mathrm{gf}}\right)\right]$ or $\left[\tau_c^{\dagger} < \max\left(\tau_c^{*\mathrm{h}}, \tau_c^{*f}\right) \cap \zeta^{gh} > \max\left(\zeta^{hf}, , \zeta^{*h}\right)\right]$	$\left(\zeta^{\mathrm{gh}}, \tau_c^{\mathrm{gh}}\right)$	On the vertex by $g_s(\zeta) = \gamma_{\mathrm{g}}$ and $\tau_{\mathrm{c}}^2 = \gamma_h^{-1} h_s(\zeta)$	$g_s\left(\zeta^{\mathrm{gh}}\right) = \gamma_{\mathrm{g}}$ $\tau_{\mathrm{c}}^{\mathrm{gh}} = \left(\gamma_h^{-1} h_s\left(\zeta^{\mathrm{gh}}\right)\right)^{\frac{1}{2}}$
E	Mild $y_{\max}$ Mild $u'_{\max}$ Tight $u_{\max}$	$\left[\tau_c^{\dagger} < \max\left(\tau_c^{*\mathrm{h}}, \tau_c^{*f}\right)\right] \cap \left[\zeta_{\min} < \zeta^{*f} < \zeta^{hf}\right]$	$\left(\zeta^{*\mathrm{f}}, \tau_c^{*\mathrm{f}}\right)$	On $f_s(\zeta, \tau_{\mathrm{c}}) = \gamma_{\mathrm{f}}$	$\gamma_{\mathrm{f}} = f_s\left(\zeta^{*\mathrm{f}}, \tau_{\mathrm{c}}^{*\mathrm{f}}\right)$ $\frac{\partial f_s(\zeta, \tau_{\mathrm{c}})}{\partial \tau_{\mathrm{c}}} \frac{\partial \Phi_s}{\partial \zeta} - \frac{\partial f_s(\zeta, \tau_{\mathrm{c}})}{\partial \zeta} \frac{\partial \Phi_s}{\partial \tau_{\mathrm{c}}} = 0$
F	Tight $y_{\max}$ Mild $u'_{\max}$ Tight $u_{\max}$	$\left[\tau_c^{\dagger} \ge \max\left(\tau_c^{*\mathrm{h}}, \tau_c^{*f}\right) \cap \left(\zeta_{\min} > \zeta^{\dagger}\right) \cap \tau_c^{gf} > \max\left(\tau_c^{*\mathrm{g}}, \tau_c^{gh}\right)\right]$ or $\left[\left(\tau_c^{\dagger} < \max(\tau_c^{*h}, \tau_c^{*\mathrm{f}})\right) \cap \left(\zeta^{*f} < \zeta_{\min} < \zeta^{hf}\right)\right]$	$\left(\zeta^{\mathrm{gf}}, \tau_c^{\mathrm{gf}}\right)$	On the vertex by $f_s(\zeta, \tau_{\mathrm{c}}) = \gamma_{\mathrm{f}}$ and $g_s(\zeta) = \gamma_{\mathrm{g}}$	$g_s\left(\zeta^{\mathrm{gf}}\right) = \gamma_{\mathrm{g}}$ $\gamma_{\mathrm{f}} = f_s\left(\zeta^{\mathrm{gf}}, \tau_c^{\mathrm{gf}}\right)$
G	Mild $y_{\max}$ Tight $u'_{\max}$ Tight $u_{\max}$	$\left[\tau_c^{\dagger} < \max\left(\tau_c^{*\mathrm{h}}, \tau_c^{*f}\right)\right] \cap \left[\zeta_{\min} < \zeta^{*\mathrm{h}} < \zeta^{hf}\right]$	$\left(\zeta^{\mathrm{fh}}, \tau_c^{\mathrm{fh}}\right)$	On the vertex by $f_s(\zeta, \tau_{\mathrm{c}}) = \gamma_{\mathrm{f}}$ and $\tau_{\mathrm{c}}^2 = \gamma_h^{-1} h_s(\zeta)$	$\gamma_{\mathrm{f}} = f_s\left(\zeta^{\mathrm{hf}}, \tau_{\mathrm{c}}^{\mathrm{hf}}\right)$ $\tau_{\mathrm{c}}^{\mathrm{hf}} = \frac{1}{2\zeta^{\mathrm{hf}}\sqrt{\gamma_{\mathrm{h}}}}$

Table 3. Global optima of the constrained optimal servo control problem.

http://dx.doi.org/10.5772/intechopen.74301

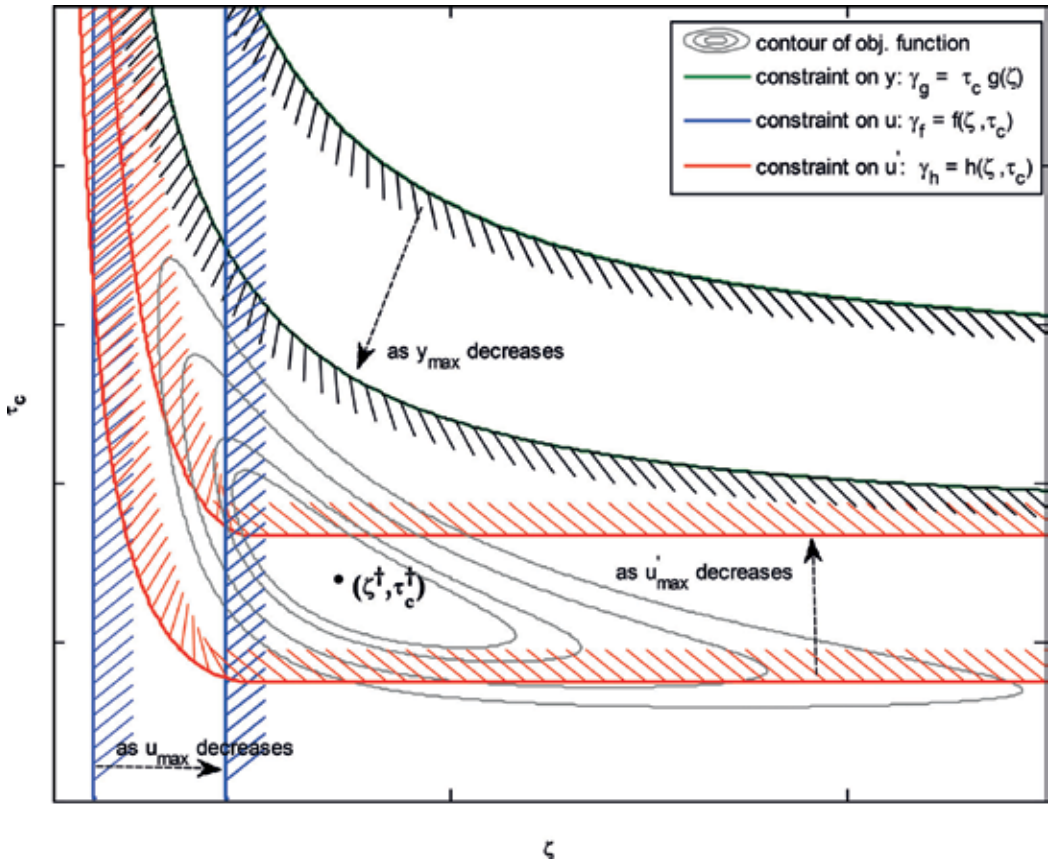

Figure 5. Effects of the constraint specifications y_{max}, u_{max}, and u'_{max} on the feasible region.

Once ζ^t is obtained, ${u'}^t{}_{max}$ can then be derived as follows:

$$ {u'}^t{}_{max} = h_r(\zeta^t)|\Delta D| \tag{18} $$

To sum up, if $u'_{max} \geq {u'}^t{}_{max}$, the constraint set (y_{max}, u'_{max}) is feasible; otherwise, it is infeasible.

Similarly, for a given u'_{max}, there is a minimum available y_{max} value below which the optimal control problem is not feasible. Let y^t_{max} be the smallest possible y_{max}. The values of y^t_{max} and ζ^t can be obtained by solving the following system of equations simultaneously:

$$ h_r\left(\zeta, \gamma_g {g_r}^{-1}\right) = \gamma_h \tag{19} $$

$$ \frac{dh_r\left(\zeta, \gamma_g {g_r}^{-1}\right)}{d\zeta} = 0 \tag{20} $$

To sum up, if $y_{max} \geq y^t_{max}$, then the constraint set (y_{max}, u'_{max}) is feasible; otherwise, it is infeasible.

Feasible $u_{\max}$ for a given feasible set $(y_{\max}, u'_{\max})$: For a feasible $(y_{\max}, u'_{\max})$, it can be intuitively inferred from the geometrical analysis of the constraint curves that any positive $u_{\max} \geq |\Delta D|$ will result in a feasible region if there is no intersection between the constraint curves of $\tau_c g_r(\zeta) = \gamma_g$ and $h_r(\zeta, \tau_c) = \gamma_h$. Furthermore, if the intersection, ζ^{gh}, exists, the constraint, $u_{\max}$, is feasible if $\zeta^{gh} \geq \zeta^{gf}$. To evaluate the existence of an intersection between the two constraint curves $\tau_c g_r(\zeta) = \gamma_g$ and $h_r(\zeta, \tau_c) = \gamma_h$, it is important to calculate $\tau_c(\infty)$, the value of τ_c where the two constraint curves are secant when $\zeta \to \infty$. $\tau_c(\infty)$ of each constraint curve can be obtained by solving the following equations:

$$\left[\tau_c(\infty) g_r(\zeta) = \gamma_g\right]_{\zeta \to \infty} \tag{21a}$$

$$\left[h_r(\zeta, \tau_c(\infty)) = \gamma_h\right]_{\zeta \to \infty} \tag{21b}$$

Because $\lim_{\zeta \to \infty} g_r(\zeta) = 1$ and $\lim_{\zeta \to \infty} h_r(\zeta, \tau_c) = 1/\tau_c = \gamma_h$, $\tau_c(\infty)$ of the two constraint curves are as follows:

$$\tau_c^g(\infty) = \gamma_g \tag{22a}$$

$$\tau_c^h(\infty) = \frac{1}{\gamma_h} \tag{22b}$$

A vertex ζ^{gh} exists when $\tau_c^g(\infty) \geq \tau_c^h(\infty)$. Therefore,

$$\gamma_g \geq \frac{1}{\gamma_h} \tag{23}$$

which yields

$$\left|\frac{y_{\max}}{K_p \Delta D}\right| \left|\frac{u'_{\max}}{\Delta D}\right| \geq 1 \tag{24}$$

Overall, for a given feasible $(y_{\max}, u'_{\max})$, $u_{\max}$ is feasible under either of the following conditions: (1) Eq. (24) is not satisfied or (2) Eq. (24) is satisfied and $\zeta^{gh} \geq \zeta^{gf}$. Otherwise, $u_{\max}$ is not feasible and should be increased until one of the conditions is satisfied. Note that if $\left|\frac{y_{\max}}{K_p \Delta D}\right| \left|\frac{u'_{\max}}{\Delta D}\right| < 1$, no vertex point is formed by $\gamma_g = \tau_c g_r(\zeta)$ and $\gamma_h = h_r(\zeta, \tau_c)$, i.e., case D does not exist. In such a situation, for the purpose of evaluating the conditions presented in **Table 2**, any extremely large value can be assigned to ζ^{gh}.

Figure 6 illustrates a procedure applied to design a feasible constraint set $(y_{\max}, u'_{\max}, u_{\max})$ and test its feasibility.

4.2. Optimal servo control

It is clear from their approaching values of $y(t), u(t), u'(t)$ as $t \to \infty$ that for the constraints by $y_{\max}$ and $u_{\max}$ to be feasible, they must be greater than $|\Delta Y_{sp}|$ and $|\Delta Y_{sp}/K|$, respectively, whereas the constraint by $u'_{\max}$ can be set to any nonnegative value. **Figure 7** illustrates how

http://dx.doi.org/10.5772/intechopen.74301

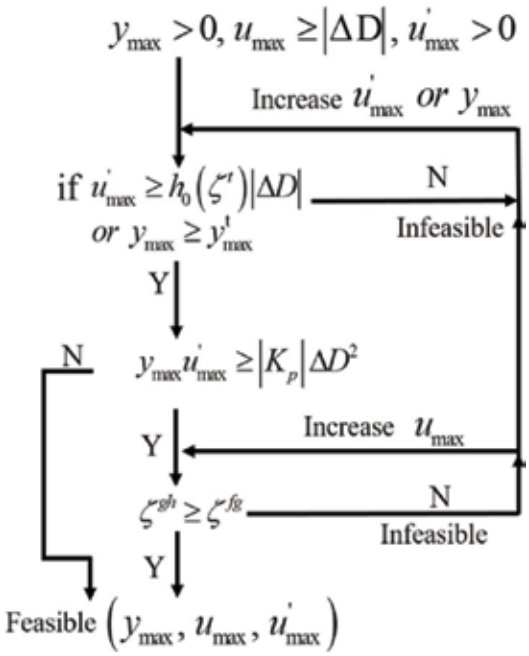

Figure 6. Procedure to design and test a feasible constraint set for optimal regulatory PI control of integrating system.

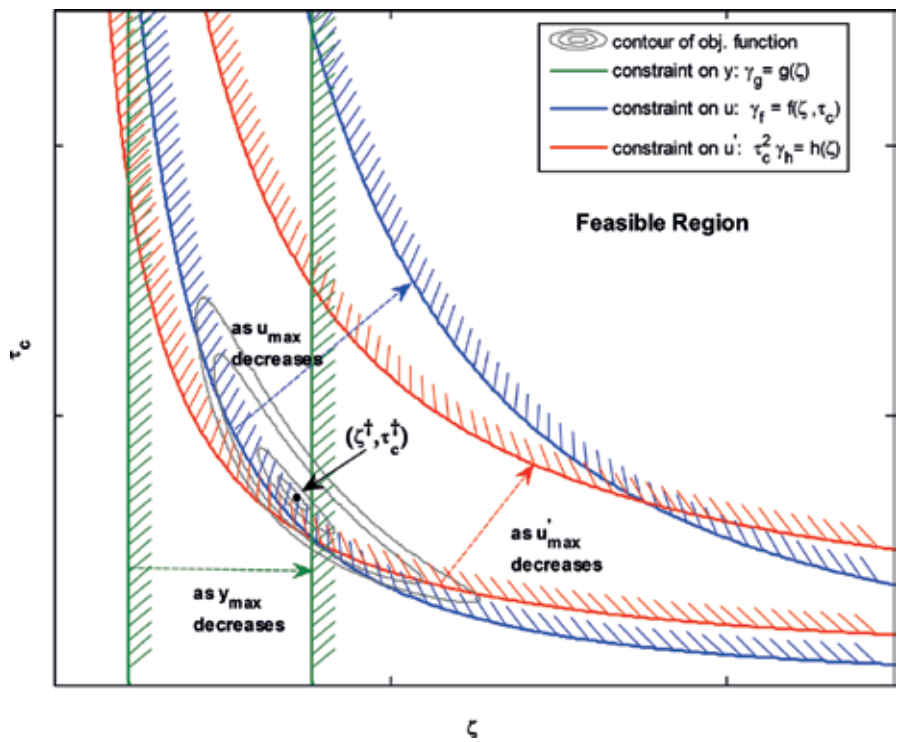

Figure 7. Effects of the constraint specifications y_{max}, u_{max}, and u'_{max} on the feasible region.

the three constraint specifications affect the feasible region. The constraint $\gamma_g \geq g_s(\zeta)$ vertically splits the region into two, while the constraints imposed by $\tau_c^2\gamma_h \geq h_s(\zeta)$ and $\gamma_f \geq f_s(\zeta, \tau_c)$ have a similar shape in (ζ, τ_c) space. It shows that for any feasible constraint set $\left(y_{max}, u'_{max}, u_{max}\right)$, the feasible region is bounded below but unbounded in the upper side. This means that a decrease in y_{max}, u_{max} and u'_{max} will narrow down the feasible region delimited by the three constraints, but the feasible region will always exist. Moreover, the shape of the three constraints indicates the feasible region is always convex.

5. Closed-loop performance

5.1. Optimal regulatory control

Consider the following integrating process as

$$G_p(s) = \frac{1}{s} \tag{25}$$

Table 4 presents the examples of the seven possible aforementioned cases, as based on various constraint specifications. Simulations are carried out for weighting factors $\omega_y = \omega_{u'} = 0.5$.

Figure 8 presents the resulting process variable, $y(t)$, controller output, $u(t)$, and its rate of change, $u'(t)$, for the seven examples. As can be seen from the figure, the PI controller designed by the proposed method not only yields optimal control performance, but also strictly satisfies the respective y_{max}, u_{max}, and u'_{max} constraint requirements.

5.2. Optimal servo control

Consider the following integrating process

Example	Case	Constraint specification			PI parameter	
		y_{max}	u_{max}	u'_{max}	K_C	τ_I
1	A	0.70	2.70	2.70	1.41	1.41
2	B	0.70	2.70	1.11	1.10	1.10
3	C	0.36	2.70	2.70	1.93	1.51
4	D	0.285	2.70	2.10	2.10	0.69
5	E	0.70	1.105	2.70	1.96	2.95
6	F	0.30	1.20	2.70	2.18	0.98
7	G	0.70	1.20	1.37	1.37	1.56

Table 4. Constraint requirements and corresponding optimal PI parameters for regulatory control example.

http://dx.doi.org/10.5772/intechopen.74301

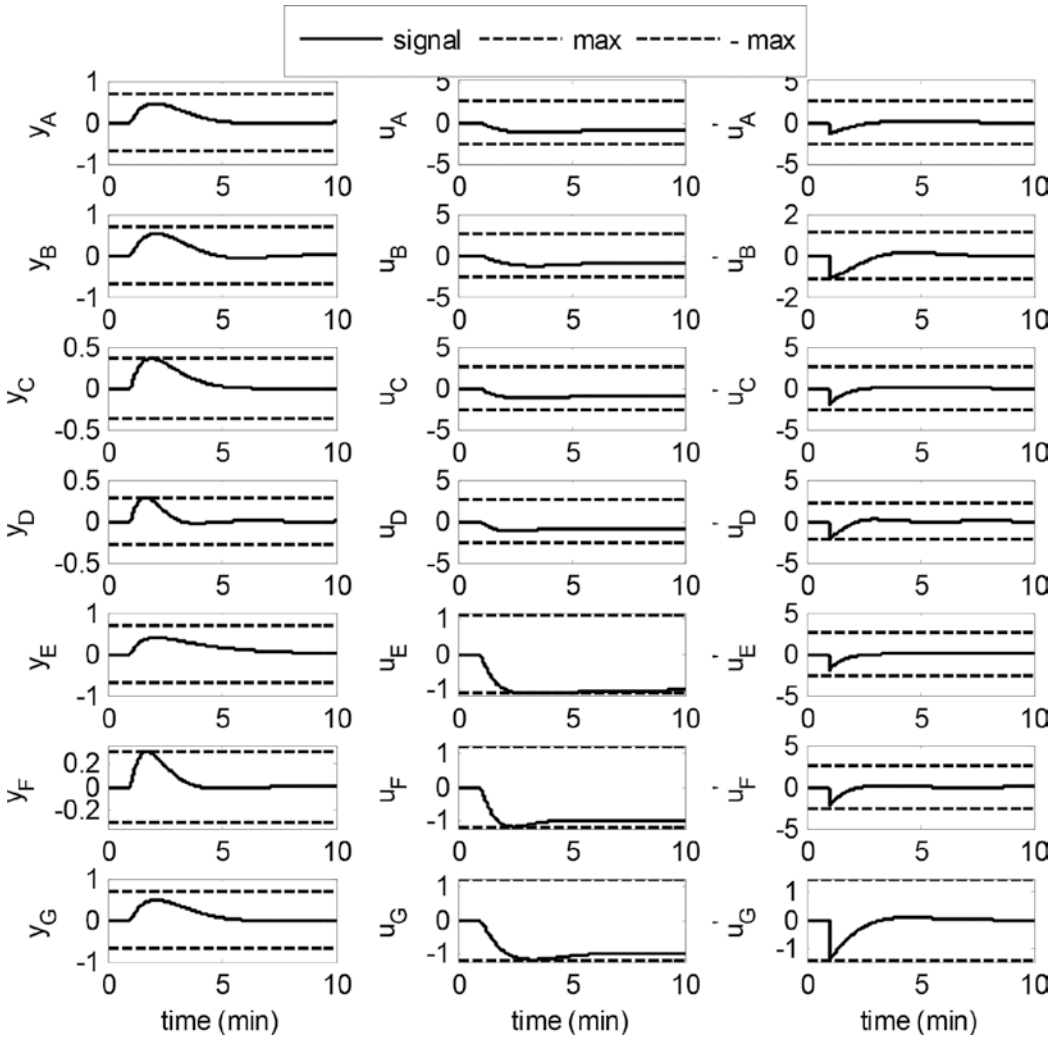

Figure 8. Time responses of the system for cases A to G: regulatory system.

$$G_{\mathrm{p}}(s) = \frac{10}{s} \tag{26}$$

Table 5 lists the examples of the seven possible cases based on various constraint specifications. Simulations are carried out for weighting factors, $\omega_{\mathrm{y}} = \omega_{u'} = 0.5$. **Figure 9** presents the time responses by the proposed optimal PI controller for the seven examples. As seen in the responses, the resulting optimal PI controllers not only provide the stable and optimal closed-loop responses, but also satisfy the $y_{\max}$, $u_{\max}$, and $u'_{\max}$ requirements, strictly.

Example	Case	Constraint specification			PI parameter	
		$y_{\max}$	$u_{\max}$	$u'_{\max}$	K_C	τ_I
1	A	1.2	0.5	1.5	1.41	1.414
2	B	1.2	0.5	0.5	0.79	1.58
3	C	1.03	0.5	1.5	1.52	1.46
4	D	1.03	0.5	1.03	1.51	1.47
5	E	1.2	0.3	1.5	1.53	2.42
6	F	1.03	0.41	1.5	1.38	1.61
7	G	1.2	0.4	1.17	2.15	1.83

Table 5. Constraint requirements and corresponding optimal PI parameters for servo control example.

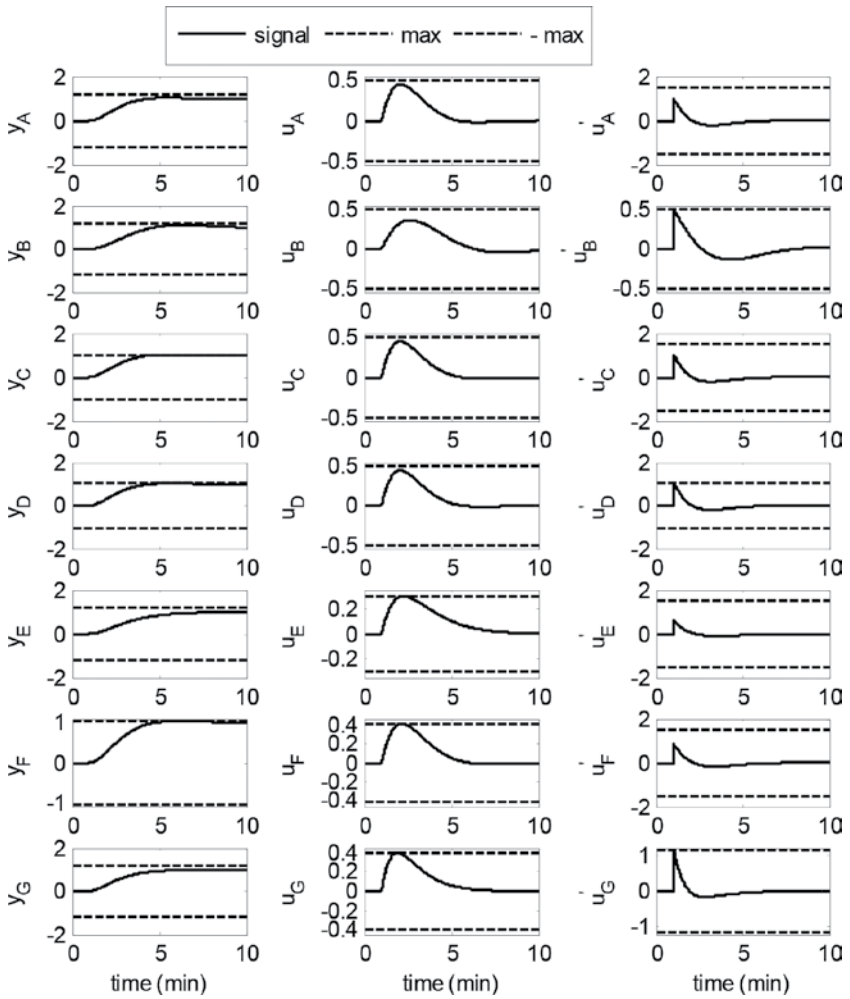

Figure 9. Time responses of the system for cases A to G: servo system.

6. Conclusions

A novel analytical design approach is introduced for optimal regulatory and servo PI control subjected to operational constraints and examined to integrating processes. Owing to incisive parameterization, a complex constrained optimal control problem can be reformulated and converted to a simple algebraic form in the new design parameter (ζ, τ_c) space, which allows finding the conditions and locations for the global optima by graphical analysis without having to rely on the numerical or black-box optimization effort. The proposed closed-form solution of the constrained optimal controller establishes a direct relationship between the control and plant parameters by which the optimal PI parameters can be obtained in an easy and quick manner. This approach also provides the following useful insights into how the control parameters affect the plant and how a feasible constraint set can be designed and checked in the constrained optimal control.

Acknowledgements

This research was supported by the Basic Science Research Program through the National Research Foundation of Korea (NRF) funded by the Ministry of Education (2015R1D1A3A01015621) and by the Priority Research Centers Program through the National Research Foundation of Korea (NRF) funded by the Ministry of Education (2014R1A6A1031189).

Conflict of interest

The authors confirm there are no conflicts of interest.

Author details

Rodrigue Tchamna and Moonyong Lee*

*Address all correspondence to: mynlee@yu.ac.kr

School of Chemical Engineering, Yeungnam University, Gyeongsan, Korea

References

[1] Lewis FL, Vrabie DL, Syrmos VL. Optimal Control. 3rd ed. New York: John Wiley and Sons; 2012. p. 553. DOI: 10.1002/9781118122631

[2] Siebenthal CD, Aris R. Studies in optimization—VII The application of Pontryagin's methods to the control of batch and tubular reactors. Chemical Engineering Science. 1964;**19**:747-761. DOI: 10.1016/0009-2509(64)85086-7

[3] Shin J, Lee J, Park S, Koo KK, Lee M. Analytical design of a proportional-integral controller for constrained optimal regulatory control of inventory loop. Control Engineering Practice. 2008;**16**:1391-1397. DOI: 10.1016/j.conengprac.2008.04.006

[4] Lee M, Shin J. Constrained optimal control of liquid level loop using a conventional proportional-integral controller. Chemical Engineering Communications. 2009;**196**:729-745. DOI: 10.1080/00986440802557393

[5] Lee M, Shin J, Lee J. Implement a constrained optimal control in a conventional level controller. Hydrocarbon Processing. 2010;**89**:71-76

[6] Lee M, Shin J, Lee J. Implement a constrained optimal control in a conventional level controller. Hydrocarbon Processing. 2010;**89**:81-85

[7] Nguyen VH, Yoshiyuki Y, Lee M. Optimization based approach for industrial PI controller design for optimal servo control of integrating process with constraints. Journal of Chemical Engineering of Japan. 2011;**44**:345-354. DOI: 10.1252/jcej.10we325

[8] Thu H, Lee M. Analytical design of proportional-integral controllers for the optimal control of first-order processes with operational constraints. Korean Journal of Chemical Engineering. 2013;**30**:2151-2162. DOI: 10.1007/s11814-013-0153-1

[9] Tchamna R, Lee M. Constraint handling optimal PI control of open-loop unstable process: Analytical approach. Korean Journal of Chemical Engineering. 2017;**34**:3067-3076. DOI: https://doi.org/10.1007/s1181

[10] Tchamna R, Lee M. Optimization approach for the analytical design of an industrial PI controller for the optimal regulatory control of first order processes under operational constraints. Journal of the Taiwan Institute of Chemical Engineers. 2017;**80**:85-99. DOI: 10.1016/j.jtice.2017.08.012

[11] Tchamna R, Lee M. Analytical design of an industrial two-term controller for optimal regulatory control of open-loop unstable processes under operational constraints. ISA Transactions. 2018;**72**:66-76. DOI: 10.1016/j.isatra.2017.11.002

[12] Vapnyarskii IB. Lagrange Multipliers. 1st ed. Heidelberg: Springer; 2001

[13] Boyd S, Vandenberghe L. Convex Optimization. 1st ed. Cambridge: Cambridge University Press; 2004. p. 727

Chapter 8

Decoupling Control and Soft Sensor Design for an Experimental Platform

Thamiles Rodrigues de Melo,
Nathália Arthur Brunet Monteiro, Danilo Pequeno,
Jaidilson Jó da Silva and José Sérgio da Rocha Neto

Additional information is available at the end of the chapter

http://dx.doi.org/10.5772/intechopen.75708

Abstract

This chapter presents the design and implementation of a decoupling control strategy for an experimental platform and pilot plant, dedicated to the study of the fouling phenomena which occur in industrial tubes. Initially, a set of tests was done for the identification and validation of FOPDT models suitable to the four processes of the multivariable system: flow-voltage, flow-current, pressure-voltage, and pressure-current. After, the interaction between the inputs and outputs of the system was analyzed by the RGA and RNGA matrices. The static decoupling and decentralized PID controllers tuned by the Ziegler-Nichols and IMC methods were designed. Then, the set point tracking response was simulated and implemented using MATLAB and LabVIEW software, respectively. Finally, the concept of soft sensor was applied to monitor the output variables of the experimental platform, for a better performance of the decoupling control.

Keywords: multivariable system, FOPDT process, PID control, decoupling, soft sensor

1. Introduction

Automatic control arose from the need to improve performance of the systems, in search of better products at lower costs, and has made great advances in engineering, becoming of great importance in industrial processes. The increase in the complexity of the systems and the high level of automation present in the most diverse areas of the productive sectors has indicated the need to develop more precise and robust models, in order to make processes more reliable and to reduce the operating costs [1].

In general, industrial processes have a multivariable nature, with multiple inputs and outputs, which configure multi-input multi-output (MIMO) systems. If these processes have two inputs and two outputs, then they can be referred to as two-input two-output (TITO) systems. Besides, many MIMO systems are treated as several TITO subsystems in practice [2].

Multivariable systems are more difficult to control due to interactions between input and output variables on each control loop. Thus, many problems associated with multivariable control are solved by means of the application of decentralized control theory. In this type of control, design techniques for single-input single-output (SISO) control systems are used in the pairing of manipulated variables (i.e., plant input signals on control) and process variables (i.e., output signals of the plant on control) [3, 4].

When the interactions between the control loops are not so significant, a diagonal controller (decentralized control) may be sufficient to guarantee control of the system. However, if the interactions are more significant, a complete matrix controller (centralized control) is more appropriate. One of the strategies for implementing centralized control is the use of decoupling devices together with a decentralized controller. Furthermore, the decoupling in a MIMO control system also allows the application of SISO control techniques, such as the proportional-integral-derivative (PID) controller tuning methods [5, 6].

The main advantage of PID control in industry can be attributed by the simplicity and ease of implementation for robustness over a wide range of operating conditions. The PID structure has three elements: a proportional term to close the feedback loop, an integral term to assure zero error to constant reference and disturbance inputs, and a derivative term to improve or realize the stability and good dynamic response. The preference for using the time constants of this controller in the industry refers to the physical meaning given to the operator on the system behavior to be controlled [7].

The task of a control system is to ensure the stability of the process, to minimize the influence of disturbances, and to optimize the overall performance. Thus, the industrial processes are instrumented with a large number of sensors. The purpose of sensors is to acquire data of the system. Currently, soft sensors have been used in industries to make physical systems meet the specifications of performance previously established with success, such as reconstructing the missing measurements during the operating of process and assisting in monitoring, control, and optimization of plant [8].

The soft sensors can be considered as the result of the intersection of the techniques of system modeling and identification and the intelligent instrument technology, instruments that, combined with digital systems like microprocessors or microcontrollers, modify their behavior, manipulating computationally the information to adapt to the collection and manipulation of the process data and transmitting them in the best possible way. The term “soft sensor” is a combination of the words “software” and “sensors,” because the models are usually a set of software routines and represent similar measurements of the real sensors [9].

Specific modeling techniques for soft sensors using artificial neural networks (ANNs) constitute an interesting development to be searched. This study has led to the interest in the development of soft sensors, using a computer program; the variables are estimated from the information collected by other measurements, without the industrial process being paralyzed.

In this context, the aim of this chapter is the design and implementation of a decoupling control strategy for an experimental platform dedicated to study the fouling phenomena. Besides, the concept of soft sensor allied to neural networks is applied to start the output variable monitoring of the platform, for a better performance of the decoupling control.

This chapter is structured as follows. Section 2 presents the basic concepts of MIMO control system using decoupling. Section 3 describes the experimental platform under study. Section 4 presents the methodology used for modeling and control of the system. Section 5 discusses the results obtained. Section 6 presents the special topic on an application of soft sensor for the closed-loop control. Section 7 summarizes a conclusion about the implementation.

2. Fundamentals of multivariable control systems

Multivariable systems, also called MIMO systems, are systems that have more than one input variable and more than one output variable. The main difference between a SISO system and a MIMO system is the presence of combinations (or directions) in the system.

The combinations are present in vectors and matrices, which compose the MIMO systems, but are not in scalars, that characterize the SISO systems, as observed in **Figure 1**. However, ideas and techniques applied to SISO systems can be extended to multivariable systems [10].

Consider a multivariable system with m inputs $u(t)$ and n outputs $y(t)$ in the time domain. The matrix representation of the system in the Laplace s domain is given according to Eq. (1):

$$\mathbf{Y}(s) = \mathbf{G_p}(s)\mathbf{U}(s) \Rightarrow \begin{bmatrix} Y_1(s) \\ Y_2(s) \\ \vdots \\ Y_n(s) \end{bmatrix} = \begin{bmatrix} G_{p_{11}}(s) & G_{p_{12}}(s) & \cdots & G_{p_{1m}}(s) \\ G_{p_{21}}(s) & G_{p_{22}}(s) & \cdots & G_{p_{2m}}(s) \\ \vdots & \vdots & \ddots & \vdots \\ G_{p_{n1}}(s) & G_{p_{n2}}(s) & \cdots & G_{p_{nm}}(s) \end{bmatrix} \cdot \begin{bmatrix} U_1(s) \\ U_2(s) \\ \vdots \\ U_m(s) \end{bmatrix} \quad (1)$$

where $\mathbf{Y}(s)$ is the output vector representing a set of process variables $Y_1(s)$, $Y_2(s)$, …, $Y_n(s)$, with order $n \times 1$; $\mathbf{U}(s)$ is the input vector representing a set of manipulated variables $U_1(s)$, $U_2(s)$, …, $U_m(s)$, with order $m \times 1$; and $\mathbf{G_p}(s)$ is the transfer function matrix of the plant, with order $n \times m$.

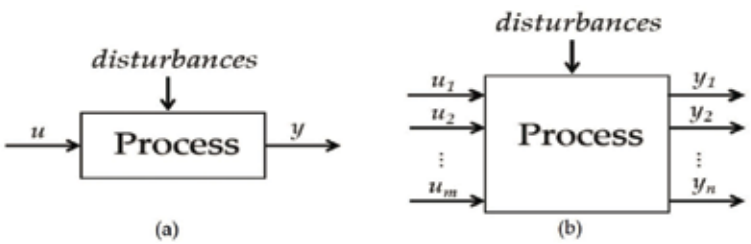

Figure 1. Block diagrams for (a) SISO and (b) MIMO systems. *Source*: Own author (2018).

In the multivariable system, if one of the inputs is modified and this affects the other outputs, then there is an *interaction* between the inputs and the outputs of the system. The interaction determines the level of coupling of the multivariable system, which can be:

- *Poorly coupled or uncoupled*, when u_1 only affects y_1, u_2 only affects y_2, and so on.
- *Strongly coupled*, when the change in u_i, with $i = 1, \ldots, m$, affects all outputs of the system, i.e., $y_1, y_2, \ldots, y_n$. If the effect of the manipulated variable is greater than the others in the plant, then the coupling has dominance in the system [11].

Thus, a *multivariable control system* can be treated as a control system that involves several manipulated and process variables to reduce the interferences caused by the interaction between the control loops. A feedback control loop for a MIMO system is observed in **Figure 2**, where $e(t)$ is the error between the output $y(t)$ and the reference $y_r(t)$.

When the elements outside the diagonal of the plant matrix are elevated, one type of MIMO control strategy denominated as *decoupling control* has the ability to removing the interactions between two or more variables. For example, the decoupling configuration of a TITO system with decentralized control is observed in **Figure 3**. The process variable $\mathbf{Y}(s) = [Y_1(s) \;\; Y_2(s)]^T$ tracks the set point $\mathbf{Y_r}(s) = [Y_{r_1}(s) \;\; Y_{r_2}(s)]^T$ by means of the control strategies implemented in the decentralized controller matrix $\mathbf{G_c}(s)$. Furthermore, this matrix produces the manipulated variable $\mathbf{U}(s) = [U_1(s) \;\; U_2(s)]^T$ to actuate in the plant matrix $\mathbf{G_p}(s)$.

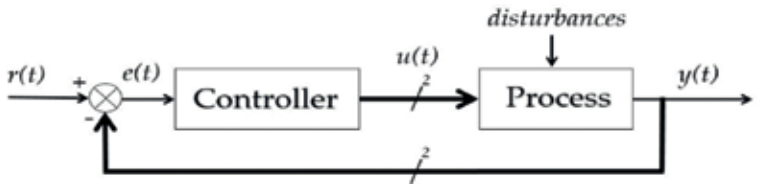

Figure 2. General structure of a feedback control loop for a MIMO system. *Source*: Own author (2018).

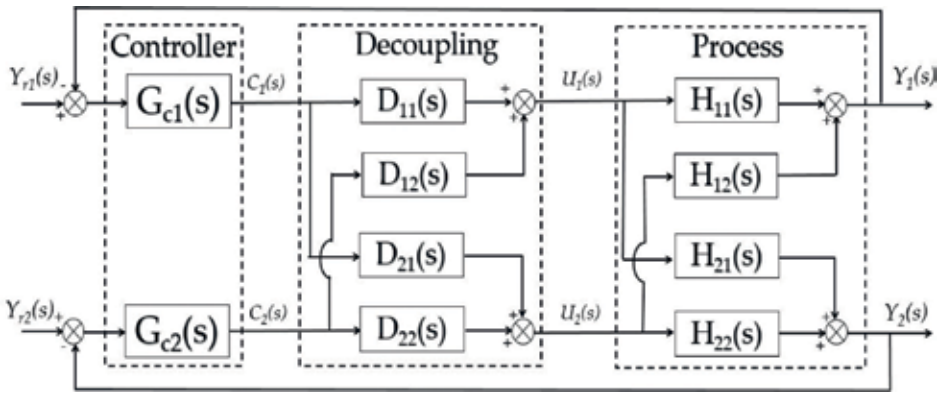

Figure 3. The decoupling configuration of a TITO system. *Source*: Own author (2018).

For a TITO system, the plant matrix $\mathbf{G_p}(s)$ can be expressed by Eq. (2):

$$\mathbf{G_p}(s)=\begin{bmatrix} G_{p_{11}}(s) & G_{p_{12}}(s) \\ G_{p_{21}}(s) & G_{p_{22}}(s) \end{bmatrix}=\begin{bmatrix} \frac{Y_1(s)}{U_1(s)} & \frac{Y_1(s)}{U_2(s)} \\ \frac{Y_2(s)}{U_1(s)} & \frac{Y_2(s)}{U_2(s)} \end{bmatrix} \tag{2}$$

where $G_{p_{ij}}(s)$, with i, j ranging from 1 to 2, is the transfer function of each SISO process in the Laplace domain, resulting from possible input-output combinations in a TITO system.

Since the decentralized controller matrix $\mathbf{G_c}(s)$ has order compatible with the plant matrix $\mathbf{G_p}(s)$, then it can be expressed according to Eq. (3):

$$\mathbf{G_c}(s)=\begin{bmatrix} G_{c_1}(s) & 0 \\ 0 & G_{c_2}(s) \end{bmatrix} \tag{3}$$

where $G_{c_i}(s)$, with i varying from 1 to 2, is the transfer function of the implemented controller in the decentralized control structure in the Laplace domain.

If the interaction between the inputs and outputs was poorly coupled, then the output $\mathbf{C}(s)$ of the decentralized controller equals the manipulated variable $\mathbf{U}(s)$. Otherwise, if necessary to apply the decoupling on the system, then the controller output and the plant input are distinct by means of the design of the decoupling matrix $\mathbf{D}(s)$, as represented in Eq. (4):

$$\mathbf{U}(s)=\mathbf{D}(s)\mathbf{C}(s)\Rightarrow\begin{bmatrix} U_1(s) \\ U_2(s) \end{bmatrix}=\begin{bmatrix} D_{11}(s) & D_{12}(s) \\ D_{21}(s) & D_{22}(s) \end{bmatrix}\cdot\begin{bmatrix} C_1(s) \\ C_2(s) \end{bmatrix} \tag{4}$$

When replacing Eq. (4) in Eq. (1), considering this matrix with compatible order to the TITO system, the resulting matrix $\mathbf{T}(s)$ is obtained with the decoupling, as represented in Eq. (5):

$$\mathbf{Y}(s)=\mathbf{G_p}(s)\mathbf{U}(s)=\mathbf{G_p}(s)\mathbf{D}(s)\mathbf{C}(s)\Rightarrow\mathbf{Y}(s)=\mathbf{T}(s)\mathbf{C}(s) \tag{5}$$

In this case, the resulting matrix becomes diagonal and represents the desired dynamic for the decoupled TITO system [12], according to Eq. (6):

$$\mathbf{T}(s)=\mathbf{G_p}(s)\mathbf{D}(s)\Rightarrow\begin{bmatrix} T_{11}(s) & 0 \\ 0 & T_{22}(s) \end{bmatrix}=\begin{bmatrix} G_{p_{11}}(s) & G_{p_{12}}(s) \\ G_{p_{21}}(s) & G_{p_{22}}(s) \end{bmatrix}\cdot\begin{bmatrix} D_{11}(s) & D_{12}(s) \\ D_{21}(s) & D_{22}(s) \end{bmatrix} \tag{6}$$

Therefore, the product of the inverse of plant matrix with the resulting matrix obtains the decoupling matrix, according to Eq. (7):

$$\mathbf{D}(s)=\mathbf{G_p}(s)^{-1}\mathbf{T}(s)=\frac{1}{G_{p_{11}}(s)G_{p_{22}}(s)-G_{p_{12}}(s)G_{p_{21}}(s)}\cdot\begin{bmatrix} G_{p_{22}}(s)T_{11}(s) & -G_{p_{12}}(s)T_{22}(s) \\ -G_{p_{21}}(s)T_{11}(s) & G_{p_{11}}(s)T_{22}(s) \end{bmatrix} \tag{7}$$

For a simulation example on MIMO system, consider a Luyben and Vinnate distillation column model, cited in [13], with diagonal pairing ($y_1 - u_1$ /$y_2 - u_2$), is given by Eq. (8).

$$\mathbf{G_p}(s)=\begin{bmatrix} \dfrac{-2.16}{8s+1}e^{-s} & \dfrac{1.26}{9.5s+1}e^{-0.3s} \\ \dfrac{-2.75}{9.5s+1}e^{-1.8s} & \dfrac{4.28}{9.2s+1}e^{-0.35s} \end{bmatrix} \tag{8}$$

The static decoupling matrix $\mathbf{D}(s)$ is given by Eq. (9):

$$\mathbf{D}(j0) = \begin{bmatrix} 1 & 0.5833 \\ 0.6425 & 1 \end{bmatrix} \tag{9}$$

The set point tracking response of the control loops simulated by means of MATLAB software is shown in **Figure 4**, using the PI controllers tuned by Internal Model Control (IMC) method (better explained in Section 4), according to **Table 1**.

After the basic concepts of a multivariable control system, the description of the plant under test and the formulation of the control problem are shown in Section 3.

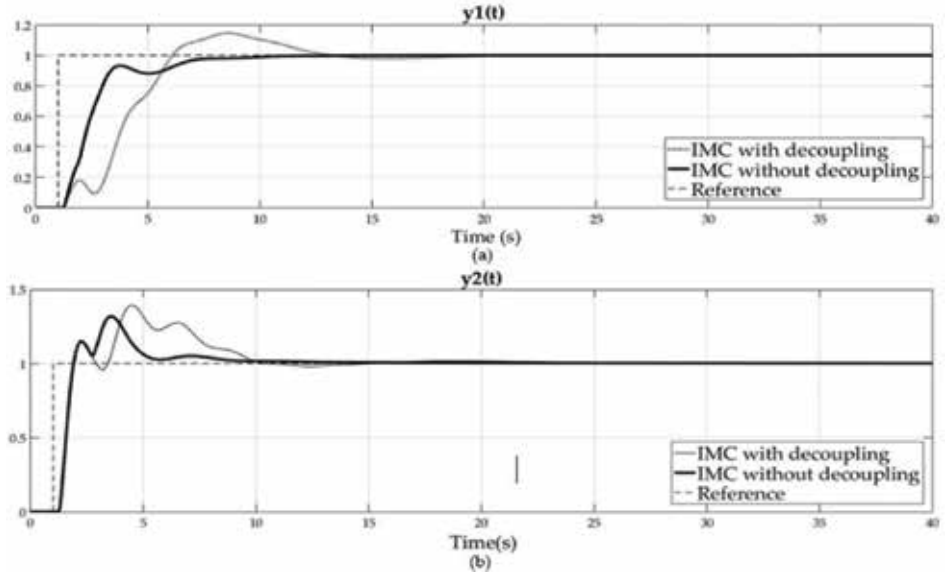

Figure 4. The simulation of set-point tracking response: (a) the flow and (b) pressure control loops with static decoupling – ZN and IMC methods. *Source*: Own author (2018).

Tuning method	Process	Controller	$K_{P_{in}}$	$T_{I_{in}}$
IMC	11	$G_{c1}(s)$	−3.9352	8.5000
	22	$G_{c2}(s)$	6.2583	9.3750

Source: Own author (2018).

Table 1. PID controllers obtained with IMC tuning method.

http://dx.doi.org/10.5772/intechopen.75708

3. Experimental platform

To study the process of fouling formation in industrial tubes, an experimental platform was built in the Laboratory of Electronic Instrumentation and Control (LIEC) of the Electrical Engineering Department at Federal University of Campina Grande, Brazil.

The experimental platform shown in **Figure 5** is characterized as a distributed monitoring of fluid transport system with galvanized iron tubes of different diameters (1″, 1 1/2″, 2″). The 2″ tubes are assumed as the main tube, and the other tubes are used for generation of disturbances in the system.

For the monitoring and control of the phenomena in study, three flow sensors and three pressure sensors were chosen, which were fixed in each type of tube and one temperature sensor which was submerged in the fluid (in this case, the water) stored in a 100 liter tank. Besides, on the experimental platform, there is one control valve with electric actuator and two manual valves for outflow control, even as one frequency inverter used for the rotate velocity control of the water pump.

Furthermore, there is one programmable logic controller (PLC) responsible by the integration between sensors, actuators, and computer on the experimental platform. The sensors communicate with the PLC via 4–20 mA standard, and the actuators communicate with controller using the 4–20 mA or 0–10 V standard.

To determine the control structure for the experimental platform considering as a TITO system, the following definitions were done [14]:

- The $U_1(s)$ and $U_2(s)$ represent the voltage signal $V(s)$ and the current signal $I(s)$ applied on the actuators of the experimental platform, i.e., the frequency inverter and the control valve.

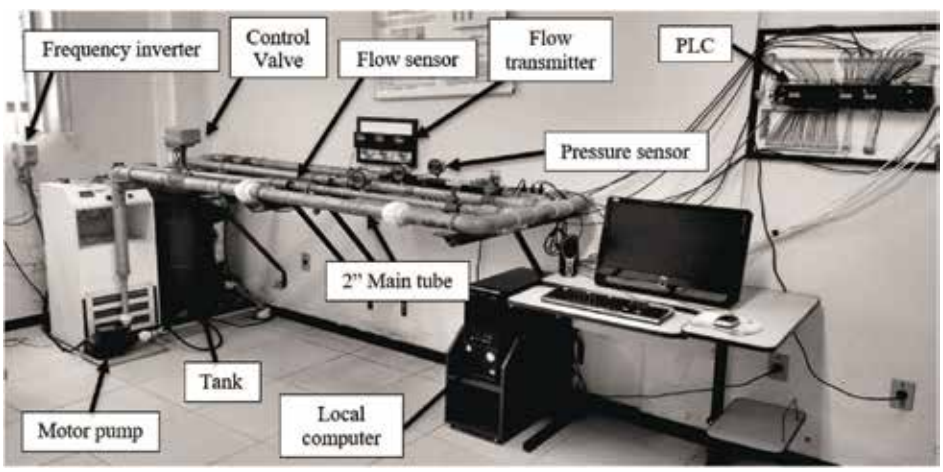

Figure 5. Photograph of experimental platform in study. *Source*: Own author (2018).

- The $Y_1(s)$ and $Y_2(s)$ represent the flow measure $Q(s)$ and the pressure measure $P(s)$ monitored by means of the flow and pressure sensors in the main tube.
- The $Y_{r_1}(s)$ and $Y_{r_2}(s)$ represent the reference flow $Q_r(s)$ and the reference pressure $P_r(s)$ which will be adopted for operating in the main tube.

In the implementation of the control structure proposed for the experimental platform, it is necessary that:

- The plant operates in the percentage range of the reference values, in order to minimize the unplanned interventions resulting from the fouling phenomena.
- The conditions of the multivariable control system do not exceed the operating limits of the plant, such as the measurements made by the flow sensors and pressure and the actuations performed by the frequency inverter and control valve within the full-scale range of these transducers.

The methodology adopted for the development of a decoupling control on the experimental platform is discussed in Section 4.

4. System modeling, interaction analysis, and control design

The plant matrix $\mathbf{G_p}(s)$ in the experimental platform is composed of four processes: $G_{p_{11}}(s)$ representing the flow-voltage process, $G_{p_{12}}(s)$ representing the flow-current process, $G_{p_{21}}(s)$ representing the pressure-voltage process, and $G_{p_{22}}(s)$ representing the pressure-current process. In this work, each transfer function $G_{p_{ij}}(s)$ is assumed as a first-order plus dead time (FOPDT) process, according to Eq. (10):

$$G_{p_{ij}}(s) = \frac{K_{ij}e^{-L_{ij}s}}{\tau_{ij}s + 1} \tag{10}$$

where K_{ij} is the gain of the process [dimensionless], L_{ij} is the dead time [s], and τ_{ij} is the time constant of FOPDT process [s].

For the identification of the models experimentally, the behavior of the output signals is observed by means of the application of known input signals in each process. In practice, consecutive tests are done on the system, and the input and output data are stored. Then, these data are processed in a specific software to adjust the experimental curves obtained to the known theoretical models. At last, the model obtained is valid for each process.

Thus, these tests were executed in the four processes of the system. All FOPDT process models were obtained individually from the experiments based on the critical point of the plant, which consists in the application of consecutive switches in the manipulated variable in a determined time interval, taking into account the dynamics of the system. At the end of the switches, the application of a pulse was executed. Subsequently, the parameters of each FOPDT process

model were estimated and validated by means of a software developed in C#, better described in Barros et al. [15], in which the frequency response method was used as the identification method and Theil coefficient as validation method.

The standard coefficient U, proposed by Theil [16], can be interpreted as the division of the root mean square error (RMSE) of the proposed prediction for the variable, by the RMSE value of the original variable, as expressed by Eq. (11):

$$U = \frac{\sqrt{\frac{1}{N}\sum_{t=1}^{N}\left(\widehat{y}(t) - y(t)\right)^2}}{\sqrt{\frac{1}{N}\sum_{t=1}^{N}\widehat{y}^2(t)} + \sqrt{\frac{1}{N}\sum_{t=1}^{N}y^2(t)}} \tag{11}$$

where $\widehat{y}(t)$ is the predicted (estimated) value, $y(t)$ is the observed (measured) value, and N is the number of measurements.

If U equals 1, it means that the proposed model is as good as the real system. If U is greater than 1, the predicted model should be discarded. Thus, the coefficient U should only be considered when it is greater than 0 and less than 1, indicating a greater accuracy of the obtained model. When U is closer to 0, the prediction should be improved [17].

To determine the best loop pairing in the control structure, the Relative Gain Array (RGA) and Relative Normalized Gain Array (RNGA) matrices were calculated, as proposed by Bristol [18] and He et al. [19], respectively. The RGA matrix only requires information on the steady-state system to measure the process interactions and thus to recommend on the most efficient parity. In this way, the elements of RGA matrix are dependent on the steady-state system gains, according to Eq. (12):

$$\mathbf{\Lambda} = \mathbf{K} \otimes \mathbf{K}^{-\mathbf{T}} \tag{12}$$

where $\mathbf{K}=\mathbf{G_p}(j0)$, with $K_{ij} = G_{p_{ij}}(j0)$ being the steady-state gain, and $\otimes$ denotes element-by-element multiplication.

For a TITO system, the corresponding RGA matrix can be calculated from Eq. (13):

$$\mathbf{\Lambda} = \begin{bmatrix} \lambda_{11} & \lambda_{12} \\ \lambda_{21} & \lambda_{22} \end{bmatrix} = \begin{bmatrix} \lambda_{11} & 1-\lambda_{11} \\ 1-\lambda_{11} & \lambda_{11} \end{bmatrix} \tag{13}$$

where $\lambda_{11} = \frac{1}{1-\kappa}$, with $\kappa = \frac{K_{21}K_{12}}{K_{11}K_{22}}$ being the interaction coefficient.

The correct interpretation of the elements of the RGA matrix allows quantifying the interaction measure involved in all the possible control configurations of a $N \times N$ system. Thus, it is recommended to choose the control configuration that has the least interaction as follows:

i. Choose the control configuration with the diagonal or off-diagonal elements λ_{ij} as close to 1.

ii. If possible, avoid to choose a control configuration where $\lambda_{ij} >> 1$.

iii. Settings with $\lambda_{ij} < 0$ are totally undesirable, because the negative values indicate the possibility of a closed-loop unstable.

In order to overcome the deficiency of the RGA method of not including the dynamic behavior, the RNGA matrix was used. In this matrix, steady-state behavior can be easily characterized by the matrix **K,** whereas dynamic behavior can be obtained by the response time of the process variable relative to the manipulated variable.

Thus, the RNGA matrix is defined in Eq. (14), and it depends of the normalized gain matrix $\mathbf{K_N}$, which considers both characteristics mentioned above. Similar to RGA matrix, the best loop pairing is chosen when the diagonal or off-diagonal elements ϕ_{ij} are close to 1:

$$\mathbf{\Phi} = \mathbf{K_N} \otimes \mathbf{K_N^{-T}} \tag{14}$$

where $\mathbf{K_N} = \mathbf{G_p}(j0) \odot \mathbf{T_{ar}}$, with $k_{Nij} = \frac{G_{p_{ij}}(j0)}{\tau_{arij}}$ being the normalized gain, where $G_{p_{ij}}(j0)$ is the steady-state gain and τ_{arij} is the mean residence time, which is an indicator of the speed of the response of y_i given the action of u_j, and $\odot$ being the element-by-element division.

Once loop pairing has been defined, the decoupling matrix $\mathbf{D}(s)$ was calculated using the static decoupling. This type of decoupling allows the resulting matrix $\mathbf{T}(s)$ to be diagonal at steady state, i.e., only $s = j0$. In the case of a TITO system, the static decoupled matrix can be given according to Eq. (15):

$$\mathbf{D}(j0) = \begin{bmatrix} 1 & -\dfrac{G_{p_{12}}(j0)}{G_{p_{11}}(j0)} \\ -\dfrac{G_{p_{21}}(j0)}{G_{p_{22}}(j0)} & 1 \end{bmatrix} = \begin{bmatrix} 1 & -\dfrac{K_{12}}{K_{11}} \\ -\dfrac{K_{21}}{K_{22}} & 1 \end{bmatrix} \tag{15}$$

For closing the control loop proposed, the elements of decentralized controller matrix $\mathbf{G_c}(s)$ were obtained by means of the PID theory, which combines proportional, integral, and derivative actions to control each process, as expressed by Eq. (16):

$$G_{c_i}(s) = K_{P_i}\left(1 + \frac{1}{T_{I_i}s} + T_{D_i}s\right) \tag{16}$$

where K_{P_i} is the proportional gain [dimensionless], T_{I_i} is integral time constant [s], and T_{D_i} is the derivative time constant [s].

To calculate the parameters for each decentralized controller $G_{c_i}(s)$, the PID tuning methods were applied on the control structure proposed. The tuning method proposed by Ziegler and Nichols [20] determines that the controller parameters are obtained from the time response of the process to be controlled. Thus, for a FOPDT process model, the PID controller parameters can be calculated with the Ziegler-Nichols (ZN) method according to **Table 2**.

Other PID tuning methods originally proposed by Garcia and Morari [21] consider the process model as an integral part of the controller. The central idea of the Internal Model Control (IMC)

method is that the controller can be obtained only if the control system incorporates, explicitly or implicitly, some representation of the process to be controlled.

For a FOPDT process model, this method considers that the dead time process can be approximated using the *first-order Padé approximation*. Besides, the general form of the PID controller tuned by the IMC method has a low pass filter with a filtering component τ_c, which is used precisely to decrease the sensitivity to modeling errors [22]. The calculation of PID controller parameters can be calculated according to **Table 3**.

At last, to evaluate the output control performance, the Integral Absolute Error (IAE) and Integral Squared Error (ISE) metrics were used as quantitative performance measures, according to Eqs. (17) and (18), respectively:

$$\text{IAE} = \int_0^T |e(t)|dt \tag{17}$$

$$\text{ISE} = \int_0^T e^2(t)dt \tag{18}$$

where T = t_s, which is the settling time of the system.

With all the necessary parameters obtained, the decoupling control was simulated in the MATLAB software and implemented using a Human Machine Interface (HMI) developed in the LabVIEW software. For the system test, 20 liters per minute (LPM) was used as flow set point and 40 mBar as pressure set point, according to the turbulent flow regime of the experimental platform proposed in Melo et al. [23].

The results obtained on the development of the decoupling control are shown in Section 5.

Controller	**Parameters**		
$G_{c_i}(s)$	K_{P_i}	T_{I_i}	T_{D_i}
PID	$\frac{1.2\tau_{ij}}{K_{ij}L_{ij}}$	$2L_{ij}$	$\frac{L_{ij}}{2}$

Source: Own author (2018).

Table 2. PID tuning by the ZN method.

Controller		**Parameters**	
$G_{c_i}(s)$	K_{P_i}	T_{I_i}	T_{D_i}
PID	$\frac{2\tau_{ij}+L_{ij}}{K_{ij}\left(\tau_c+L_{ij}\right)}$	$\tau_{ij}+\frac{L_{ij}}{2}$	$\frac{\tau_{ij}L_{ij}}{2\tau_{ij}+L_{ij}}$

Source: Own author (2018).

Table 3. PID tuning by the IMC method.

5. Results and discussion

The actual response curve of the flow-voltage process is shown in **Figure 6a**, while the comparative of the responses curve between the identified mathematical model and the experimental model of the process is shown in **Figure 6b**. Similar results were obtained for other processes of the plant matrix, thus validating the mathematical models identified. Besides, the input and output signals in this figure are represented as words on a decimal basis of the analog-to-digital converter (ADC) on the PLC, which can be converted in the measuring units by means of the equivalence relations in the HMI.

The obtained models were approximated by FOPDT process model with sufficient dead time to reliably model the system in question. Among the models obtained using the software developed in C#, the best models that were chosen according to the Theil coefficient criterion are shown in **Table 4**.

From these models, the best loop pairing present in the system was defined according to the RGA and RNGA matrices obtained, as expressed in Eqs. (19) and (20), respectively:

$$\mathbf{\Lambda} = \begin{bmatrix} -1.9116 & 2.9116 \\ 2.9116 & -1.9116 \end{bmatrix} \tag{19}$$

$$\mathbf{\Phi} = \begin{bmatrix} -4.1699 & 5.1699 \\ 5.1699 & -4.1699 \end{bmatrix} \tag{20}$$

Based on the elements of both matrices, it can be observed that the loop pairing suggested to control the TITO system in study is the off-diagonal pairing, i.e., $y_1 - u_2 / y_2 - u_1$. Therefore, the flow variable must be controlled by the current signal, applied to the control valve, while the pressure variable must be controlled by voltage applied to the frequency inverter.

After the choice of the best loop pairing for the control loops, the static decoupling matrix was calculated, as expressed in Eq. (21). The objective of the decoupling is to make the decentralized controllers operate on two independent processes in control loops: pressure-voltage and flow-current. Therefore, to ensure the correctness of operating the decoupling control, the processes associated to both control loops were reallocated for diagonal elements of the plant matrix:

$$\mathbf{D}(j0) = \begin{bmatrix} 1 & -0.7276 \\ -0.9023 & 1 \end{bmatrix} \tag{21}$$

Besides, the decentralized controllers were designed for the selected control loops. The controller parameters obtained by tuning methods described are shown in **Table 5**. For the calculation of the filtering component τ_c in the IMC method, this work proceeded according to Skogestad [24].

The set point tracking response of the flow and pressure control loops simulated by means of MATLAB software is shown in **Figure 7**, using the PID controllers tuned by the Ziegler-Nichols and IMC methods with static decoupling. In this case, the choice of τ_c leads to

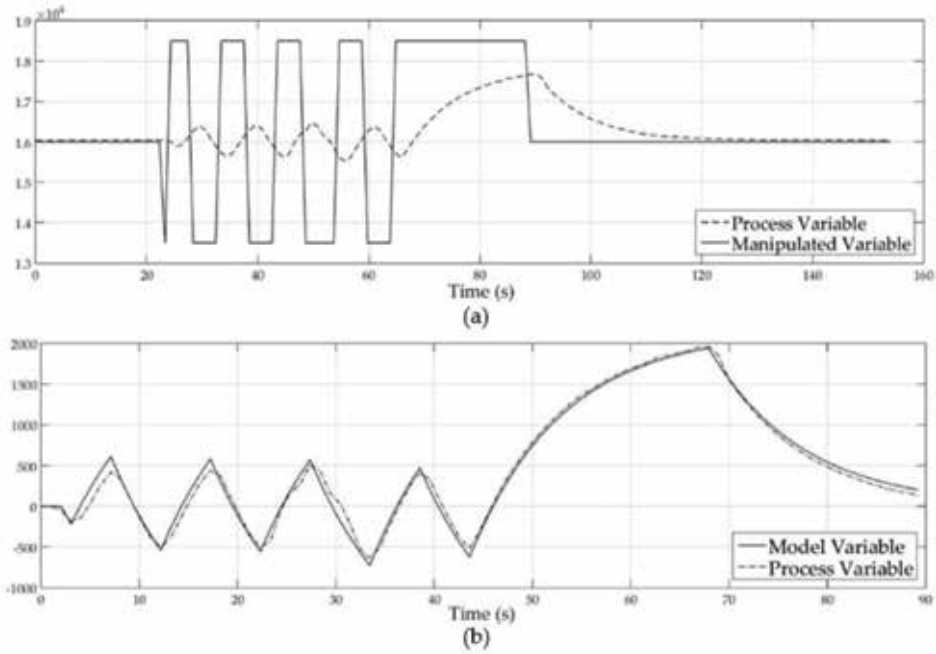

Figure 6. System modeling: (a) the response curve of the flow-voltage process and (b) the response curve of the identified model and the experimental model. *Source*: Own author (2018).

aggressive control action, principally to compensate the sluggish dynamic of the flow-current process.

In order to compare the output control performance of both PID tuning methods, the ISE and IAE metrics were used. The values obtained for these metrics are shown in **Table 6**. According to these performance metrics, it was verified that the strategy of control with the lowest values was the IMC controller for both control loops used.

The set point tracking response of the flow and pressure control loops on the experimental platform, supervised by the HMI developed in LabVIEW software, is shown in **Figure 8**, using the PID controllers tuned by the ZN and IMC methods with static decoupling.

Process	**Transfer function**	**U**
Flow-voltage	$G_{p_{11}}(s) = \frac{0.8622}{9.9680s+1} e^{-8.2500s}$	0.0448
Pressure-voltage	$G_{p_{21}}(s) = \frac{0.0469}{5.2040s+1} e^{-10.0100s}$	0.1119
Flow-current	$G_{p_{12}}(s) = \frac{1.1850}{18.7900s+1} e^{-6.0840s}$	0.0660
Pressure-current	$G_{p_{22}}(s) = \frac{0.0423}{10.8200s+1} e^{-6.0840s}$	0.0796

Source: Own author (2018).

Table 4. FOPDT process models obtained experimentally.

Tuning method	Process	Controller	$K_{P_{in}}$	$T_{I_{in}}$	$T_{D_{in}}$
ZN	Pressure-voltage	$G_{c_1}(s)$	0.6239	20.0200	5.0050
	Flow-current	$G_{c_2}(s)$	3.7061	12.1680	3.0420
IMC	Pressure-voltage	$G_{c_1}(s)$	14.4972	10.2090	2.5513
	Flow-current	$G_{c_2}(s)$	2.0188	21.8320	2.6181

Source: Own author (2018).

Table 5. PID controllers obtained with both tuning methods.

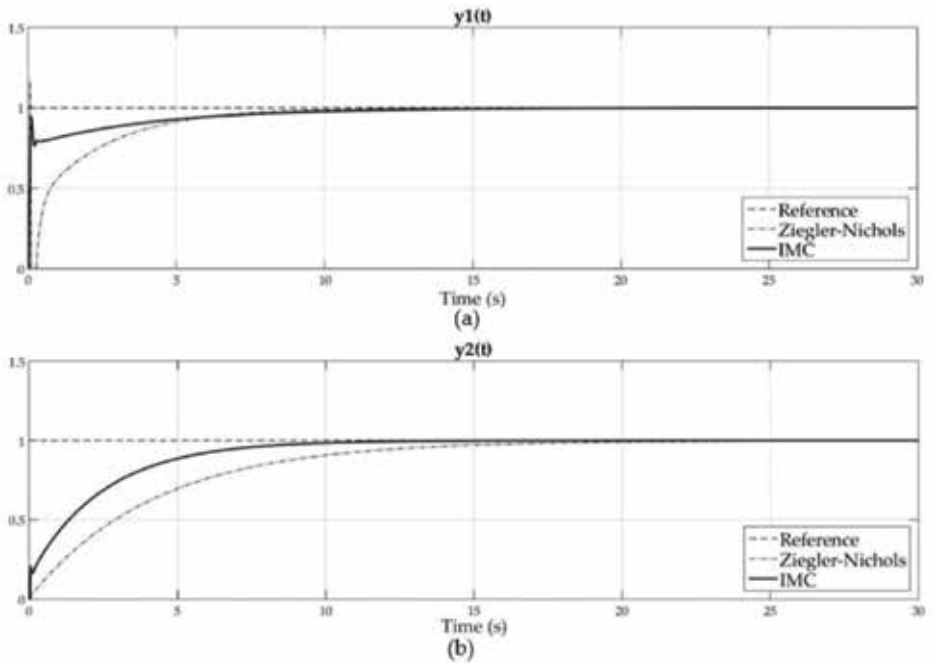

Figure 7. The simulation of set-point tracking response: (a) the flow and (b) pressure control loops with static decoupling – ZN and IMC methods. *Source*: Own author (2018).

Tuning method	Process	Controller	IAE	ISE
ZN	Pressure-voltage	$G_{c_1}(s)$	64.1477	46.7040
	Flow-current	$G_{c_2}(s)$	52.1777	42.4687
IMC	Pressure-voltage	$G_{c_1}(s)$	49.1532	34.0354
	Flow-current	$G_{c_2}(s)$	39.0924	28.9877

Source: Own author (2018).

Table 6. IAE and ISE performance metrics.

http://dx.doi.org/10.5772/intechopen.75708

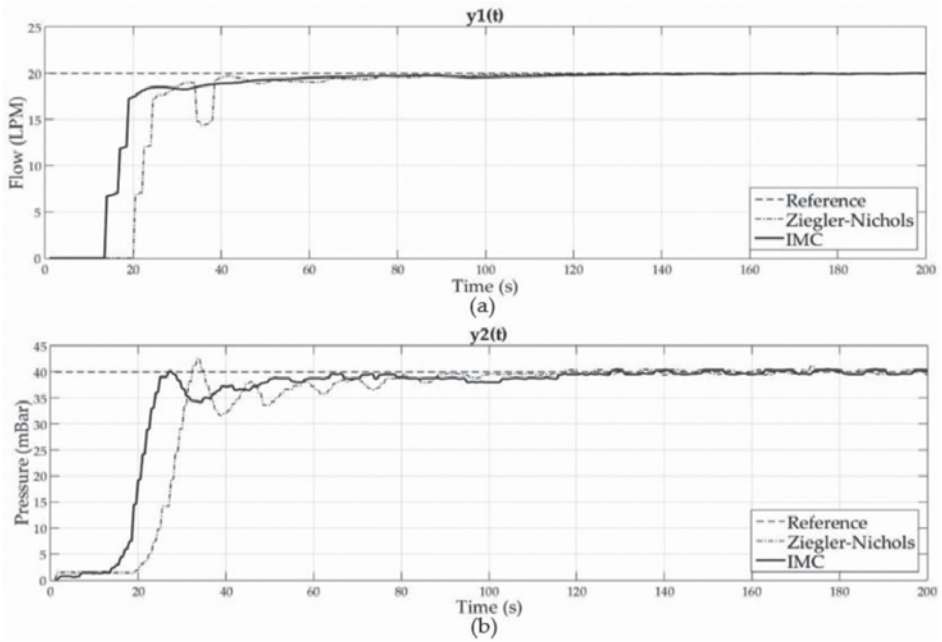

Figure 8. The implementation of set-point tracking response: (a) the flow and (b) pressure control loops on the experimental platform. *Source*: Own author (2018).

During the time interval around 30 s, it is observed that rapid pressure fluctuations in the system with ZN method resulted in flow reversals, i.e., a suction phenomenon was caused by the action opening of control valve, and this situation leads to an undesirable response in the closed-loop control. From the 140 s, both the process variables had already reached the steady state.

For the control system implemented to continue operating correctly, a good process instrumentation is fundamental. From this, the use of the soft sensor with the control system already designed with the objective of reducing the dependence of the physical sensors, as described in Section 6, is proposed.

6. Practical application of soft sensor

The concept of the use of the soft sensor aims at mathematical modeling of processes with focus on the prediction of the property, from available measurements of the other plant variables [25]. Mathematical models of processes designed to estimate relevant process variables to control can help to reduce the need for measuring devices, improve system reliability, and develop tight control policies. Thus, soft sensors offer a number of attractive properties to make the control process more reliable.

Irrespective of whether a maintenance intervention is programmed or accidental, the measuring hardware needs to be turned off and suitably substituted. The backup of measuring

instrumentation is a typical application of soft sensors. Thus, soft sensor is a mechanism used to replace the temporary or permanent unavailability of a physical sensor in a plant, which can happen due to the real sensor failure or removal for maintenance [26, 27].

For example, in the network scheme for a MIMO system as shown in **Figure 9**, the soft sensor running in parallel with the physical process is updated in real time with the same control signal data transmitted on the network to the actuators. When the physical sensor is not available for measurement, the switch at the sensor output changes from the position *P* to position *S* to get the output generated by the soft sensor [28].

The use of artificial intelligence techniques in the modeling of nonlinear dynamic systems has been diffused in the literature in recent years. This interest is motivated by the characteristics of these techniques that allow the development of models that are universal approximation of functions. In fact, depending on the technique, it is possible to approximate with arbitrary precision a continuous nonlinear function defined in a compact region (limited and closed) based on quantitative and qualitative information [29, 30].

Among the techniques of artificial intelligence used in the modeling of dynamic systems, artificial neural networks can be emphasized. The application of artificial neural networks in the prediction of variables can be auxiliary in the implementation of the soft sensor to process monitoring, in search of the processes with better performance and that are more reliable. Thus, the concept of soft sensor allied to ANNs is applied to start the output variables monitoring of the experimental platform.

On this platform, as mentioned in Section 3, there are two processes for monitoring and control which can be distinguished by the actuator element: valve position (current) or variation in the operation frequency of the motor pump (voltage). It is necessary to define a fixed operating point for one of the actuators. For example, in **Figure 10** the illustration of the inputs and outputs of the process can be observed, where, in the case 1, the position of the valve is fixed and the operation frequency of the motor pump is varied and, in the case 2, the motor pump working with fixed operating frequency is used and the position of the valve is varied, in both cases, to monitor and control the flow and pressure values in the tube.

Initially, to visualize a soft sensor working in the process, the monitoring of the flow values was done on the platform using a soft sensor designed by neural networks, with the fixed valve position, and varying the frequency (voltage) to pump the water inside the tube.

To test flow value monitoring, a frequency was applied to pump the water inside the tube, and the flow values measured and estimated (soft sensor) were observed. In a certain time, the flow

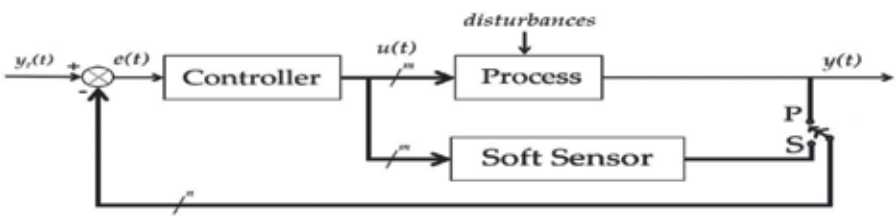

Figure 9. Feedback control loop with a soft sensor. *Source*: Own author (2018).

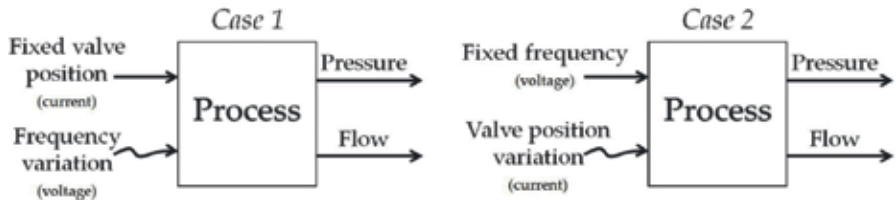

Figure 10. Operating point of the process for soft sensor design. *Source*: Own author (2018).

sensor was withdrawn, losing the measured signal by the real sensor. With the loss of the measured signal, to avoid stop the process, the neural network, based on the process input, estimates the flow value, so that the process can be monitored by continuing its operation, with the estimated values (soft sensor), while the real sensor signal is not recovered.

In **Figure 11**, the graph with the monitoring of the flow values as a function of time, for a better visualization of time duration of the transition from the estimated value response (soft sensor) to the measured real value, is observed. In the transition with the return of the real sensor signal, three samples were passed, lasting 3.39 seconds, which is the duration that the system worked without both signals, real and soft sensor. The purpose is a transition as short as possible, obtaining a process monitored for a longer time.

As presented, it was possible to estimate the flow values. In the case of the signal loss of the real sensor, it is possible to use the implemented soft sensor for monitoring of the process, avoiding unnecessary stopping. The conclusions obtained with this work and the perspectives for the improvement of the control system proposed are shown in Section 7.

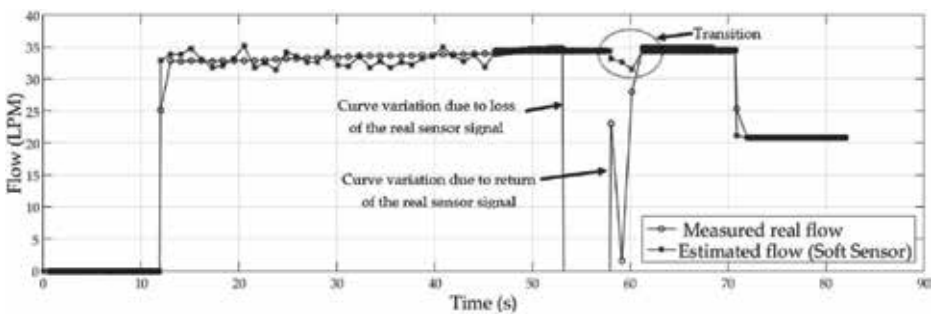

Figure 11. Flow variable monitoring in the MATLAB software. *Source*: Own author (2018).

7. Conclusion and future works

The present chapter consisted in the design and implementation of a decoupling control strategy for an experimental platform dedicated to study the fouling phenomena. This platform is considered as a TITO system, i.e., the voltage and current signals as the input system and the flow and pressure measurements as the output system.

Initially, a set of tests were done to identify FOPDT process models of the plant matrix, using the frequency response method for parameter estimation in each model and the Theil coefficients for the validation models. Then, the interaction between the inputs and outputs of the system was analyzed using RGA and RNGA matrices, which suggested the off-diagonal pairing as the best pairing loops, i.e., the flow-current and pressure-voltage processes for the closed-loop control.

Due to strong coupling loops, the static decoupling matrix was calculated, and finally the decentralized controller matrix was obtained using the ZN and IMC methods as PID tuning techniques. After the simulation and implementation of the decoupling control proposed, using MATLAB and LabVIEW software, respectively, the IAE and ISE performance metrics were calculated to analyze the output performance of the control loops.

Therefore, for the system under study, the best decoupling control strategy is associated with the IMC method. Even if the decoupling to be calculate for an exact mathematical model, the PID controllers obtained using this tuning method has the ability to ensure robust control against possible modeling errors.

For a better performance of the decoupling control, the soft sensor design was applied to start the output variable monitoring of the experimental platform. The general idea was to design a fully monitored process via computer program, so that if the measurement of the output variable fails for any reason, it is possible to use the soft sensor to infer the flow rate values (in this case, variable of interest in monitoring).

In the future works, it is possible to develop other soft sensors that will be integrated into the feedback control loop proposed to avoid interruptions performed to solve problems that could be solved without stopping the process. This makes the process more reliable, with better performance and with less difficulty to detect and solve possible failures.

Acknowledgements

The authors would like to thank CNPq and PPgEE-COPELE for financial support of project.

Author details

Thamiles Rodrigues de Melo[1]*, Nathália Arthur Brunet Monteiro[1], Danilo Pequeno[1], Jaidilson Jó da Silva[2] and José Sérgio da Rocha Neto[2]

*Address all correspondence to: thamiles.melo@ee.ufcg.edu.br

1 Post-Graduate Program in Electrical Engineering, PPgEE, COPELE, Federal University of Campina Grande (UFCG), Campina Grande, PB, Brazil

2 Department of Electrical Engineering (DEE), Federal University of Campina Grande (UFCG), Campina Grande, PB, Brazil

References

[1] Ogata K. Modern Control Engineering. 5th ed. São Paulo: Prentice Hall; 2009. 894 p. DOI: ISBN-10: 0136156738. ISBN-13: 978-0136156734

[2] Liu T, Zhang W, Danying G. Analytical multiloop PI/PID controller design for two-by-two processes with time delays. Industrial & Engineering Chemistry. 2005;**44**(6):1832-1841. DOI: 10.1021/ie0493715

[3] García MA, Salgado ME, Silva EI. Achievable performance bounds for tall MIMO systems. IET Control Theory & Applications. 2011;**5**(5):736-743. DOI: 10.1049/iet-cta.2010.0328

[4] Kookos IK, Lygeros AI. An algorithmic method for control structure selection based on the RGA and RIA interaction measures. Chemical Engineering Research and Design. 1998;**76**(4):458-464. DOI: 10.1205/026387698525072

[5] Garrido J, Vázquez F, Morilla F. Generalized inverted decoupling for TITO processes. In: Proceedings of the 18th International Federation of Automatic Control (IFAC) World Congress; August 28–September 2; Milan. Italy: 2011. pp. 7535-7540

[6] Chen P, Zhang W. Improvement on an inverted decoupling technique for a class of stable linear multivariable processes. ISA Transactions. 2007;**46**(2):199-210. DOI: 10.1016/j.isatra.2006.09.002

[7] Franklin GF, Powell JD, Emami-Naeini A. Feedback Control of Dynamic Systems. 7th ed. London: Pearson Education Limited; 2014. 860 p. DOI: ISBN-10: 0133496597. ISBN-13: 978-0133496598

[8] Corriou JP. Process Control: Theory and Applications. 2nd ed. Switzerland (Cham): Springer International Publishing AG; 2018. 860 p. ISBN-13: 978-3319611433

[9] Kadlec P, Gabrys B, Strandt S. Data-driven soft sensors in the process industry. Computers & Chemical Engineering. 2009;**33**(4):995-814. DOI: 10.1016/j.compchemeng.2008.12.012

[10] Skogestad S, Postlethwaite I. Multivariable Feedback Control: Analysis and Design. 2nd ed. Chichester: John Wiley & Sons, Inc.; 2005. 590 p. DOI: ISBN-10: 0470011688. ISBN-13: 978-0470011683

[11] Albertos P, Sala A. Multivariable Control Systems: An Engineering Approach. 4th ed. London: Springer; 2004. 340 p. DOI: ISBN-10: 1852337389. ISBN-13: 978-1852337384

[12] Gagnon E, Pomerleau A, Desbiens A. Simplified, ideal or inverted decoupling? ISA Transactions. 1998;**37**(4):265-276. DOI: 10.1016/S0019-0578(98)00023-8

[13] Wang QG, Cai WJ, Hang CC. PID control for multivariable processes. Berlin (Heidelberg): Springer Verlag; 2008. 266 p. ISBN-13: 978-3540784821

[14] Melo TR, Silva JJ, Rocha Neto JS. Development of a multivariable control system on an experimental platform dedicated to the study of fouling phenomena. In: Proceedings of the IEEE International Instrumentation and Measurement Technology Conference (I2MTC); 11–14 May; Pisa. Italy: IEEE; 2015. pp. 1314-1319

[15] Barros PR, Campos MCMM, Júnior GA, Carvalho RC d'A, Santos JBM. Application of computer software for system identification and PID control loop tuning to a petrochemical plant. Computer Aided Chemical Engineering. 2009;**27**:693-698. DOI: 10.1016/S1570-7946(09)70336-0

[16] Theil H. Economic Forecasts and Policy. Amsterdam, The Netherlands: North-Holland; 1961. 567 p

[17] Dixon KR. Modeling and Simulation in Ecotoxicology with Applications in MATLAB and Simulink. Lubbock: CRC Press; 2011. 270 p. ISBN-10: 143985517X. ISBN-13: 978-1439855171

[18] Bristol E. On a new measure of interaction for multivariable process control. IEEE Transactions on Automatic Control. 1965;**11**(1):133-134. DOI: 10.1109/TAC.1966.1098266

[19] He M-J, Cai W-J, Ni W, Xie L-H. RNGA based control system configuration for multivariable processes. Journal of Process Control. 2009;**19**(6):1036-1042. DOI: 10.1016/j.jprocont.2009.01.004

[20] Ziegler JG, Nichols NB. Optimum settings for automatic controllers. Transactions of the American Society of Mechanical Engineers (ASME). 1942;**64**(11):759-765

[21] Garcia CE, Morari M. Internal model control. 1. A unifying review and some new results. Industrial & Engineering Chemistry Process Design and Development. 1982;**21**(2):308-323. DOI: 10.1021/i200017a016

[22] Rivera DE, Morari M, Skogestad S. Internal model control. 4. PID controller design. Industrial & Engineering Chemistry Process Design and Development. 1986;**25**(1):252-265. DOI: 10.1021/i200032a041

[23] Melo TR, Silva JJ, Rocha Neto JS. Implementation of a decentralized PID control system on an experimental platform using LabVIEW. IEEE Latin America Transactions. 2017; **15**(2):213-218. DOI: 10.1109/TLA.2017.7854614

[24] Skogestad S. Simple analytic rules for model reduction and PID controller tuning. Journal of Process Control. 2003;**13**(4):291-309. DOI: 10.1016/S0959-1524(02)00062-8

[25] Joseph JB, Brosilow CB. Inferential control of processes: Part I, II and III. American Institute of Chemical Engineering. 1978;**24**(3):485-509. DOI: 10.1002/aic.690240313

[26] Fortuna L, Graziani S, Xibilia MG. Soft Sensor for Monitoring and Control of Industrial Processes. London: Springer; 2007. 271 p. ISBN-10:1846284791. ISBN-13: 978-1846284793

[27] Mansano RK, Godoy EP, Porto AJV. The benefits of soft sensor and multi-rate control for the implementation of wireless networked control systems. Sensors. 2014;**14**(12):24441-24461. DOI: 10.3390/s141224441

[28] Bhuyan M. Intelligent Instrumentation: Principles and Applications. USA: CRC Press; 2011. 524 p. DOI: ISBN-10: 1420089536. ISBN-13: 978-1420089530

[29] Cybenko G. Approximation by superpositions of a sigmoid function. Mathematics of Control Signals and Systems. 1989;**2**(4):303-314. DOI: 10.1007/BF02551274

[30] Wang H, Oh Y, Yoon ES. Strategies for modeling and control of nonlinear chemical processes using neural networks. Computers & Chemical Engineering. 1998;**22**(1):832-862. DOI: 10.1016/S0098-1354(98)00157-4

Chapter 9

PID Controller Design Methods for Multi-Mass Resonance System

Hidehiro Ikeda

Additional information is available at the end of the chapter

http://dx.doi.org/10.5772/intechopen.74298

Abstract

Motor drive systems are indispensable for applications in the industrial field. High-speed and high-accuracy control is required for motor drive systems. However, solutions to meet these requirements can cause mechanical resonance vibrations to occur in the system as a result of miniaturization and system weight reduction. It is therefore necessary to model these systems as multi-mass resonance systems with multiple masses and finite rigid shafts, gears, and loads. In addition, vibration suppression control should be applied to these systems. This chapter provides two off-line tuning methods for a digital proportional-integral-derivative (PID)-type controller for a two-mass resonance system to suppress its mechanical resonance vibrations. These methods include a coefficient diagram method and a fictitious reference iterative tuning method. The former method uses a nominal mathematical model of the object while the latter method uses only the initial experimental data without use of the mathematical model. In this chapter, the two methods are compared. A controller is proposed that consists of a modified integral-proportional derivative (I-PD) speed controller and a proportional-integral (PI) current controller, and requires no information about the load side state variables. Finally, the effectiveness of the proposed method is confirmed through computer simulations and experimental results.

Keywords: two-mass resonance system, vibration suppression control, modified I-PD controller, coefficient diagram method, fictitious reference iterative tuning

1. Introduction

Motor drive systems are used in a wide range of applications, including industrial robots, home electrical appliances, automobiles, steel rolling mills, computers, and space work surfaces. In

general, motor drive systems consist of electric motors, gears, belts, flexible shafts, and mechanical load equipment. Recently, the overall stiffness of these systems has been decreasing because of demands for high-speed and high-accuracy system responses, miniaturization, system weight reduction, and low system costs. Additionally, the system constructions have become more complex and the central processing unit (CPU) processing speeds that are required to perform the system calculations have increased exponentially. Consequently, torsional resonance vibrations occur between the motor and the load side. It is therefore necessary to model the system as a multi-mass resonance system, which is composed of several masses with finite rigid shafts, gears, and loads. In addition, a vibration suppression control method should be applied to the system.

The first-order approximation model of the multi-mass resonance system has the form of a two-mass resonance model. Several control methods are effective for control of a two-mass resonance system [1–5]. PID-type controllers are the most commonly used controllers for industrial applications because of their simplicity and their practicality for use with multi-mass systems. Various PID controller design methods have been proposed; examples of these methods include the limit sensitivity method, the Ziegler and Nichols tuning method, and methods that use the system polynomial. These controller design methods, which are called model-based design methods, may be able to produce the required results in cases where both the system equation and the real system's parameters are unknown.

In the industrial fields in which many typical motor drive systems are used, experienced technicians often adjust the control system on site to suit the needs of the manufacturing equipment. However, engineer shortages in these fields are becoming a serious problem. It is therefore essential to develop a simple controller design method for industrial applications.

Under these circumstances, and to save both the time required and the cost of tuning the controllers for the motor drive systems, some direct controller tuning methods have been proposed based on the transient response data from closed-loop systems, without modeling of the plant. The fictitious reference iterative tuning (FRIT) method is one of the most promising candidate methods for practical direct parameter tuning [6, 7]. Using the FRIT method, the controller gains can be designed using only single-shot experimental input-output data without knowledge of the model parameters of the object to be controlled.

This chapter introduces two types of approaches to PID-type controller design for suppression of the two-mass resonance system. The first method is based on the assumption that the mathematical model of the object to be controlled is known. This design method is called the coefficient diagram method (CDM) [8–10]. The CDM is an algebraic approach designed to produce the characteristic polynomial directly in the parameter space. The design of the coefficient diagram of the control system is performed using a differential evolution (DE) procedure to obtain the optimal controller gains in a short time [11–13]. The second design method is a FRIT method, which is a PID controller design approach based on one-shot experimental data only and does not use the mathematical model of the object to be controlled [14–16]. The effectiveness of the two proposed design methods is confirmed using a combination of computer simulations and experiments.

http://dx.doi.org/10.5772/intechopen.74298

2. Two-mass speed control system applying PID-type control

2.1. Description of two-mass resonance model

The model consists of two rigid masses and a torsional shaft. The multiple masses on the load side of the actual system are approximated as one inertial element. Similarly, several shafts and gears are approximated as a single torsional shaft. The typical two-mass model is depicted schematically in **Figure 1** below [14–17].

Here, J and ω denote the moment of inertia and the angular speed, respectively, and the suffixes M and L indicate the motor side and the load side, respectively. T_{in} is the input torque, T_{dis} is the torsional torque, T_L is the load torque, and K_s is the shaft stiffness. The continuous state equations of this two-mass resonance model are shown as Eqs. (1) to (3). Additionally, a current loop is considered in this research for high-speed torque control. Eq. (4) is indicative of the voltage equation when using a permanent magnet dc servo motor as the driving motor. In the equations, K_t is the torque constant of the dc motor, L_a is the armature current, R_a is the total resistance, u_c is the control input, K_e is the back-electromotive force (back-EMF) constant, and the viscous friction and nonlinear friction sources such as the Coulomb torque are neglected. Therefore, the torque input is calculated using $T_{in} = K_t i_a$.

$$J_M \frac{d\omega_M}{dt} = K_t i_a - T_{dis} \tag{1}$$

$$J_L \frac{d\omega_L}{dt} = T_{dis} - T_L \tag{2}$$

$$\frac{\mathrm{dT_{dis}}}{\mathrm{dt}} = \mathrm{K_s}(\omega_\mathrm{M} - \omega_\mathrm{L}) \tag{3}$$

$$L_a \frac{di_a}{dt} + R_a i_a = E u_c - K_e \omega_M \tag{4}$$

The research in this case deals with a normalized model to provide generality for the design of the proposed control system. Eqs. (5)–(8) show the normalized state equations. The state equation parameters are normalized as shown in Eq. (9), where the suffix *pu* indicates a normalized parameter, K_0 [V/pu] is the converter gain, K_a [pu/A] is the current feedback coefficient, K_ω [pu/(rad/s)] is the angular speed feedback gain, and τ_e [s] is an electrical time constant.

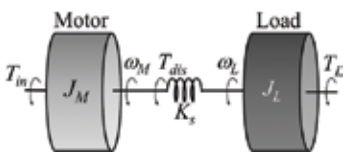

Figure 1. Two-mass resonance model.

$$J_{Mpu}\frac{d\omega_M}{dt} = i_a - T_{dis} \tag{5}$$

$$J_{Lpu}\frac{d\omega_L}{dt} = T_{dis} - T_L \tag{6}$$

$$\frac{dT_{dis}}{dt} = K_{spu}(\omega_M - \omega_L) \tag{7}$$

$$\tau_e\frac{di_a}{dt} + i_a = u_c - K_{epu}\omega_M \tag{8}$$

$$J_{Mpu} = \frac{K_a}{K_t K_\omega}J_M,\quad J_{Lpu} = \frac{K_a}{K_t K_\omega}J_L,\quad K_{spu} = \frac{K_a}{K_t K_\omega}K_s,\quad K_{epu} = \frac{1}{K_0 K_\omega}K_e \tag{9}$$

Therefore, the unit for all state variables is [pu]. **Figure 2** shows a block diagram of the normalized two-mass resonance model.

Eq. (10) gives the resonance angular frequency, the anti-resonance angular frequency, and the inertia ratio, respectively.

$$\omega_r = \sqrt{\frac{K_{spu}}{J_{Mpu}} + \frac{K_{spu}}{J_{Lpu}}},\quad \omega_a = \sqrt{\frac{K_{spu}}{J_{Lpu}}},\quad R = \frac{J_{Lpu}}{J_{Mpu}} \tag{10}$$

The next equation gives the simplified transfer function for the two-mass mechanical element, in which the input and the output are i_a and ω_M, respectively.

$$\frac{\Omega_M(s)}{I_a(s)} = \frac{s^2 + \omega_a^2}{J_{Mpu}s\left(s^2 + \omega_r^2\right)} \tag{11}$$

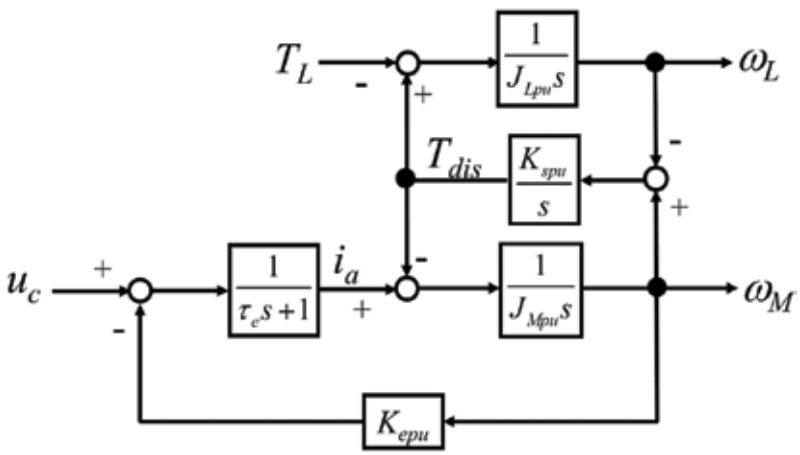

Figure 2. Block diagram of normalized two-mass resonance model.

Symbol	Value	Symbol	Value
J_M	2.744×10^{-4} (kgm^2)	J_L	2.940×10^{-4} (kgm^2)
K_s	18.5 (Nm/rad)	R_a	2.884 (Ω)
L_a	6.676 (mH)	E	25.0 (V)
K_t	0.2778 (Nm/A)	K_e	0.2778 (V/(rad sec))

Table 1. Nominal parameters of the two-mass resonance model.

The nominal parameters for the two-mass resonance model in this chapter are given in **Table 1** below. In this chapter, the proposed CDM method is evaluated through computer simulations, while the proposed FRIT method is evaluated experimentally using the experimental setup shown below.

Figure 3 shows a photograph of the experimental system that was constructed in this research. The two-mass resonance system is simulated using the dc servo motor and a dc generator with a finite rigid coupling. The controller is realized using a digital signal processor that calculates the pulse-width modulation (PWM) signal to send to a four-quadrant dc chopper [17].

The digital signal processor (DSP) board (PE-PRO/F28335 Starter Kit, Myway Plus Corp.), consists of the DSP (TMS320F28335PGFA), a digital input/output (I/O), ABZ counters for the encoder signals, analogue-to-digital (A/D) converters and digital-to-analogue (D/A) converters [18]. The motor and load angles and the angular speeds are detected using 5000 pulses-per-revolution encoders. The dc servo motor current is measured using a current sensor and the A/D converter.

The control period (T_s) and the detection period of the encoder are both 1 ms and the current detection period is 10 μs. While we considered the application of the system to specific apparatus, we then constructed a digital control system that contains a discrete controller. In addition, we used MATLAB/Simulink software to perform the proposed off-line tuning process based on simulations and constructed the PID-type control system as a continuous system [19]. A disturbance is added to the dc generator as a torque using the electric load device on constant current mode. **Figure 4** shows the apparatus for the two-mass resonance model that was used in the experimental setup. **Figure 5** shows the experimental system configuration [17].

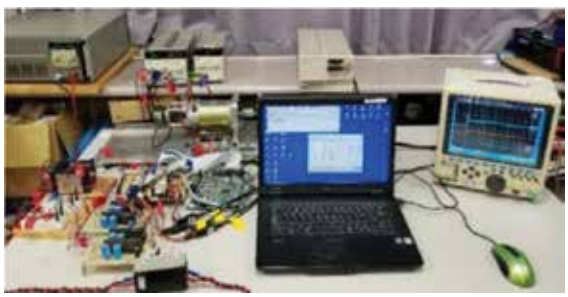

Figure 3. Overview of the experimental system.

Figure 4. Photograph of the experimental two-mass resonance model.

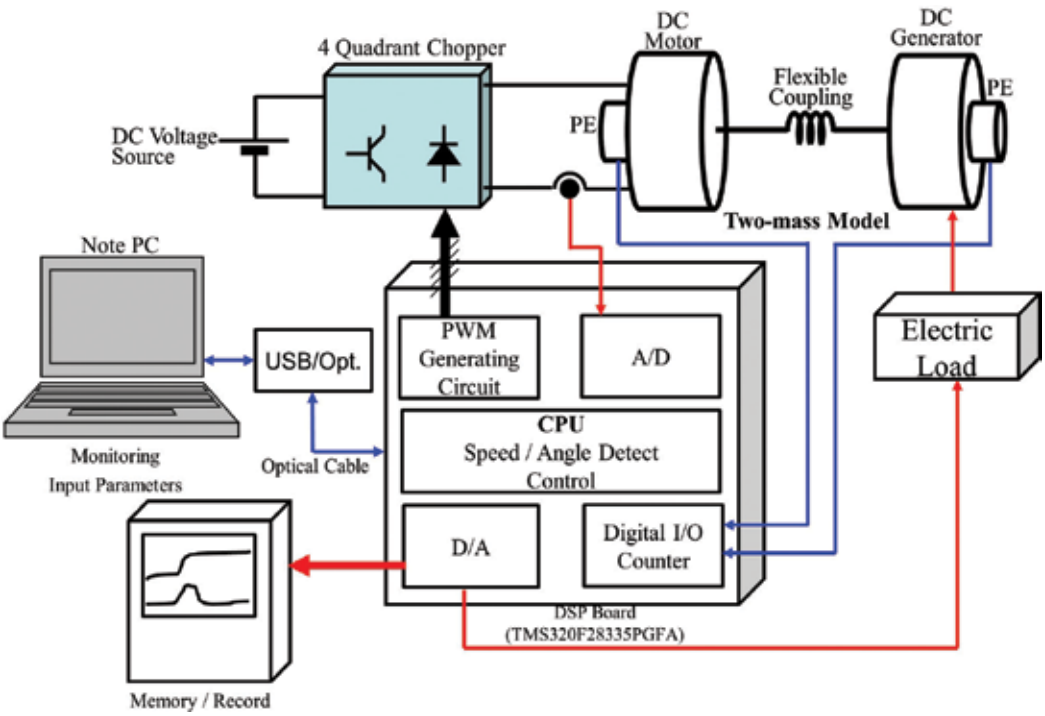

Figure 5. Configuration of the experimental system (for the two-mass resonance model).

2.2. Modified-IPD speed controller and PI current controller

In this chapter, classical PID speed and current controllers are used to suppress the resonance vibrations for the two-mass resonance model. In general, the PI controller, which consists of a proportional controller and an integral controller that are placed in parallel to determine the speed error, is used as the angular speed controller. However, because the resonance system has a complex structure, it is difficult to suppress the vibrations using the classic PI controller alone. Therefore, the I-PD controller is used in this chapter and a first-order lag element is also used to increase the degrees of freedom for the controller design. Additionally, a simple PI controller is

used to realize the high-speed torque response for the current minor loop. The continuous control system proposed here is shown in **Figure 6**. In the figure, ω_{ref} is the reference angular speed, K_p, K_i, K_d, and T_d represent the m-IPD speed controller gains, and K_{ap} and K_{ai} are the PI current controller gains. This chapter proposes two design methods for these six controller gains (i.e., K_p, K_i, K_d, T_d, K_{ap}, and K_{ai}). Then, during the simulations and experiments, a digital control system is used, as shown in **Figure 7**. In this case, the D-control element of the speed controller performs a z-transform in combination with the first lag element of the speed controller to construct a difference equation and avoid the need for a complete differentiation procedure.

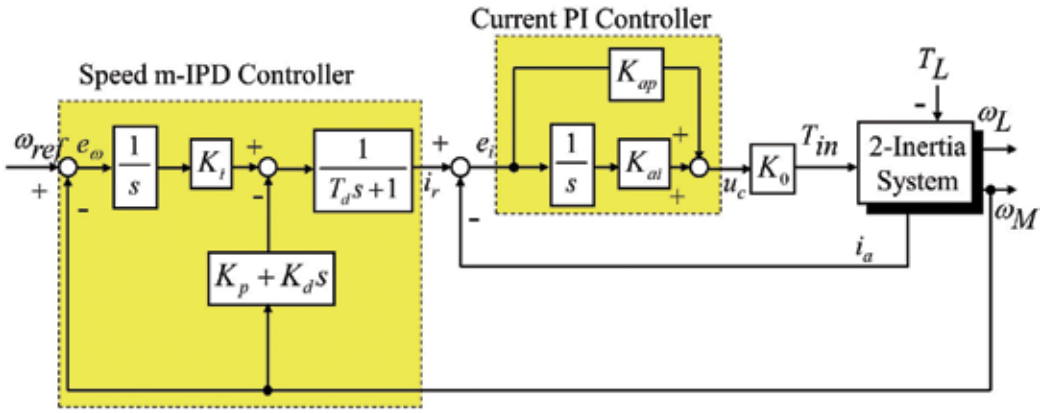

Figure 6. Proposed control system (continuous controller model).

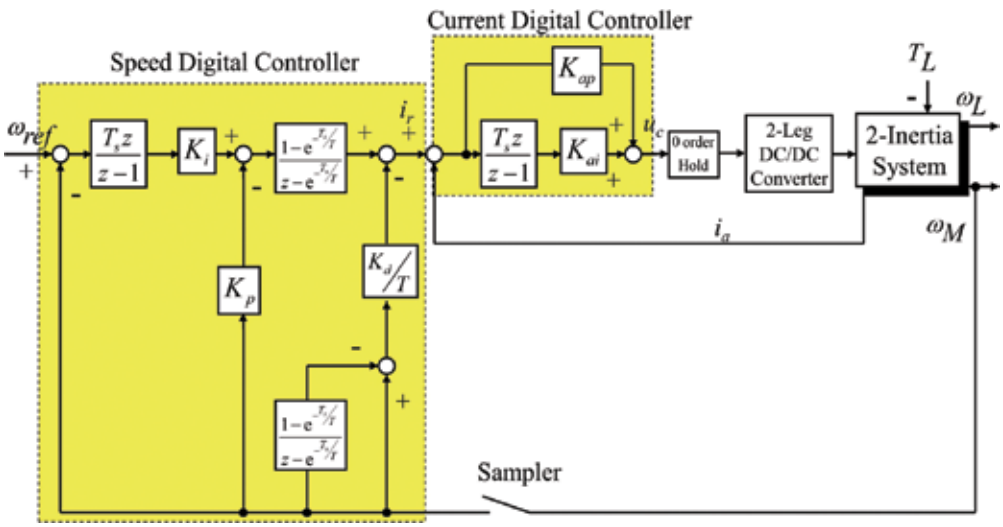

Figure 7. Proposed control system (discrete controller model).

3. Controller design using coefficient diagram method

3.1. Coefficient diagram method

First, this section explains the coefficient diagram method (CDM) for design of the proposed controller, which is required to suppress the resonance vibrations for the two-mass resonance model. The CDM is an algebraic approach that is used to design the characteristic polynomial directly in the parameter space. In the CDM, a coefficient diagram (CD) is used to perform the controller design. The CD provides the ability to analyze the time response, stability and robustness qualities of the controller using a diagram. In the CD, the vertical axis shows the coefficient of the characteristic polynomial (a_i), the stability indices (γ_i), and the equivalent time constant (τ) logarithmically, while the horizontal axis shows the order i values that correspond to the coefficient. Here, the characteristic polynomial is as shown in Eq. (12).

$$P(s) = a_n s^n + a_{n-1} s^{n-1} + \cdots + a_1 s + a_0 = \sum_{i=0}^{n} a_i s^i \tag{12}$$

In the CDM, the stability indices (γ_i), which are defined in Eq. (13) below, are indicators of the stability of the control system.

$$\gamma_i = \frac{a_i^2}{a_{i+1} a_{i-1}}, \qquad i = 1\tilde{n} - 1 \tag{13}$$

The equivalent time constant τ, which represents the transient response characteristic, is expressed using the following equation:

$$\tau = \frac{a_1}{a_0} \tag{14}$$

The coefficient a_i can then be calculated using τ and the stability indices γ_i as shown in Eq. (15).

$$a_{i+1} = \frac{a_0 \tau^i}{\gamma_{i-1} \gamma_{i-2}^2 \cdots \gamma_2^{i-2} \gamma_1^{i-1}} \tag{15}$$

In the CDM, use of the standard values of the stability indices is recommended, and these values are listed as follows:

$$\gamma_{n-1} = \cdots = \gamma_3 = \gamma_2 = 2.0, \qquad \gamma_1 = 2.5 \tag{16}$$

This form is called "the standard form of the stability indices."

3.2. Design method for the controller gains using the CDM

The CDM is a very simple and effective method for controller design. However, in higher order systems, it is difficult to complete the design by trial and error alone. In this work, the

design of the CD for the control system is performed using the differential evolution (DE) method. The DE method is an optimization search method [12, 13].

In the proposed design method, the reference value of the equivalent time constant τ_{ref} is first specified. Then, the coefficients of the characteristic polynomial are calculated using the six controller gains with random initial settings. Each of the coefficients is determined using the following equations:

$$a_7 = J_{Mpu} T \tau_e \tag{17}$$

$$a_6 = J_{Mpu} \tau_e + J_{Mpu} T + J_{Mpu} K_{ap} T \tag{18}$$

$$a_5 = J_{Mpu} + J_{Mpu} K_{ap} + K_{ap} K_d + K_{epu} T + J_{Mpu} K_{ai} T + J_{Mpu} T \tau_e \omega_r^2 \tag{19}$$

$$a_4 = K_{epu} + J_{Mpu} K_{ai} + K_{ai} K_d + K_{ap} K_p + J_{Mpu} T \omega_r^2 + J_{Mpu} \tau_e \omega_r^2 + J_{Mpu} K_{ap} T \omega_r^2 \tag{20}$$

$$a_3 = J_{Mpu} \omega_r^2 + K_{ap} K_i + K_{ai} K_p + J_{Mpu} K_{ap} \omega_r^2 + K_{ap} K_d \omega_a^2 + K_{epu} T \omega_a^2 + J_{Mpu} K_{ai} T \omega_r^2 \tag{21}$$

$$a_2 = K_{epu} \omega_a^2 + K_{ai} K_i + J_{Mpu} K_{ai} \omega_r^2 + K_{ai} K_d \omega_a^2 + K_{ap} K_p \omega_a^2 \tag{22}$$

$$a_1 = K_{ap} K_i \omega_a^2 + K_{ai} K_p \omega_a^2 \tag{23}$$

$$a_0 = K_{ai} K_i \omega_a^2 \tag{24}$$

The stability indices are then computed using these calculated coefficients and the evaluation function F in Eq. (25) is calculated using the terms from Eqs. (26)–(30). In this case, the evaluation function F consists of an evaluation to match with the set reference value of the equivalent time constant, an evaluation to reduce the change in the next stability index, and an evaluation to match the standard forms of the stability indices $\gamma_{s,i}$. The weights w_1 to w_5 of the evaluation functions are set to have values of (w_1, w_2, w_3, w_4, w_5) = (100, 2, 10, 1, 4), respectively. These steps are subsequently repeated to obtain the optimal controller gains by the DE method.

$$F = \frac{1}{w_1 f_1 + w_1 f_1 + w_1 f_1 + w_1 f_1 + w_1 f_1} \tag{25}$$

$$f_1 = \sqrt{(\tau_{ref} - \tau)^2} \tag{26}$$

$$f_2 = \sum_{i=1}^{2} \sqrt{\left(\gamma_{s,i} - \gamma_i\right)^2} \tag{27}$$

$$f_3 = \sqrt{\left(\gamma_{s,3} - \gamma_3\right)^2} \tag{28}$$

$$f_4 = \sum_{i=3}^{5} \sqrt{(\gamma_i - \gamma_{i+1})^2} \tag{29}$$

$$f_5 = \sum_{i=4}^{6} \sqrt{\left(\gamma_{s,i} - \gamma_i\right)^2} \tag{30}$$

3.3. Simulation results

Figure 8 shows an example of the simulation results in the form of the angular speed step responses for the control input. The resonance vibrations can be seen in this figure.

Figure 9 shows the frequency response characteristics of the two-mass resonance model from the control input u_c to the motor angular speed ω_M. The peak point of the mechanical resonance can be observed in this figure. It is therefore essential to construct the controller design method such that it reduces this resonance peak gain.

Table 2 shows the controller gains that were designed using the proposed method, where the reference time constant τ_{ref} is set to 0.05. **Figure 10** shows the designed CD. In the figure, each coefficient is multiplied by 100^n, where n is the order of the characteristic polynomial. The figure shows that the form of the diagram is very smooth and that the convex shape is appropriately upward. The designed stability indices are shown in **Figure 11**. The results in this figure confirm that the stability indices nearly fit the standard form of these indices, and the fluctuations in the numerical values of adjacent indices are also small.

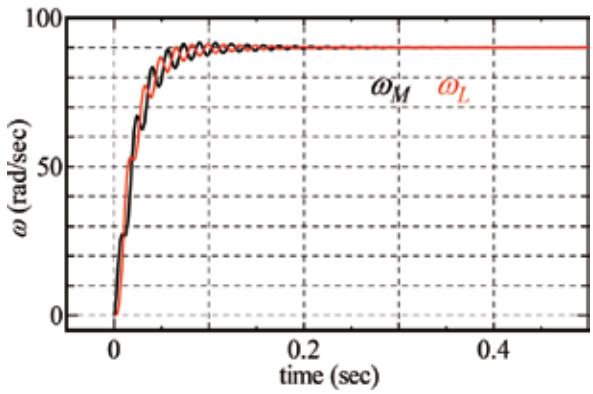

Figure 8. Angular speeds of the step responses of the two-mass model.

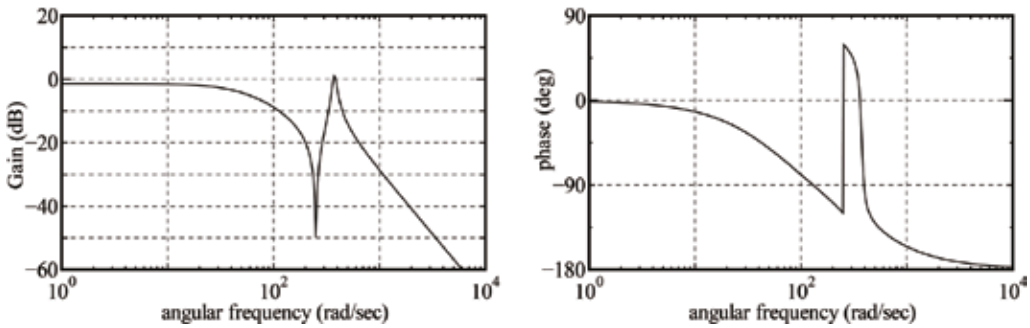

Figure 9. Frequency responses of the two-mass resonance model from u_c to ω_M.

Gain name	Value	Gain name	Value	Gain name	Value
K_p	2.792×10^2	K_i	9.007×10^3	K_d	3.522
T	0.4368	K_{ap}	1.834	K_{ai}	96.53

Table 2. Controller gain results when designed using the proposed CDM method.

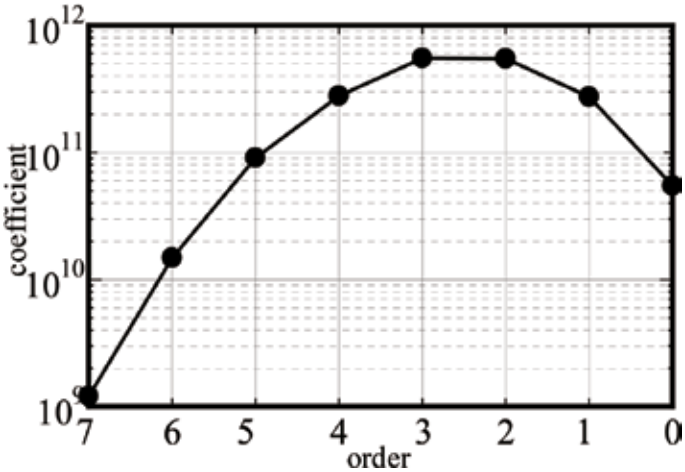

Figure 10. Designed coefficient diagram.

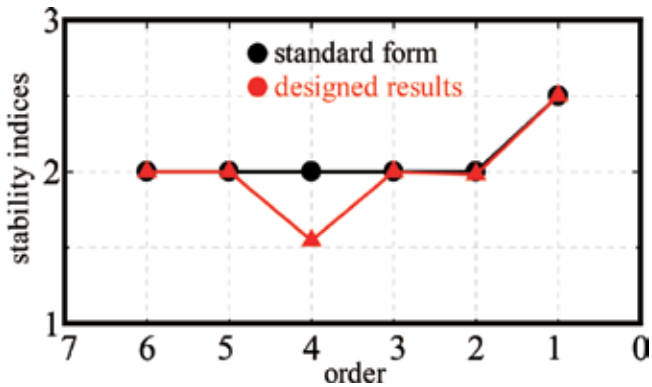

Figure 11. Designed and standard form stability indices.

Figure 12 shows the simulation results, where the speed reference command input ω_{ref} is changed from 0 to 30 rad/s at t = 0 s, and the disturbance torque input is changed from 0 to 20% of the rated torque at t = 0.25 s. The figure indicates that the wave provides a good reference-following performance and illustrates the validity of the vibration suppression characteristics and the disturbance response simultaneously. Additionally, the gain characteristic that was derived using the proposed method over the range from the reference speed ω_{ref} to

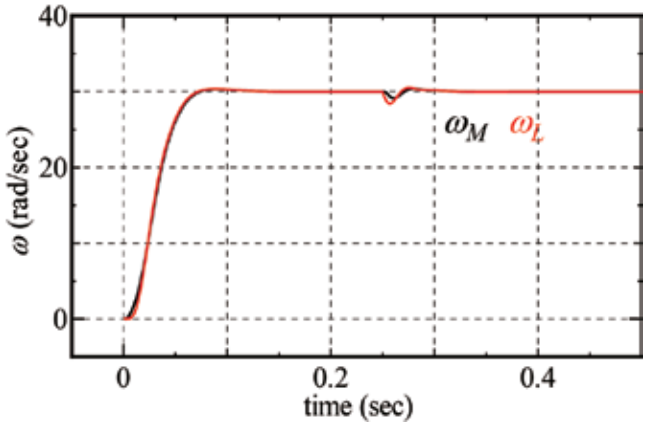

Figure 12. Simulation results when using the proposed method.

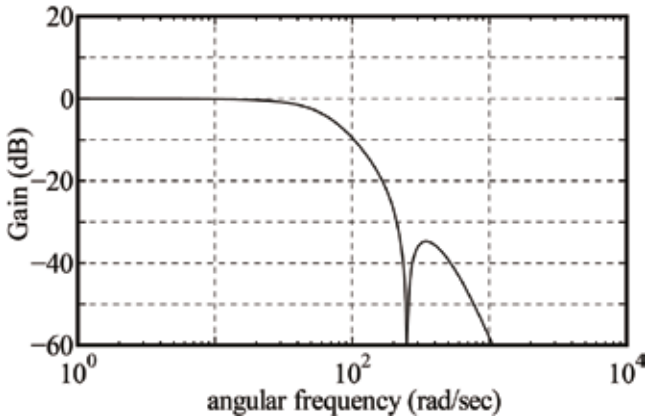

Figure 13. Gain characteristics when using the proposed method over the range from ω_{ref} to ω_M.

the motor angular speed ω_M is illustrated in **Figure 13**. The effectiveness of the proposed method is confirmed by the characteristic shown in this figure because the resonance peak is reduced considerably. Therefore, the results for the proposed method show that it is effective as a design method for the vibration suppression controller for the two-mass resonance system.

4. Controller design using fictitious reference iterative tuning (FRIT)

In this section, an off-line tuning method for the vibration suppression-type speed and current controller gains for the two-mass system is proposed based on the FRIT method; this method uses only single-shot experimental input-output data and does not use either the model parameters or the state equation of the two-mass resonance model. While most FRIT designs only use one state variable, this method uses specific multiple state variables to design the controller gains when using the FRIT method [6, 7, 14–16].

4.1. Frit

Figure 14 shows a typical control system, in which G is the transfer function of the object to be controlled, r is the reference signal, $\boldsymbol{\rho}$ represents the controller gains, $C(\boldsymbol{\rho})$ represents the controller, u is the control input parameter, and y is the output parameter. In this case, the mathematical model of G is not known in advance and is not required for this method.

Initially, as shown in **Figure 15**, a single-shot experiment is performed using the initial controller gains ρ_0, and the control input u_0 and output y_0 are measured. Then, the reference model $M(s)$, which matches the desired response, is determined. A fictitious reference signal is then generated using the controller, the control input u_0, and the output y_0, as shown in Eq. (31) below. This means that the initial data u_0 and y_0 can be obtained using any value of ρ if $\tilde{r}(\boldsymbol{\rho})$ is input to the closed-loop system used to implement $C(\boldsymbol{\rho})$.

$$\tilde{r}(\boldsymbol{\rho}) = C(\boldsymbol{\rho})^{-1}u_0 + y_0 \tag{31}$$

The optimal controller gains that are required to achieve $y_M = y_0$ are then determined, as shown in **Figure 16**, using an optimization search method. Finally, these controller gains then represent the best available solutions that allow the desired control system response to be obtained. Therefore, the controller design process can be performed without any prior information about either the model parameters or the state equations.

4.2. Vibration suppression controller design method by FRIT

Figure 17 shows a simplified form of the proposed vibration suppression control system, where $C_{\omega 1}$, $C_{\omega 2}$, $C_{\omega 3}$, and C_i are the controllers. While the FRIT method generally uses one

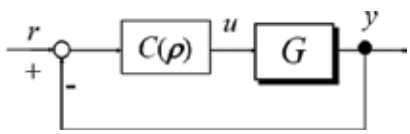

Figure 14. Typical closed-loop system.

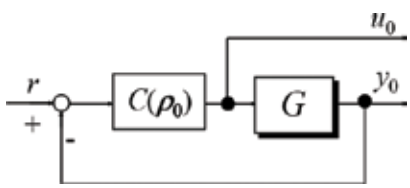

Figure 15. Measurement of the initial data.

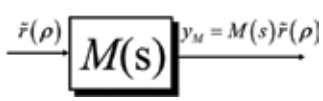

Figure 16. Reference model showing the input of the fictitious reference signal.

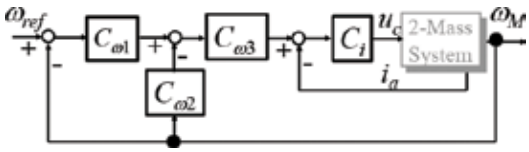

Figure 17. Simplified proposed control system.

control input and one state variable for the initial experimental data, the proposed method uses one control input, u_c, plus two state variables, ω_M and i_a. The controller gain vector $\boldsymbol{\rho}$ is given as follows:

$$\boldsymbol{\rho} = \begin{bmatrix} K_p & K_i & K_d & TK_{ap} & K_{ai} \end{bmatrix}^T \tag{32}$$

Therefore, the fictitious reference signal $\tilde{\omega}_{ref}(\boldsymbol{\rho})$ can be calculated using the following equation without any need for the two-mass resonance model.

$$\tilde{\omega}_{ref}(\boldsymbol{\rho}) = \left(1 + C_{\omega 1}^{-1} C_{\omega 2}\right)\omega_{M0} + C_{\omega 1}^{-1} C_{\omega 3}^{-1} i_{a0} + C_{\omega 1}^{-1} C_{\omega 3}^{-1} C_i^{-1} u_{c0} \tag{33}$$

Here, u_{c0}, ω_{M0} and i_{a0} represent the initial experimental data. The reference model $M(s)$, as shown in Eq. (34), is then used depending on the purpose of the system, where the time constant τ is a reference model parameter.

$$M(s) = \frac{1}{(\tau s + 1)^3} \tag{34}$$

Here, τ is calculated using the following equation with the 99% response time parameter T_{99}.

$$\tau = \frac{T_{99}}{4.4 \times 3^{0.6}} \tag{35}$$

The differential evolution method is then used to search for the optimal gains. The performance index function F is then defined as shown in Eq. (36) below using ω_{M0} and $y_M = M(s)\tilde{\omega}_{ref}(\boldsymbol{\rho})$.

$$F(\boldsymbol{\rho}) = \left\| M(s)\tilde{\omega}_{ref}(\boldsymbol{\rho}) - \omega_{M0} \right\|_2 \tag{36}$$

4.3. Experimental results

Figure 18 shows an example of the experimental results in the form of the angular speed step response of the control input. The resonance vibrations can again be observed in a similar manner to the case of the simulation results shown in **Figure 8** above.

Figure 19 shows the gain characteristics of the frequency responses from the experimental results shown in **Figure 18**, which relate the input voltage to the motor angular speed ω_M and the load angular speed ω_L. From these characteristics, the peak resonance vibrations at approximately 300 rad/s are also observed. These results were calculated based on the experimental

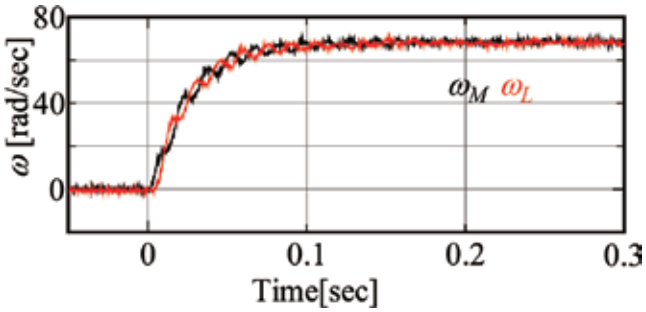

Figure 18. Angular speeds of the step responses (DC voltage input).

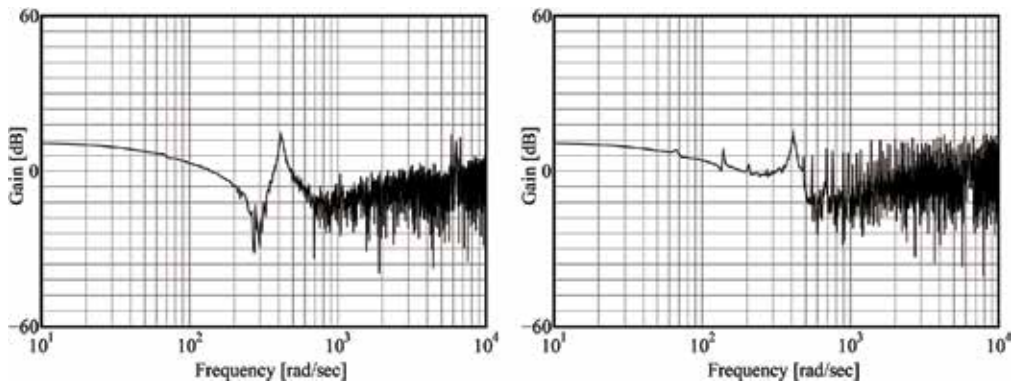

Figure 19. Calculated frequency responses to dc voltage input (left: u_c to ω_M, right: u_c to ω_L).

input and output waves of the voltage step response using the method that was proposed in [20]. Additionally, both the resonance and anti-resonance points can be found in these figures.

Figure 20 shows the experimental results obtained when using the general PI speed and current controller for comparison with the effects of the proposed control system. **Figure 21** shows the gain characteristics for the frequency responses shown in **Figure 20**, which relate ω_{ref} to ω_M and ω_L, where ω_{ref} is 30 rad/s. These characteristics show that the peak gain of the

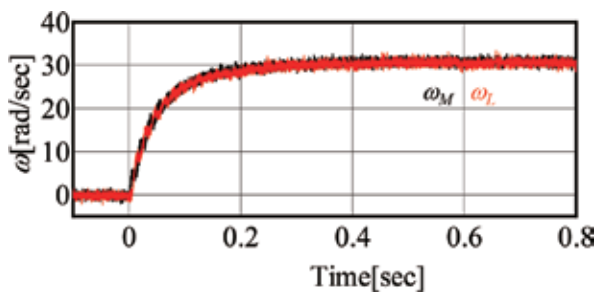

Figure 20. Experimental results obtained using conventional PI controller.

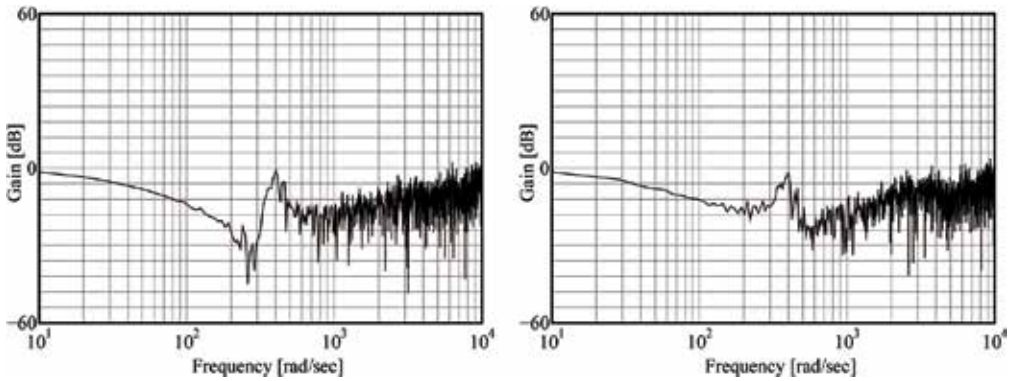

Figure 21. Frequency responses of conventional PI speed control system (left: ω_{ref} to ω_M; right: ω_{ref} to ω_L).

resonance is not greatly attenuated. **Figures 22–24** show the initial experimental waves for ω_{M0}, i_{a0} and u_{c0}, respectively, that were obtained using the values of the initial controller gain ρ_0, which are listed as follows:

$$\boldsymbol{\rho}_0 = [\,0.1 \quad 30 \quad 0.0001 \quad 0.001 \quad 1 \quad 10\,]^T \tag{37}$$

Both the initial rise and the oscillation can be observed in these figures.

Table 3 shows the results for the controller gains determined using the proposed FRIT design method with searching by the DE method, where T_{99} was set at 0.2 s. **Figure 25** shows a comparison of the experimental results obtained using the controller gains that were designed using the proposed method with the simulated results for the reference output y_M. The results in the figure show that the proposed off-line tuning method works very well, despite the fact that the design was performed using the initial one-shot experimental data alone. **Figure 26**

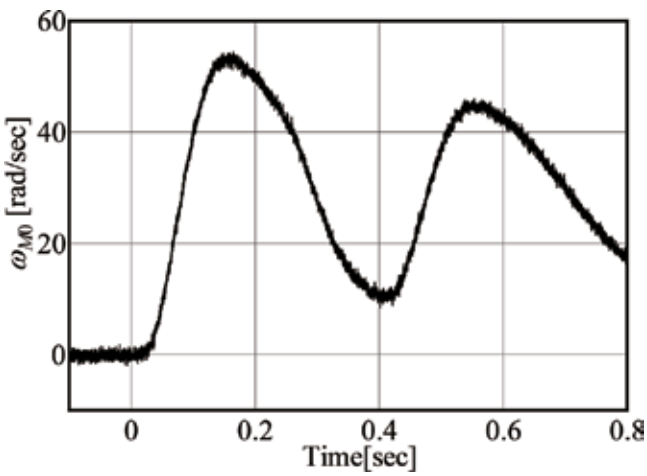

Figure 22. Initial ω_{M0} data.

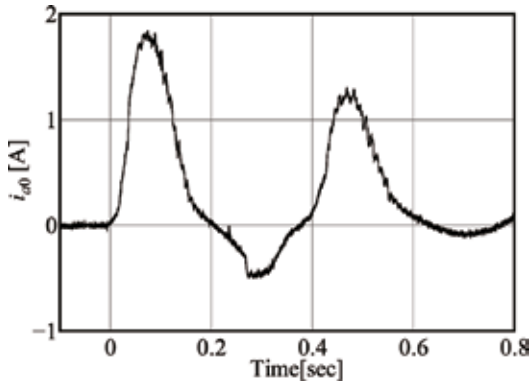

Figure 23. Initial i_{a0} data.

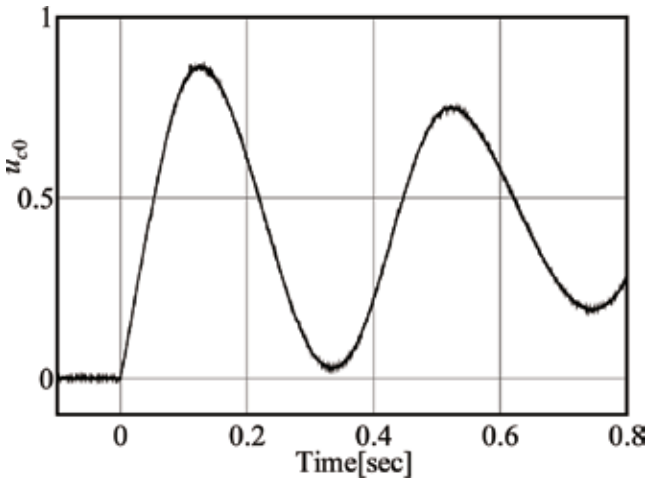

Figure 24. Initial u_{c0} data.

Gain name	Value	Gain name	Value	Gain name	Value
K_p	1.24	K_i	17.0	K_d	6.53×10^{-3}
T	8.59×10^{-4}	K_{ap}	2.37	K_{ai}	135

Table 3. Controller gain results when designed using the proposed FRIT method.

shows the experimental results that were obtained for ω_M, ω_L, and i_a when the proposed FRIT method was used. Here, ω_{ref} is stepped from 0 to 30 rad/s when t is 0 s. The figure shows the good response of the proposed vibration suppression speed controller. **Figure 27** shows the experimental results, where ω_{ref} is stepped from 30 to 50 rad/s when t is 0 s and the disturbance torque is increased from 0 to 10% of the rated torque when t is 0.5 s. As these figures show, good waves were observed in terms of their reference-following performance and disturbance response.

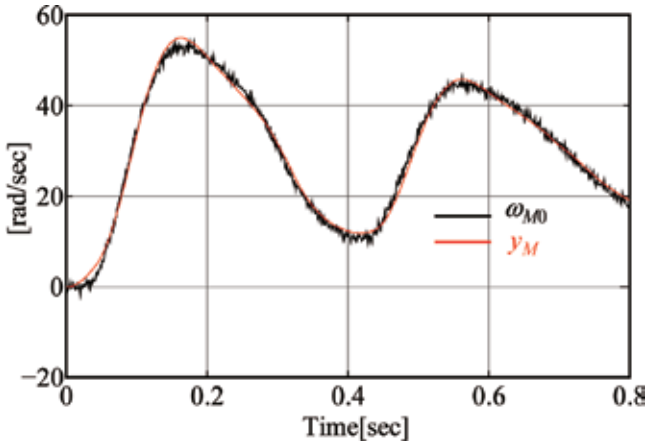

Figure 25. Initial experimental results for ω_{M0} and simulation results for y_M.

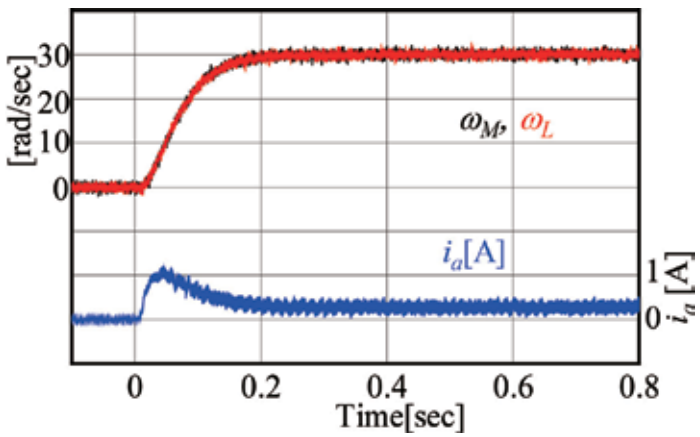

Figure 26. Experimental results for ω_M, ω_L, and i_a obtained when the proposed FRIT method.

Figure 28 shows the gain characteristics of the frequency responses of the proposed control system, where these characteristics are shown from the perspectives of ω_{ref} relative to ω_M and ω_L. The resonance vibration suppression effect can be observed in these figures. Therefore, the effectiveness of the proposed control system and the design method based on use of the FRIT method can be confirmed. Additionally, **Figure 29** shows the experimental results (ω_L) that were obtained for various values of the speed reference time parameter, where T_{99} = 0.15, 0.175, 0.2, 0.25, 0.3, and 0.35. As shown in this figure, the response times change satisfactorily and the proposed design method for the controller gains can thus also be used to design the response times arbitrarily.

http://dx.doi.org/10.5772/intechopen.74298

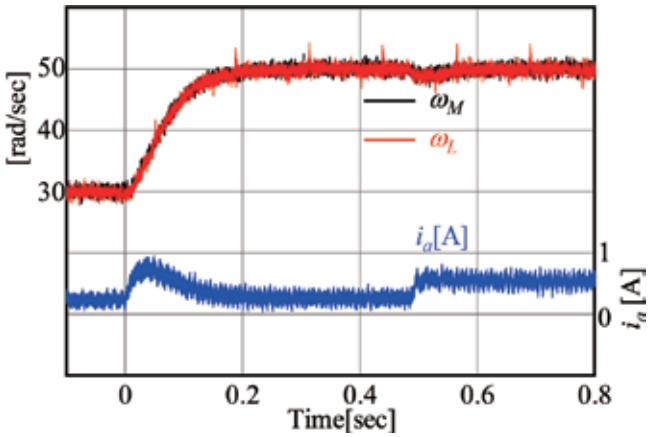

Figure 27. Experimental results for speed step response and disturbance response.

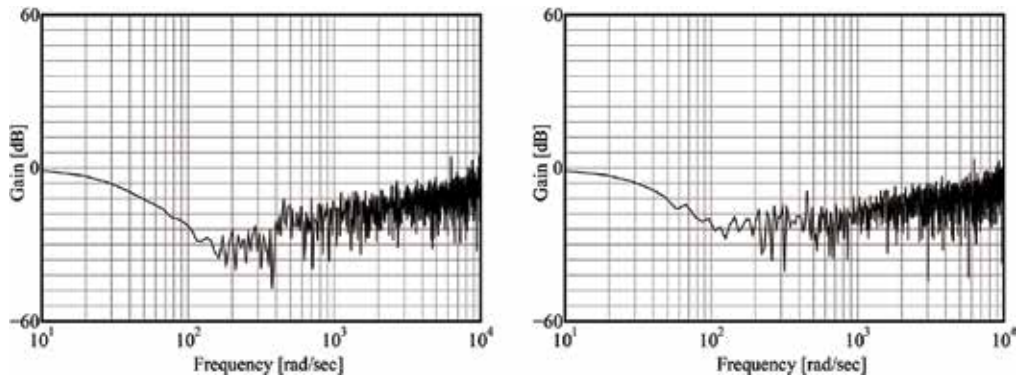

Figure 28. Frequency responses of the proposed control system (left: ω_{ref} to ω_M; right: ω_{ref} to ω_L).

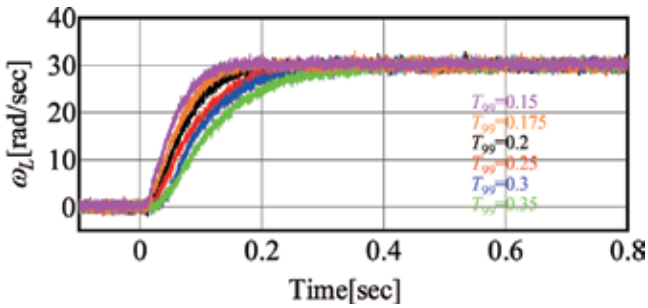

Figure 29. Experimental responses of ω_L to various values of T_{99}.

5. Conclusion

This chapter has proposed two design methods for the controller gains required for vibration suppression control in a two-mass resonance system. The proposed controller consists of a modified-IPD speed controller and a PI current controller. The proposed controller design methods are based on application of the coefficient diagram method (CDM) and application of the fictitious reference iterative tuning (FRIT) method. Both methods use the motor side variables only, including the motor's angular speed and the armature current. The CDM method uses the coefficient of the characteristic polynomial of the control system and can determine the control performance based on the shape of the coefficient diagram and the stability indices. In this chapter, the fitting performances for the standard form of the stability indices and the coefficient values were used to determine the controller gains, which were designed using the differential evolution method. The effectiveness of the proposed CDM was confirmed by the simulation results. The FRIT method can be used to design the controller without knowledge of the model state equations and their parameters. Furthermore, a fictitious signal that was calculated using the initial experimental data for multi-state variables was also proposed in this chapter. The effectiveness of the proposed FRIT method was confirmed using the experimental results. Consequently, the CDM and the FRIT method were shown to produce the same design performance. The CDM is useful for controller design when the mathematical model and the object parameters are known. The FRIT method is effective when the mathematical model is unknown but the initial experimental data can be observed.

Author details

Hidehiro Ikeda

Address all correspondence to: ikeda@nishitech.ac.jp

Department of Electrical Engineering, Nishi-Nippon Institute of Technology, Japan

References

[1] Hori Y, Sawada H, Chun Y. Slow resonance ratio control for vibration suppression and disturbance rejection in torsional system. IEEE Transactions on Industrial Electronics. 1999;**46**(1):162-168

[2] Yoon K-H et al. Hybrid robust controller design for a two mass system with disturbance compensation. Proceedings of ICCAS 2008; **2008**:1367-1372

[3] Ikeda H, Hanamoto T, Tsuji T, Tanaka Y. Position control of 2-mass systems with speed minor loop designed by pole placement method. IEEJ Transactions on Industry Applications. 1999;**119-D**(4):544-545 (in Japanese)

[4] Ikeda H, Hanamoto T, Tsuji T. Design of multi-inertia digital speed control system using Taguchi method. Proc. of ICEM 2008; 2008. pp. 1-6. Paper ID 1167, PB.3.9

[5] Ikeda H, Hanamoto T, Tsuji T, Tomizuka M. Design of vibration suppression controller for 3-inertia systems using Taguchi method. Proc. of SPEEDAM 2006, Mechatronic Systems; 2006. pp. S10–19-S10–25

[6] Matsui Y, Ayano H, Nakano K. A controller tuning for 2-mass system using closed-loop transient data, Proc. of 11th IFAC International Workshop, THS6T2. 1; 2013. pp. 564-569

[7] Azuma T, Watanabe S. A design of PID controllers using FRIT-PSO. Proc. of 8th ICST; 2014. pp. 459-464

[8] Manabe S, Kim Y-C. Recent development of coefficient diagram method. Proc. of 3rd Asian Control Conference; 2000. pp. 2055-2060

[9] Hanamoto T, Takenouchi T, Ikeda H. Vibration suppression control of 3-mass resonance system using particle swarm optimization for Design of Coefficient Diagram Method. Journal of Japan AEM. 2011:S16-S20

[10] H. Ikeda, T. Hanamoto. Vibration suppression control for multi-mass system using CDM designed by group-based-PSO. Proc of ICEE 2012, P-EM-12; 2012. pp. 1160-1165

[11] Ikeda H, Hanamoto T. Fuzzy controller of three-inertia resonance system designed by differential evolution. Journal of International Conference on Electrical Machines and Systems. 2014:184-189

[12] Ikeda H, Hanamoto T. Fuzzy controller of multi-inertia resonance system designed by differential evolution. Proc of ICEMS 2013, MC-1883; 2013. pp. 2291-2295

[13] Ikeda H, Hanamoto T. Design of m-IPD controller of multi-inertia system using differential evolution. Proc of IPEC 2014, 21J1–2; 2014. pp. 2476-2482

[14] Ikeda H, Hanamoto T. Design of vibration suppression controller for 2-inertia system by fictitious reference iterative tuning. Proc of ICEE 2015, ICEE15A-123; 2015. p. 6

[15] Ikeda H, Ajishi H, Hanamoto T. Application of fictitious reference iterative tuning to vibration suppression controller for 2-inertia resonance system. Proc of IECON 2015, TS-48, YF-008451. 2015. pp. 1825-1830

[16] Ikeda H, Kogura Y, Kim K, Era R, Hanamoto T. Vibration suppression controller tuning method for 2-mass resonance system using FRIT, Proc of ICEMS 2016, DS4G-3-2; 2016. p. 6

[17] Ikeda H. Vibration Suppression Controller of Multi-Mass Resonance System Using Fuzzy Controller. In: Chapter 19 of Modern Fuzzy Control Systems and Its Applications. Rijeka: InTech; 2017. pp. 399-417. ISBN 978-953-51-3390-2

[18] Myway Plus Corporation, https://www.mayway.co.jp/, Yokohama, Japan

[19] The Mathworks, https://www.mathworks.com, Massachusetts, U.S.A

[20] Matsui Y, Kimura T, Nakao K. Frequency response estimation for mechanical systems using closed-loop step response data. IEEJ Transactions on Electronics, Information and Systems. 2011;**131**(5):751-757

Edited by Mohammad Shamsuzzoha

PID Control for Industrial Processes presents a clear, multidimensional representation of proportional–integral–derivative (PID) control for both students and specialists working in the area of PID control. It mainly focuses on the theory and application of PID control in industrial processes. It incorporates recent developments in PID control technology in industrial practice. Emphasis has been given to finding the best possible approach to develop a simple and optimal solution for industrial users. This book includes several chapters that cover a broad range of topics and priority has been given to subjects that cover real-world examples and case studies. The book is focused on approaches for controller tuning, i.e., method bases on open-loop plant tests and closed-loop experiments.

Published in London, UK

IntechOpen

ISBN 978-1-83881-401-4